

**HYDROGEN AND CARBON NANO-MATERIALS
FROM THE PYROLYSIS-CATALYSIS OF WASTES**

Yeshui Zhang

Submitted in accordance with the requirements for the
degree of Doctor of Philosophy

The University of Leeds

School of Chemical and Process Engineering

July 2017

The candidate confirms that the thesis submitted is her own, except where work has formed part of jointly authored publications has been included. The contribution of the candidate and the other authors to this work has been explicitly indicated overleaf. The candidate confirms that appropriate credit has been given within the thesis where reference has been made to the work of others.

The work concerning investigation of different catalysts and process conditions reported in Chapter 4 is based on the published papers [1, 2].; Investigation of different rubbers and tyre pyrolysis oil model compounds reported in Chapter 5 is based on the published paper [3]; Investigation of plastics for hydrogen and carbon nanotubes production reported in Chapter 6 is based on the published papers [4-6]. The candidate was responsible for all of the experimental work and the writing of the draft manuscripts.

Published journal papers:

1. Zhang, Y., et al., Pyrolysis–Catalytic Reforming/Gasification of Waste Tires for Production of Carbon Nanotubes and Hydrogen. *Energy & Fuels*, 2015. **29**(5): p. 3328-3334.
2. Zhang, Y. and P.T. Williams, Carbon nanotubes and hydrogen production from the pyrolysis catalysis or catalytic-steam reforming of waste tyres. *Journal of Analytical and Applied Pyrolysis*, 2016. **122**: p. 490-501.
3. Zhang, Y., et al., High-value resource recovery products from waste tyres. *Proceedings of the Institution of Civil Engineers - Waste and Resource Management*, 2016. **169**(3): p. 137-145.
4. Zhang, Y., et al., Pyrolysis-catalysis of waste plastic using a nickel-stainless steel mesh catalyst for high value carbon products. *Environmental Technology*, 2017: p. 1-27.

5. Zhang, Y. et al., Influence of catalyst support material on H₂ production and catalyst coking for the pyrolysis-catalysis of waste tyres. Waste management & research, May 2017.
6. Zhang, Y., et al., Fe-Ni-MCM-41 catalysts for hydrogen-rich syngas production from waste plastics by pyrolysis-catalytic steam reforming, Energy & Fuel, July 2017.

The candidate (Yeshui Zhang) performed the experimental work and prepared the initial drafts of the published papers. The co-authors, Prof. Paul Williams, Dr. Chunfei Wu and Dr. Mohamad Anas Nahil supervised the work and Prof. Paul Williams and Dr. Chunfei Wu made corrections to the draft papers.

This copy has been applied on the understanding that it is copyright materials and that no quotation from the thesis may be published without proper acknowledgement.

The right of Yeshui Zhang to be identified as Author of this work has been asserted by her accordance with the Copyright, Designs and Patents Act 1988.

Acknowledgement

Foremost, I would like to express my sincere gratitude to my supervisors Prof. Paul Williams and Dr. Chunfei Wu for the continuous support of my PhD study and related research, for their patience, motivation, and immense knowledge. Their guidance helped me in all the time of the research and writing of this thesis. I could not have imagined having a better supervisor and mentor for my PhD study.

Besides my supervisors, I would also like to express my enormous gratitude to my parents for financially and spiritually supporting for PhD study. Enormous gratitude also to my beloved fiancée Hualun Zhu, for his unconditional love, patience on my personal attitude, and accompany with me all the time no matter what happened. I feel so lucky there was a romantic encounter with him at the beginning of my PhD, which offered us the chance to build up our own home. Also, my deepest appreciation for his family for cultivating such great person to be with me. Without their supports I would have no chance to pursue PhD study in UK.

Special thanks to Dr. Mohamad Anas Nahil and Dr. Jude Onwudili for their involvement with this research who provided me an opportunity to join their team as intern, and who gave access to the laboratory and research facilities. Without their precious support it would not be possible to conduct this research. Thanks to Mr. Ed Woodhouse for his technical support.

I also want to thank to my colleagues in my research group: Dr. Juniza Md Saad, Dr. Amal Al-Rahbi, Dr. Jonathan Acomb, Dr. Eyup Yildirim, Dr. Chika Muhammad, Dr. Ramzi Cherad, Dr. Paula Blanco Sanchez, Kenneth, Japhet, Andrew, Peace, Devy, for your help and friendships.

Abstract

In this work, a two-stage fixed-bed reaction system was used for the production of carbon nanotubes along with hydrogen production from waste tyres and plastics from a pyrolysis-catalysis/catalytic-reforming process.

The preliminary investigations concerned different metal catalysts ($\text{Ni}/\text{Al}_2\text{O}_3$, $\text{Co}/\text{Al}_2\text{O}_3$, $\text{Fe}/\text{Al}_2\text{O}_3$ and $\text{Cu}/\text{Al}_2\text{O}_3$), which were investigated to determine the effects on carbon nanotube and hydrogen production by pyrolysis-catalysis of waste truck tyres. The results showed catalyst addition in the pyrolysis-catalysis of waste tyre process can increase hydrogen production. The $\text{Ni}/\text{Al}_2\text{O}_3$ catalyst gave the highest hydrogen production at $18.14 \text{ mmol g}^{-1}$ along with production of relatively high quality carbon nanotubes which were homogenous. The influence of catalyst support was investigated with different $\text{SiO}_2:\text{Al}_2\text{O}_3$ ratios (3:5, 1:1, 3:2, 2:1) with nickel. The results showed that the Ni-based $\text{SiO}_2:\text{Al}_2\text{O}_3$ supported catalyst at a 1:1 ratio at $900 \text{ }^\circ\text{C}$ with sample to catalyst ratios at 1:2 gave the highest hydrogen production at $27.41 \text{ mmol g}^{-1}$, and the 1:1 ratio gave the highest filamentous carbon production at 201.5 mg g^{-1} . The influence of process parameters on hydrogen and CNTs production were investigated with the $\text{Ni}/\text{Al}_2\text{O}_3$ catalyst. Hydrogen production reached the highest amount which was $27.41 \text{ mmol g}^{-1}$ at $900 \text{ }^\circ\text{C}$ with sample to catalyst ratio was 1:2. The highest filamentous carbon production was produced with the sample to catalyst ratio at 1:1 at $900 \text{ }^\circ\text{C}$ catalyst temperature. The water injection rates were also investigated, the results showed that water introduction inhibited filamentous carbon production but increased the hydrogen production.

An in-depth study to better understand the process involved investigation of three different tyre rubbers and five tyre pyrolysis oil model compounds to understand the mechanism of carbon nanotubes formation in waste tyres by the pyrolysis-catalysis process. The results showed that natural rubber which is the main component of tyre samples which used for this thesis, dominated hydrogen production at 25 mmol g^{-1} and SBR gave the highest carbon formation which was 40 wt. %. The aliphatic model compounds (hexadecane and decane) favoured gaseous hydrocarbons formation instead of solid carbon formation, but the aromatic model compounds (styrene, naphthalene and

phenanthrene) favour solid carbon formation where the majority of carbon formation was filamentous carbon.

The study was extended to investigate waste plastics and different types of waste plastic feedstock used in the pyrolysis catalysis/catalytic reforming process to produce hydrogen and carbon nanotubes. As carbon nanotubes separation from the catalyst is a challenge for this project, the nickel metal catalyst was loaded on stainless steel mesh and applied in the high-density polyethylene pyrolysis-catalysis process. The benefit of this catalyst has been shown in that the carbon formation could be easily separated by physical shaking from the stainless steel-nickel mesh catalyst. However, further investigation on waste plastics was concentrated on hydrogen production and where carbon nanotubes were the by-product from the process. Fe-based and Ni-based catalysts as bimetallic catalysts supported by MCM-41 with different Fe:Ni ratios were investigated using simulated mixed waste plastics. A synergistic effect of the iron and nickel was observed, particularly for the (10:10) Fe/Ni/MCM-41 catalyst where the highest gas yield (95 wt.%) and highest H₂ production (46.1 mmol g⁻¹_{plastic}) have been achieved. Along with lowest carbon deposition which was 6 wt.% with carbon nanotubes formation. Seven real world waste plastics were used to produce hydrogen and carbon nanotubes in the presence of a Fe:Ni at 10:10 ratio catalyst with an MCM-41 support. The results showed that the agricultural waste plastic gave the highest hydrogen production that was 55.99 mmol g⁻¹ with carbon nanotubes formation. The calorific values of the produced gases from different plastic samples were in the range of 12.13 - 24.06 MJ m⁻³, which could provide the process fuel that shows the possibility to apply the technology for further larger scale of research.

Table of contents

List of figures	XI
List of tables	XVII
Abbreviations	XIX
Chapter 1. Introduction	1
1.1 Waste hydrocarbons	1
1.2 Waste tyres production and management	1
1.3 Waste plastics production and management	2
1.4 Hydrogen and carbon nanotubes	5
1.4.1 Hydrogen	5
1.4.2 Carbon nanotubes	6
1.4.3 Tyres and plastics as potential feedstock for hydrogen and CNTs	7
1.5 Aim and objectives	9
References	11
Chapter 2. Literature review	15
2.1 Hydrogen production from waste sources	15
2.1.1 Waste tyres	15
2.1.2 Waste plastics	17
2.1.3 Other alternative feedstock resource - Glycerol	18
2.1.4 Summary of thermal treatments for waste carbonaceous material	21
2.2 Process conditions for thermal treatments of wastes	22
2.3 Catalysts development for waste thermal treatment	24
2.3.1 Nickel-based catalysts	24
2.3.2 Noble metals-based catalysts	27
2.3.3 Other catalysts	30
2.3.4 Catalyst supports	32
2.3.5 Summary	33
2.4 Carbon nanotubes (CNTs) applications and production	34
2.4.1 Applications of carbon nanotubes	34
2.4.2 Production of carbon nanotubes	37
2.4.3 Summary	52
2.5 Production of Carbon nanotubes (CNTs) from alternative sources: methods and catalysts	53
2.5.1 Catalytic pyrolysis of waste plastics	54

2.5.2	Carbon nanotubes from waste tyres	55
2.5.3	Carbon nanotubes from other sources.....	56
2.5.4	Summary	57
	References	58
Chapter 3.	Materials and methodology	74
3.1	Materials	74
3.1.1	Waste tyres	74
3.1.2	Tyre pyrolysis oil model compounds.....	76
3.1.3	Plastics samples	77
3.1.4	Catalysts preparation.....	79
3.2	Reaction system and reproducibility of products	82
3.2.1	Two-stage fixed-bed reactor.....	82
3.2.2	Reproducibility of products by pyrolysis-catalysis with two-stage fixed-bed reactor.....	85
3.3	Materials analysis and characterisations.....	86
3.3.1	X-Ray diffraction	86
3.3.2	Porous catalysts characterization.....	88
3.3.3	Gas chromatography	91
3.3.4	Thermal gravimetric analyser	97
3.3.5	Scanning electron microscopy	100
3.3.6	Transmission electron microscopy with energy dispersive X-Ray analyser	102
3.3.7	Raman analysis	104
	References	107
Chapter 4.	Investigation of different catalysts and process conditions for carbon nanotubes production and by-product hydrogen by pyrolysis-catalysis of waste tyres.....	109
4.1	Effect of different metals including Co, Fe, Ni and Cu with Al ₂ O ₃ catalyst support	110
4.1.1	Characterisations of the fresh catalysts	111
4.1.2	Pyrolysis-catalysis of waste tyres: Mass balance and hydrogen production	115
4.1.3	Carbon Nanotubes (CNTs) Production	120
4.1.4	Conclusion	124
4.2	Effect of SiO ₂ :Al ₂ O ₃ ratios of Ni/SiO ₂ /Al ₂ O ₃ catalysts on the production of carbon nanotubes production and by-product hydrogen.....	125

4.2.1	Product yields and gas composition.....	125
4.2.2	Characteristics of carbon production.....	127
4.2.3	Effect of catalyst temperature on carbon nanotube production and by-product hydrogen from the pyrolysis- catalysis of tyres	132
4.2.4	Effect of tyre:catalyst ratio on carbon nanotube production and by-product hydrogen from the pyrolysis catalysis of tyres.....	139
4.2.5	Conclusion	144
4.3	Investigation of process conditions for the pyrolysis-catalysis/ catalytic reforming of waste truck tyres for hydrogen and by- product carbon nanotube productions with Ni/Al ₂ O ₃ catalysts ...	145
4.3.1	Effect of water injection rate on pyrolysis-catalytic reforming	146
4.4	Conclusions for hydrogen production from waste tyres by pyrolysis-catalytic reforming	157
	Reference	160
Chapter 5. Influence of different rubbers and tyre pyrolysis oil compounds on hydrogen and carbon nanotube production166		
5.1	Pyrolysis catalysis of butadiene rubber (BR), Styrene butadiene rubber (SBR), natural rubber (NR), waste car tyre and waste truck tyre.....	166
5.1.1	Characterisation of the Feedstock Rubber Samples	167
5.1.2	Product yields from pyrolysis-catalysis of tyres and rubbers	169
5.1.3	Carbon formation	172
5.1.4	Conclusions.....	177
5.2	Investigation of tyre oil compounds on hydrogen and carbon nanotube production	178
5.2.1	Carbon production and characterisation	180
5.2.2	Gas compositions	192
5.2.3	Conclusion	193
	Reference	195
Chapter 6. Pyrolysis-catalysis/catalytic reforming of plastics for hydrogen and carbon nanotubes production.....198		
6.1	Investigation of carbon nanotubes production from high density polypropylene (HDPE) with nickel loading on a stainless steel (NiSS) catalyst.....	198
6.1.1	Catalyst characterisation	199
6.1.2	Product yield	200

6.1.3	Carbon production and characterization	203
6.1.4	Conclusion	212
6.2	Hydrogen and carbon nanotubes productions from waste plastics waste with Fe/Ni/MCM41 catalysts by pyrolysis-catalytic reforming	213
6.2.1	Characterisation of fresh catalysts	213
6.2.2	The effect of Fe:Ni ratio on gaseous products.....	217
6.2.3	Effect of Fe:Ni ratios on catalyst deactivation/carbon deposition.....	220
6.2.4	Conclusion	227
6.3	Hydrogen produced from different waste plastics with Fe/Ni/MCM-41 (10:10) catalyst by pyrolysis-catalytic reforming process.....	228
6.3.1	Mass balance and gaseous products.....	228
6.3.2	Carbon deposition.....	231
6.3.3	Conclusion	234
	References	235
Chapter 7. Conclusions and future work.....		239
7.1	Conclusions.....	239
7.1.1	Pyrolysis-catalysis of waste tyres for hydrogen and carbon nanotubes production	239
7.1.2	Investigations on different tyre rubbers and tyre pyrolysis oil model compounds for carbon nanotubes and hydrogen productions.....	241
7.1.3	Investigation of the hydrogen production along with value-added carbon nanotubes production from waste plastics by pyrolysis- catalysis/catalytic-reforming.....	243
7.2	Future work.....	245
7.2.1	Mechanism study	245
7.2.2	Carbon nanotubes purifications study.....	246
7.2.3	Quality control of carbon production	246

List of figures

Figure 1-1 Evolution of EU end-of-life tyres (ELT) arising by ETRMA [10].....	2
Figure 1-2 The proportions of plastics management between 2006 to 2012 in EU[16].	3
Figure 1-3Treatments of post-consumer plastics across the EU in 2012 [16].	4
Figure 1-4 The supply and demand of hydrogen [19].	6
Figure 2-1 The reaction pathways of pyrolysis of glycerol[36].	19
Figure 2-2 Products from pyrolysis and gasification of carbonaceous materials [52].	21
Figure 2-3 Schematic diagram of a chemical vapour deposition (CVD) method for synthesizing carbon nanotubes (CNTs) [140].	38
Figure 2-4 The most accepted mechanism for carbon nanotubes growth: (a) tip-growth model. (b) base-growth model [140].	40
Figure 2-5 The vapour-liquid-solid mechanism of carbon nanotube growth [145].	42
Figure 2-6 The carbon diffusion and sub-diffusion of MWCNTs growth mechanism (Red arrows indicate the prohibited paths for carbon diffusion and green arrows indicate the possible carbon diffusion paths) [148].	43
Figure 3-1 Waste truck (left) and car tyres (right) samples	74
Figure 3-2 Plastic samples (From left to right: HDPE, LDPE, PS, PET and PP).	77
Figure 3-3 Real world waste plastics (A: Plastics from motor oil flasks; B: Plastics from vehicle fuel tank; C: Plastics from detergent containers; D: Mineral water containers plastics; E: Household food packaging plastics; F: Plastics from building re-construction; G: Waste plastics from agriculture).	78
Figure 3-4 Ni on the pre-treated stainless steel mesh (NiSS) catalysts with scanning electron micrographs.	81
Figure 3-5 Schematic diagram of two-stage fixed-bed reaction system [8]..	82
Figure 3-6 Two-stage fixed-bed reaction system for pyrolysis catalysis/catalytic-gasification experiments.	83
Figure 3-7 XRD analysis of the used Fe-Ni-MCM-41 catalysts from the pyrolysis-catalytic reforming of simulated mixed waste plastics with different Fe:Ni ratios (00:20, 05:15, 10:10, 15:05, 20:00). The Ni peaks at 44 and 52 2-Theta indicate the stable face centred cubic phase. The iron peaks indicate the α - Fe or iron carbide.	84
Figure 3-8 Bruker D8 X-Ray diffraction spectroscopy (Modified figure based on [9]).	86

Figure 3-9 Typical XRD spectrum of fresh Ni/Al ₂ O ₃ catalyst.....	87
Figure 3-10 NOVA 2200e instrument used to characterize the porous properties of catalysts.	88
Figure 3-11 Example of the adsorption and desorption isothermal for 20 wt. % Fe/Ni/MCM-41 catalyst with Fe:Ni ratio at 1:1 by a NOVA 2200e instrument.....	89
Figure 3-12 Varian 3380 gas chromatography	92
Figure 3-13 GC response peaks for standard gas (a) permanent gas chromatogram; (b) alkanes chromatogram; (c) alkenes chromatogram; (d) carbon dioxide chromatogram.	94
Figure 3-14 Shimadzu thermal gravimetric analyser (TGA-50).	98
Figure 3-15 Typical TGA-TPO and DTG-TPO results of reacted Ni/Al ₂ O ₃ catalyst.....	98
Figure 3-16 Thermal gravimetric analysis (TGA) of waste truck tyre.....	99
Figure 3-17 Stanton-Redcroft thermo gravimetric analyser	100
Figure 3-18 Hitachi SU8230 Scanning electron microscope [19].	101
Figure 3-19 Sample of SEM images of (a) fresh 10 wt. % Cu/Al ₂ O ₃ catalyst and (b) reacted catalyst with filamentous carbon production by pyrolysis-catalysis waste truck tyre.....	102
Figure 3-20 TECNAI TF20 Transmission electron microscopy (From TECNAI TF20 operation manual).	103
Figure 3-21 Samples of TEM and EDX mapping of reacted catalyst.	104
Figure 3-22 Renishaw Invia Raman spectroscope [25].....	105
Figure 3-23 (a) Example of Raman result for the reacted 10 wt. % Ni/Al ₂ O ₃ catalyst after the pyrolysis-catalysis of waste tyre experiment at 800 °C; (b) example of Raman result for the reacted 20 wt.% Fe/MCM-41 catalyst after pyrolysis-catalytic reforming of simulated mixed waste plastics.	106
Figure 4-1 SEM images of the fresh Co/Al ₂ O ₃ , Cu/Al ₂ O ₃ , Fe/Al ₂ O ₃ and Ni/Al ₂ O ₃ catalysts before pyrolysis-catalysis.	112
Figure 4-2 DTG-TPR results of the Co/Al ₂ O ₃ , Cu/Al ₂ O ₃ , Fe/Al ₂ O ₃ and Ni/Al ₂ O ₃ catalysts fresh catalysts	113
Figure 4-3 XRD analysis of the fresh Co/Al ₂ O ₃ , Cu/Al ₂ O ₃ , Fe/Al ₂ O ₃ and Ni/Al ₂ O ₃ catalysts.....	115
Figure 4-4 TPO results of different reacted catalysts from the pyrolysis-catalysis of waste tyre. (Catalyst temperature was 600 °C)	118
Figure 4-5 DTG-TPO results of different reacted catalysts from the pyrolysis-catalysis of waste tyre. (catalyst temperature was 600 °C ..	119
Figure 4-6 SEM analysis of the reacted Co/Al ₂ O ₃ , Cu/Al ₂ O ₃ , Fe/Al ₂ O ₃ and Ni/Al ₂ O ₃ catalysts after the pyrolysis-catalysis of waste tyre.	121

Figure 4-7 TEM analysis of the reacted Co/Al ₂ O ₃ , Cu/Al ₂ O ₃ , Fe/Al ₂ O ₃ and Ni/Al ₂ O ₃ catalysts derived from pyrolysis-catalysis of waste tyre	122
Figure 4-8 Raman analysis of the 4 reacted catalysts (Fe/Al ₂ O ₃ , Cu/Al ₂ O ₃ , Co/Al ₂ O ₃ , Ni/Al ₂ O ₃)	123
Figure 4-9 Product yields from the pyrolysis-catalysis of waste tyres with a 20 wt. % Ni/Al ₂ O ₃ /SiO ₂ catalyst with different Al ₂ O ₃ to SiO ₂ ratios.	127
Figure 4-10 TGA-TPO and DTG-TPO analyses for reacted catalysts from the pyrolysis-catalysis of waste tyres with different alumina:silica ratios for 20 wt. % Ni/Al ₂ O ₃ /SiO ₂ catalyst with different Al ₂ O ₃ to SiO ₂ ratios (AS1 = alumina:silica ratio is 1:1; AS2 = alumina:silica ratio is 2:1; AS4 = alumina:silica ratio is 3:2; AS5 = alumina:silica ratio is 3:5).	128
Figure 4-11 SEM images of reacted catalysts from the pyrolysis-catalysis of waste tyres with a 20 wt. % Ni/Al ₂ O ₃ /SiO ₂ catalyst with different Al ₂ O ₃ to SiO ₂ ratios.....	129
Figure 4-12 TEM images of reacted catalysts from the pyrolysis-catalysis of waste tyres with a 20 wt. % Ni/Al ₂ O ₃ /SiO ₂ catalyst with different Al ₂ O ₃ to SiO ₂ ratios.....	130
Figure 4-13 Raman analysis of reacted catalysts from the pyrolysis-catalysis of waste tyres with a 20 wt. % Ni/Al ₂ O ₃ /SiO ₂ catalyst with different Al ₂ O ₃ to SiO ₂ ratios.	131
Figure 4-14 Proportions of amorphous and filamentous carbons produced from the pyrolysis-catalysis of waste tyres with a 20 wt. % Ni/Al ₂ O ₃ /SiO ₂ catalyst with different Al ₂ O ₃ to SiO ₂ ratios.	132
Figure 4-15 (a) TGA-TPO and DTG-TPO analysis results of the used catalysts; (b) Proportions of disordered and filamentous types of carbon formed from the pyrolysis-catalysis of tyres at different temperatures (700, 800 and 900 °C) with no water and tyre:catalyst ratio is 1:0.5.	135
Figure 4-16 SEM and TEM images of the used catalysts from the pyrolysis-catalysis of tyres at different temperatures (700, 800 and 900 °C) with no water and tyre:catalyst ratio is 1:0.5.	137
Figure 4-17 Raman analysis results of the used catalysts from the pyrolysis-catalysis of tyres at different temperatures (700, 800 and 900 °C) with no water and tyre:catalyst ratio is 1:0.5.	138
Figure 4-18 (a) TGA-TPO and DTG-TPO results of reacted catalysts; (b) Proportions of disordered and filamentous types of carbon formed from the pyrolysis-catalysis of tyres at different tyre:catalyst ratios (1:0.5; 1:1; 1:2) with no water and 900°C.	141
Figure 4-19 SEM and TEM images of reacted catalysts from the pyrolysis-catalysis of waste tyres at different tyre:catalyst ratios (1:0.5; 1:1; 1:2) with no water and 900°C	142

Figure 4-20 Raman analysis results of reacted catalysts from the pyrolysis-catalysis of tyre at different tyre:catalyst ratios (1:0.5; 1:1; 1:2) with no water and 900°C	143
Figure 4-21 (a) TGA-TPO and DTG-TPO analysis results of the used catalysts from the pyrolysis-catalytic reforming of waste tyre at different water injection rates; (b) Proportions of disordered and filamentous types of carbon formed from the pyrolysis-catalytic reforming of tyres with different water injection rates (0, 2 and 5 ml h ⁻¹) at 800 °C and tyre:catalyst ratio 1:0.5.....	149
Figure 4-22 SEM and TEM images of the used catalysts from the pyrolysis-catalytic reforming of waste tyres at different water injection rates (0, 2 and 5 ml h ⁻¹) at 800 °C and tyre:catalyst ratios 1:0.5.	150
Figure 4-23 Raman analysis of the used catalysts from the pyrolysis-catalytic reforming of waste tyres at different water injection rates (0, 2 and 5 ml h ⁻¹) at 800 °C and tyre:catalyst ratios 1:0.5.....	151
Figure 4-24 TGA-TPO and DTG-TPO results of reacted catalysts produced from the pyrolysis-catalytic reforming of waste tyres with a 20 wt. % Ni/Al ₂ O ₃ /SiO ₂ catalyst with an Al ₂ O ₃ :SiO ₂ ratio of 1:1.....	155
Figure 4-25 SEM images of reacted catalysts produced from the pyrolysis-catalytic reforming of waste tyres with a 20 wt. % Ni/Al ₂ O ₃ /SiO ₂ catalyst with an Al ₂ O ₃ :SiO ₂ ratio of 1:1.....	156
Figure 4-26 TEM images of reacted catalysts produced from the pyrolysis-catalytic reforming of waste tyres with a 20 wt. % Ni/Al ₂ O ₃ /SiO ₂ catalyst with an Al ₂ O ₃ :SiO ₂ ratio of 1:1.....	156
Figure 4-27 Raman analyses reacted catalysts produced from the pyrolysis-catalytic reforming of waste tyres with a 20 wt. % Ni/Al ₂ O ₃ /SiO ₂ catalyst with an Al ₂ O ₃ :SiO ₂ ratio of 1:1.....	157
Figure 5-1 TGA and DTG analysis results of the feedstock truck tyre, car tyre, poly-butadiene rubber (BR), styrene-butadiene rubber (SBR) and natural rubber (NR).	168
Figure 5-2 TGA-TPO and DTG-TPO results of the used catalysts from the pyrolysis-catalysis of truck tyre, car tyre, poly-butadiene rubber (BR), styrene-butadiene rubber (SBR) and natural rubber (NR).....	173
Figure 5-3 Proportion of amorphous and graphitic type carbons formed from the pyrolysis-catalysis of truck tyre, car tyre, poly-butadiene rubber (BR), styrene-butadiene rubber (SBR) and natural rubber (NR).	174
Figure 5-4 SEM and TEM images of the carbon deposited on the catalyst from the pyrolysis-catalysis of truck tyre, car tyre, poly-butadiene rubber (BR), styrene-butadiene rubber (SBR) and natural rubber (NR).	175
Figure 5-5 Raman analysis of the carbon deposited on the catalyst from the pyrolysis-catalysis of truck tyre, car tyre, poly-butadiene rubber (BR), styrene-butadiene rubber (SBR) and natural rubber (NR)	176

Figure 5-6 TGA-TPO results of reacted catalysts produced from pyrolysis catalysis of tyre oil model compounds.....	181
Figure 5-7 DTG-TPO results of reacted catalysts produced from pyrolysis catalysis of tyre oil model compounds.....	182
Figure 5-8 Proportions of disordered and filamentous types of carbon formed from pyrolysis of tyre oil model compounds.....	183
Figure 5-9 Gaseous carbon conversion.....	183
Figure 5-10 SEM images of reacted catalysts produced from pyrolysis catalysis of tyre oil model compounds.....	185
Figure 5-11 TEM images of reacted catalysts produced from pyrolysis tyre oil model compounds.	188
Figure 5-12 (a) Raman results of reacted catalysts produced from pyrolysis-catalysis of aliphatic tyre oil model compounds (hexadecane and decane); (b) single ring aromatic tyre oil model compounds (styrene); (c) polyaromatic tyre oil model compounds (naphthalene and phenanthrene); (d) commercial carbon nanofibers and multi-walled carbon nanotubes.	190
Figure 6-1 Scanning electron micrograph of the prepared nickel-loaded stainless steel mesh catalyst.	199
Figure 6-2 X-ray diffraction analysis of the prepared nickel-loaded stainless steel mesh catalyst	200
Figure 6-3 TGA-TPO and DTG-TPO results of the deposited carbon in relation to catalyst temperatures and different plastic to catalyst ratios.	204
Figure 6-4 Proportions of disordered carbon and filamentous carbon produced from HDPE by pyrolysis-catalysis with the nickel-stainless steel mesh catalyst (The X-axis indicates the reaction temperature and amount of feedstock, for example 2-700 indicates the feedstock amount is 2 g and reaction temperature was 700 °C).....	205
Figure 6-5 SEM results of different amounts of HDPE at different temperatures (a) 700 °C with 2g; (b) 800 °C with 2g; (c) 900 °C with 2g; (d) 900 °C with 4g.....	206
Figure 6-6 TEM results of the selected catalyst tested at 800 °C	207
Figure 6-7 Raman analyses of carbon deposited on the wire mesh catalyst for the pyrolysis-catalysis of waste high density polyethylene in relation to temperature	207
Figure 6-8 Carbon nanotubes amount estimation by TEM images.....	212
Figure 6-9 XRD analysis of fresh Fe/Ni/MCM-41 catalysts with different Fe:Ni ratios (00:20, 05:15, 10:10, 15:05, 20:00)	214
Figure 6-10 SEM fresh Fe/Ni/MCM-41 catalysts with different Fe:Ni ratios include (a) 00:20, (b) 05:15, (c) 10:10, (d) 15:05, (e) 20:00).	216

Figure 6-11 XRD analysis of the used Fe/Ni/MCM-41 catalysts from the pyrolysis-catalytic reforming of simulated mixed waste plastics with different Fe:Ni ratios (00:20, 05:15, 10:10, 15:05, 20:00).	217
Figure 6-12 DTG-TPO results of the used catalysts from the pyrolysis-catalytic reforming of simulate mixed waste plastics (SMWP) with Fe/Ni/MCM-41 catalysts with different Fe:Ni ratios (00:20, 05:15, 10:10, 15:05, 20:00).	221
Figure 6-13 SEM images of the used catalysts from the pyrolysis-catalytic reforming of simulated mixed waste plastics (SMWP) with Fe/Ni/MCM-41 catalysts with different Fe:Ni ratios (00:20, 05:15, 10:10, 15:05, 20:00).	222
Figure 6-14 Transmission electron microscopy with energy dispersive X-ray spectroscopy (TEM-EDXS) elemental mapping analysis of C, Fe and Ni for reacted (05:15, 10:10, 15:05) Fe/Ni/MCM-41 catalysts.	225
Figure 6-15 TEM images of the used catalysts from the pyrolysis-catalytic reforming of simulated mixed waste plastics (SMWP) with Fe/Ni/MCM-41 catalysts with different Fe:Ni ratios include (a) 00:20, (b) 05:15, (c) 10:10, (d) 15:05, (e) 20:00).	226
Figure 6-16 TGA-TPO analysis results of the used catalysts from the pyrolysis-catalytic reforming of different waste plastics.	231
Figure 6-17 DTG-TPO analysis results of the used catalysts from the pyrolysis-catalytic reforming of different waste plastics (Feedstock to catalysts ratio at 4:1, reforming temperature at 800 °C, heating rate at 50 °C min ⁻¹ , water injection rate 2 g h ⁻¹ and Fe-Ni/MCM-41 catalysts with Fe to Ni ratio at 10:10).	232
Figure 6-18 SEM images of reacted catalysts from the pyrolysis-catalytic reforming of different waste plastics.	233

List of tables

Table 2-1 Comparison of CNTs formed by chemical vapour deposition of methane in the presence of different catalysts and supports[152]	46
Table 3-1 Elemental analysis of Truck tyre, car tyre, BR, SBR, and NR	75
Table 3-2 The calculations for preparing the alumina-silica catalyst support with different alumina to silica ratios.	80
Table 3-3 Reproducibility analysis of the products mass balance	85
Table 3-4 Repeatability of the gas concentrations by GC-FID and GC-TCD (STDEV is standard deviation).	95
Table 4-1 Mass balance and gas concentrations for the pyrolysis-catalysis of waste tyres.	116
Table 4-2 Product yields and gas concentrations from the pyrolysis-catalysis of waste tyres with a 20 wt. % Ni/Al ₂ O ₃ /SiO ₂ catalyst with different Al ₂ O ₃ to SiO ₂ ratios (the yields were calculated based on the weight of feedstock).	126
Table 4-3 Product yield and gas concentrations from the pyrolysis-catalysis of tyres at different temperatures (700, 800 and 900 °C) with no water and tyre:catalyst ratio is 1:0.5.	133
Table 4-4 Product yield and gas concentrations from the pyrolysis-catalysis of tyre at different tyre:catalyst ratios (1:0.5; 1:1; 1:2) with no water and 900°C	139
Table 4-5 Product yield and gas concentrations from the pyrolysis-catalytic reforming of tyres at different water injection rates (0,2 and 5 ml/h) at 800°C and tyre:catalyst ratio 1:0.5 (Reacted water was calculated based on the assumption that the oxygen source was only from injected water).	146
Table 4-6 Product yields and gas concentrations from the pyrolysis-steam reforming of waste tyres with a 20 wt. % Ni/Al ₂ O ₃ /SiO ₂ catalyst with an Al ₂ O ₃ :SiO ₂ ratio of 1:1 (Reacted water was calculated based on the assumption that the oxygen source was only from injected water).	153
Table 5-1 Product yield and gas concentrations from the pyrolysis-catalysis of truck tyre, car tyre, poly-butadiene rubber (BR), styrene-butadiene rubber (SBR) and natural rubber (NR).	170
Table 5-2 Carbon formation from the pyrolysis-catalysis of tyre pyrolysis oil model compounds	180
Table 5-3 Gas concentrations and weights from pyrolysis catalysis of tyre oil model compounds	193
Table 6-1 Mass balance and gas concentrations for the pyrolysis-catalysis of high density polyethylene (HDPE) in relation to catalyst temperature and different plastic to catalyst ratio.	201

Table 6-2 BET surface area, pore volume and average pore radius of Fe/Ni/MCM-41 catalysts with different Fe:Ni ratios (00:20, 05:15, 10:10, 15:05, 20:00).....	215
Table 6-3 Product yields and gas concentrations from pyrolysis-catalytic reforming of simulated mixed waste plastics (SMWP) with Fe/Ni/MCM-41 catalysts with different Fe:Ni ratios (00:20, 05:15, 10:10, 15:05, 20:00).....	218
Table 6-4 Product yields and gas concentrations from the pyrolysis-catalytic reforming of different waste plastics(Feedstock to catalysts ratio at 4:1, reforming temperature at 800 °C, heating rate at 50 °C min ⁻¹ , water injection rate 2 g h ⁻¹ and Fe-Ni/MCM-41 catalysts with Fe to Ni ratio at 10:10).....	229

Abbreviations

PE- polyethylene

PET-polyethylene terephthalate

PP – polypropylene

PS - polystyrene

HDPE – high-density polyethylene

LDPE – low-density polyethylene

CNTs - carbon nanotubes

MWCNTs- multi-walled carbon nanotubes

SWCNTs – single-walled carbon nanotubes

CNFs- carbon nanofibers

CVD- chemical vapour deposition

TGA- Thermal gravimetric analyser

DTG-TPO-derivative thermal gravity - temperature programmed oxidization

TPR- temperature programmed reduction

FTIR- Fourier Transform Infrared Spectroscopy

PC/PCG- pyrolysis catalysis/pyrolysis catalytic-gasification

PCF- pyrolysis catalytic-reforming

XRD- X-Ray diffraction

BET- Brunauer, Emmett and Teller

GC- gas Chromatography

SEM- scanning electron microscopy

TEM- transmission electron microscopy

EDX- energy dispersive X-ray analysis

FID - flamed ionized detector

TCD – thermal conductivity detector

Chapter 1. Introduction

1.1 Waste hydrocarbons

1.2 Waste tyres production and management

A large amount of used tyres are generated around the world each year. For example, in 2011, there were around 3.27 million tonnes of used tyre arising in the European Union [7]. In the US, the used tyre production was around 3.87 million tonnes in the same year [8]. In 2012, around 1.01 million tonnes of scrap tyre was generated which represented a 15 thousand tonnes increment compared with the previous year in Japan [9].

The significant growth of end-of-life tyres generated in the EU since 2004 is shown in Figure 1-1, which attained 2.64 million tonnes in 2011 from 2.48 million tonnes in 2004. Following with continuous increments in 2012 and 2013 representing 2.76 and 2.88 million tonnes per year respectively. The automotive retail economies are still growing throughout Europe accompanied with growth of the transport sector, therefore the increasing trend of end-of-life tyres generated in EU is still expected to show an upward trend [10].

Waste tyres are considered as one of the most difficult waste materials to degrade. This is illustrated by the chemical and biological resistance of waste tyres to degradation resulting in extremely long time periods of survival of tyres in waste landfill sites. Also, landfilling of waste tyres represents a waste of resource. Therefore, most of the developed countries have banned the landfilling of waste tyres. In the EU, the Waste Landfill Directive banned whole used tyres going to landfill in 2003 and shredded used tyres were banned going to landfill since 2006 [11]. In the US, there are 38 states which ban whole used tyres deposited in landfill and 11 states ban all kinds of used tyres to landfill [12].

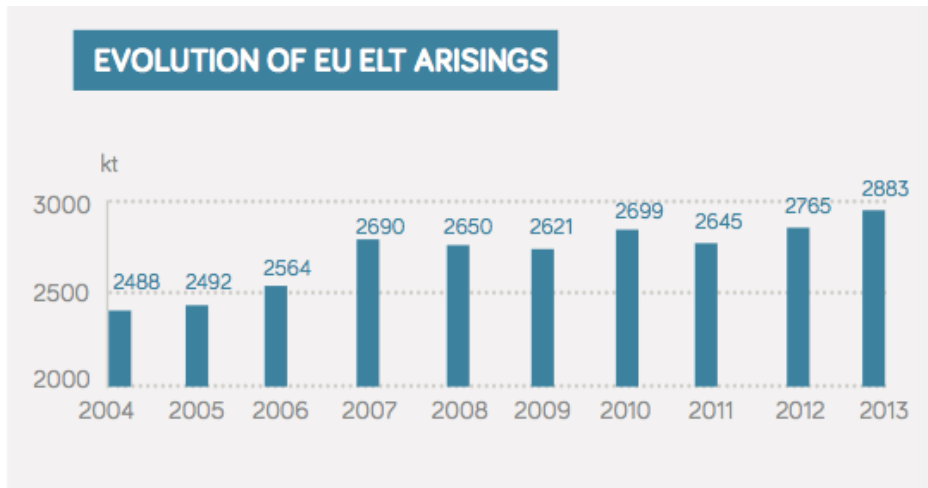


Figure 1-1 Evolution of EU end-of-life tyres (ELT) arising by ETRMA [10]

With the demand for automobiles growing globally each year, the environmental issues caused by waste tyre disposal have become more serious [11]. Waste tyres are a mixture of elastomers (e.g. natural rubber, butadiene and styrene-butadiene rubbers), carbon black filler/strengthener, metal reinforcements, zinc, sulphur and other additives [11]. The approaches to manage the waste tyre issue include energy recovery, recycling and reuse.

1.3 Waste plastics production and management

The large quantity of plastics consumption around the world causes enormous amounts of waste plastics to be produced. In 2012, 65.41 million tonnes of polyethylene (PE), 52.75 million tonnes of polypropylene (PP), 19.8 million tonnes of polyethylene terephthalate (PET) and 10.55 million tonnes of polystyrene (PS) were produced in the world [13]. There is approximately 19.9 million tonnes of waste plastics generated every year in Europe. One of the main waste plastics generated in the EU is polyethylene which includes high density polyethylene (HDPE) and low density polyethylene (LDPE) [14]. The Resin Identification Coding for classifying plastics produced from different resins has been introduced by the plastics industry in 1988. The code 1 is for PET, code 2 is for HDPE, code 3 is for PVC, code 4 is for LDPE, code 5 is for PP, code 6 is for PS, and code 7 is for other types of resins such as acrylic, styrene, fiberglass or mixtures [15].

The annual average of post-consumer plastics waste generation from 2006 to 2012 is 25 Mtonne.

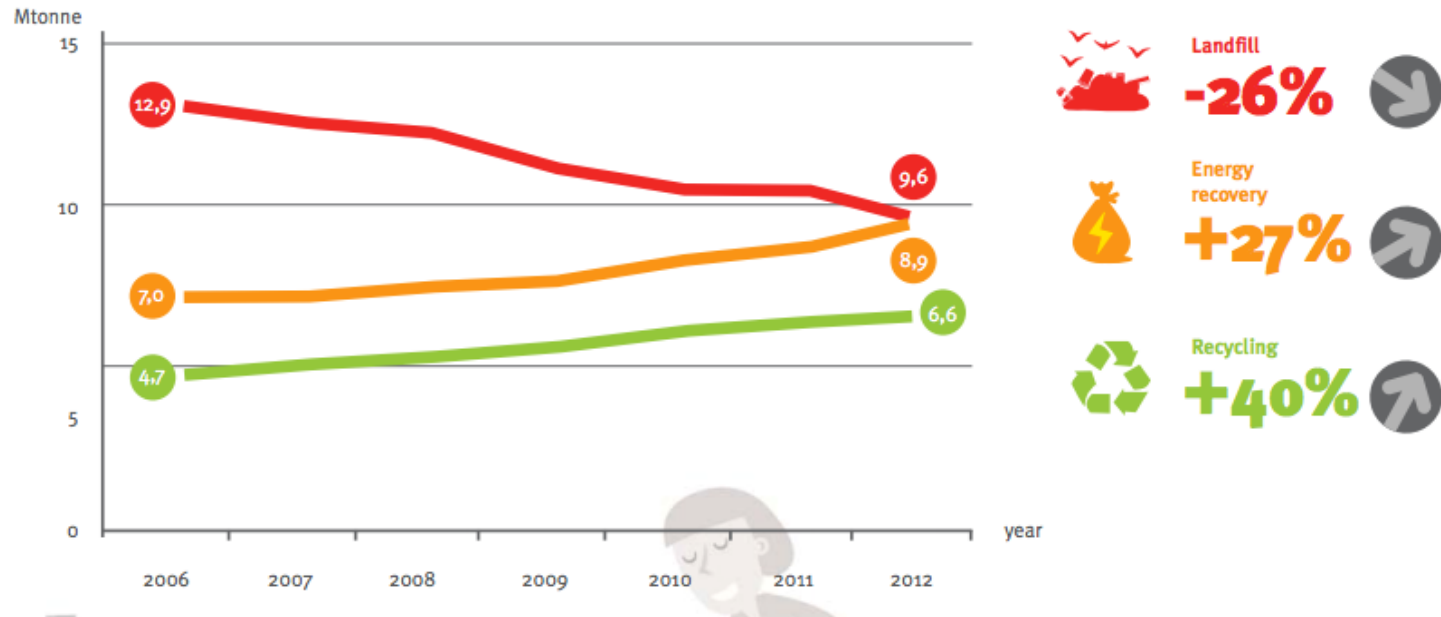


Figure 1-2 The proportions of plastics management between 2006 to 2012 in EU[16].

In general, countries with landfill ban achieve higher recycling rates

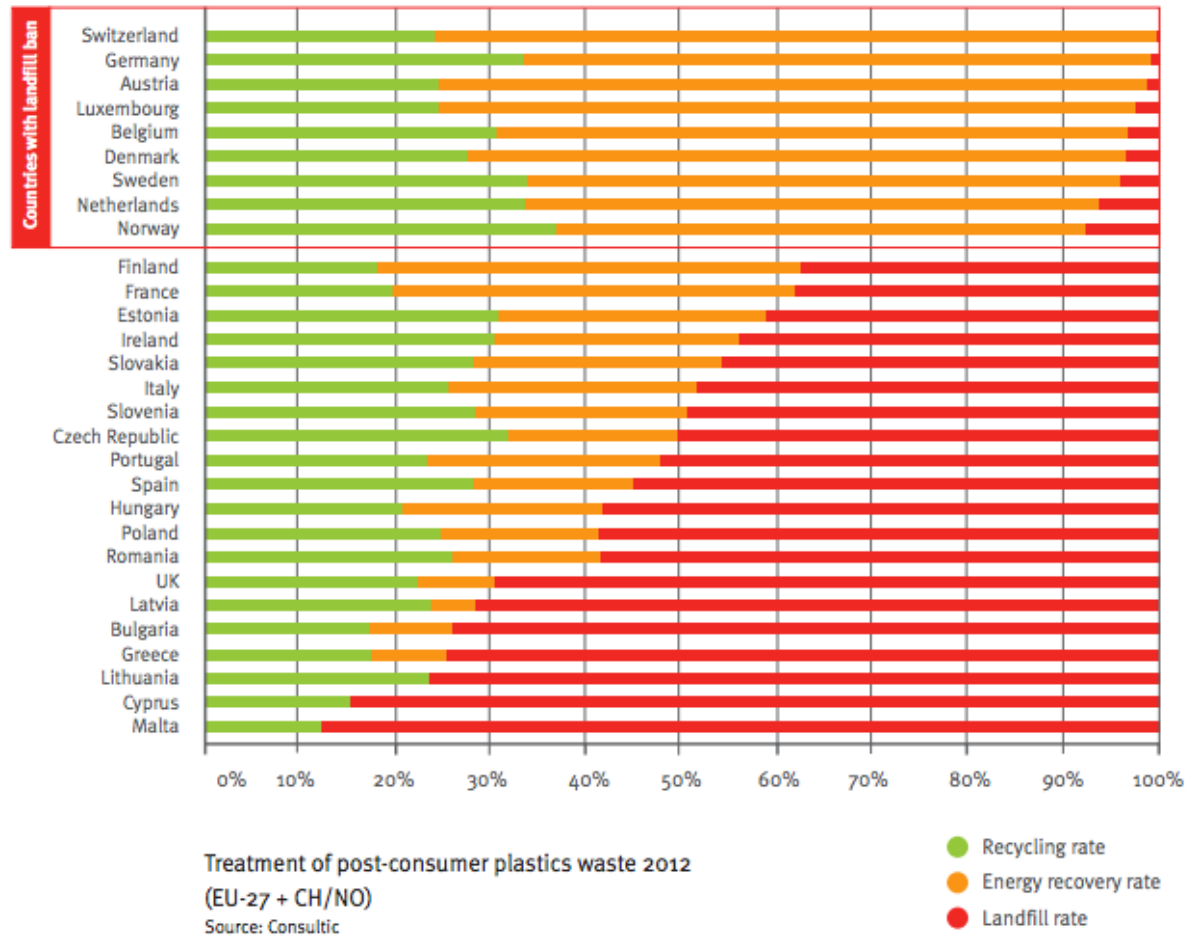


Figure 1-3 Treatments of post-consumer plastics across the EU in 2012 [16].

Figure 1-2 shows the proportions of waste plastics that have been managed through landfill, energy recovery and recycling options between 2006 to 2012 in the EU. The landfill of waste plastics has generally reduced by 26 % since 2006, but landfilling is commonly still the first option as the disposal route for waste plastics in Europe as it is the most cheapest and easiest method. In 2012, 25.2 million tonnes of post-consumer plastics waste was produced in the EU and ended up in the waste stream. Some of the European countries with landfill bans have achieved high waste plastics recovery rates compared with countries without landfill bans as shown in Figure 1-3, such as Switzerland, Germany, Austria, Luxembourg, Belgium, Denmark, Sweden, Netherlands and Norway [16].

1.4 Hydrogen and carbon nanotubes

1.4.1 Hydrogen

Hydrogen is considered as a clean energy fuel that has potential to reduce the world consumption of fossil fuels to meet sustainability development. Currently, the methods to produce hydrogen energy are highly costly. There is around 5×10^{11} N m³ of hydrogen production in the world, and around 96% of hydrogen is produced from fossil fuels. The principal production routes are methane reforming (48%), oil/naphtha reforming (30%), coal gasification (18%) and electrolysis (3.9%) [17]. The costs and energy sources are issues for hydrogen economy development [18].

There are more and more researchers interested in investigating new feedstock to produce hydrogen. The use of waste hydrocarbons can be a potential significant source because it can help solve waste disposal issues and maximise the value of wastes by producing hydrogen and value added products such as carbon nanotubes.

The hydrogen utility economy based on the emerging energy sourcing issues, for examples: fossil fuel usage, climate change, local regulations and sustainable energy generation. The applications for hydrogen as a renewable energy include: fuel cell engines, turbines, internal combustion engines, etc., as Figure 1-4 shows.

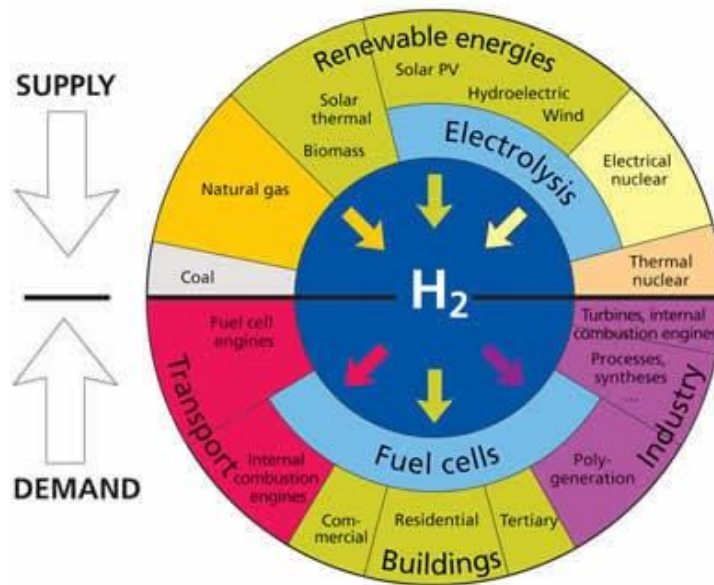


Figure 1-4 The supply and demand of hydrogen [19].

1.4.2 Carbon nanotubes

Since the discovery of carbon nanotubes (CNTs) in the early 1990's, CNTs have been applied in science and engineering which has attracted many researchers' interest because of their unique physical and chemical properties [20, 21]. Bulk CNTs have been used for rechargeable batteries, automotive parts and it also be used in sporting goods and boat hulls [22, 23]. The initial applications of CNTs on super-capacitors, actuators and lightweight electromagnetic shields have already achieved commercial acceptability. CNTs can be used as multifunctional coating materials, for example: multi-walled carbon nanotubes (MWCNTs) can be added into paint which can discourage algae and barnacles attached on the boat hulls and therefore reduce bio-fouling [22, 24]. MWCNTs have been used widely in lithium ion batteries by blending MWCNTs with active materials and polymer binder [22, 25, 26]. MWCNTs can increase electrical connectivity and mechanical integrity therefore the rate capacity and life cycle of batteries can be enhanced [22, 27, 28]. Considering the low electron scattering and band gap of the high quality of single walled carbon nanotubes (SWCNTs), they have been used in transistors. CNTs also

have been used in biosensors and medical devices because their chemical and dimensional compatibility with biomolecules [22, 29].

However, the commercial applications of CNTs have still not reached to their full potential, and there is still room for the development of CNT production from wastes as a complementary process for large-scale CNT production. The current existing methods for CNT production are energy and resource intensive, include but are not limited to the electric arc-discharge method, laser ablation method, catalytic chemical vapour deposition (CVD), flame synthesis and solar energy route [30]. Among these methods, CVD is currently the most promising and preferred method for large-scale production. The typical reactor used for CVD is a fluidized bed reactor which improves the gas diffusion and heat transfer to catalysts nanoparticles [30]. The low-cost feedstock, efficiency improvement, energy consumption reduction and waste reduction are the main factors that affect the scale-up of CNTs produced by CVD [31]. There is a successful example of scaled up Camphor CVD for MWCNT production that has been commercialized in Japan (Meijo Nano carbon Co. Ltd.) [32]. It has been reported that due to the relatively low price of camphor, the cost for producing CNTs has been reduced to a low level of around \$100 kg⁻¹ that is the lowest commercial price reported for purified CNTs [33].

Nevertheless, researchers are still looking for more efficient and cost-effective ways for large-scale production of CNTs which has been defined as the production of 10 thousand tonnes of CNTs per year. Hence, in recent years, there have been efforts regarding possible alternative routes for producing CNTs or investigating alternative feedstock [33].

1.4.3 Tyres and plastics as potential feedstock for hydrogen and CNTs

The typical tyre has a high carbon content at ~ 81.2 wt.% and at hydrogen ~7.2 wt.% [34]. The recovery of valuable products from tyres has been studied by many researchers [12, 34-36]. Pyrolysis as a thermal degradation process to recover more valuable products from waste tyres has been investigated [35, 36]. It is also known that waste plastic has a high content of hydrogen. Many researchers have studied the thermo-chemical decomposition of plastics and

proposed the possibility of producing hydrogen [37-40]. It is suggested that the availability of large quantities of waste plastic could produce a significant amount of hydrogen.

Pyrolysis/gasification of waste tyres or plastics are thermal chemical treatments which have become more desirable for energy recovery of waste plastics or tyres to prevent the waste going to landfill [41, 42]. Pyrolysis is a thermal process that breaks down the waste hydrocarbon into smaller molecules in a oxygen lean environment. The products from the pyrolysis of solid carbonaceous materials are gas, oil and char. The pyrolysis gases can be used as fuel gas due to the high content of H₂ and C₁-C₄ hydrocarbons; the oil products can be used as fuel directly or by mixing with petroleum or upgrading with catalyst or as chemical feedstock; The solid char is mainly carbon black which can be used as a solid fuel or upgraded to activated carbon [35]. The carbonaceous adsorbents produced from waste tyre can be used for wastewater treatment by adsorbing toxic metals and organic pollutants. This can be a very effective solution to solve environmental pollution caused by waste tyre disposal [11, 12].

For thermal-chemical conversion of waste plastic to produce hydrogen, a catalyst plays a key role to maximize the hydrogen production. In addition, a two-stage pyrolysis-catalysis system is more controllable than one-stage catalysis process, as it can separate the pyrolysis residues containing contaminants from the catalyst [14]. From previous studies, nickel-based catalysts are the most common catalyst used for hydrogen production from biomass or plastics by thermal processing because of their high thermal stability, and hydrogen selectivity etc. [14, 37, 40]. Many types of Ni-based catalysts have been investigated such as Ni/Al₂O₃[43], Ni-Mg-Al catalyst [14] and Ni/MgO catalyst [44].

Mohanty et al. [45] pointed out one of the main indicators for the catalyst lifetime test was catalyst deactivation which resulted from coke deposition in steam gasification of waste polyethylene. Wu and Williams [46] investigated the coke formation on the surface of a Ni-Mg-Al catalyst in plastics pyrolysis-catalysis process. Both the formation of amorphous and filamentous carbons were

confirmed, and the deposited filamentous carbons included carbon nanotubes (CNTs). As the carbon deposition deactivates the catalyst and reduces the efficiency of thermo-chemical conversion of plastic, enhances the production of CNTs as well as reducing the production of amorphous carbon will add significant values to the process of hydrogen production from plastics, thus, effectively increase the economic feasibility of hydrogen production from plastics by pyrolysis-catalysis.

1.5 Aim and objectives

The promising thermal chemical treatment of waste hydrocarbons include of waste tyres and plastics are more desirable, compared to the traditional treatments, and this could ease the environmental issues caused by landfilling or incineration. Also, the waste plastics and tyres can be the alternative feedstock for hydrogen and carbon nanotube productions due to the much lower costs of feedstock. So, this project aims to investigate the hydrogen and carbon nanotube productions from the pyrolysis-catalysis of wastes including of waste tyres and plastics.

The objectives have been listed below:

- The transition metals are commonly used as catalysts for hydrogen production from waste hydrocarbons by pyrolysis-catalysis, so Co/Al₂O₃, Ni/Al₂O₃, Fe/Al₂O₃ and Cu/Al₂O₃ have been chosen to investigate the influences of different metal catalysts effects on hydrogen and carbon nanotube production from the waste tyre pyrolysis-catalysis process;
- Catalyst supports are normally used to increase the catalysts stability and therefore improve the catalyst activity. Silica and alumina are the most common catalyst supports because their high thermal stability. So, the effects of SiO₂ to Al₂O₃ ratios of nickel-based catalysts have been introduced to the waste tyre pyrolysis-catalysis process to investigate the effects on hydrogen and carbon nanotube (CNT) production;

- Process condition investigations (temperatures, sample to catalyst ratios and water injection rates) for hydrogen and carbon nanotube (CNT) production by pyrolysis-catalysis/catalytic-reforming of waste tyres have been investigated;
- A more in-depth study on the mechanism of hydrogen and carbon nanotubes formation in the waste tyres pyrolysis-catalysis process has also been investigated to determine how the main components of waste tyre would influence the yields of carbon nanotubes coupled with a relatively high hydrogen yield;
- The synergistic effect of bimetallic catalysts has been reported to improve the metal dispersion of catalysts which consequently improves catalytic activity. Therefore, different Fe and Ni ratios of mesoporous material (MCM-41) supported catalysts have been investigated to find out how the synergy of bimetallic catalyst plays a role in hydrogen and carbon nanotubes production by pyrolysis catalytic-reforming of simulated mixed waste plastics;
- Carbon nanotubes separation from the catalyst is one of the issues which need to be considered. Therefore, a novel stainless steel mesh supported nickel-based catalyst has been applied to investigate hydrogen and carbon nanotubes formation by pyrolysis-catalysis of waste plastic in the form of high density polyethylene (HDPE);
- Real world waste plastics normally contain different compositions and contaminants. To consider the possibility of the project to be commercialized, seven different real world waste plastics have been investigated for hydrogen production by pyrolysis catalytic-reforming.

References

1. Zhang, Y., et al., *Pyrolysis–Catalytic Reforming/Gasification of Waste Tires for Production of Carbon Nanotubes and Hydrogen*. Energy & Fuels, 2015. **29**(5): p. 3328-3334.
2. Zhang, Y., et al., *Carbon nanotubes and hydrogen production from the pyrolysis catalysis or catalytic-steam reforming of waste tyres*. Journal of Analytical and Applied Pyrolysis, 2016. **122**: p. 490-501.
3. Zhang, Y., et al., *High-value resource recovery products from waste tyres*. Proceedings of the Institution of Civil Engineers - Waste and Resource Management, 2016. **169**(3): p. 137-145.
4. Zhang, Y., et al., *Pyrolysis-catalysis of waste plastic using a nickel-stainless steel mesh catalyst for high value carbon products*. Environmental Technology, 2017: p. 1-27.
5. Zhang, Y. et al., *Influence of catalyst support material on H₂ production and catalyst coking for the pyrolysis-catalysis of waste tyres*. Waste management & research, May 2017.
6. Zhang, Y., et al., *Fe-Ni-MCM-41 catalysts for hydrogen-rich syngas production from waste plastics by pyrolysis-catalytic steam reforming*. Energy & Fuels, 2017.
7. European Tyre & Rubber Manufactureres' Association, *ELT Management*, 2011, ETRMA, Brussles, Belgium.
8. Rubber Manufacturers Association, *2011 U.S.Scrap Tire Market Summary*, 2001, Washington D.C., US.
9. Masaaki, H.N., *Tyre Industry of Japan 2013*, 2013, JATMA.
10. ETRMA, *End of life tyres 2015*, 2015, European Tyres & Rubbers Manufacturers' Association, Brussles, Belgium.
11. Saleh, T.A., et al., *Processing methods, characteristics and adsorption behavior of tire derived carbons: A review*. Advances in Colloid and Interface Science, 2014. **211**: p. 93-101.
12. Alexandre-Franco, M., et al., *Adsorption of cadmium on carbonaceous adsorbents developed from used tire rubber*. Journal of Environmental Management, 2011. **92**(9): p. 2193-2200.
13. Wang, C.-q., et al., *Flotation separation of waste plastics for recycling—A review*. Waste Management, 2015. **41**: p. 28-38.
14. Wu, C., et al., *Pyrolysis–gasification of plastics, mixed plastics and real-world plastic waste with and without Ni–Mg–Al catalyst*. Fuel, 2010. **89**(10): p. 3022-3032.

15. Kutz, M., *Applied plastics engineering handbook: processing and materials* 2011, William Andrew. p. 177-192.
16. Europe, Plastic. "Plastics- The facts 2014/2015." *The unknown life of plastics*, www.plasticeuropemarketresearchgroup (2015).
17. Ewan, B.C.R., et al., *A figure of merit assessment of the routes to hydrogen*. International Journal of Hydrogen Energy, 2005. **30**(8): p. 809-819.
18. Authayanun, S., et al., *Thermodynamic study of hydrogen production from crude glycerol autothermal reforming for fuel cell applications*. International Journal of Hydrogen Energy, 2010. **35**(13): p. 6617-6623.
19. Dijon, J., et al., *How to switch from a tip to base growth mechanism in carbon nanotube growth by catalytic chemical vapour deposition*. Carbon, 2010. **48**(13): p. 3953-3963.
20. Iijima, S., *Helical microtubules of graphitic carbon*. nature, 1991. **354**(6348): p. 56-58.
21. Monthieux, M., et al., *Who should be given the credit for the discovery of carbon nanotubes?* Carbon, 2006. **44**(9): p. 1621-1623.
22. Michael F. L., D.V., *Carbon Nanotubes: Present and Future Commercial Applications*. Science, 2013(339).
23. Peng, B., et al., *Measurements of near-ultimate strength for multiwalled carbon nanotubes and irradiation-induced crosslinking improvements*. Nat Nano, 2008. **3**(10): p. 626-631.
24. Beigbeder, A., et al., *Preparation and characterisation of silicone-based coatings filled with carbon nanotubes and natural sepiolite and their application as marine fouling-release coatings*. Biofouling, 2008. **24**(4): p. 291-302.
25. Dai, L., et al., *Carbon Nanomaterials for Advanced Energy Conversion and Storage*. Small, 2012. **8**(8): p. 1130-1166.
26. Köhler, A.R., et al., *Studying the potential release of carbon nanotubes throughout the application life cycle*. Journal of Cleaner Production, 2008. **16**(8–9): p. 927-937.
27. Evanoff, K., et al., *Towards Ultrathick Battery Electrodes: Aligned Carbon Nanotube – Enabled Architecture*. Advanced materials, 2012. **24**(4): p. 533-537.
28. Sotowa, C., et al., *The Reinforcing Effect of Combined Carbon Nanotubes and Acetylene Blacks on the Positive Electrode of Lithium-Ion Batteries*. ChemSusChem, 2008. **1**(11): p. 911-915.
29. Heller D., et al., *Single-Walled Carbon Nanotube Spectroscopy in Live Cells: Towards Long-Term Labels and Optical Sensors*. Advanced materials, 2005. **17**(23).

30. Endo, M., et al. *Large-scale production of carbon nanotubes and their applications*. Pure and Applied Chemistry, 2006. **78**(9): p. 1703-1713.
31. Zhang, Q., et al., *Carbon nanotube mass production: principles and processes*. ChemSusChem, 2011. **4**(7): p. 864-889.
32. Kumar, M., et al., *Chemical vapor deposition of carbon nanotubes: a review on growth mechanism and mass production*. Journal of Nanoscience and Nanotechnology, 2010. **10**(6): p. 3739-3758.
33. De Volder, M.F., et al., *Carbon nanotubes: present and future commercial applications*. Science, 2013. **339**(6119): p. 535-539.
34. Zhang, Y., et al., *High-value resource recovery products from waste tyres*. Proceedings of the Institution of Civil Engineers - Waste and Resource Management, 2016. **0**(0): p. 1-9.
35. Williams, P.T., *Pyrolysis of waste tyres: A review*. Waste Management, 2013. **33**(8): p. 1714-1728.
36. Sienkiewicz, M., et al., *Progress in used tyres management in the European Union: A review*. Waste Management, 2012. **32**(10): p. 1742-1751.
37. Wu, C., et al., *Hydrogen production by steam gasification of polypropylene with various nickel catalysts*. Applied Catalysis B: Environmental, 2009. **87**(3): p. 152-161.
38. Czernik, S., et al., *Production of hydrogen from plastics by pyrolysis and catalytic steam reform*. Energy & Fuels, 2006. **20**(2): p. 754-758.
39. Williams, P.T., *Waste incineration*. Waste Treatment and Disposal, Second Edition, 2005: John Wiley & Son, p. 245-323.
40. Wu, C., et al., *Investigation of Ni-Al, Ni-Mg-Al and Ni-Cu-Al catalyst for hydrogen production from pyrolysis-gasification of polypropylene*. Applied Catalysis B: Environmental, 2009. **90**(1-2): p. 147-156.
41. Williams, P.T. "Pyrolysis of waste tyres: a review." *Waste Management*33.8 (2013): 1714-1728.
42. Acomb, J.C., et al. *The use of different metal catalysts for the simultaneous production of carbon nanotubes and hydrogen from pyrolysis of plastic feedstocks*. Applied Catalysis B: Environmental, 2016. **180**: p. 497-510.
43. Srinakruang, J., et al., *A highly efficient catalyst for tar gasification with steam*. Catalysis Communications, 2005. **6**(6): p. 437-440.
44. Minowa, T., et al., *Cellulose decomposition in hot-compressed water with alkali or nickel catalyst*. The Journal of Supercritical Fluids, 1998. **13**(1-3): p. 253-259.

45. Mohanty, P., et al., *Hydrogen production from steam reforming of acetic acid over Cu-Zn supported calcium aluminate*. *Bioresource Technology*, 2012. **123**: p. 558-565.

46. Wu, C., et al., *Investigation of coke formation on Ni-Mg-Al catalyst for hydrogen production from the catalytic steam pyrolysis-gasification of polypropylene*. *Applied Catalysis B: Environmental*, 2010. **96**(1-2): p. 198-207.

Chapter 2. Literature review

2.1 Hydrogen production from waste sources

Around 96% of the global production of hydrogen is from fossil fuels. Hydrogen is mainly produced through methane reforming (48%), oil/naphtha reforming (30%), coal gasification (18%) and electrolysis (3.9%) [1]. Costs and alternative material sources are key challenges for the development of a sustainable hydrogen economy. Therefore, using alternative sources to generate hydrogen is imperative.

2.1.1 Waste tyres

A typical tyre has a high carbon content of ~ 81.2 wt.% and a hydrogen content of ~7.2 wt.% [2]. The recovery of valuable products from tyres has been studied by many researchers, including production of hydrogen, aromatic compounds, activated carbons, and others [2-5]. Pyrolysis as a thermal degradation process for recovering more valuable products from waste tyres has been investigated as a process option [3, 5]. Typical pyrolysis temperatures are around 500°C, to which the waste tyres are heated in inert atmospheres to produce tyre degradation products, including gases, solid chars and oils. The gaseous products contain hydrogen and C₁-C₄ hydrocarbons (methane, ethene, ethane, propene, propane, butene, butane, and butadiene), and have a high calorific value of up to 65 MJm⁻³, depending on process conditions [3]. The solid char contains carbon black fillers that could be used as solid fuels or upgraded to activated carbons, which have been widely used for purification and separation in many fields [6]. Oils from pyrolysis of waste tyres are complex liquids with the texture of oil/wax, dark brown or black colours and sulphurous odours. They consist of over 100 identified compounds with chemical structures between C₅-C₆₀. By fractionation these oils have been shown to contain aliphatic hydrocarbons (including decane, undecane, dodecane, tridecane, tetradecane and others), aromatic hydrocarbons (including toluene, ethylbenzene, xylene,

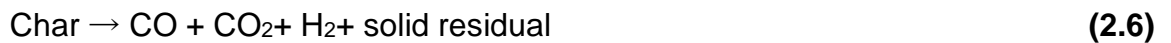
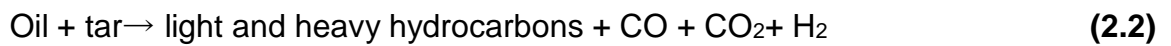
propylbenzene, ethylbenzene, naphthalene, phenanthrene, and pyrene), heteroatoms and polar fractions [7].

Different compositions of tyre pyrolysis oils have been reported by different researchers by using different reactors. This could be caused by the various reaction conditions, such as residence time of the reacting feedstock and temperatures. Using a circulating fluidized-bed reactor at 500°C, Dai et al. [8] obtained a tyre pyrolysis oil which contained 26.77 wt.% of alkanes, 42.09 wt.% aromatics, 26.64 wt.% non-hydrocarbons and 4.05 wt.% asphalt. Conesa et al. [9] reported that a pyrolysis oil produced with a fluidized-bed reactor at 700°C consisted of 39.5 wt.% aliphatic fraction, 19.1 wt.% aromatic fraction, 21.3 wt.% hetero-atom fraction and 20.1 wt.% polar fraction. Aylon et al. [10] produced a tyre pyrolysis oil at 600°C, by using a screw kiln reactor, which contained 6.7 wt.% alkane fraction, 65.5 wt.% aromatic fraction and 27.8 wt.% polar fraction.

Pyrolysis processes are normally carried out at relatively low temperatures (around 500 to 600°C) with a higher yield of oils than gaseous products [3]. Gasification processes on the other hand are usually carried out at temperatures above 600°C, yielding more gaseous products than pyrolysis at lower temperatures [11]. During gasification of waste tyres, hydrogen-enriched syngas is normally the target product. Syngas can be used for power generation in internal combustion gas engines or for producing chemicals through the Fischer-Tropsch process [12-15]. Hydrogen is regarded as a clean energy carrier for a projected future hydrogen economy, as it can be produced from many sources, its combustion only generates water and it has broad applications such as use in fuel cells [16].

Tyres are composed of a mixture of rubber polymeric materials made of single or double-bonded carbon atoms, where the rubbers are characterised by carbon-carbon double bonds [17]. The thermal decomposition of tyre rubber produces sub-units of the tyre rubber's molecular structure which are highly reactive free radicals [18]. The mechanism of tyre decomposition can be explained by the following reactions 2.1-2.6 [19]:





In-depth studies of the mechanisms of tyre decomposition have also been carried out by various researchers. Groves et al. [20] explained that the mechanism for dimer formation in rubber pyrolysis processes is possibly because of monomer recombination by the Diels-Alder reaction; an organic chemical reaction between a conjugated diene and a substituted alkene called dienophile to form a cyclohexene system. This mechanism was firstly defined by Otto Diels and Kurt Alder in 1928 [21]. Mastral et al. [22] explained the decomposition of tyres through polyisoprene depolymerisation and cyclisation, and Pakdel et al. [23] further explained the thermal decomposition of polyisoprene of rubber to isoprene intermediate radicals by a β -scission mechanism, and then these isoprene intermediate radicals can be transformed to isoprene which, in the gas phase, can be dimerised to dipentene. Kwon et al. [24] described a mechanism for the thermal decomposition of waste tyres which occurs through bond scission of monomers (the main constituent of tyres) corresponding with more reactions in the gas phase, including hydrogenation and recombination.

2.1.2 Waste plastics

It is well-known that waste plastics have high contents of hydrogen. Many researchers have studied the thermo-chemical decomposition of plastics and proposed the possibility of producing hydrogen [25-28]. It is often suggested that the large quantities of waste plastics available can be used to produce significant amounts of hydrogen. For example, approximately 25.1 million tonnes of waste plastics were generated in Europe in 2010 [29]. Polyethylene, including high density polyethylene (HDPE) and low density polyethylene (LDPE), is one of the main types of waste plastics [30].

Many researchers have focused on the thermal decomposition of plastics and their results are indicative of the viability of using plastics to produce hydrogen [25-27, 31]. Gasification of waste plastics to produce synthesis gases (H₂, CH₄ and CO) could effectively convert all of the carbon-compounds in waste plastics to valuable products [32]. The reactions can be explained as the following equations 2.7, 2.8, 2.9 and 2.10 [33]. By using waste plastics as a replacement for conventional feedstock used in hydrogen production, there is a potential to mitigate the high demands for fossil fuels [31].



In the thermo-chemical conversion of waste plastics to produce hydrogen, catalysts play a key role of maximizing hydrogen production. Also, two-stage pyrolysis-catalysis systems are more controllable than one-stage catalysis processes, because they separate the pyrolysis residues containing contaminants from catalysts [30]. From previous studies, nickel-based catalysts are the most common catalysts used for hydrogen production from biomass or plastics by thermal processing, mainly because of their high thermal stabilities, and hydrogen selectivity [25, 28, 30]. Many types of Ni-based catalysts have been investigated to find out the effects of the different Ni-based catalysts with different catalyst supports and metal promoters for hydrogen production, such as Ni/Al₂O₃[34], Ni-Mg-Al catalyst [30] and Ni/MgO catalysts [35].

2.1.3 Other alternative feedstock resource - Glycerol

Many reactions occur during the pyrolysis of glycerol, when the temperatures range between 650°C and 800°C (as shown in the reactions in Figure 2-1). Products formed from pyrolysis of glycerol include gases, liquids and chars. Gas components include H₂, CO, CO₂, CH₄, C₂H₂; the liquid components include methanol, ethanol, acetone, acetaldehyde, acrolein, acetic acid and water. Reactions 1-3, as shown in Figure 2-1, occur concurrently; the liquid, gas and char are produced by dehydration reactions when the temperatures are

relatively low; when temperatures are relatively high, H₂, CO and char are produced as the main products by consecutive thermal cracking reactions shows as reactions 4 to 6 in Figure 2-1 [36]. Valliyappan et al. [36] surmised that the total char production from pyrolysis of glycerol is below 10 wt. %, which means the process is feasible and effective.

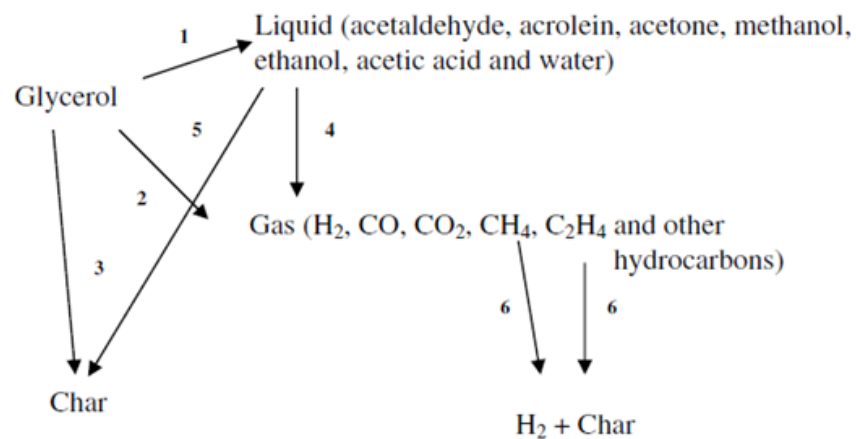


Figure 2-1 The reaction pathways of pyrolysis of glycerol[36].

The chemical equation for conversion of glycerol to CO and H₂ is shown in equation 2.11 CO and H₂ are the main gaseous products from pyrolysis of glycerol. There are also small contents of other gases such as CO₂, CH₄, C₂H₄, C₂H₅ and C₃H₆. There are also simultaneous reactions happening during the pyrolysis of glycerol, as shown in equation 2.12 [36]. Subsequent reactions, such as water-gas shift and methanation reactions, are shown as equation 2.13 and equation 2.14 [37].

Decomposition of glycerol:



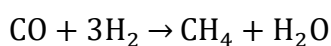
Simultaneous reactions:



Water-gas shift reaction:



Methanation reaction:



(2.14)

Glycerol can be a potential feedstock for producing H₂, with a theoretical production ratio of glycerol/hydrogen of 1:4. [38, 39]. Comparing all the processes of glycerol production, recovery of hydrogen from the glycerol reforming process is the most effective way to improve the utilization of glycerol [40-42].

The aqueous phase reforming of glycerol offers several different advantages, including low energy consumption (because aqueous phase reforming can occur at relatively lower temperatures compared with conventional gas phase reforming) and it is compatible with other wet feedstocks, so it is unnecessary to do pre-drying [43]. Also, aqueous phase reforming of glycerol results in less catalyst deactivation and lower levels of CO concentrations [41, 43, 44]. The classic gas phase reforming uses a conventional reaction system with reactions at safe atmospheric pressures, and production of H₂ with high selectivity [9].

There are different methods for catalytic reforming of glycerol, such as steam reforming, partial oxidation (also called oxidative reforming), auto-thermal and supercritical water gasification, dry reforming (or CO₂ reforming), dry auto-thermal (a combination of dry, oxidative and steam reforming) and pyrolysis [45]. Avasthi et al. [46] surmised that hydrogen production from glycerol can be a very good option because of the amount of hydrogen produced from glycerol reforming processes is stoichiometrically more than the conventional methods.

At high temperatures, gasification of glycerol can produce H₂ and carbon monoxide (CO) of which the gaseous mixture is syngas. Fischer-Tropsch synthesis is a way to produce green biodiesel using syngas as feedstock, at a H₂/CO ratio of 2:1 [38, 47]. The gases produced from glycerol can be used to produce electricity because of their medium heating value [38, 48]. Valliyappan et al. [49] produced syngas by pyrolysis of glycerol, in experiments carried out at atmospheric pressure and controlled by changing the nitrogen flow rate, temperatures and types or sizes of the packing material in the reactor. Simonetti et al. [50] focused on syngas production from glycerol by gas phase reactions. They used carbon supported platinum (Pt) and platinum-rhenium (Pt-Re) catalysts in the experiments, and measured rates of glycerol conversion to

H₂/CO ratio by controlling the reaction conditions kinetically. They found that Re (Rhenium) promotes glycerol conversion at conditions and leads to higher CO pressures. The interaction of CO with the surface is decreased by the primary promotional effect of Re. Therefore, the coverage of CO decreased and then the catalyst can operate more effectively when the gaseous CO is present. Peres et al. [51] found that the optimized output of converting glycerol to gas in their pyrolysis of glycerol (they used commercial glycerol with a purity of 99% in experiments) reached up to 80%wt. The best hydrogen concentration can reach up to 40% and the best CO concentration can reach up to 48%.

2.1.4 Summary of thermal treatments for waste carbonaceous material

Pyrolysis of carbonaceous materials such as waste tyres, waste plastics and crude glycerol from the biodiesel industry have potentials to become profitable liquid, gaseous and solid products, as shown in Figure 2-2 [52, 53]. Liquid products containing naphtha, tars and phenols can be applied straightaway or upgraded as fuels [54]; Gas products containing syngas (H₂+CO), methane and others can also be used as fuels[55]; and solid products are mainly chars that can be upgraded to activated carbons[56].

As gasification is different from pyrolysis, it requires gasifying agents such as water, air or carbon dioxide to enhance the gaseous products and consequently results in lower production of oils. The gaseous products are mainly H₂, CO, CO₂, CH₄ and H₂O [52].

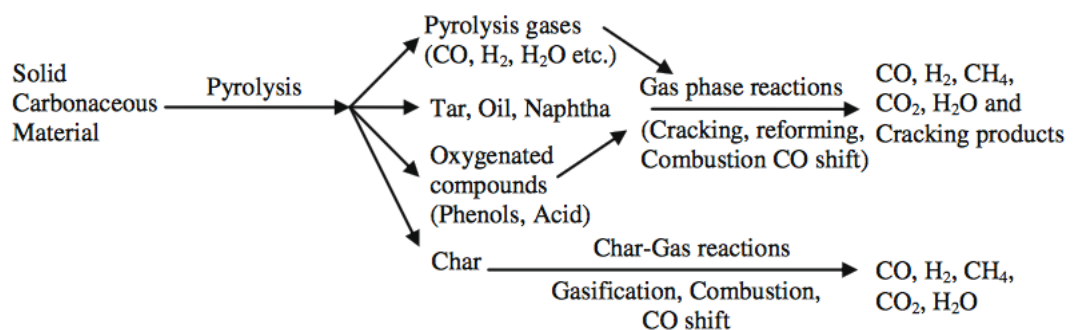


Figure 2-2 Products from pyrolysis and gasification of carbonaceous materials [52].

2.2 Process conditions for thermal treatments of wastes

Pyrolysis of waste tyres can be influenced by process conditions, for example the type of raw material, sample sizes, residence times, temperatures and tyre feeding rates. Characteristics of waste tyre pyrolysis have been studied by many researchers [9, 13, 41, 57-59]. Dai et al. [8] investigated pyrolysis temperatures, residence times and particle sizes of samples by using a circulating fluidized-bed reactor in which pyrolysis and secondary reactions occurred. They reported that secondary reactions are favoured by long residence times, carbonization is favoured by lower temperatures and heating rates, but not oil yield. Gas products increased as temperatures increased from 400 to 800°C. Methane, hydrogen and carbon monoxide productions increased with temperature, but carbon dioxide and heavier hydrocarbon gases decreased. As the residence time increased, the syngas (hydrogen and carbon monoxide) and light hydrocarbon productions increased, but carbon dioxide production decreased, which is because of the secondary reactions such as the further cracking of heavy pyrolysis oils, char reduction and shift reactions. Temperatures and residence times played a predominant role on higher gas production and lower tar/oil production. However, the particle sizes of samples did not affect gas production to any significant degree.

Aylon et al. [10] produced tyre pyrolysis oils by using a moving bed reactor at different temperatures (600, 700 and 800°C). Yields of pyrolysis oils decreased dramatically from 41.5 to 27.5 wt.% as temperatures increased from 600 to 800°C. However, gas production significantly increased from 17.9 to 31.5 wt.%. The reason for the higher tar cracking ratios at higher temperatures was due to the more primary cracking of heavy hydrocarbons at higher temperatures.

Cunliffe and Williams [59] investigated the influence of temperature and chemical constitutions of tyre pyrolysis oil by using a fixed bed reactor, they found a clear increase of the aromatic fraction from 36.7 to 45.6 wt.% and decrease of the aliphatic fraction from 51.3 to 36.1 wt.% as temperatures increased from 450 to 600°C. They also pointed out that the extended resident time of pyrolysis gases leading to more secondary conversion of volatile compounds in the reactor could possibly increase the aromatic fraction.

Kyari et al. [57] compared pyrolysis products from seven different types of tyres (Countries of origin: Poland, Korea, Japan, South Africa, Italy and Great Britain) with a fixed bed reactor to investigate the influence of tyre origin on the pyrolysis product yields. They found that yields of gases, chars and oil products that were not significantly affected by types of tyre. However, the compositions of the pyrolysis gas and pyrolysis oil varied between different tyres.

Leung et al. [13] studied the influences of operational parameters (equivalence ratio, tyre feed rate, temperatures and particle sizes) on hydrogen production from a waste tyre gasification process, using a tubular reactor. They concluded that gaseous yields are proportional to equivalence ratio, tyre feed rate and tyre particle size. Char yields decreased slightly when the equivalence ratio, feed rate or particle size increased. Oil yields reduced considerably with the increase of equivalence ratio and tyre feeding rate. The gaseous products were mainly H₂, CO, CO₂, H₂S and other heavier hydrocarbons (C₂-C₄), with relatively high heating values ranging between 20 to 37 MJ m⁻³.

Rodriguez et al. [58] used an unstirred stainless steel 3.5 dm³ autoclave to run tyre pyrolysis experiments at temperatures in a range of 300 to 700 °C with 100 °C intervals. They found pyrolysis temperatures significantly affected gas production in waste tyre pyrolysis process, and the highest temperature of 700 °C resulted in the highest gas yield. The calorific value of pyrolysis gases were in the range of 68 to 84 MJm⁻³, much higher than are typically found in literature (20-37 MJ m⁻³) [60-62]. Ucar et al. [41] also investigated two types of tyres' (passenger car tyre and truck tyre) effects on the pyrolysis products from a fixed bed reactor. They reported there were no significant differences in gas compositions, especially of C₁-C₄. Hydrogen production from the waste car tyre was higher than production from the waste truck tyre. The compositions of pyrolysis oil obtained from the two types of tyre were not similar; oil produced from the passenger car tyre contained more sulphur and aromatic compounds compared to the oil produced from the truck tyre, this is due to the rubber component of car tyre with more synthesis rubber but truck tyre contents more natural rubber. Solid char obtained from the truck tyre contained less ash, which is more suitable for upgrading to activated carbon.

All investigations of the effects of process conditions on waste tyre pyrolysis products indicate that product yields are significantly affected by temperature, but not limited to temperature. The types of reactors, heating rates, residence time and the specific characteristics of the system could also influence the product yields.

2.3 Catalysts development for waste thermal treatment

Catalysts are normally used to enhance hydrogen production [33, 63-65] and play an important role in gasification processes to maximize hydrogen production. Pyrolysis/catalytic-reforming of plastics is known as an effectual way to produce hydrogen by thermal decomposition. Also, two-stage pyrolysis-gasification systems are more controllable than one-stage gasification because they can effectively separate residues from solid products [30]. Several methods of catalyst synthesis have been explored, including impregnation, precipitation and sol-gel synthesis methods. The sol-gel synthesis method is still under investigation, while impregnation and precipitation have been widely used in reforming processes [66].

2.3.1 Nickel-based catalysts

Transition metals are considered good catalysts for the reforming of hydrocarbons [67]. Nickel-based catalysts are most frequently used in the production of hydrogen by thermochemical processing of plastics and biomass, primarily because of their stability at high temperatures and high selectivity for hydrogen [25, 30, 31]. The wide range of nickel-based catalysts which have been investigated have included Ni/Al₂O₃ [34], Ni-Mg-Al catalysts [30] and Ni/MgO catalysts [35].

Elbaba et al. [12, 68-70] investigated several nickel-based catalysts to improve the production of hydrogen from waste tyres. They used a two-stage pyrolysis couple with a catalytic steam reforming reactor with nickel catalysts to produce a syngas with a high content of hydrogen (65 vol.%) from waste tyres [70].

Elbaba et al. [12, 70] reported that higher nickel contents in catalysts, increased temperatures and steam inputs produced higher levels of hydrogen.

Wu et al. [71] used Ni-Mg-Al catalysts for a glycerol pyrolysis/catalytic-gasification process. They found the stability of the catalysts were still effective after six hours of testing hydrogen production or changes in the concentrations of the gases. Ni, Co and noble metals (such as Pt, Pd and Rh) can be used in the glycerol reforming process. However, noble metal catalysts will increase the costs of hydrogen production from glycerol reforming [72-75]. Ni-based catalysts are the most common catalyst used in glycerol reforming processes [75].

Adhikari et al. [76] considered that active catalysts for ethanol steam reforming could also be active in glycerol steam reforming. So they used Ni and noble metal-based catalysts in glycerol reforming experiments to produce hydrogen. There are also some other common catalysts which have been used in hydrocarbon reforming processes to obtain hydrogen, such as Al_2O_3 , $\gamma\text{-Al}_2\text{O}_3$, MgO , MgAl_2O_4 , SiO_2 , ZrO_2 , CeO_2 and TiO_2 [77]. Catalysts used in each reforming process depend on the feedstock, and the most common catalysts are nickel-based. However, the problem brought by using Ni-based catalysts is that coke formation on the surface of catalysts cannot be avoided [72, 78].

Dou et al. [79] used a commercial Ni-based catalyst and dolomite sorbent in a glycerol conversion process. CO_2 removal progressed simultaneously with hydrogen production from the glycerol conversion process. Results showed the optimum temperature for the reactions was around 500°C . The recent research they carried out on a crude glycerol conversion process showed that the maximum hydrogen production and purity could be achieved to 100% and 68% respectively at 600°C . Czernik et al. [80] investigated a glycerol steam reforming process in a fluidized-bed reactor by using a commercial Ni-based catalyst. The hydrogen production efficiency reached around 80% of the theoretical yield.

The current research indicates that when using nickel-based catalysts in the reforming process, efficiency mainly depends on the temperature of reaction which needs to be a minimum of 550°C . An impregnation method was used in

research by Buffoni et al. [78] to modify a catalyst by adding ZrO_2 and CeO_2 oxides on a commercial $\alpha-Al_2O_3$ support or on the activity and stability of Ni catalyst. The results proved that the modified Ni/Ce α catalyst could reduce the coke formation and was more stable in the reforming process. This is because the character of Ni/Ce α restrains lateral dehydration, rearrangement and condensation reactions which result in coke formation with intermediate components [78].

A precipitation method was used by Zhang et. al. [73] to prepare a M/CeO₂ (M=2% Ir, 15% Co and 15% Ni in weight) catalyst. The process for catalyst preparation started with CeO₂ being suspended in aqueous solutions which contained metal precursors ((H₂IrCl₆·6H₂O, Ni(OAc)₂·4H₂O and Co(OAc)₂·4H₂O, respectively). These solutions were then heated to 75 °C with simultaneous stirring. Subsequently, a 0.25M Na₂CO₃ aqueous solution was gradually added to make the pH value of the mixture reach 9.0. After an hour, the metal hydroxide species were deposited on the surface of ceria. Solids were filtered out, washed by hot water, and dried at 100 °C overnight. Finally, the catalyst were prepared by calcining at 400°C in the air for 4 hours. Results showed this kind of catalyst is highly active and selective for hydrogen production from glycerol reforming. The conversions of glycerol to hydrogen achieved were up to 85% at temperatures as low as 400 °C, using the Ir/CeO₂ catalyst in the glycerol reforming process [73]. To achieve the same conversion efficiency using Co/CeO₂ and Ni/CeO₂ catalysts required temperatures of 425 °C and 450 °C, respectively [72, 73].

Adhikari et al. [81] focused their research on the kinetics and reactor modelling of hydrogen production using Ni/MgO, Ni/TiO₂ and Ni/CeO₂ catalysts in a glycerol reforming process. The findings were an activation energy of 103 KJ/mol and the reaction order was 0.223. The surface area of the Ni/CeO₂ catalyst was the highest (67.0 m²g⁻¹) and therefore it gave the maximum hydrogen selectivity (74.7%) compared with the Ni/MgO and Ni/TiO₂ catalysts when the experimental conditions were the same: 600 °C, water to glycerol molar ratio of 12:1 and feed flow rate of 0.5ml min⁻¹ [81, 82].

Iriondo et al. [83] investigated hydrogen production from a glycerol reforming process by using an alumina supported nickel based catalyst modified with Mg, Zr, Ce, and La. They found that application of promoters can promote hydrogen selectivity in the glycerol reforming process. The results showed when Mg was used as a promoter in the catalyst, the high surface concentration of the catalyst comes with high hydrogen selectivity. Also, when Zr is used as a promoter in the catalyst, the capacity of activating steam can be increased. High stability of the catalyst was achieved when Ce and La were used as promoters in the catalyst. The glycerol conversion can stay at 100% over 50 h when using a Ni/Al₂O₃-ZrO₂ catalyst [72]. Iriondo et al. [72, 84] also investigated the possibility of improving the activity of an alumina supported Ni-based catalyst by adding intermediate amounts of La to the catalyst.

Alkali metals are effective at eliminating tar formation or upgrading the gas products formed in thermochemical conversion of carbonaceous materials. Hauserman [85] investigated primary alkali catalysts for hydrogen production from coal or wood gasification. Sutton et al. [86] concluded the alkali carbonate increases the carbon conversion to gases from the condensable liquid from gasification processes.

2.3.2 Noble metals-based catalysts

Soares and Simonetti et al [50, 87] found that a carbon supported platinum (Pt/C) catalyst gave the best reaction performance in a glycerol reforming process when comparing to Pt catalysts with different supports. The supported Pt catalysts consisting of Al₂O₃, ZrO₂, CeO₂/ZrO₂ and MgO/ZrO₂ deactivated the glycerol conversion reaction. On the other hand, the Pt/C catalyst had stability and selectivity for H₂/CO at the reaction temperature (around 620K). Pt/Al₂O₃ catalyst was able to activate the reaction at certain periods and then suddenly turn and deactivate the reaction. However, the high activity of Pt/C catalyst required temperatures to be lower than 300 °C. Also considering that Fischer-Tropsch synthesis of syngas from glycerol reforming to fuel requires reaction temperatures between 200-280 °C, Soares and Simonetti [87] found that a carbon supported Pt-Re catalyst could be used at this temperature. When the

Pt/Re ratio was 1:1, it gave the reaction stability, high activity and selectivity to H₂/CO at the desired temperature. They prepared the carbon supported Pt-Re catalyst by incipient wetness, impregnating aqueous solutions of H₂PtCl₆ · 6H₂O and HReO₄ with carbon black. The support needed to be dried up for 12 hours at a temperature of 373 K before impregnation. For every gram of support, 1.7g of solvent was needed. After the impregnation and drying at 403 K for 12 hours, catalyst preparation was done [50, 87]. Temperature programmed reduction (TPR) studies about Pt/C, Pt-Re/C, Re/C catalysts gave results showing Pt catalyses the reduction of Re, leading to the Pt-Re alloy formation that supported on carbon [50].

Slinnet al. [88] found that when using a Pt/Al₂O₃ catalyst in the glycerol reforming process, optimum hydrogen production could be achieved at 860°C with a flow rate of 0.12 mol glycerol/min per kg catalyst and a steam to carbon ratio (S/C) of 2.5. The optimisation of hydrogen selectivity was 70% and the glycerol conversion to gas was 100%.

Adhikari et al. [76] also performed different experiments at 900°C, while WGMR was 9:1 and FFR was 0.15ml/min by using 14 different catalysts in a glycerol steam reforming process. These included Al₂O₃, Rh/Al₂O₃, Pt/Al₂O₃, Pd/Al₂O₃, Ir/Al₂O₃, Ru/Al₂O₃, Ni/Al₂O₃, Ce/Al₂O₃, Rh/Ce/Al₂O₃, Pt/Ce/Al₂O₃, Pd/Ce/Al₂O₃, Ir/Ce/Al₂O₃, Ru/Ce/Al₂O₃, and Ni/Ce/Al₂O₃. The catalysts were prepared on 92% alumina ceramic foam monoliths which contained 8% silica (Silica from Vesuvius Hi Tech Ceramics, Champaign, IL) by the wetness technique, using nitrate and chlorate precursors. Among the 14 different catalysts, Ni/Al₂O₃ and Rh/CeO₂/Al₂O₃ performed the best H₂ selectivity and glycerol conversion. Results showed the highest hydrogen selectivity of 80% was achieved by using Ni/Al₂O₃, and H₂ selectivity reached up to 71% by using Rh/CeO₂/Al₂O₃. They also found that the increase of water/feedstock ratio leads to an increase in H₂ selectivity and glycerol conversion. However, the efficiency of H₂ production from the glycerol conversion process could reduce because of the increase of enthalpy needed for water evaporation.

Sanchez et al. [89] found that the glycerol reforming efficiency could increase from 96.8% to 99.4% when the temperature was increased from 600°C to

700°C at 1atm and 16:1 water/feedstock ratio by using a Ni/Al₂O₃ catalyst (5.8wt% Ni). The maximum glycerol conversion efficiency reached 99.7% at 650°C and started to decrease at 600°C over time. But, Chiodo et al. [90] found that a Rh/Al₂O₃ catalyst showed higher activity and stability compared to a Ni/Al₂O₃ catalyst in hydrogen production from their glycerol steam reforming process.

Profeti et al. [91] found that a Ni/CeO₂-Al₂O₃ catalyst can be promoted by noble metals (Pt, Ir, Pd, and Ru) since the dispersed CeO₂ on alumina can prevent the formation of inactive nickel aluminate. The addition of noble metals can stabilize the Ni sites in the reduced state in the reforming process, leading to a decrease in coke formation and increase in glycerol conversion. In their experiments, the higher catalytic performance which came with the highest H₂ yield and lower CO yield was achieved by using the Ni/Pt catalyst. Ni/CeO₂-Al₂O₃ catalysts were prepared by a sequential impregnation method. The first step was to impregnate CeO₂ on γ -Al₂O₃ using the incipient wetness method. An aqueous solution of Ce(NO₃)₂ prepared in a rotary evaporator at 60°C was also required. For the removal of adsorbed contaminants, the γ -Al₂O₃ pellets needed to be sieved to 80-100 mesh particles and treated at 550 °C for 3 hours under the synthetic flow. The sample was calcined at 550 °C for 3 hours under 20 cm³min⁻¹ airflow after drying at 80 °C for 10 hours. Then, Ni was impregnated on CeO₂-Al₂O₃ support also by using the incipient wetness method with an aqueous solution of Ce(NO₃)₂·6H₂O. Finally, the catalyst was obtained by calcination at 550°C for 3 hour, after drying at 80 °C for 10 hours.

The modified Ni/CeO₂-Al₂O₃ catalysts were prepared by methods similar to that reported by Profeti et al [91]. Impregnation of Ni/CeO₂-Al₂O₃ was carried out after calcination with the aqueous solutions of Pt (H₂PtCl₆·2H₂O) or Pd (PdCl₂) or Ru (RuCl₃·H₂O) or Ir (IrCl₄·xH₂O). After impregnation, solutions were dried at 80°C for 10 hours and calcination was done at 550°C in air, for 3 hours. The same process of sieving γ -Al₂O₃ using 80-100 mesh sieves was repeated, with further calcination at 600 °C to remove impurities. As higher concentrations of nickel can very effectively increase the activity of catalysts, it could overlap with the influence of the addition of noble metals into the catalysts, leading to a difficulty in comparing the different catalysts. So a small amount of noble metals

promoter (loading of 0.3wt.%) and a relatively small amount of nickel loading (5wt.%) were chosen in the catalyst preparation process [91].

Catalytic performances of Ni/CeO₂-Al₂O₃ catalysts were promoted by the addition of noble metals (Pt, Pd, Ru, Ir). Results showed the modified catalyst with noble metals promotion led to higher H₂ yields than the catalysts without noble metal promotions. The best result from their glycerol reforming process was achieved when the NiPt/CeO₂-Al₂O₃ catalyst was used at 700°C [91].

2.3.3 Other catalysts

Adhikari et al. [81] found that when the temperature was 650 °C and pressure was 1 atm, hydrogen production ratio by glycerol reforming using a Ni/MgO catalyst reached a maximum of 56.5% compared with Ni/TiO₂ and Ni/CeO₂. [92]. The catalysts were prepared using Ni(NO₃)₂·6H₂O over three supports which were MgO, TiO₂ and CeO₂, by a wet impregnation method. The same content of Ni loading (15wt.%) was used in all prepared catalysts. All catalysts were dried at 110°C for 12 hours and then calcined at 500°C in air for 6 hours. The final step was to sieve the catalyst using sieves with 16-35 mesh sizes.

Czernik et al. [80] analysed hydrogen production from glycerol steam reforming by using thermodynamic and experimental analyses. Results showed the maximum moles of hydrogen produced per mole of glycerol could reach up to 6 thermodynamically, but the stoichiometric limit was 7. Moreover, the experimental results were far away from the thermodynamic equilibrium by using Ni/MgO catalyst [72].

Rossettiet. al. [93] prepared Ni-based catalysts supported on TiO₂, ZrO₂ and SiO₂ by synthesising supports in the liquid phase. These were followed by impregnation with the active phase and calcination at 800°C. Otherwise, the catalysts can be synthesised by direct pyrolysis which can make catalysts with high stability at high temperatures and high metal dispersion. The metal-support interaction and surface acidity are the most important parameters for assessing catalysts. The metal-support interaction strongly depends on the catalyst preparation procedure. If the metal-support interaction is stronger, the activity

and stability of catalyst will be relatively higher. The nature of acid sites is differentiated.

Cui et al. [94] investigated the $\text{La}_{1-x}\text{Ce}_x\text{NiO}_3$ catalyst activities in a glycerol steam reforming process by comparing the catalyst activities with a Pt metal catalyst. They found that Ni can be easily reduced in $\text{La}_{0.3}\text{Ce}_{0.7}\text{NiO}_3$ structure. Results were calculated by a non-stoichiometric method and compared with the thermodynamic equilibrium. The result showed that the catalyst had the highest activity in the glycerol steam reforming process. The glycerol conversion efficiency was close to the thermodynamic equilibrium when the temperature was in the range of 500 to 700°C. The minimum carbon formation on the surface of the catalyst was achieved by using the $\text{La}_{0.3}\text{Ce}_{0.7}\text{NiO}_3$ catalyst with a good stability of the catalyst's surface [72].

Hirai et al. [95] found that H_2 selectivity can reach up to 90% in the glycerol steam reforming process with complete conversion at 600°C by using a $\text{Ru}/\text{Y}_2\text{O}_3$ catalyst. Also, a $\text{Ru}/\text{Y}_2\text{O}_3$ catalyst with 3 wt.% Ru loading was considered a more durable catalyst for limiting deactivation of catalysts caused by carbon deposits in the glycerol steam reforming process. They reported that this catalyst afforded very high activity in a prolonged experiment. In their experiments, Group 8-10 metals were used to prepare the catalysts over Y_2O_3 , ZrO_2 , CeO_2 , La_2O_3 , SiO_2 , MgO , and Al_2O_3 supports. The results showed that the order of catalysts activity was as follows: $\text{Ru} \approx \text{Rh} > \text{Ni} > \text{Ir} > \text{Co} > \text{Pt} > \text{Pd} > \text{Fe}$. Kikuchi et al. [96] found the order of the catalysts activities on silica in the steam reforming methane was as follows: $\text{Ru} \approx \text{Rh} > \text{Ni} > \text{Ir} > \text{Pt} \approx \text{Pd} > \text{Co} \approx \text{Fe}$.

Hirai et al. [95] surmised that active metals in the steam reforming of methane also afforded high activity in the glycerol steam reforming process. Their results showed that Ru afforded the highest H_2 yield at a reaction temperature of 600°C. Although Al_2O_3 can be a favourable support for the steam reforming of hydrocarbons, Ru on an Al_2O_3 support gave the lowest conversion in the glycerol steam reforming process. The greater the CH_4 produced and the lower the CO_2 produced, the less the amount of H_2 was produced. So, the $\text{Ru}/\text{Y}_2\text{O}_3$ catalyst gave the best result in the glycerol steam reforming process. Optimal

Ru loading was attained at 500°C. The results also showed that when the Ru loading increased the H₂ yield increased until the Ru loading was up to 3 wt. %. The further increase of Ru loading up to 5 wt.% had no significant effect on the H₂ yield [95].

2.3.4 Catalyst supports

Catalyst supports are normally used to increase the catalyst stability. Alumina supports have been applied widely in many reactions and are considered to be the most effective supports for catalysts. Mirodatos et al. [97] found that Ni/Al₂O₃ catalysts demonstrate the highest amount of carbon deposition in the methanation reaction compared to Ni/SiO₂ catalysts. Ni/Al₂O₃ catalysts present the highest catalytic stability in the reforming process. A similar situation occurred in the reforming methane reaction using Ni/Al₂O₃ and Ru/Al₂O₃ catalysts carried out by Zhang et al. [98] and Slagtern et al. [99].

The use of different catalyst supports also has an effect on the performance of a catalyst through interaction of the active metal with the support, surface area and porosity of the support material, among others. Miyazawa et al. [100] investigated the performance of nickel catalysts on various supports for the steam reforming of biomass pyrolysis tars. Ni-Al₂O₃, Ni-ZrO₂, Ni-TiO₂, Ni-CeO₂ and Ni-Ni/MgO catalysts were examined. The Ni-Al₂O₃ catalyst was found to be the most active and the Ni-MgO catalyst showed the lowest activity in relation to hydrogen production. It was suggested that the type of support used influenced the nickel metal particle size, which is key to catalyst activity. Inaba et al. [101] investigated Ni-SiO₂, Ni-ZrO₂, Ni-CeO₂ and a series of Ni-zeolites for use as catalysts for hydrogen production from the gasification of cellulose. The production of hydrogen followed the order Ni-SiO₂> Ni-ZrO₂> Ni-CeO₂. The production of hydrogen using the Ni-zeolites was dependent on the type of zeolite used.

Wu and Williams [25] used a two-stage pyrolysis-catalytic steam reforming process to produce hydrogen from polypropylene using various substrate supports with nickel, including Ni-Al₂O₃, Ni-MgO, Ni-CeO₂ and Ni-ZSM-5. Yields of hydrogen were influenced by the amount and type of carbon deposition on

the catalyst surface during reaction, which was in turn influenced by the type of catalyst support material.

MCM-41 is a mesoporous material with high surface area up to $1000 \text{ m}^2\text{g}^{-1}$, pore diameters in a range of $\sim 2\text{-}10 \text{ nm}$ and a flexible structure of the amorphous silica walls [102]. It has been used as a catalyst for hydrogen production, Wu et al. [102] investigated Ni on a MCM-41 support for H_2 production from biomass and Zhao et al. [102] compared Ni- Al_2O_3 and Ni-MCM-41 supports for hydrogen production from cellulose. Zhao et al. [103] reported that the highly ordered mesoporous structure of an MCM-41 support improved the dispersion of active nickel particles and subsequently increased the interaction between the nickel sites and gaseous products. However, there are few studies investigating the production of H_2 from waste plastics using Ni-MCM-41 and also the role of the addition of metal promoters such as iron to the Ni-catalyst.

However, catalyst deactivation resulting from coke formation on the surface of catalyst is one of the challenges in hydrogen production from tyre gasification [100, 104-107]. Catalyst deactivation is also affected by sulphur poisoning. Elbaba et al. [12] found that the deactivation of a Ni/ Al_2O_3 catalyst in gasification of a waste tyre for hydrogen production was due to sulphur poisoning and carbon deposition. It was noted that there are different forms of carbons generated in the process, including amorphous carbon and graphite carbon, for instance carbon nanotubes. Giannakeas et al. [108] found evidence from XRD to prove there is carbon deposition on the surfaces of the catalysts which causes catalyst deactivation in the waste tyre reforming.

2.3.5 Summary

Catalysts play the most important role in the waste hydrocarbon pyrolysis-catalysis/catalytic reforming process. The most common catalysts used in this process are transition metals-based catalysts like Ni-, Co-, Cu- and Fe-based catalysts. Noble metal-based catalysts also promote the catalysis or reforming process, however, the cost of noble metals are considerable, and as such, noble metals-based catalysts cannot be commercialized for large-scale

production. Catalysts supports also affect the process, and the most commonly used catalyst supports are alumina, zeolite and silica, among others.

2.4 Carbon nanotubes (CNTs) applications and production

In recent years, carbon nanotubes (CNTs) as one of popular carbon nano-materials which have been one of the most frequently investigated materials due to their physical, chemical, mechanical and thermal properties, and their potential applications in different industries which have grown rapidly since they were first discovered by Ijima [109]. The commercial interest in CNTs is reflected in the production of thousands of tonnes produced every year.

2.4.1 Applications of carbon nanotubes

Single-walled carbon nanotubes (SWCNTs) are formed by a single graphite sheet wrapped around to form a cylinder with diameters in a range of 0.8-1 nm. Multi-walled carbon nanotubes (MWCNTs) are formed by nested cylinders of graphene sheet in which the diameters are typically in a range of 5-20 nm and also can exceed 100nm. The length of CNTs varies from 100 nanometers to centimeters [110]. CNTs have several of featured properties, such as relatively high tensile strengths (around 100 GPa), which is 100 times greater than stainless steel, high modulus (around 1 Tpa) [111], large aspect ratio of length to diameter, cylindrical structure, lower density (around 1100-1300 kg m⁻³) which equates to one-sixth of that of stainless steel, small size on a nano-scale, good chemical and environmental stability. CNTs have relatively high thermal conductivities of about 3500 Wm⁻¹K⁻¹ at room temperature similar to diamonds and the relatively high electrical conductivity of 10⁹A cm⁻² comparable to that of copper [112, 113]. Applications of CNTs are widely varied, making CNTs a high value material.

The initial applications of CNTs in super-capacitors, actuators and lightweight electromagnetic shields appear to have been successful. CNTs can be used as multifunctional coating materials. For example, multi-walled carbon nanotubes (MWCNTs) can be added into paints to discourage the attachment of algae and

barnacles to the hulls of boats and therefore reducing bio-fouling [114, 115]. MWCNTs have been used widely in lithium ion batteries by blending MWCNTs with active materials and polymer binders [3, 114, 116]. MWCNTs can increase the electrical connectivity and mechanical integrity with the result that the rate capacity and life cycle of batteries have been enhanced [114, 117, 118]. Considering the low electron scattering and band gap of high quality of single walled carbon nanotubes (SWCNTs), they have been used in making transistors. CNTs could also be used in biosensors and medical devices due to their chemical and dimensional compatibility with biomolecules [114, 119].

2.4.1.1 Composite materials

MWCNTs can be used as electrically conductive fillers in plastics. The percolation network can be formed with only a 0.01wt.% concentration of MWCNTs due to their high aspect ratio. The conductivity of disordered polymers with 10 wt.% CNTs composition can reach $10,000 \text{ s m}^{-1}$ [120]. MWCNTs have also been applied in the automotive industry to the composition of plastics to enable electrostatic-assisted painting of mirror housings, fuel lines and filters in order to prevent electrostatic charge. MWCNTs can also be added to products in the microelectronics industry, such as electromagnetic interference shielding packages and wafer carriers [110].

Due to the different features of CNTs with different diameters, aspect ratios, alignment, dispersion and interfacial interaction with the matrix, CNTs mixed with polymers or precursor resins can meaningfully improve the stiffness, strength and toughness of composite materials which have been widely used in load-bearing applications. It is reported in literature that with a 1 wt.% addition of CNTs into epoxy resins, the stiffness has increased by 6 % and fracture toughness has increased by 23 % [121, 122]. The resins mixed with CNTs have recently been used to manufacture lightweight and strong wind turbine blades and boat hulls.

MWCNTs can also be added to plastics as flame-retardants, which can potentially replace environmentally hazardous halogenated flame retardants. Reasons for the use CNTs as flame-retardant additives are due to changes of

rheology [123]. CNTs cannot only be added to polymers to form composite materials, but can also be added into metals to enhance the modulus and tensile strengths. These metals with improved features can be applied in aerospace and automotive industries [124]. For example, commercial aluminium and MWCNTs mixtures have strengths close to stainless steel which are in the range of 0.7 to 1 GPa, however, the density is only 2.6 g cm^{-3} . The mixture of MWCNTs and aluminium provides higher strength with lower cost than the Al-Li alloy.

2.4.1.2 Coatings and films

CNTs are emerging as multifunctional coating materials due to the development of the dispersion technique and functionalization technique. The addition of MWCNTs into paints could reduce biofouling of ship hulls which could possibly replace the conventional environmentally hazardous biocide-containing paints by preventing attachments of algae and barnacles on the boat hulls [115].

Indium tin oxide is commonly used in displays, touch-screen devices and photovoltaics. The price of indium tin oxide continues to rise due to a scarcity of indium [125]. As an alternative, CNT-based transparent conducting films could take the place of indium tin oxide to form more flexible transparent conductors for displays. Currently, SWCNTs films have been commercially produced. The surface resistivity is suitable for some applications such as CNT thin film heaters, defrosting windows and sidewalks, but are of considerably higher price than the indium tin oxide coatings [126].

2.4.1.3 Energy storage

MWCNTs can be blended with active materials and polymer binders in lithium ion batteries for laptops and mobile phones, since they can substantially enhance electrical connectivity and mechanical integrity, consequently increasing rate capability and cycle life [127, 128].

SWCNTs have been studied for packaged cells which show a remarkable performance of super capacitors with a forest-grown SWCNTs application. An

energy density of 16 Wh kh^{-1} and a power density of 10 kW kg^{-1} have been achieved for a 40-F super capacitor, while the maximum voltage was 3.5 V. The lifetime of this super capacitor has also been forecasted to reach 16 years at 105°C [110].

CNTs can be used as catalyst supports for fuel cell electrolysis since they can reduce more than half of Pt usage compared with normal carbon black [129]. Further research has also proven that the application of doped CNTs in fuel cells may not need Pt [130, 131].

2.4.2 Production of carbon nanotubes

2.4.2.1 Methods and purification

CNTs are currently produced by the synthesised electric arc discharge method [109], laser ablation method, catalytic chemical vapour deposition (CVD), flame synthesis, solar energy route and others [132]. The electric arc discharge method requires two graphite electrodes with 1 mm gap under an inert gas atmosphere at a pressure of 500 Torr. A current of 50-120 A with a voltage of 20-25 V produces an arc that generated between the two electrodes. The carbon evaporates from the electrodes which then condense on the cathodes with CNTs formation. The advantage of this method is that both SWCNTs and MWCNTs can be synthesised at low cost for CNTs production [133]. The laser ablation method applies all the same conditions as the arc-discharge method, including condensation of the graphite vapour to form CNTs. It has been reported that graphite to CNTs conversions of 60-90 % can be achieved by using the laser ablation method [134].

Dasgupta et al. [135] surmised that the most featured character of arc discharge and laser ablation methods is the large amount of energy required to induce the reorganization of carbon atoms into CNTs. The temperature for the process needs to reach 3000°C or higher to beneficially form good crystallizations of CNTs. Therefore, products from both arc discharge and laser ablation methods always have good graphite alignments. Difficulties have emerged in meeting the basic required conditions for large-scale production of CNTs, such as vacuum

conditions and continuous graphite target replacement. Also, CNTs produced by the arc-discharge method and laser ablation are normally in carbonaceous soot, which consists of amorphous carbon and metal particles from catalysts. Transition metal carbide has been considered by many researchers to promote filamentous carbon deposition [136-138]. The high-performance of aligned SWCNTs can be synthesised by an attractive coagulation-based spinning of CNT suspensions, which has the potential to enlarge the scale and be extended to the production of MWCNTs [139].

Chemical vapour deposition (CVD) is the most common and popular method to commercially synthesis CNTs. The CVD method is based on the hydrocarbon vapour thermal decomposition, and the process can be promoted by adding metal-based catalysts. A schematic diagram of a CVD setup is shown in Figure 2-3. The general process includes the passing of a hydrocarbon vapour through a tubular reactor at high temperatures of around 600 to 1200°C, in the presence of a catalyst. As the hydrocarbon decomposes in the reactor, CNTs grow on the surface of the catalyst. The growth ends with the system cooling down to room temperature. Precursors for CNTs synthesis by the CVD method can be in various phases, such as liquid and solid hydrocarbons [140].

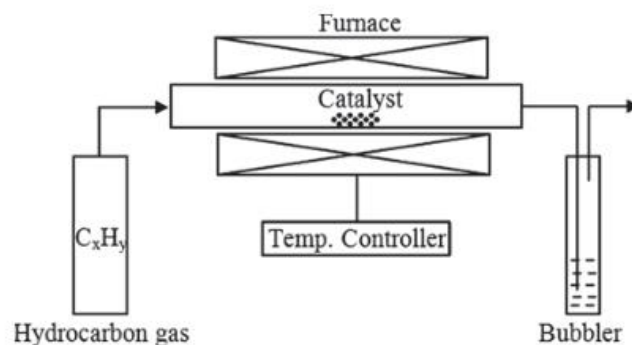


Figure 2-3 Schematic diagram of a chemical vapour deposition (CVD) method for synthesizing carbon nanotubes (CNTs) [140].

In the CVD method, carbon is deposited from a hydrocarbon in the presence of a catalyst with the required temperature lower than 1200°C. This is energy-saving compared with the arc discharge method and laser ablation method. Also, the structure of CNTs can be properly controlled in the CVD process, such

as the wall number, length, diameter and alignment. In consideration of the different advantages of CVD, such as mild operations, low cost and well-controlled process, CVD can be the most promising and feasible method for large-scale production of CNTs [141]. However, the disadvantage still exists that the CNTs produced could be a mixture of MWCNTs and SWCNTs [133].

In order to improve the purity of CNTs formed by different methods and to apply them in different industries, non-CNTs impurities should be removed. The two most popular methods used to remove impurities from CNTs products are the dry method which involves oxidizing in air and wet treatment which involves dissolving in an acid. The dry method depends on the higher thermal stability of CNTs compared with amorphous carbon and other highly reactive impurities. The wet method is normally applied after the dry treatment, and dissolves the metals or metal oxides in nitric acid. Filtration and centrifugation steps are also applied to improve the quality and yield of CNTs.

Ebbesen et al. [142] used a dry method to oxidize CNTs produced by the electric arc discharge method, to remove impurities. The CNTs produced were oxidized at 750°C and held for half an hour. However, the method was unsuccessful as most of the carbon, even CNTs, were burnt off. Xu et al. [143] purified CNTs produced by the CVD method using carbon monoxide in a combined dry and wet method. The produced CNTs were first dry-treated to remove the more active amorphous carbon. Then the samples were wet-treated in HCl to remove the iron catalyst particles. When the oxidization temperature was 350°C, 98% of CNTs were obtained with a significant reduction of iron content from 30% to 1%. The total weight loss of the CNTs yield was only around 30 wt.%.

Moon et al. [144] obtained CNTs with 96% purity which were also treated by a combination method. The CNTs produced by the electric arc discharge method were first heated to 450°C and held for 50 minutes to remove amorphous carbon. Then, produced CNTs with impurities were dissolved in HCl to remove catalyst particles and finally the CNTs were boiled in 30% nitric acid to unbundle the CNTs.

Overall, common CNTs synthesis methods like CVD always come with impurities from the production process, such as amorphous carbon and catalyst particles. Furthermore, the incorporation of dry and wet treatments can improve the purity of CNTs dramatically.

2.4.2.2 Mechanism of carbon nanotubes growth

The mechanism of carbon nanotubes growth has been debated since they were discovered. Mechanisms proposed by different researchers are often contradicting. However, the most acceptable mechanism for CNTs formed by the CVD method has been proposed by Kumar and Ando [140]. They claimed that hydrocarbon vapours start to decompose into carbon and hydrogen atoms when in contact with metal nanoparticles at higher temperatures; then the carbon atoms dissolve into the metals until the metals are saturated with carbon at a certain temperature; The carbon precipitates out and crystallizes as hollow tubes which have no dangling bonds and are thus energetically stable. There are two models to explain this growth mechanism according to the catalyst metal and support interaction as shown in Figure 2-4.

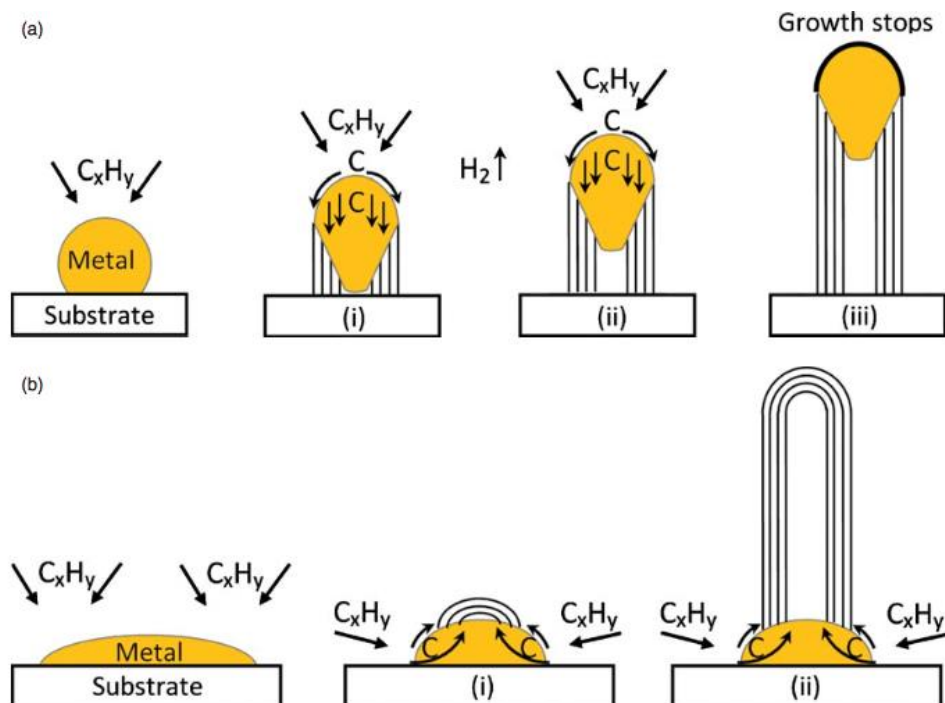


Figure 2-4 The most accepted mechanism for carbon nanotubes growth: (a) tip-growth model. (b) base-growth model [140].

Figure 2-4(a) shows the tip-growth model, and describes the growth of CNTs on the catalyst where there is weak metal-support interaction when the metal particles are at an acute contact angle with the support. The hydrocarbons decompose on the tip of the metal particle, then carbon atoms diffuse down through the metal particles and accumulate at the bottom of the metal particles. Because of the weak interaction between metal particle and support, the accumulated carbon on the bottom of the particle would push the metal particle away from the support. The accumulated carbon are hollow carbon CNTs which can keep growing until they reach the carbon-solubility of the metal particle. Figure 2-4(b) illustrates the base-growth model which describes the growth of CNTs on the catalyst where there is strong metal-support interaction. The strong metal-support interaction indicates the metal particle has an obtuse contact angle with the support. The beginning stage of the hydrocarbon decomposition and carbon atoms diffusion are similar to the tip-growth model. Due to the strong interaction between metal particles and support, the carbon precipitates out on the top of the metal particles as a hemispherical dome. As more and more hydrocarbons decompose and diffuse to the lower peripheral surface of the metal particles, the carbon atoms accumulate as crystallized carbon nanotubes [140]. The authors also broadly concluded that SWCNTs are formed when the catalyst particle sizes are of a few nanometers in size and the MWCNTs are formed when the catalyst particle sizes are in a few tens of nanometers. However, CNTs growth are also affected by important parameters, which are hydrocarbon precursors and type of catalyst. Other factors such as synthesis temperature, pressure, residence time, reactor type and flow rate of reactant could also influence the quality of CNTs formation. Tessonnier and Su [145] reached a similar conclusion that the diameter of the SWCNTs increases as the size of the catalysts particles increases. However, the nature of the CNTs would change at a certain point where double walled carbon nanotubes (DWCNTs) and MWCNTs are formed. They also highlighted that large metal particles at diameters above micro-meter size could dominate graphene or graphite formation. The shapes of catalyst particles also affect features of the filamentous carbon formation; round shape catalyst particles lead to hollow

CNTs while irregular metal particles with sharp edges lead to fishbone carbon nanofibers [146].

Tessonnier and Su [145] proposed a vapour-solid-solid growth mechanism based on the vapour-liquid-solid mechanism proposed by Baker et al. [147] as shown in Figure 2-5. The vapour-liquid-solid mechanism includes three main steps. The first step is the elementary carbon atom formation by the absorption and dissociation of a gaseous carbon precursor on the catalyst particle surface; In the second step, the carbon atoms dissolve in the bulk of nanoparticles and the liquid metastable carbide could be formed and carbon diffusion occurs in the particles; Finally the carbon atoms precipitate out at the side of the catalyst particles to accumulate as carbon filaments. The vapour-liquid-solid mechanism has been supported by many other researchers, since the calculated activation energy for carbon nanofiber formation agrees with the calculation of carbon dissolution in metals [147, 148] .

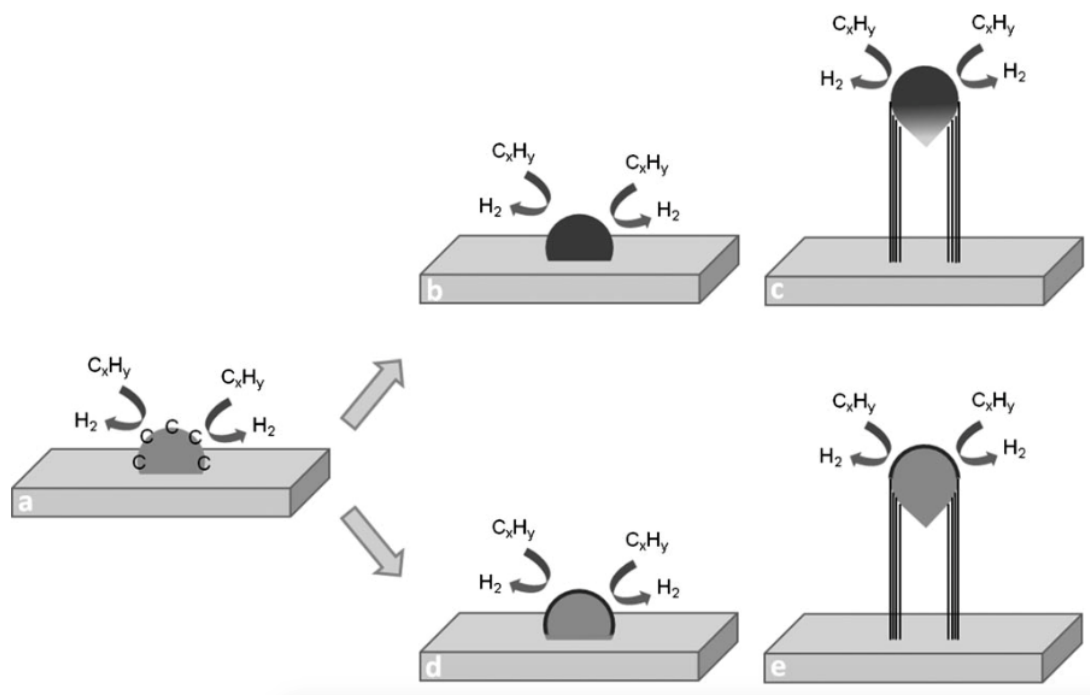


Figure 2-5 The vapour-liquid-solid mechanism of carbon nanotube growth [145].

There are still debates on the vapour-liquid-solid mechanism because the diffusion step is not clear, especially the driving force pushing the carbon atoms to diffuse on the catalysts particle surface has not been stated clearly. The

vapour-liquid-solid mechanism could possibly explain the CNTs growth mechanism when the metal particles melt. The study of CNTs growth mechanism has been modified as the carbon diffusion occurs at the surface of the catalyst particle instead of through the bulk of catalysts particles, which has been supported by many researchers. Tessonnier and Su [145] investigated the vapour-solid-solid mechanism including the carbon precursor dissociation, carbon atoms diffusion on the surfaces of catalyst particles and carbon precipitation to form CNTs. They also proposed a hypothesis about the sub-diffusion of carbon atoms according to the calculation that each carbon atom could gain 0.3 eV energy by diffusing on the sub-surface. The MWCNTs grow by integrating the carbon atoms diffused by sub-surface which is shown in Figure 2-6. The outermost wall formed by carbon atoms diffusion and the second layer of the wall are likely formed by subsurface diffusion of carbon atoms [148].

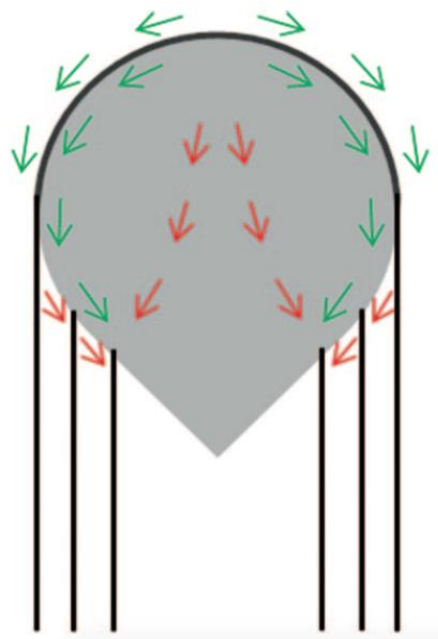


Figure 2-6 The carbon diffusion and sub-diffusion of MWCNTs growth mechanism (Red arrows indicate the prohibited paths for carbon diffusion and green arrows indicate the possible carbon diffusion paths) [148].

Dasgupta et al. [135] summarized the mechanisms of CNT formation in a fluidized bed in eleven steps which are listed below:

- Hydrocarbon gas mass transfers from bubble phase to emulsion phase;
- Hydrocarbon mass transfers from emulsion to the external surface of support which is carbon black;
- Hydrocarbon diffusion from the pore mouth of the carbon black support to the catalyst surface;
- Adsorption of the hydrocarbon on the active site of the catalyst surface;
- Carbon molecules produced by the reaction on the surface of the catalyst;
- Carbon molecules dissolution in the catalyst;
- Super-saturation of the catalyst with carbon;
- Nucleation and growth of CNTs;
- Hydrogen and other gaseous products desorption;
- Gaseous products diffusion from the catalyst to the carbon black support;
- Gaseous products mass transfer from the carbon black support to the emulsion phase.

2.4.2.3 Catalysts and precursors

Although noble metals are the most effective catalysts to promote hydrogen production [149, 150], they are not the ideal catalysts for the large scale industries considering their cost. Currently, Ni-, Fe- and Co-based catalysts have been commonly used for gasification of hydrocarbons [140]. The most common carbon precursors used for CNTs production are methane [151, 152], ethylene [153, 154], acetylene [155], benzene [156], xylene [157] and carbon monoxide [158]. Hernadi et al. [151] investigated Fe-based catalysts with different supports to produce carbon nanotubes via CVD of different hydrocarbons, including acetylene, ethylene and propylene. They found that a Fe/silica catalyst presented the highest activity in carbon nanotubes formation compared with other types of catalysts, such as graphite and ZSM-5.

Weidenkaff et al. [159] produced MWCNTs with diameters in the range of 5 to 20 nm from carbon monoxide and gaseous hydrocarbons by CVD in the presence of an Fe-based catalyst in a fluidized bed reactor. Venegoni et al. [160] produced MWCNTs from a hydrogen and ethylene mixture as the carbon precursor in the presence of an Fe/SiO₂ catalyst by a CVD method in a fluidized bed reactor. Homogeneous MWCNTs were produced with diameters in the range of 10 to 20 nm. Morançais et al. [161] very selectively synthesised MWCNTs from ethylene by a CVD method in a fluidized bed reactor, in the presence of an Fe/Al₂O₃ catalyst. The improved CVD process with efficient mixing of the grains with catalyst powder led to a high selectivity of MWCNTs formation and with high purity. Philippe et al. [162] also produced MWCNTs by a CVD method with a fluidized bed reactor in the presence of Fe/Al₂O₃ catalyst. They also proposed a two-stage MWCNTs growth mechanism based on their experiments and characterizations, which started with the MWCNTs nucleation and grew by reconstruction as well as simultaneous carburization of the catalytic film. When the catalytic film has been consumed, the catalyst particles inside of the mesoporous support were reduced and tangled CNTs were formed.

Li et al. [163] used Fe/Al₂O₃ catalysts prepared by an ion-beam assisted deposition method to produce well-aligned CNTs arrays with lengths in a range of 500 μm to 1.5 mm by a CVD method. See et al. [164] used Fe/Co/Al₂O₃ catalysts in their experiments to investigate how the interaction of process parameters would affect the process of CNTs synthesis in fluidized beds. Results showed that the synthesis temperature affected formation of CNTs greatly while the influence on CNT diameter, quality, and yield were not clear. With the increase of synthesis temperature in all of their experiments, carbon yields increased more rapidly than the increase in yields of CNTs. This suggests that the selectivity of CNTs production decreases when temperatures increase. Nevertheless, See and co-researchers [165] found that the quality of CNTs had improved, in that the CNTs products were more graphitized as temperatures increased. Results also showed that higher fluidization ratios resulted in a pronounced increase of carbon yield compared with the increase of the deposition time. Catalyst types and the interaction between catalyst types and temperature were proved to have significant effects on carbon yields. The

selectivity of CNTs significantly depended on catalyst types. In general, their experimental results showed that the Fe-Co/Al₂O₃ catalyst had a relatively higher selectivity toward CNTs formation than the Fe/Al₂O₃ catalyst in the CNTs synthesis process.

Table 2-1 Comparison of CNTs formed by chemical vapour deposition of methane in the presence of different catalysts and supports[152] .

Catalyst composition	Support material	SWNTs	Description of synthesized material
Fe ₂ O ₃	alumina	Yes	abundant individual SWNTs; some bundles; occasional double-walled tubes
Fe ₂ O ₃	Silica	Yes	abundant SWNT bundles
CoO	alumina	Yes	some SWNT bundles and individual SWNTs
CoO	Silica	No	no tubular materials synthesized
NiO	alumina	No	mainly defective multi-walled structures with partial metal filling
NiO	Silica	No	no tubular materials synthesized
NiO/CoO	alumina	No	no tubular materials synthesized
NiO/CoO	Silica	Yes	some SWNT bundles

Some researchers have used Co-based catalysts to enhance the CNTs obtained from hydrocarbon reforming processes [166]. Qian et al. [166] used Co- and Ni-based catalysts in a methane decomposition process to enhance CNTs production in a fluidized bed reactor. They compared the methane decomposition process with and without catalyst reduction. The CNTs produced by the process without catalyst reduction yielded 3 to 4 times less than the CNTs yielded from the methane decomposition process with catalyst reduction. They explained that the in-situ catalyst reduction provides energy for endothermic methane decomposition. Also, the in-situ catalyst reduction consumed hydrogen and carbon to form water and carbon monoxide which led the equilibrium of the decomposition to shift in the direction of hydrogen and CNTs formation. Kong et al. [152] synthesised CNTs by CVD of methane in the presence of different catalysts. They compared the effects of different metals (Fe-, Ni-, Co- and Fe/Co- based) and different supports (alumina and silica) on the CNTs formation. The results are listed in **Table 2-1**.

Wei et al. [167] investigated the thickness of Fe- and Ni-based catalysts films on CNTs formation by a CVD method. They found that the critical catalyst film thickness for CNTs formation had no correlation with the diameter of the CNTs. However, the vertically oriented CNTs formed by using plasma enhanced CVD with nickel catalyst showed a strong correlation between the diameter of CNTs and the thickness of catalyst film. Fang et al. [168] reported Ce-Ni mixed oxides can be one of the most effective and stable catalysts in the steam reforming of ethanol to produce hydrogen and carbon nano-materials. Results from their research showed that the Ce-Ni catalyst is not only an active catalyst in hydrogen production but also the most effective catalyst to produce the value-added product of carbon nano-materials. They also found that the most suitable method of preparing a Ce-Ni catalyst for the ethanol steam reforming process to produce hydrogen and carbon nano-materials is the co-precipitation method. The co-precipitation method can form the small size of NiO with a diameter of 15 nm and CeO₂ with a diameter of 4 nm as well as give high activity. These led to less formation of nano-fibrous carbon materials formed by carbon deposition and the size of the nano-fibrous carbon materials depended on the size of Ni related nanoparticles. Ce-Ni catalysts prepared by the co-precipitation method

can form smaller and more homogeneous sizes of graphitic filaments compared to catalysts prepared by other methods. The graphitic filaments are CNTs and carbon nanofibres (CNFs). The catalytic stability of Ce-Ni catalysts has an influence on the type of carbon formation.

Ni-based catalysts have significant catalytic activities despite the catalyst preparation methods. The catalytic activity and stability of catalysts are determined by the sizes of NiO and CeO₂ and the interaction between nickel and cerium species, which are defined by the method of preparation. Considering the strong relationship between catalytic stability and the type of carbon formation in the reaction, catalytic stability can be analysed from the small and homogeneous size of graphitic filaments [169].

Fe, Co and Ni are the most common metals used in CNTs synthesis for two reasons: firstly, the carbon solubility can reach high levels at high temperatures; secondly, carbon diffusion can attain high rates in these metals. Apart from the common transition metals used in CNTs production, Cu, Au, Ag, Pt and Pd were also found to catalyse hydrocarbon decomposition to form CNTs [170].

Kong et al. [171] synthesised single-walled carbon nanotubes (SWCNTs) of high quality by CVD of methane with Fe-based catalysts at 1000°C. Different catalyst supports were investigated, and the authors concluded that the catalysts supported by amorphous silica particles could produce SWCNTs bundles. However, the catalysts supported by crystalline alumina nanoparticles produced individual SWCNTs and small bundles.

Fan et al. [153] produced self-oriented regular arrays of carbon nanotubes by CVD of ethylene with patterned porous silicon as substrate. Satishkumar et al. [154] produced bundles of aligned carbon nanotubes by pyrolysis of ferrocene and hydrocarbon mixtures. They found that the ferrocene-acetylene mixture is ideal for producing compact aligned nanotube bundles. The bundles of carbon nanotubes were associated with nanoparticles in a size range of 2-13 nm, and the alignment of catalyst nanoparticles was dominated by the ferromagnetism of the transition metal nanoparticles.

Li et al. [155] enlarged the scale of aligned carbon nanotubes production by CVD of xylene with iron nanoparticles embedded mesoporous silica catalyst, the growth direction of aligned carbon nanotubes was controlled by the pores of the mesoporous silica catalyst support. Sen et al. [156] investigated the effects of metallocenes such as ferrocene, cobaltocene and nickelocene on carbon nanotubes synthesis by pyrolysis of benzene. The wall thickness of nanotubes were associated with the metallocene content.

Organometallobenes have also been widely used as catalysts to produce CNTs, because the metal particles can be liberated in-situ and effectively promote hydrocarbon decomposition to form carbon nanotubes [140]. Wei et al. [157] synthesised multi-walled carbon nanotubes in a promoted method by exposing a silica substrate to a xylene and ferrocene mixture at 800°C. The authors reported that this xylene and ferrocene vapour mixture boosted the selectivity of multi-walled carbon nanotubes formation. Nikolaev et al. [158] synthesised single walled carbon nanotubes by gas-phase catalytic growth from carbon monoxide. The catalysts were used in situ by decomposing iron pentacarbonyl in the hot carbon monoxide flow.

Cyclohexane [172, 173] and fullerene [174, 175] are also commonly used as carbon precursors to produce multi-walled carbon nanotubes. Liu et al. [172] prepared carbon nanotubes by catalytic decomposition of cyclohexane. Li et al. [173] synthesised three-dimensional hierarchical carbon nanotubes by electrochemical iron deposition of cyclohexane. The CNTs were shown to have high electrical conductivity. Nerushev et al. [174] used fullerene and acetylene as carbon sources to investigate the catalytic particle size dependence in a CVD process. They found the carbon nanotube diameters increased when the catalytic particle size increased, but not on a scale of 1:1. Morjan et al. [175] used fullerene as a carbon precursor to synthesize multi-walled carbon nanotubes films by an iron-catalysed thermal chemical vapour deposition process. The structural properties of carbon nanotubes produced from fullerene were different from the carbon nanotubes produced from acetylene.

Catalyst supports used in carbon nanotubes production by chemical vapour deposition process also include graphite [147], quartz [176, 177], silicon [178,

179], silicon carbide [180, 181], silica [182, 183], alumina [97, 98, 184, 185], alumina-silicate (zeolite) [186, 187], CaCo₃ [188], magnesium oxide [189-191], among others. The interactions between catalytic particles and supports play an important role in CNTs formation. The chemical bond formation between catalytic metal particles and supports could inhibit the catalytic ability of the metal particles. Also, the morphology and textural properties of the catalyst support could affect the yield and quality of CNTs [140]. For example, zeolite with nano-scale pores can significantly boost CNTs yields with a relatively small particle size [187].

Alumina materials have been reported to be better catalyst supports than silica due to their strong metal-support interaction which could promote metal dispersion to achieve high density of catalytic sites on the catalysts [192].

Stainless steel meshes have been applied by many researchers in CNTs production from different sources [193-197]. For example, the use of a stainless steel mesh as catalyst support has been introduced in CNTs and hydrogen production from the reforming of toluene, which can easily separate the CNTs products from the catalysts [193]. Alves et al. [194] produced carbon nanotubes using a stainless steel type 304 alloy which consisted of 67% iron, 18-20% chromium and 11% nickel. The conclusion that stainless steel can promote CNTs growth has also been reported by other researchers [195, 196]. Sano et al. [195] produced aligned multi-walled carbon nanotubes on the surface of stainless steel by phenol decomposition. The stainless steel mesh was activated by intensive oxidising in air and then dry reducing in H₂. Wal and Hall [197] used an activated type 304 stainless steel mesh as catalyst to produce carbon nanotubes from mixtures of gases such as a C₂H₂/benzene mixture or a CO/benzene mixture by chemical vapour deposition method (CVD).

2.4.2.4 Effects of reaction conditions on production of carbon nanotubes

In addition to the effects of catalysts and precursors on CNTs production, process conditions such as temperature and addition of oxidants, also play dominant roles in CNTs formation. Zhou et al, [198] and Zhao et al. [199] concluded that the orientation of graphene sheets of CNTs can be turned to 0 -

90° relative to the filament axis. The nature of the carbon precursor and synthesis temperature could lead to the re-construction of carbon particles.

Hata et al. [178] investigated water addition in SWCNTs formation by a CVD method. Results showed that the water stimulated catalyst activity and increased catalysis lifetime by an etching effect, which oxidized the carbon encapsulated on the catalysts particles. The enhanced aligned SWCNTs with 2.5 mm height were formed within 10 minutes with 99.98% carbon purity by this water-assisted CVD of ethylene, also called “super growth”. However, relatively low concentrations of oxidant are required (normally less than 1000 ppm), because high concentrations of oxidant would also etch the CNTs product. Magrez et al. [200] mixed carbon dioxide with ethylene to grow CNTs at a ratio of 1:1. Zhang et al. [201] tried to add ethanol (C_2H_5OH) into the CNTs formation process to grow vertical aligned CNTs forests. The modified process had insufficient H_2O or CO for the etching effect in this process with ethanol addition, but there was still a small amount of water formed by the ethanol decomposition into H_2O and C_2H_4 . Results showed the walls of the CNTs can be reduced by ethanol addition and the catalysts lifetime also increased by more than 3 times. They used online dewpoint and mass spectrometry measurements and found that the ethanol decomposition into active carbon could enhance the growth of CNTs, and the water was used to etch the amorphous carbon accumulated on the catalysts surface whereas the catalyst activity was subsequently improved and lifetime was prolonged.

Motta et al. [202] investigated the effects of sulphur on SWCNTs and MWCNTs production at high temperatures between 1200 and 1300°C in the presence of Fe-based catalysts. The results showed that sulphur could enhance the growth of CNTs by the diffusion of sulphur atoms into the first layers of iron atoms to form Fe-S. The surface energy could possibly be modified by the liquid Fe-S layer due to the lower melting point compared to iron. Also, the presence of sulphur prevented the diffusion of carbon inside bulk catalyst particles, making production of SWCNTs more dominant instead of MWCNTs which need sub-surface diffusion of carbon atoms.

2.4.3 Summary

The most common precursors for CNTs synthesis are ethanol, methane, ethylene, acetylene, benzene, xylene and carbon monoxide, while ethanol has become the most popular precursor for SWCNTs synthesised at low temperatures [110, 181]. The molecular structures of the precursors affect the morphology of CNTs directly. Hydrocarbons with linear structures such as methane, ethylene, acetylene result in a dominance of linear structures of CNTs, since the hydrocarbon could decompose into atomic carbons, linear dimers or trimers of carbon and form the straight hollow filamentous carbons. Likewise, cyclic hydrocarbons such as benzene, xylene, cyclohexane, and fullerene would lead to a dominance of curved CNT formations, with bridges inside of the tubes [174]. SWCNTs formation requires higher temperatures than MWCNTs, which are 600-900 and 900-1200°C, respectively[140].

The most popular transition metals used for CNTs synthesis are Fe, Ni, and Co due to their high solubility of carbon at high temperatures, high diffusion rates, relatively high melting points and low equilibrium-vapour pressures. Authors have also reported that Fe, Ni and Co have stronger adhesion to CNTs. These transition metals-based catalysts are also suitable for CNTs formulated by arc-discharge and laser-vaporization methods, in addition to the CVD method. Solid organometallobenes like ferrocene, cobaltocene and nickelocene are used as catalysts for CNTs formation because they could liberate metal particles in-situ and effectively improve the catalysis activity [140]. It has been reported that the same metal-based catalyst supported on different supports could have different catalytic activities. The common catalyst supports are graphite, quartz, silicon, silicon carbide, silica, alumina, zeolite, calcium oxide, and magnesium oxide, among others. The quality and yield of CNTs are affected by the morphology and textures of supports. Aluminium supports are more suitable for CNTs formation compared to silica supports, because stronger metal-interaction would promote higher metal dispersion [192].

Reaction parameters such as temperature and the addition of oxidants such as water and carbon dioxide could improve CNTs yields by improving the catalyst

activity and prolonging catalyst life, by removing encapsulated carbon on the surface of catalysts.

2.5 Production of Carbon nanotubes (CNTs) from alternative sources: methods and catalysts

Hydrogen production could be significantly enhanced by including catalysts in the thermal decomposition processes for plastics processing. Unfortunately, catalyst deactivation, caused by formation of coke on the surfaces of catalysts is a major challenge facing hydrogen production from the gasification of tyres. Catalyst deactivation by coke deposition on the surface of reacted catalysts cannot be avoided [203-205]. He et al. [33] pointed out that one of the main indicators for influencing catalyst lifetime was catalyst deactivation,[33] which resulted from coke deposition in the steam gasification of waste polyethylene. Wu and Williams [206] investigated coke formation on the surface of a Ni-Mg-Al catalyst in a plastics pyrolysis-catalysis process. The formation of both amorphous and filamentous carbons were confirmed, and the deposited filamentous carbons included carbon nanotubes (CNTs).

The catalyst deactivation would decrease the efficiency of the reforming process because the coke would encapsulate the catalyst particles [46, 72]. However, carbon nanotubes (CNTs) produced in the process of tyre gasification for hydrogen production can be regarded as a secondary product, instead of considering it as un-wanted coke. It is therefore interesting to manipulate the gasification process e.g. using a catalyst to maximize the production of CNTs. Thus, the economic feasibility of hydrogen production would be effectively increased from waste hydrocarbons by pyrolysis-catalysis because of the by-product formation of CNTs.

Although the most common method to synthesis CNTs is via a chemical vapour deposition (CVD) process from hydrocarbons like methane, benzene, xylene or other hydrocarbons [207, 208]. Waste hydrocarbons such as waste tyres, plastics and crude glycerol, with their high content of hydrocarbons also represent potential feedstock for the production of CNTs. A large amount of publications have been reviewed by Bazargan [132] in relation to synthesising

carbon nanotubes from waste plastics. Yang et al. [209] successfully used waste tyres as an alternative carbon source to produce CNTs by a CVD method over a cobalt based catalyst.

2.5.1 Catalytic pyrolysis of waste plastics

Recently, co-production of hydrogen and carbon nanotubes (CNTs) by pyrolysis-catalysis of plastics has become more attractive to researchers [210]. Kukovitsky et al. [211] confirmed that crooked carbon nanotubes with 10-40 nm diameters were produced from polyethylene by pyrolysis at 420 - 450°C in a quartz tube in the presence of a nickel plate catalyst. The CNTs production rate can reach up to 200-300 mg per hour.

Liu et al. [212] investigated the influence of temperature on MWCNTs and hydrogen rich syngas production from polypropylene by a pyrolysis catalytic-reforming process. The two-stage reaction process involved polypropylene pyrolysis over a HZSM-5 zeolite catalyst in a screw kiln reactor and further catalysis of the pyrolysis vapour over a nickel-based catalyst in a moving-bed reactor. They found that 700 °C was the optimum temperature for MWCNTs and hydrogen production.

Acomb et al. [213] investigated different metal catalysts ($\text{Ni}/\text{Al}_2\text{O}_3$, $\text{Co}/\text{Al}_2\text{O}_3$, $\text{Cu}/\text{Al}_2\text{O}_3$ and $\text{Fe}/\text{Al}_2\text{O}_3$) for both hydrogen and CNTs production from LDPE by a catalytic pyrolysis process at 800 °C. Except for the Cu-based catalyst, MWCNTs were successfully formed with the three other catalysts. Fe-based and Ni-based catalysts gave the highest amounts of CNTs and hydrogen production due to the weaker metal-support interaction of $\text{Ni}/\text{Al}_2\text{O}_3$ and $\text{Fe}/\text{Al}_2\text{O}_3$ catalysts, and the interaction is believed to have been the key factor that affected CNTs formation. The authors also compared Ni-based catalysts at different calcination temperatures and reported different metal-support interactions. Results showed that the $\text{Ni}/\text{Al}_2\text{O}_3$ catalyst calcined at a lower temperature would result in sintering of active metal particles and larger active metal particles which were not suitable for CNTs formation. The $\text{Fe}/\text{Al}_2\text{O}_3$ catalyst gave the highest CNTs production due to its adequate metal-support interaction and larger carbon solubility of iron. The authors mentioned that

purification processes would be necessary to separate CNTs from contaminants in future applications. Wu et al. [71] also pointed out that intensive work is needed to separate CNTs from Ni-Mg-Al catalysts for end-use applications.

Hao et al. [214] synthesised CNTs by using an Fe/Mo/Al₂O₃ catalyst in the catalytic pyrolysis of propylene in a nano-agglomerate fluidized bed reactor. The researchers [214] studied the formation of CNTs during this process including the initial fragmentation of the support of the catalyst, sub-agglomerate formation and the growth of CNTs which expands the agglomerates. CNTs product yields were higher when the agglomerates were fully developed.

2.5.2 Carbon nanotubes from waste tyres

Recent work [12, 68-70, 215] by some authors have shown that under certain process conditions, carbon deposited on the surfaces of catalysts during pyrolysis catalysis of waste tyres is composed mainly of carbon nanotubes. Yang et al. [209] successfully used waste tyres as an alternative carbon source to produce CNTs by a CVD method over a cobalt-based catalyst. This indicates there is a potential for waste tyres to be used as carbon precursors to synthesis CNTs. Murr et al. [216] investigated a novel electric arc discharge method for synthesis of MWCNTs from tyre powder. Poyraz et al. [217] produced CNTs from devulcanized ground tyre rubber particles. The short-term microwave irradiation devulcanization of ground tyre rubber was firstly carried out in a microwave for less than 4 mins. The microwave-treated ground tyre rubber particles were coated with polypyrrole as substrate to grow CNTs by secondary microwave treatment. The successful growth of CNTs were confirmed by TGA, FTIR, SEM and TEM techniques.

Hydrocarbons generated from the pyrolysis of waste tyres contain more than 100 hydrocarbon species [3]. For example, the gas phase produced from pyrolysis of tyres contains alkane and alkene hydrocarbon gases from C₁–C₄. Higher molecular weight hydrocarbons are also generated during pyrolysis of tyres. The condensed oil fractions from pyrolysis of waste tyres have been shown to contain a wide range of hydrocarbon species, including aliphatic, aromatic, hetero-atom and polar hydrocarbons. For example, alkanes from C₁₀–

C₃₅, alkenes from C₆–C₉, single ring aromatic compounds such as benzene, toluene, xylene, styrene and alkylated derivatives, polycyclic aromatic hydrocarbons such as naphthalene, biphenyl, phenanthrene, anthracene, pyrene and alkylated derivatives and a wide range of other hydrocarbons including phenols, organic acids and sulphur and nitrogen containing hydrocarbons [3]. The sulphur contents of waste tyres can deactivate Ni/Al₂O₃ catalysts activity in the waste tyre pyrolysis catalytic-gasification process due to the sulphur deposited on the active nickel particles. But the sulphur poisoning was not significant for a Ni/dolomite catalyst [69].

2.5.3 Carbon nanotubes from other sources

Coke formation on the surface of catalysts during hydrogen production from glycerol reforming processes is also a challenge. The coke formation on the surface of catalysts during the glycerol reforming process cannot be avoided, similar to carbon deposition in waste tyre and plastics pyrolysis catalysis/catalytic reforming processes. Efficiencies of reforming processes could be reduced dramatically due to catalyst surface area reduction. Therefore, it would reduce the heat transfer from gas to catalyst [46, 72]. Ebshish et al. [72, 79] reported that coke formation during their glycerol steam reforming process was because of the acidic catalyst support. It affected the glycerol conversion process. Also, it will affect the quantity of hydrogen produced because of the impurities.

Chiodo et al. [90] concluded that coke formation is because of large amounts of olefins that exist in reaction streams. Investigations on how to convert coke to value-added products would increase the feasibility of reforming raw glycerol to value-added products [71]. Wu et al. [71] concluded this process would reduce CO₂ emissions compared with the conventional way to regenerate the catalyst by combustion of the coke formed on the surface of the catalyst. However, for future applications this process needs further investigation because of impurities contained in the crude glycerol which include spent, excess alkali metal catalysts, salts, excess methanol, fattyacids and esters.

2.5.4 Summary

To the best knowledge of the author, there are limited reports concerning co-producing hydrogen and CNTs from catalytic tyre gasification, although, simultaneously producing H₂ and CNTs has been reported for gasification of plastics [96, 218].

Currently, Ni-, Fe-, Cu- and Co-based catalysts are normally used for gasification of waste polymers [103, 219-222].

In the reforming processes, formation of coke on the surfaces of catalysts cannot be avoided. It can decrease the efficiency of reforming processes because coke formation readily deactivates catalysts [46, 72]. However, carbon nanotubes (CNTs) produced in the process of tyre gasification for hydrogen production can be regarded as by-products, instead of considering them to be un-wanted coke. It is therefore of interest to manipulate the gasification process, for instance through catalysts, to maximize production of CNTs.

References

1. Ewan, B.C.R., et al., *A figure of merit assessment of the routes to hydrogen*. International Journal of Hydrogen Energy, 2005. **30**(8): p. 809-819.
2. Zhang, Y., et al., *High-value resource recovery products from waste tyres*. Proceedings of the Institution of Civil Engineers - Waste and Resource Management, 2016. **169**(3): p. 137-145.
3. Williams, P.T., *Pyrolysis of waste tyres: A review*. Waste Management, 2013. **33**(8): p. 1714-1728.
4. Williams, P., et al., *Enhanced pyrolysis processing of scrap tyres*. Journal of the Institute of Energy, 2001. **74**(501): p. 100-112.
5. Sienkiewicz, M., et al., *Progress in used tyres management in the European Union: A review*. Waste Management, 2012. **32**(10): p. 1742-1751.
6. Suzuki, M., *Activated carbon fiber: Fundamentals and applications*. Carbon, 1994. **32**(4): p. 577-586.
7. Williams, P.T., et al., *Aromatic chemicals from the catalytic pyrolysis of scrap tyres*. Journal of Analytical and Applied Pyrolysis, 2003. **67**(1): p. 143-164.
8. Dai, X., et al., *Pyrolysis of waste tires in a circulating fluidized-bed reactor*. Energy, 2001. **26**(4): p. 385-399.
9. Conesa, J.A., et al., *Gas from the Pyrolysis of Scrap Tires in a Fluidized Bed Reactor*. Energy & Fuels, 1996. **10**(1): p. 134-140.
10. Aylón, E., et al., *Valorisation of waste tyre by pyrolysis in a moving bed reactor*. Waste management, 2010. **30**(7): p. 1220-1224.
11. Roos, C.J., *Clean heat and power using biomass gasification for industrial and agricultural projects*. 2010: Northwest CHP Application Center.
12. Elbaba, I.F., et al., *Hydrogen production from the pyrolysis–gasification of waste tyres with a nickel/cerium catalyst*. International Journal of Hydrogen Energy, 2011. **36**(11): p. 6628-6637.
13. Leung, D.Y.C., et al., *Fluidized-bed gasification of waste tire powders*. Fuel Processing Technology, 2003. **84**(1–3): p. 175-196.
14. Xiao, G., et al., *Low-temperature gasification of waste tire in a fluidized bed*. Energy Conversion and Management, 2008. **49**(8): p. 2078-2082.
15. Galvagno, S., et al., *Steam gasification of tyre waste, poplar, and refuse-derived fuel: A comparative analysis*. Waste Management, 2009. **29**(2): p. 678-689.

16. Dell, R.M., et al., *Chapter 8 - Hydrogen, Fuel Cells and Fuel Cell Vehicles*, in *Towards Sustainable Road Transport*, R.M.D.T.M.A.J. Rand, Editor. 2014, Academic Press: Boston. p. 260-295.
17. Zadgaonkar, A., *Process and equipment for conversions of waste plastics into fuels*. *Feedstock Recycling and Pyrolysis of Waste Plastics: Converting Waste Plastics into Diesel and Other Fuels*, 2006: p. 709-728.
18. de Marco Rodriguez, I., et al., *Pyrolysis of scrap tyres*. *Fuel processing technology*, 2001. **72**(1): p. 9-22.
19. Benito, A., et al., *Carbon nanotubes production by catalytic pyrolysis of benzene*. *Carbon*, 1998. **36**(5): p. 681-683.
20. Groves, S.A., et al., *Natural rubber pyrolysis: Study of temperature-and thickness-dependence indicates dimer formation mechanism*. *Journal of Analytical and Applied Pyrolysis*, 1991. **19**: p. 301-309.
21. Diels, O., et al., *Synthesen in der hydroaromatischen Reihe*. *Justus Liebigs Annalen der Chemie*, 1928. **460**(1): p. 98-122.
22. Mastral, A., et al., *Influence of process variables on oils from tire pyrolysis and hydropyrolysis in a swept fixed bed reactor*. *Energy & Fuels*, 2000. **14**(4): p. 739-744.
23. Pakdel, H., et al., *Production of dl-limonene by vacuum pyrolysis of used tires*. *Journal of Analytical and Applied Pyrolysis*, 2001. **57**(1): p. 91-107.
24. Kwon, E., et al., *Fundamental understanding of the thermal degradation mechanisms of waste tires and their air pollutant generation in a N₂ atmosphere*. *Environmental science & technology*, 2009. **43**(15): p. 5996-6002.
25. Wu, C., et al., *Hydrogen production by steam gasification of polypropylene with various nickel catalysts*. *Applied Catalysis B: Environmental*, 2009. **87**(3): p. 152-161.
26. Czernik, S., et al., *Production of hydrogen from plastics by pyrolysis and catalytic steam reform*. *Energy & Fuels*, 2006. **20**(2): p. 754-758.
27. Williams, P.T., *Waste incineration*. *Waste Treatment and Disposal*, Second Edition, 2005: p. 245-323.
28. Wu, C., et al., *Investigation of Ni-Al, Ni-Mg-Al and Ni-Cu-Al catalyst for hydrogen production from pyrolysis-gasification of polypropylene*. *Applied Catalysis B: Environmental*, 2009. **90**(1-2): p. 147-156.
29. Group, P.E.M.R., *An analysis of European plastics production, demand and waste data for 2011, 2012*, Consulté sur www.plasticseurope.org.
30. Wu, C., et al., *Pyrolysis-gasification of plastics, mixed plastics and real-world plastic waste with and without Ni-Mg-Al catalyst*. *Fuel*, 2010. **89**(10): p. 3022-3032.

31. Lakhapatri, S.L., et al., *Analysis of catalyst deactivation during steam reforming of jet fuel on Ni-(PdRh)/ γ -Al₂O₃ catalyst*. Applied Catalysis A: General, 2011. **405**(1–2): p. 149-159.
32. Sierra Gallego, G., et al., *Production of hydrogen and MWCNTs by methane decomposition over catalysts originated from LaNiO₃ perovskite*. Catalysis Today, 2010. **149**(3–4): p. 365-371.
33. He, M., et al., *Syngas production from catalytic gasification of waste polyethylene: influence of temperature on gas yield and composition*. International Journal of Hydrogen Energy, 2009. **34**(3): p. 1342-1348.
34. Srinakruang, J., et al., *A highly efficient catalyst for tar gasification with steam*. Catalysis Communications, 2005. **6**(6): p. 437-440.
35. Minowa, T., et al., *Cellulose decomposition in hot-compressed water with alkali or nickel catalyst*. The Journal of Supercritical Fluids, 1998. **13**(1–3): p. 253-259.
36. Valliyappan, T., et al., *Pyrolysis of glycerol for the production of hydrogen or syn gas*. Bioresource Technology, 2008. **99**(10): p. 4476-4483.
37. Adhikari, S., et al., *Hydrogen production from glycerol: An update*. Energy Conversion and Management, 2009. **50**(10): p. 2600-2604.
38. Romero, A., et al., *Ni(II)–Mg(II)–Al(III) catalysts for hydrogen production from ethanol steam reforming: Influence of the Mg content*. Applied Catalysis A: General, 2014. **470**(0): p. 398-404.
39. da Silva, A.L., et al., *Cobalt particle size effects on catalytic performance for ethanol steam reforming—Smaller is better*. Journal of Catalysis, 2014. **318**: p. 67-74.
40. Soares, R.R., et al., *Glycerol as a Source for Fuels and Chemicals by Low-Temperature Catalytic Processing*. Angewandte Chemie, 2006. **118**(24): p. 4086-4089.
41. Ucar, S., et al., *Evaluation of two different scrap tires as hydrocarbon source by pyrolysis*. Fuel, 2005. **84**(14–15): p. 1884-1892.
42. Nichele, V., et al., *Ni/ZrO₂ catalysts in ethanol steam reforming: Inhibition of coke formation by CaO-doping*. Applied Catalysis B: Environmental, 2014. **150–151**(0): p. 12-20.
43. Sekine, Y., et al., *Effect of small amount of Fe addition on ethanol steam reforming over Co/Al₂O₃ catalyst*. Applied Catalysis A: General, 2014. **472**(0): p. 113-122.
44. Seker, E., *The catalytic reforming of bio-ethanol over SiO₂ supported ZnO catalysts: The role of ZnO loading and the steam reforming of acetaldehyde*. International Journal of Hydrogen Energy, 2008. **33**(8): p. 2044-2052.

45. Schwartz, N.V., et al., *Observations on the thermogravimetric oxidation of carbon blacks in vulcanizates*. *Thermochimica Acta*, 1978. **26**(1–3): p. 349-359.
46. Avasthi, K.S., et al., *Challenges in the Production of Hydrogen from Glycerol – A Biodiesel Byproduct Via Steam Reforming Process*. *Procedia Engineering*, 2013. **51**(0): p. 423-429.
47. Palma, V., et al., *CeO₂-supported Pt/Ni catalyst for the renewable and clean H₂ production via ethanol steam reforming*. *Applied Catalysis B: Environmental*, 2014. **145**(0): p. 73-84.
48. Claude, S., *Research of new outlets for glycerol-recent developments in France*. *Lipid*, 1999.(101): p. 101.
49. Valliyappan, T., et al., *Pyrolysis of glycerol for the production of hydrogen or syn gas*. *Bioresour Technol*, 2008. **99**(10): p. 4476-83.
50. Simonetti, D., et al., *Gas-phase conversion of glycerol to synthesis gas over carbon-supported platinum and platinum–rhenium catalysts*. *Journal of Catalysis*, 2007. **247**(2): p. 298-306.
51. Peres, A.P.G., et al., *Syngas Production and Optimization from Glycerol Pyrolysis*. *International Journal on Energy Conversion (IRECON)*; Vol 1, No 1 (2013), 2013.
52. Ahmed, I., et al., *Syngas yield during pyrolysis and steam gasification of paper*. *Applied energy*, 2009. **86**(9): p. 1813-1821.
53. Williams, P.T., *Waste treatment and disposal*. 2005: John Wiley & Sons.
54. Demirbas, A., *Effects of temperature and particle size on bio-char yield from pyrolysis of agricultural residues*. *Journal of analytical and applied pyrolysis*, 2004. **72**(2): p. 243-248.
55. Kodera, Y., et al., *Novel process for recycling waste plastics to fuel gas using a moving-bed reactor*. *Energy & Fuels*, 2006. **20**(1): p. 155-158.
56. Esfandiari, A., et al., *Preparation and evaluation of activated carbons obtained by physical activation of polyethyleneterephthalate (PET) wastes*. *Journal of the Taiwan Institute of Chemical Engineers*, 2012. **43**(4): p. 631-637.
57. Kyari, M., et al., *Characterization of Oils, Gases, and Char in Relation to the Pyrolysis of Different Brands of Scrap Automotive Tires*. *Energy & Fuels*, 2005. **19**(3): p. 1165-1173.
58. de Marco Rodriguez, I., et al., *Pyrolysis of scrap tyres*. *Fuel Processing Technology*, 2001. **72**(1): p. 9-22.
59. Cunliffe, A.M., et al., *Composition of oils derived from the batch pyrolysis of tyres*. *Journal of Analytical and Applied Pyrolysis*, 1998. **44**(2): p. 131-152.

60. Leung, D., et al., *Pyrolysis of tire powder: influence of operation variables on the composition and yields of gaseous product*. Fuel Processing Technology, 2002. **79**(2): p. 141-155.
61. Roy, C., et al., *Recycling of scrap tires to oil and carbon black by vacuum pyrolysis*. Resources, Conservation and Recycling, 1990. **4**(3): p. 203-213.
62. Napoli, A., et al., *Scrap tyre pyrolysis: Are the effluents valuable products?* Journal of Analytical and Applied Pyrolysis, 1997. **40**: p. 373-382.
63. Coll, R., et al., *Steam reforming model compounds of biomass gasification tars: conversion at different operating conditions and tendency towards coke formation*. Fuel Processing Technology, 2001. **74**(1): p. 19-31.
64. Lee, D.C., et al., *Carbon nanotube synthesis in supercritical toluene*. Journal of the American Chemical Society, 2004. **126**(15): p. 4951-4957.
65. Lakhapatri, S.L., et al., *Deactivation due to sulfur poisoning and carbon deposition on Rh-Ni/Al₂O₃ catalyst during steam reforming of sulfur-doped n-hexadecane*. Applied Catalysis A: General, 2009. **364**(1–2): p. 113-121.
66. Kwon, E., et al., *Investigation of mechanisms of polycyclic aromatic hydrocarbons (PAHs) initiated from the thermal degradation of styrene butadiene rubber (SBR) in N₂ atmosphere*. Environmental Science & Technology, 2008. **42**(6): p. 2175-2180.
67. Abu El-Rub, Z., et al., *Review of Catalysts for Tar Elimination in Biomass Gasification Processes*. Industrial & Engineering Chemistry Research, 2004. **43**(22): p. 6911-6919.
68. Elbaba, I.F., et al., *Two stage pyrolysis-catalytic gasification of waste tyres: Influence of process parameters*. Applied Catalysis B: Environmental, 2012. **125**(0): p. 136-143.
69. Elbaba, I.F., et al., *Deactivation of Nickel Catalysts by Sulfur and Carbon for the Pyrolysis–Catalytic Gasification/Reforming of Waste Tires for Hydrogen Production*. Energy & Fuels, 2014. **28**(3): p. 2104-2113.
70. Elbaba, I.F., et al., *Catalytic Pyrolysis-Gasification of Waste Tire and Tire Elastomers for Hydrogen Production*. Energy & Fuels, 2010. **24**(7): p. 3928-3935.
71. Wu, C., et al., *Renewable hydrogen and carbon nanotubes from biodiesel waste glycerol*. Scientific reports, 2013. **3**.
72. Ebshish, A., et al., *Review of hydrogen production via glycerol reforming*. Proceedings of the Institution of Mechanical Engineers, Part A: Journal of Power and Energy, 2012. **226**(8): p. 1060-1075.
73. Zhang, B., et al., *Hydrogen production from steam reforming of ethanol and glycerol over ceria-supported metal catalysts*. International Journal of Hydrogen Energy, 2007. **32**(13): p. 2367-2373.

74. Iriondo, A., et al., *Glycerol steam reforming over Ni catalysts supported on ceria and ceria-promoted alumina*. International Journal of Hydrogen Energy, 2010. **35**(20): p. 11622-11633.
75. Freitas, A.C., et al., *Comparison of several glycerol reforming methods for hydrogen and syngas production using thermodynamic analysis*. 2014. **39**(31): p. 17969-17984.
76. Adhikari, S., et al., *Production of hydrogen by steam reforming of glycerin over alumina-supported metal catalysts*. Catalysis Today, 2007. **129**(3-4): p. 355-364.
77. Anthony Le Valant, N.B., et al., *Preparation and characterization of Ni/Rh/Al₂O₃ catalyst and catalytic methane-steam reforming*. Applied Catalysis B: Environmental, 2010.
78. Buffoni, I.N., et al., *Nickel catalysts applied in steam reforming of glycerol for hydrogen production*. Catalysis Communications, 2009. **10**(13): p. 1656-1660.
79. Dou, B., et al., *Hydrogen production by sorption-enhanced steam reforming of glycerol*. Bioresource Technology, 2009. **100**(14): p. 3540-3547.
80. Czernik, S., et al., *Hydrogen by Catalytic Steam Reforming of Liquid Byproducts from Biomass Thermoconversion Processes*. Industrial & Engineering Chemistry Research, 2002. **41**(17): p. 4209-4215.
81. Adhikari, S., et al., *Kinetics and Reactor Modeling of Hydrogen Production from Glycerol via Steam Reforming Process over Ni/CeO₂ Catalysts*. Chemical Engineering & Technology, 2009. **32**(4): p. 541-547.
82. Adhikari S., et al., *conversion of glycerol to hydrogen via a steam reforming process over nickel catalysts*. 2008(22). p.1220-1226.
83. Iriondo, A., et al., *Hydrogen Production from Glycerol Over Nickel Catalysts Supported on Al₂O₃ Modified by Mg, Zr, Ce or La*. Topics in Catalysis, 2008. **49**(1-2): p. 46-58.
84. Iriondo, A., et al., *Influence of La₂O₃ modified support and Ni and Pt active phases on glycerol steam reforming to produce hydrogen*. Catalysis Communications, 2009. **10**(8): p. 1275-1278.
85. Hauserman, W.B., *High-yield hydrogen production by catalytic gasification of coal or biomass*. International journal of hydrogen energy, 1994. **19**(5): p. 413-419.
86. Sutton, D., et al., *Review of literature on catalysts for biomass gasification*. Fuel Processing Technology, 2001. **73**(3): p. 155-173.
87. Soares, R.R., et al., *Glycerol as a source for fuels and chemicals by low-temperature catalytic processing*. Angewandte Chemie (International ed.in English), 2006. **45**(24): p. 3982-3985.

88. Slinn, M., et al., *Steam reforming of biodiesel by-product to make renewable hydrogen*. Bioresource Technology, 2008. **99**(13): p. 5851-5858.
89. Sánchez, E.A., et al., *Hydrogen production from glycerol on Ni/Al₂O₃ catalyst*. International Journal of Hydrogen Energy, 2010. **35**(11): p. 5902-5907.
90. Chiodo, V., et al., *Catalytic features of Rh and Ni supported catalysts in the steam reforming of glycerol to produce hydrogen*. Applied Catalysis A: General, 2010. **381**(1–2): p. 1-7.
91. Profeti, L.P.R., et al., *Production of hydrogen via steam reforming of biofuels on Ni/CeO₂–Al₂O₃ catalysts promoted by noble metals*. International Journal of Hydrogen Energy, 2009. **34**(12): p. 5049-5060.
92. Adhikari, S., et al., *Hydrogen production from glycerin by steam reforming over nickel catalysts*. Renewable Energy, 2008. **33**(5): p. 1097-1100.
93. Rossetti, I., et al., *Nickel Catalysts Supported Over TiO₂, SiO₂ and ZrO₂ for the Steam Reforming of Glycerol*. ChemCatChem, 2013. **5**(1).
94. Cui, Y., et al., *Steam reforming of glycerol: The experimental activity of La_{1-x}Ce_xNiO₃ catalyst in comparison to the thermodynamic reaction equilibrium*. Applied Catalysis B: Environmental, 2009. **90**(1–2): p. 29-37.
95. Hirai, T., et al., *Production of Hydrogen by Steam Reforming of Glycerin on Ruthenium Catalyst*. Energy & Fuels, 2005. **19**(4): p. 1761-1762.
96. Kikuchi, R., et al., *Semi-pilot scale test for production of hydrogen-rich fuel gas from different wastes by means of a gasification and smelting process with oxygen multi-blowing*. Fuel Processing Technology, 2005. **86**(12–13): p. 1279-1296.
97. Mirodatos, C., H. Praliaud, and M. Primet, *Deactivation of nickel-based catalysts during CO methanation and disproportionation*. Journal of Catalysis, 1987. **107**(2): p. 275-287.
98. Zhang, Z., et al., *Carbon dioxide reforming of methane to synthesis gas over Ni/La₂O₃ catalysts*. Applied Catalysis A: General, 1996. **138**(1): p. 109-133.
99. Slagtern, A., et al., *Specific Features Concerning the Mechanism of Methane Reforming by Carbon Dioxide over Ni/La₂O₃Catalyst*. Journal of Catalysis, 1997. **172**(1): p. 118-126.
100. Miyazawa, T., et al., *Catalytic performance of supported Ni catalysts in partial oxidation and steam reforming of tar derived from the pyrolysis of wood biomass*. Catalysis Today, 2006. **115**(1): p. 254-262.
101. Inaba, M., et al., *Hydrogen Production by Gasification of Cellulose over Ni Catalysts Supported on Zeolites*. Energy & Fuels, 2006. **20**(2): p. 432-438.

102. Wu, C., et al., *Effect of Ni Particle Location within the Mesoporous MCM-41 Support for Hydrogen Production from the Catalytic Gasification of Biomass*. ACS Sustainable Chemistry & Engineering, 2013. **1**(9): p. 1083-1091.
103. Zhao, M., et al., *The influence of supported Ni catalysts on the product gas distribution and H₂ yield during cellulose pyrolysis*. Applied Catalysis B: Environmental, 2009. **92**(1): p. 185-193.
104. Simell, P.A., et al., *Effects of gasification gas components on tar and ammonia decomposition over hot gas cleanup catalysts*. Fuel, 1997. **76**(12): p. 1117-1127.
105. Venezia, A.M., *X-ray photoelectron spectroscopy (XPS) for catalysts characterization*. Catalysis Today, 2003. **77**(4): p. 359-370.
106. Lim, H.E., et al., *Growth of carbon nanotubes via twisted graphene nanoribbons*. Nat Commun, 2013. **4**.
107. Bokobza, L., et al., *Raman spectroscopic characterization of multiwall carbon nanotubes and of composites*. Express Polym. Lett, 2012. **6**(7): p. 601-608.
108. Giannakeas, N., et al., *Hydrogen from scrap tyre oil via steam reforming and chemical looping in a packed bed reactor*. Applied Catalysis B: Environmental, 2012. **126**(0): p. 249-257.
109. Iijima, S., *Helical microtubules of graphitic carbon*. nature, 1991. **354**(6348): p. 56-58.
110. De Volder, M.F., et al., *Carbon nanotubes: present and future commercial applications*. science, 2013. **339**(6119): p. 535-539.
111. Peng, B., et al., *Measurements of near-ultimate strength for multiwalled carbon nanotubes and irradiation-induced crosslinking improvements*. Nature nanotechnology, 2008. **3**(10): p. 626-631.
112. Wei, B., R., et al., *Reliability and current carrying capacity of carbon nanotubes*. Applied Physics Letters, 2001. **79**(8): p. 1172-1174.
113. Pop, E., et al., *Thermal conductance of an individual single-wall carbon nanotube above room temperature*. Nano letters, 2006. **6**(1): p. 96-100.
114. Michael F. L., D.V., *Carbon Nanotubes: Present and Future Commercial Applications*. Science, 2013, 339(6119), p.535-539.
115. Beigbeder, A., et al., *Preparation and characterisation of silicone-based coatings filled with carbon nanotubes and natural sepiolite and their application as marine fouling-release coatings*. Biofouling, 2008. **24**(4): p. 291-302.
116. Williams, P.T., et al., *The Batch Pyrolysis of Tyre Waste—Fuel Properties of the Derived Pyrolytic Oil and Overall Plant Economics*.

Proceedings of the Institution of Mechanical Engineers, Part A: Journal of Power and Energy, 1993. **207**(1): p. 55-63.

117. Martínez, J.D., et al., *Waste tyre pyrolysis – A review*. Renewable and Sustainable Energy Reviews, 2013. **23**(0): p. 179-213.

118. Sotowa, C., et al., *The Reinforcing Effect of Combined Carbon Nanotubes and Acetylene Blacks on the Positive Electrode of Lithium-Ion Batteries*. ChemSusChem, 2008. **1**(11): p. 911-915.

119. Evans, A.E.a.R., *The Composition of a Tyre: Typical Components*, 2006, The Waste & Resource Action Programme: Banbury.

120. Bauhofer, W., et al., *A review and analysis of electrical percolation in carbon nanotube polymer composites*. Composites Science and Technology, 2009. **69**(10): p. 1486-1498.

121. Chou, T.-W., et al., *An assessment of the science and technology of carbon nanotube-based fibers and composites*. Composites Science and Technology, 2010. **70**(1): p. 1-19.

122. Gojny, F., et al., *Carbon nanotube-reinforced epoxy-composites: enhanced stiffness and fracture toughness at low nanotube content*. Composites science and technology, 2004. **64**(15): p. 2363-2371.

123. Kashiwagi, T., et al., *Nanoparticle networks reduce the flammability of polymer nanocomposites*. Nature materials, 2005. **4**(12): p. 928-933.

124. Bakshi, S.R., et al., *An analysis of the factors affecting strengthening in carbon nanotube reinforced aluminum composites*. Carbon, 2011. **49**(2): p. 533-544.

125. Wu, Z., et al., *Transparent, conductive carbon nanotube films*. Science, 2004. **305**(5688): p. 1273-1276.

126. De, S., et al., *The effects of percolation in nanostructured transparent conductors*. Mrs Bulletin, 2011. **36**(10): p. 774-781.

127. Dai, L., et al., *Carbon nanomaterials: carbon nanomaterials for advanced energy conversion and storage (Small 8/2012)*. Small, 2012. **8**(8): p. 1122-1122.

128. Evanoff, K., et al., *Towards ultrathick battery electrodes: Aligned carbon nanotube-enabled architecture*. Advanced Materials, 2012. **24**(4): p. 533-537.

129. Matsumoto, T., et al., *Reduction of Pt usage in fuel cell electrocatalysts with carbon nanotube electrodes*. Chemical Communications, 2004(7): p. 840-841.

130. Le Goff, A., et al., *From hydrogenases to noble metal-free catalytic nanomaterials for H₂ production and uptake*. Science, 2009. **326**(5958): p. 1384-1387.

131. Gong, K., et al., *Nitrogen-doped carbon nanotube arrays with high electrocatalytic activity for oxygen reduction*. *science*, 2009. **323**(5915): p. 760-764.
132. Bazargan, A., et al., *A review–Synthesis of carbon nanotubes from plastic wastes*. *Chemical engineering journal*, 2012. **195**: p. 377-391.
133. Liu, W.-W., et al., *Synthesis and characterization of graphene and carbon nanotubes: a review on the past and recent developments*. *Journal of Industrial and Engineering Chemistry*, 2014. **20**(4): p. 1171-1185.
134. Petit, P.N.H.D.P., et al.. *Crystalline ropes of metallic carbon nanotubes*. *Science*, 1996. **273**: p. 483-487.
135. Dasgupta, K., et al., *Fluidized bed synthesis of carbon nanotubes – A review*. *Chemical Engineering Journal*, 2011. **171**(3): p. 841-869.
136. Boellaard, E., et al., *The formation of filamentous carbon on iron and nickel catalysts*. *Journal of Catalysis*, 1985. **96**(2): p. 481-490.
137. Rodriguez, N.M., et al., *Promotional Effect of Carbon Monoxide on the Decomposition of Ethylene over an Iron Catalyst*. *Journal of Catalysis*, 1993. **144**(1): p. 93-108.
138. Boehm, H., *Carbon from carbon monoxide disproportionation on nickel and iron catalysts: Morphological studies and possible growth mechanisms*. *Carbon*, 1973. **11**(6): p. 583IN1587-586IN5590.
139. Behabtu, N., et al., *Strong, light, multifunctional fibers of carbon nanotubes with ultrahigh conductivity*. *science*, 2013. **339**(6116): p. 182-186.
140. Kumar, M., et al., *Chemical vapor deposition of carbon nanotubes: a review on growth mechanism and mass production*. *Journal of nanoscience and nanotechnology*, 2010. **10**(6): p. 3739-3758.
141. Mui, E.L.K., et al., *Kinetic Modeling of Waste Tire Carbonization*. *Energy & Fuels*, 2008. **22**(3): p. 1650-1657.
142. Ebbesen, T., et al., *Purification of nanotubes*. *Nature*, 1994. **367**(6463): p. 519-519.
143. Xu, Y.-Q., et al., *Controlled multistep purification of single-walled carbon nanotubes*. *Nano Letters*, 2005. **5**(1): p. 163-168.
144. Moon, J.-M., et al., *High-yield purification process of singlewalled carbon nanotubes*. *The Journal of physical chemistry B*, 2001. **105**(24): p. 5677-5681.
145. Tessonnier, J.P., et al., *Recent progress on the growth mechanism of carbon nanotubes: a review*. *ChemSusChem*, 2011. **4**(7): p. 824-847.

146. Rinaldi, A., et al., *Dissolved carbon controls the initial stages of nanocarbon growth*. *Angewandte Chemie International Edition*, 2011. **50**(14): p. 3313-3317.
147. Baker, R.T.K., et al., *Nucleation and growth of carbon deposits from the nickel catalyzed decomposition of acetylene*. *Journal of Catalysis*, 1972. **26**(1): p. 51-62.
148. Baker, R., et al., *Formation of filamentous carbon from iron, cobalt and chromium catalyzed decomposition of acetylene*. *Journal of catalysis*, 1973. **30**(1): p. 86-95.
149. Mortola, V.B., et al., *Surface and structural features of Pt/CeO₂-La₂O₃-Al₂O₃ catalysts for partial oxidation and steam reforming of methane*. *Applied Catalysis B: Environmental*, 2011. **107**(3-4): p. 221-236.
150. Nishikawa, J., et al., *Catalytic performance of Ni/CeO₂/Al₂O₃ modified with noble metals in steam gasification of biomass*. *Catalysis Today*, 2008. **131**(1-4): p. 146-155.
151. Hernadi, K., et al., *Fe-catalyzed carbon nanotube formation*. *Carbon*, 1996. **34**(10): p. 1249-1257.
152. Kong, J., et al., *Chemical vapor deposition of methane for single-walled carbon nanotubes*. *Chemical Physics Letters*, 1998. **292**(4-6): p. 567-574.
153. Fan, S., et al., *Self-Oriented Regular Arrays of Carbon Nanotubes and Their Field Emission Properties*. *Science*, 1999. **283**(5401): p. 512-514.
154. Satishkumar, B.C., et al., *Bundles of aligned carbon nanotubes obtained by the pyrolysis of ferrocene-hydrocarbon mixtures: role of the metal nanoparticles produced in situ*. *Chemical Physics Letters*, 1999. **307**(3-4): p. 158-162.
155. Li, W.Z., et al., *Large-Scale Synthesis of Aligned Carbon Nanotubes*. *Science*, 1996. **274**(5293): p. 1701-1703.
156. Sen, R., et al., *Carbon nanotubes by the metallocene route*. *Chemical Physics Letters*, 1997. **267**(3): p. 276-280.
157. Wei, B.Q., et al., *Microfabrication technology: Organized assembly of carbon nanotubes*. *Nature*, 2002. **416**(6880): p. 495-496.
158. Nikolaev, P., et al., *Gas-phase catalytic growth of single-walled carbon nanotubes from carbon monoxide*. *Chemical Physics Letters*, 1999. **313**(1-2): p. 91-97.
159. Weidenkaff, A., et al., *Metal nanoparticles for the production of carbon nanotube composite materials by decomposition of different carbon sources*. *Materials Science and Engineering: C*, 2002. **19**(1-2): p. 119-123.

160. Venegoni, D., et al., *Parametric study for the growth of carbon nanotubes by catalytic chemical vapor deposition in a fluidized bed reactor*. Carbon, 2002. **40**(10): p. 1799-1807.
161. Morançais, A., et al., *A parametric study of the large scale production of multi-walled carbon nanotubes by fluidized bed catalytic chemical vapor deposition*. Carbon, 2007. **45**(3): p. 624-635.
162. Philippe, R., et al., *An original growth mode of MWCNTs on alumina supported iron catalysts*. Journal of Catalysis, 2009. **263**(2): p. 345-358.
163. Li, Q., et al., *Sustained growth of ultralong carbon nanotube arrays for fiber spinning*. Advanced Materials, 2006. **18**(23): p. 3160-3163.
164. See, C.H., et al., *On the Development of Fluidized Bed Chemical Vapour Deposition for Large-Scale Carbon Nanotube Synthesis: Influence of Synthesis Temperature*. Australian Journal of Chemistry, 2007. **60**(7): p. 541-546.
165. See, C.H., et al., *Process Parameter Interaction Effects during Carbon Nanotube Synthesis in Fluidized Beds*. Industrial & Engineering Chemistry Research, 2008. **47**(20): p. 7686-7692.
166. Qian, W., et al., *Enhanced production of carbon nanotubes: combination of catalyst reduction and methane decomposition*. Applied Catalysis A: General, 2004. **258**(1): p. 121-124.
167. Wei, Y., et al., *Effect of catalyst film thickness on carbon nanotube growth by selective area chemical vapor deposition*. Applied Physics Letters, 2001. **78**(10): p. 1394-1396.
168. Fang, W., et al., *Ce-Ni mixed oxide as efficient catalyst for H₂ production and nanofibrous carbon material from ethanol in the presence of water*. RSC Advances, 2012. **2**(25): p. 9626-9634.
169. Li, W., et al., *Effect of temperature on growth and structure of carbon nanotubes by chemical vapor deposition*. Applied Physics A, 2002. **74**(3): p. 397-402.
170. Moisala, A., et al., *The role of metal nanoparticles in the catalytic production of single-walled carbon nanotubes—a review*. Journal of Physics: condensed matter, 2003. **15**(42): p. S3011.
171. Kong, J., et al., *Chemical vapor deposition of methane for single-walled carbon nanotubes*. Chemical Physics Letters, 1998. **292**(4): p. 567-574.
172. Liu, Z.-J., et al., *Preparation of Fe-filled carbon nanotubes by catalytic decomposition of cyclohexane*. Synthetic Metals, 2002. **128**(2): p. 191-195.
173. Li, N., et al., *The Catalytic Synthesis of Three-Dimensional Hierarchical Carbon Nanotube Composites with High Electrical Conductivity Based on Electrochemical Iron Deposition*. Advanced Materials, 2007. **19**(19): p. 2957-2960.

174. Nerushev, O.A., et al., *Particle size dependence and model for iron-catalyzed growth of carbon nanotubes by thermal chemical vapor deposition*. Journal of Applied Physics, 2003. **93**(7): p. 4185-4190.
175. Morjan, R.E., et al., *Growth of carbon nanotubes from C60*. Applied Physics A, 2004. **78**(3): p. 253-261.
176. Andrews, R., et al., *Continuous production of aligned carbon nanotubes: a step closer to commercial realization*. Chemical Physics Letters, 1999. **303**(5–6): p. 467-474.
177. Kumar, M., et al., *A simple method of producing aligned carbon nanotubes from an unconventional precursor – Camphor*. Chemical Physics Letters, 2003. **374**(5–6): p. 521-526.
178. Hata, K., et al., *Water-Assisted Highly Efficient Synthesis of Impurity-Free Single-Walled Carbon Nanotubes*. Science, 2004. **306**(5700): p. 1362-1364.
179. Kumar, M., et al., *Field emission from camphor-pyrolyzed carbon nanotubes*. Chemical Physics Letters, 2004. **385**(3–4): p. 161-165.
180. Ding, D., et al., *Synthesis of carbon nanostructures on nanocrystalline Ni-Ni₃P catalyst supported by SiC whiskers*. Carbon, 2003. **41**(3): p. 579-582.
181. Murakami, T., et al., *Raman study of SWNTs grown by CCVD method on SiC*. Thin Solid Films, 2004. **464–465**: p. 319-322.
182. Kitiyanan, B., et al., *Controlled production of single-wall carbon nanotubes by catalytic decomposition of CO on bimetallic Co-Mo catalysts*. Chemical Physics Letters, 2000. **317**(3–5): p. 497-503.
183. Mattevi, C., et al., *In-situ X-ray Photoelectron Spectroscopy Study of Catalyst-Support Interactions and Growth of Carbon Nanotube Forests*. The Journal of Physical Chemistry C, 2008. **112**(32): p. 12207-12213.
184. Cheung, C.L., et al., *Diameter-Controlled Synthesis of Carbon Nanotubes*. The Journal of Physical Chemistry B, 2002. **106**(10): p. 2429-2433.
185. Hongo, H., et al., *Chemical vapor deposition of single-wall carbon nanotubes on iron-film-coated sapphire substrates*. Chemical Physics Letters, 2002. **361**(3–4): p. 349-354.
186. Willems, I., et al., *Control of the outer diameter of thin carbon nanotubes synthesized by catalytic decomposition of hydrocarbons*. Chemical Physics Letters, 2000. **317**(1–2): p. 71-76.
187. Kumar, M., et al., *Controlling the diameter distribution of carbon nanotubes grown from camphor on a zeolite support*. Carbon, 2005. **43**(3): p. 533-540.

188. Couteau, E., et al., *CVD synthesis of high-purity multiwalled carbon nanotubes using CaCO₃ catalyst support for large-scale production*. Chemical Physics Letters, 2003. **378**(1–2): p. 9-17.
189. Colomer, J.F., et al., *Large-scale synthesis of single-wall carbon nanotubes by catalytic chemical vapor deposition (CCVD) method*. Chemical Physics Letters, 2000. **317**(1–2): p. 83-89.
190. Ward, J.W., et al., Ajayan, *Substrate effects on the growth of carbon nanotubes by thermal decomposition of methane*. Chemical Physics Letters, 2003. **376**(5–6): p. 717-725.
191. Ago, H., et al., *Growth of double-wall carbon nanotubes with diameter-controlled iron oxide nanoparticles supported on MgO*. Chemical Physics Letters, 2004. **391**(4–6): p. 308-313.
192. Nagaraju, N., et al., *Alumina and silica supported metal catalysts for the production of carbon nanotubes*. Journal of Molecular Catalysis A: Chemical, 2002. **181**(1–2): p. 57-62.
193. Busca, G., et al., *Nickel versus cobalt catalysts for hydrogen production by ethanol steam reforming: Ni–Co–Zn–Al catalysts from hydrotalcite-like precursors*. International Journal of Hydrogen Energy, 2010. **35**(11): p. 5356-5366.
194. Alves, J.O., et al., *Synthesis of nanomaterials from unserviceable tires*. Carbon, 2012. **85**(87.4): p. 82.2.
195. Sano, N., et al., *A simple oxidation–reduction process for the activation of a stainless steel surface to synthesize multi-walled carbon nanotubes and its application to phenol degradation in water*. Carbon, 2012. **50**(1): p. 115-122.
196. Amadou, J., et al., *Synthesis of a carbon nanotube monolith with controlled macroscopic shape*. Carbon, 2006. **44**(12): p. 2587-2589.
197. Vander Wal, R.L. and L.J. Hall, *Carbon nanotube synthesis upon stainless steel meshes*. Carbon, 2003. **41**(4): p. 659-672.
198. Zhou, J.-H., et al., *Structural characterization of carbon nanofibers formed from different carbon-containing gases*. Carbon, 2006. **44**(15): p. 3255-3262.
199. Zhao, T., et al., A. Holmen. *Rational design of carbon nanofibres catalysts for oxidative dehydrogenation of ethylbenzene*, Appl. Catal. A: Gen, 2007. **323**(0): p. 135-146.
200. Magrez, A., et al., *Low-temperature, highly efficient growth of carbon nanotubes on functional materials by an oxidative dehydrogenation reaction*. Acs Nano, 2010. **4**(7): p. 3702-3708.

201. Zhang, Y., et al., *Ethanol-promoted high-yield growth of few-walled carbon nanotubes*. The Journal of Physical Chemistry C, 2010. **114**(14): p. 6389-6395.
202. Motta, M., et al., *The role of sulphur in the synthesis of carbon nanotubes by chemical vapour deposition at high temperatures*. Journal of nanoscience and nanotechnology, 2008. **8**(5): p. 2442-2449.
203. Trimm, D.L., *Coke formation and minimisation during steam reforming reactions*. Catalysis Today, 1997. **37**(3): p. 233-238.
204. La Cava, A.I., et al., *Studies of deactivation of metals by carbon deposition*. Carbon, 1982. **20**(3): p. 219-223.
205. Borowiecki, T., *Nickel catalysts for steam reforming of hydrocarbons; size of crystallites and resistance to coking*. Applied Catalysis, 1982. **4**(3): p. 223-231.
206. Wu, C., et al., *Investigation of coke formation on Ni-Mg-Al catalyst for hydrogen production from the catalytic steam pyrolysis-gasification of polypropylene*. Applied Catalysis B: Environmental, 2010. **96**(1–2): p. 198-207.
207. Das, N., et al., *The effect of feedstock and process conditions on the synthesis of high purity CNTs from aromatic hydrocarbons*. Carbon, 2006. **44**(11): p. 2236-2245.
208. Ago, H., et al., *Gas analysis of the CVD process for high yield growth of carbon nanotubes over metal-supported catalysts*. Carbon, 2006. **44**(14): p. 2912-2918.
209. Yang, W., et al., *Synthesis of carbon nanotubes using scrap tyre rubber as carbon source*. Chinese Chemical Letters, 2012. **23**(3): p. 363-366.
210. Wu, C., et al., *Sustainable processing of waste plastics to produce high yield hydrogen-rich synthesis gas and high quality carbon nanotubes*. RSC Advances, 2012. **2**(10): p. 4045-4047.
211. Kukovitskii, E.F., et al., *Carbon nanotubes of polyethylene*. Chemical Physics Letters, 1997. **266**(3–4): p. 323-328.
212. Liu, J., et al., *Catalytic pyrolysis of polypropylene to synthesize carbon nanotubes and hydrogen through a two-stage process*. Polymer Degradation and Stability, 2011. **96**(10): p. 1711-1719.
213. Acomb, J.C., et al., *The use of different metal catalysts for the simultaneous production of carbon nanotubes and hydrogen from pyrolysis of plastic feedstocks*. Applied Catalysis B: Environmental, 2016. **180**: p. 497-510.
214. Hao, Y., et al., *Agglomerated CNTs synthesized in a fluidized bed reactor: Agglomerate structure and formation mechanism*. Carbon, 2003. **41**(14): p. 2855-2863.

215. Elbaba, I.F., et al., *High yield hydrogen from the pyrolysis–catalytic gasification of waste tyres with a nickel/dolomite catalyst*. *Fuel*, 2013. **106**(0): p. 528-536.
216. Murr, L.E., et al., *Carbon nanotubes and other fullerenes produced from tire powder injected into an electric arc*. *Materials Characterization*, 2005. **55**(4): p. 371-377.
217. Poyraz, S., et al., *Devulcanization of scrap ground tire rubber and successive carbon nanotube growth by microwave irradiation*. *Current Organic Chemistry*, 2013. **17**(20): p. 2243-2248.
218. Wu, C., et al., *Hydrogen production by steam gasification of polypropylene with various nickel catalysts*. *Applied Catalysis B: Environmental*, 2009. **87**(3–4): p. 152-161.
219. Wang, C.-q., et al., *Flotation separation of waste plastics for recycling—A review*. *Waste Management*, 2015. **41**: p. 28-38.
220. Park, H.J., et al., *Steam reforming of biomass gasification tar using benzene as a model compound over various Ni supported metal oxide catalysts*. *Bioresource Technology*, 2010. **101**(1): p. S101-S103.
221. Shivakumara, P., et al., *A laplacian approach to multi-oriented text detection in video*. *Pattern Analysis and Machine Intelligence*, *IEEE Transactions on*, 2011. **33**(2): p. 412-419.
222. Blanco, P.H., et al., *Catalytic pyrolysis/gasification of refuse derived fuel for hydrogen production and tar reduction: influence of nickel to citric acid ratio using Ni/SiO₂ catalysts*. *Waste and Biomass Valorization*, 2014. **5**(4): p. 625-636.

Chapter 3. Materials and methodology

3.1 Materials

Both tyres and plastics are polymeric materials. The chemical structures of the polymer molecule are normally a linear or branched chain or a network with peripheral atoms or atom groups. Every polymer structure consists of a summation of structural groups, which include hydrocarbon groups and functional groups (such as $-\text{COOH}$ and $-\text{CONH}_2$). The polymer structures terminated with different functional groups are playing an important role in their chemical properties but not on the physical properties [1].

3.1.1 Waste tyres

Single type of tyre sample was used for investigation. The waste tyre sample used in the experiment was shredded waste truck and car tyres as shown in Figure 3-1. The sample was prepared by removing the steel and shredding into same size particles (diameter is approximately 6 mm for waste truck tyre and 1 mm for waste car tyre). The ultimate analysis was carried out to obtain the nitrogen (N), carbon (C), hydrogen (H), oxygen (O) and sulphur (S) compositions in the raw material. The ultimate analysis of two types of tyres and three types of rubbers are shown in Table 3-1, which were carried out with a CHNS/O elemental analyser (CE Instruments Wigan, UK, FLASH EA2000 CHNS-O analyser).



Figure 3-1 Waste truck (left) and car tyres (right) samples

For CHNS determination, an autosampler is connected to a quartz tube placed in a furnace at the temperature of 900 °C. This reactor is connected to the analytical column, which is connected to a channel of the thermal conductivity detector (TCD). Oxygen is determined by a second autosampler which is connected to another reactor placed in a furnace at the temperature of 1060 °C. An adsorption filter is connected to the reactor outlet connected to second TCD.

Table 3-1 Elemental analysis of Truck tyre, car tyre, BR, SBR, and NR

Components (wt.%)	Truck tyre	Car tyre	NR	BR	SBR
C	81.16	81.72	86.26	87.37	87.02
H	7.17	6.54	11.22	10.69	9.96
N	0.83	0.55	not detected	not detected	not detected
S	2.08	1.87	not detected	not detected	not detected
Zn	71.8	71.6	not detected	not detected	not detected
Fe	6.58	6.4	not detected	not detected	not detected
Ca	2.71	2.92	not detected	not detected	not detected
Cu	1.13	1.08	not detected	not detected	not detected

The three pure elastomers used in the experiments in section 5.1 are the main components used in the production of tyres which are natural rubber (NR), styrene butadiene rubber (SBR) and butadiene rubber (BR) purchased from Accrington Rubber Limited UK. The NR, BR and SBR are macromolecular compounds.

The rubber samples were cut into irregular shapes that could fit in the sample crucible of the reactor at around 5 mm. The mineral compositions of different raw materials are shown in Table 3-1, which were carried out using an Rigaku Primus 2 X-Ray fluorescence spectrometer. The basic principle for using this X-Ray fluorescence spectrometer is based on the secondary X-rays from the samples which is also called “fluorescence”. The method measures the wavelength and intensity of fluorescence emitted by energized atoms in the sample with discrete energies characteristic of the elements present in the sample. The preparation of samples before analysis included grinding the sample into fine powder of less than 100 μm by a cryomill before making pressed pellets. The sample pellets were made by filling the powdered samples in a die.

3.1.2 Tyre pyrolysis oil model compounds

Tyre pyrolysis oil is a medium viscosity oil of dark brown/black colour with sulphurous/aromatic odour which contains over 100 compounds that are aliphatic, aromatic, heteroatom and polar fractions [2]. Dai et al. [3] analysed the waste tyre pyrolysis oil produced by a circulating fluidized bed reactor and reported 26.77 wt.% of alkanes, 42.09 wt.% of aromatics, 26.64 wt. % of non-hydrocarbons and 4.05 wt.% of asphalt. Aylon et al. [4] tested the tyre pyrolysis oil produced from a screw kiln reactor at 600 °C which contained 6.7 wt. % of alkane, 65.6 wt.% of aromatics and 27.8 wt.% of polar fraction.

All five model compounds used in this research represented a typical tyre pyrolysis oil components and were all purchased from Sigma-Aldrich: two aliphatic compounds including hexadecane ($\text{C}_{16}\text{H}_{34}$) and decane ($\text{C}_{10}\text{H}_{22}$); one single ring aromatic compound styrene (C_8H_8); and two polycyclic aromatic hydrocarbons (PAHs) including naphthalene (C_{10}H_8) and phenanthrene ($\text{C}_{14}\text{H}_{10}$) [2]. The commercial carbon nanofibers with 98 % carbon basis, diameter in 100 nm and length from 20 to 200 μm . Commercial multi-walled carbon nanotubes with 98 % carbon basis, diameter in a range of 6 to 13 nm and length from 2.5 to 20 μm . These two commercial carbon samples were purchased from Sigma-

Aldrich. The commercial carbon samples were used to compare the quality and morphology of carbon produced in the research (section 5.2).

3.1.3 Plastics samples

3.1.3.1 Individual plastics composition of simulated mixed waste plastics

High-density polyethylene (HDPE), polypropylene (PP) and polystyrene (PS) were obtained from Regain Polymers Limited, Castleford, UK and were all recycled waste polymers. Low-density polyethylene (LDPE) and polyethylene terephthalate (PET) were purchased from Sigma-Aldrich. All of the plastic samples are shown in

Figure 3-2. The simulated mixed waste plastics (SMWP) was a mixture of pure plastic pellets with 2-3 mm diameters, the SMWP contained 42 wt. % of LDPE, 20 wt. % of HDPE, 16 wt. % of PS, 12 wt. % of PET and 10 wt. % of PP, which is the plastics composition which represents municipal solid waste plastic as reported by Delgado et al. [5]. They summarized the simulated mixture of waste plastics compositions based on the municipal waste plastic in Europe which are mostly from packaging, various housewares, disposable items and cases for electronics. The authors also listed the plastics fractions in the residual municipal solid waste, which LDPE is in a fraction range 38-43 wt.%, HDPE 15-20 wt.%, PS 1-17 wt.%, PET 7-12 wt.% and PP 5-10 wt.%.



Figure 3-2 Plastic samples (From left to right: HDPE, LDPE, PS, PET and PP).

3.1.3.2 Real world waste plastics

Seven types of real world waste plastic samples were collected from several municipal waste treatment plants have been investigated in Chapter 6.3. The plastic samples include mixed plastics from agricultural waste, mixed plastics from detergent containers, mixed plastics from vehicle fuel tanks, mixed plastics from mineral water containers, mixed plastics from motor oil flasks, mixed plastics from household waste packagings and mixed plastics from building re-construction sites. All of these seven real world plastic samples were supplied from the University of Pannonia, Hungary. The plastic samples were cut into small pieces at around 3 to 10 mm in irregular shapes as shown in Figure 3-3.

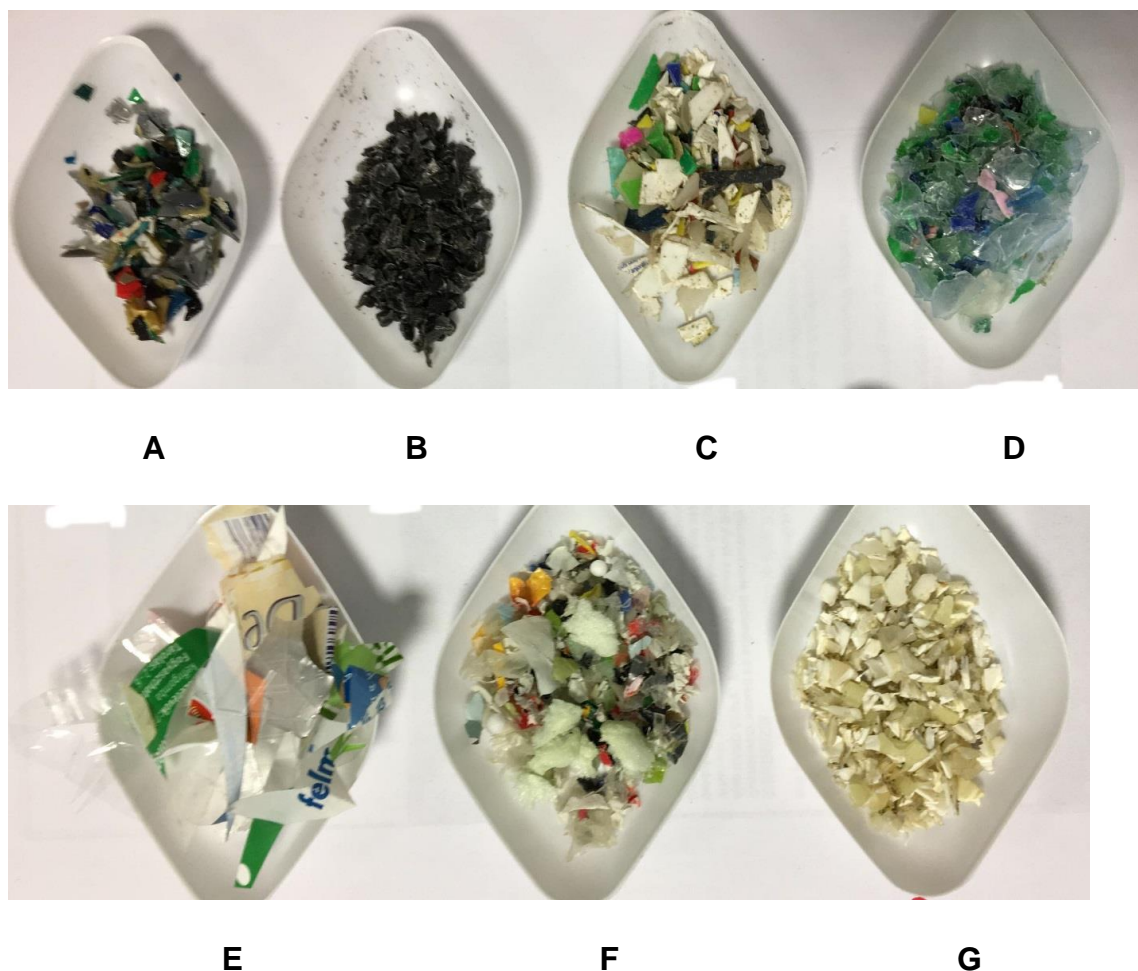


Figure 3-3 Real world waste plastics (A: Plastics from motor oil flasks; B: Plastics from vehicle fuel tank; C: Plastics from detergent containers; D: Mineral water containers plastics; E: Household food packaging plastics; F: Plastics from building re-construction; G: Waste plastics from agriculture).

3.1.4 Catalysts preparation

3.1.4.1 Ni-, Cu-, Co-, and Fe/Al₂O₃ catalysts

The Fe/Al₂O₃, Cu/Al₂O₃, Co/Al₂O₃ and Ni/Al₂O₃ catalysts were prepared by an incipient wetness method. Different metals were impregnated onto an alumina support to produce 10 wt.% of metal catalyst with alumina support. Firstly, the metal nitrates were dissolved in ethanol individually (5.68 g of nickel nitrates, 4.18 g of copper nitrates, 4.48 g of cobalt nitrate and 8.44 g of iron nitrates). Then, 10 g of α -alumina powder was added into the mixture of metal nitrates and ethanol until it became a slurry. The second step involves leaving the slurry in an oven at 50 °C until all of the excess ethanol is evaporated. The third step is to calcine at 750 °C in an air atmosphere with a heating rate is 2 °C min⁻¹ and hold for 3 hours. The final step is crushing and sieving the catalyst into the size range between 0.05 to 0.18 mm.

3.1.4.2 Ni/Al₂O₃/SiO₂ catalysts

The catalysts used in the experiments were 20 wt. % Ni/Al₂O₃/SiO₂ catalysts with 4 different Al₂O₃ to SiO₂ mole ratios (3:5, 1:1, 3:2, 2:1). The catalysts were synthesized by an incipient wetness method. 20 wt. % of Ni was impregnated onto the alumina-silica mixture support that was prepared by a sol-gel method. The 20 wt. % of Ni impregnation was obtained by dissolving the certain amount of nickel nitrates into ethanol. Silica and aluminium isopropoxide were purchased from Sigma-Aldrich which were the precursors for the silica and alumina.

The procedure for silica and alumina support prepared by the sol-gel method started with mixing the calculated amounts of SiO₂ powder and aluminium isopropoxide (Al(O₃H₇)₃) powder with distilled water. Then filter the solution with distilled water to form Al(OH)₃-SiO₂. For preparing the support with different Al₂O₃:SiO₂ ratios, the calculations are listed in Table 3-2. The obtained Al(OH)₃-SiO₂ mixtures was aged in air overnight and kept in an oven at 40 °C for one day. Finally, the dry solids were ground into fine powder for nickel impregnation preparation step.

Table 3-2 The calculations for preparing the alumina-silica catalyst support with different alumina to silica ratios.

Al ₂ O ₃ :SiO ₂	Al(OC ₃ H ₇) ₃ (g)	SiO ₂ (g)
1:1	13.6	2
2:1	27.2	2
3:2	10.2	1
3:5	12.24	3

The impregnation process starts with dissolving the calculated amount of nickel nitrates into ethanol. The catalyst support was then added with continuous stirring until the mixture becomes a slurry. The slurry was dried in an oven overnight to evaporate all of the moisture and residue ethanol. The last step was to calcine the dry solids at 750 °C in an air atmosphere with a heating rate of 2 °C min⁻¹ and holding time of 3 hours.

3.1.4.3 Fe/Ni/MCM-41 catalysts

The Fe-Ni/MCM-41 catalysts with Fe to Ni ratios 00:20, 05:15, 10:10, 15:05 and 20:00 were investigated to find out the effects of Fe to Ni ratio on both hydrogen and carbon nanotube productions from SMWP by pyrolysis-catalytic reforming. The Fe-Ni/MCM-41 catalysts with different Fe to Ni ratios were synthesised by an impregnation method [6]; The required calculated amounts of iron nitrate and nickel nitrate were dissolved into ethanol to form a solution; MCM-41 powder was synthesised according to the method reported by Cheng et al. [7] and was added into the solution, and continuously stirred for 2 hours until the mixture became a slurry; The slurry was dried overnight at 80 °C and the solid was calcined in a muffle furnace heated at 1 °C min⁻¹ ramp rate to a final temperature of 550 °C and held at that temperature for 4 hours in the presence of static air. Finally, Fe-Ni/MCM-41 catalysts with Fe to Ni ratios of 00:20, 05:15, 10:10, 15:05 and 20:00 were prepared.

3.1.4.4 Ni-stainless steel mesh catalysts

The stainless steel (SS) mesh purchased from Alfa Aesar was pre-treated by immersing the mesh into concentrated HNO₃ acid for about 30 mins, washed

with de-ionized water, followed by drying at 100 °C for 3h and calcination at 800 °C for 3h with a heating rate of 10 °C min⁻¹ in a static air atmosphere. For the loading of Ni on the pre-treated stainless steel mesh (SS), 10 mml of NiCl₂, 40 ml ammonia solution and 20 ml water were mixed for half hour in a petri dish with a cover. The SS mesh was added to the above solution, and the precursor was kept in a drying oven at 90 °C for about 12 h. Then, the SS mesh with Ni were washed with de-ionized water and dried at 105 °C for about 5 h. A calcination of the Ni/SS precursors was followed at 900 °C for 3 h with a heating rate of 2 °C min⁻¹. Figure 3-4 is the image and SEM micrographs of the NiSS catalysts.

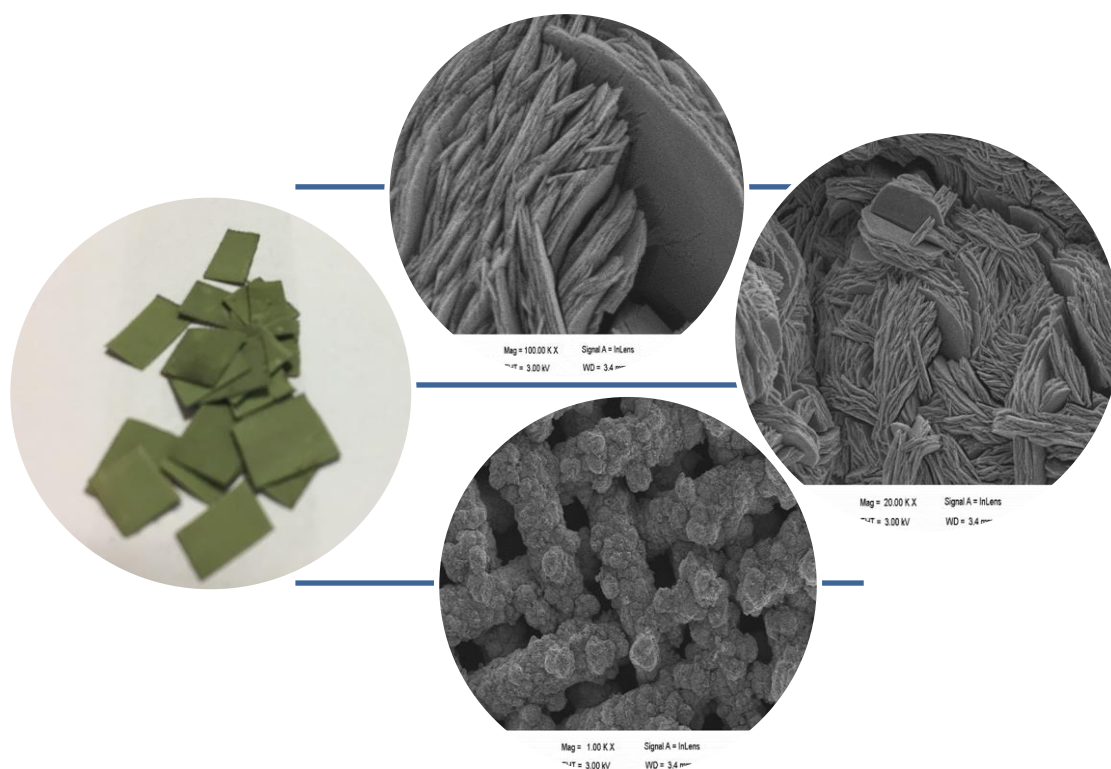


Figure 3-4 Ni on the pre-treated stainless steel mesh (NiSS) catalysts with scanning electron micrographs.

3.2 Reaction system and reproducibility of products

3.2.1 Two-stage fixed-bed reactor

A schematic diagram of the two-stage fixed-bed reactor is shown in Figure 3-5 which was used in the experiment for the pyrolysis catalysis/catalytic-reforming which consists of first and second stages. The reactor for both stages was constructed of stainless steel with a diameter of 2.2 cm and a height of 16 cm. Two thermocouples were set up on the two stages individually to independently measure and control temperature in each of the two stages. Pyrolysis of waste tyres occurred in the first stage at 600 °C and waste plastics at 500 °C. The volatiles and hot gases products pass to the second stage, where it was reacted at temperatures of 700, 800 or 900 °C. The nitrogen inlet was from the top of the first furnace at a fixed rate 80 ml min⁻¹, and gas outlet is at the bottom of the second stage. The second stage is preheated at the targeted temperature before the first stage starts to be heated up to the target temperatures. The water injection rate was controlled by using a syringer and a pump.

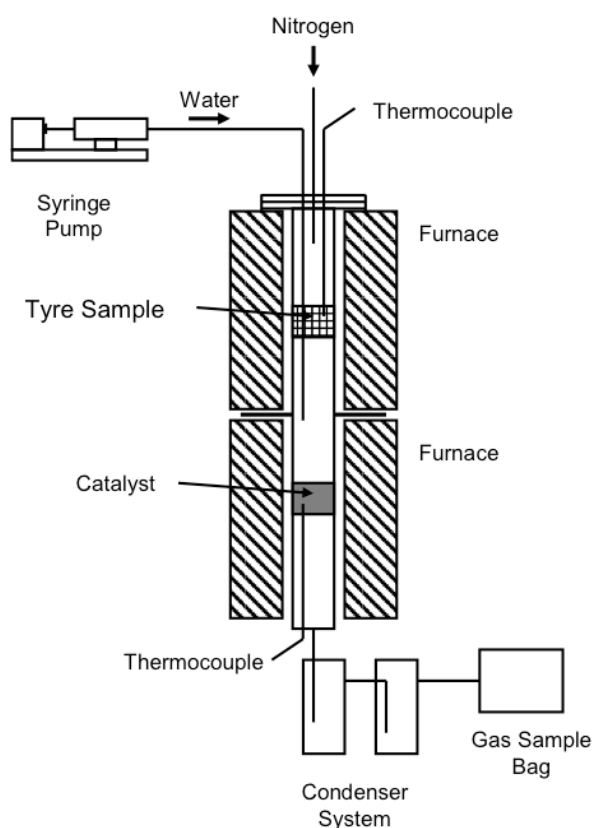


Figure 3-5 Schematic diagram of two-stage fixed-bed reaction system [8]

The second stage involves the reaction of pyrolysis-catalytic reforming or catalysis of the pyrolysis products. The carbon materials are produced on the surface of the catalyst. Reduction of the catalyst occurred in-situ by the generated process gases, particularly hydrogen and carbon monoxide. This has been supported by the XRD results in Figure 3-7, which shows the XRD spectra for the used Fe/Ni/MCM-41 catalysts after the pyrolysis-catalytic reforming process of the simulated mixed waste plastics. The results confirm that the catalysts were reduced from the metal oxide phases to the elemental metal within the initial stages of the process by the product H₂ and CO produced during the process. The gaseous products of reforming were passed to two condensers to trap the condensable products. The collected product in the first condenser were liquid products which were air-cooled at room temperature while in the second condenser those with lower condensation points were dry-ice cooled at temperature -78.5 °C. The uncondensed gases which remained in the gas stream were collected in a 25L Tedlar™ gas bag. The entire reaction system is shown in Figure 3-6.

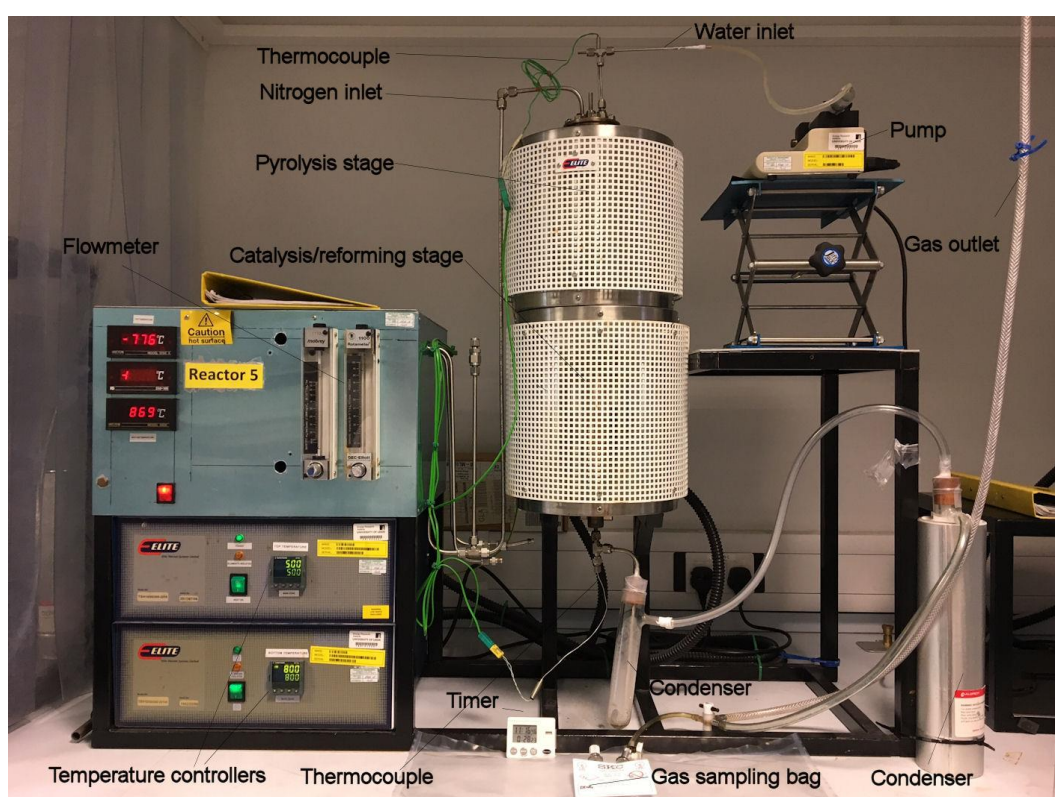


Figure 3-6 Two-stage fixed-bed reaction system for pyrolysis catalysis/catalytic-gasification experiments.

After each experiment, the mass balance was determined; the mass of tyre char residue was calculated from the mass of the pyrolysis stage sample crucible before and after the experiment; the mass of condensable oils was determined from the mass of all the condensers before and after experiments; the mass of gas was calculated from the gas chromatography analysis of the gases, together with the measured flow rate and molecular mass of each gas; the amount of carbon deposits on the catalyst were determined from temperature programmed oxidation (TPO) of the used catalyst or the weight difference of the reactor tube before and after the experiment. Repeated experiments were carried out to confirm the accuracy of the experimental results.

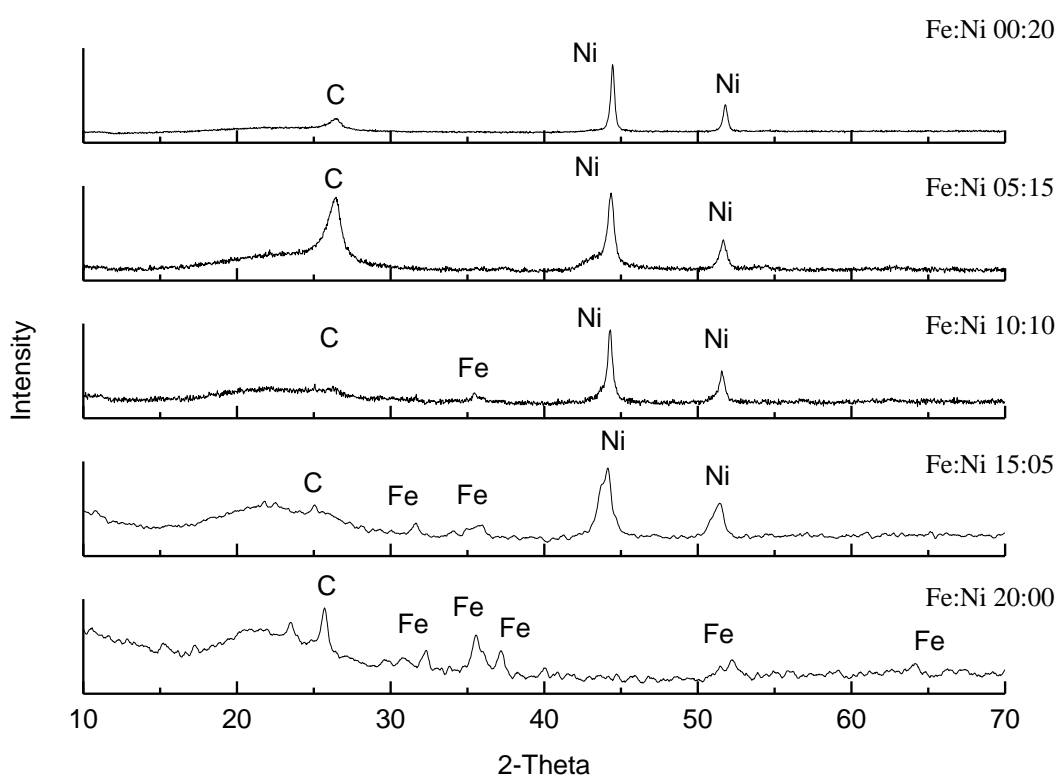


Figure 3-7 XRD analysis of the used Fe-Ni-MCM-41 catalysts from the pyrolysis-catalytic reforming of simulated mixed waste plastics with different Fe:Ni ratios (00:20, 05:15, 10:10, 15:05, 20:00). The Ni peaks at 44 and 52 2-Theta indicate the stable face centred cubic phase. The iron peaks indicate the α - Fe or iron carbide.

3.2.2 Reproducibility of products by pyrolysis-catalysis with two-stage fixed-bed reactor

The pyrolysis catalysis/catalytic-reforming experiments were carried out using the two-stage fixed-bed reactor as shown in Figure 3-6. The system was tested by repeating the experiments at the same condition for three times. The pyrolysis temperature was 600 °C, and catalysis at 800 °C, 1 g of waste truck tyre was placed in the top stage as feedstock and 0.5 g of 10 wt.% Ni/Al₂O₃ catalyst prepared by impregnation that the method was mentioned in section 3.1.4.1 and no steam was introduced in the repeat experiments.

The data displayed in Table 3-3 shows the validation of the experimental system. The repeatability is excellent with low standard deviation particularly in terms of char yield. The char yield was between 6.9 wt.% to 7 wt.% with a mean of 6.97 wt.% and standard deviation 0.05. The gas yield, liquid/oil yield and residue also with a very low standard deviation. From all the above, the standard deviation for all products was less than 10% of the mean value which indicate the acceptable repeatability. Some of the experiments were also repeated throughout the entire study to ensure the high accuracy of the results.

Table 3-3 Reproducibility analysis of the products mass balance

Truck tyres + 10 wt.%Ni/Al ₂ O ₃	Run 1	Run 2	Run 3	Mean	Standard deviation	Std. Dev (% mean)
Gas yield (wt.%)	29.00	28.51	26.56	28.02	1.05	3.76
Liquid/oil yield (wt.%)	25.90	27.00	28.20	27.03	0.94	3.47
Residue (wt.%)	37.00	38.00	36.00	37.00	0.82	2.21
Char (wt.%)	6.90	7.00	7.00	6.97	0.05	0.68
Mass balance (wt.%)	98.80	100.51	97.76	99.02	1.13	1.14

3.3 Materials analysis and characterisations

3.3.1 X-Ray diffraction

The fresh catalysts were characterized by X-ray diffraction (XRD) on a Bruker D8 as shown in **Figure 3-8** to identify the composition of the catalysts. The diffractometer used a Cu-K α X-Ray source with a Vantec position sensitive detector. A typical XRD spectrum for fresh Ni/Al $_2$ O $_3$ catalyst is shown in Figure 3-9, the peaks at different diffraction angles in the spectra indicate the metal oxides sites which can be identified by Pan Analytical Xpert High Score plus.

The sample preparation includes placing each of powdered samples on the pan before the start of the analysis. The analysis range (2 theta) was 10 to 70° with a scanning step of 0.05°. The entire analysis for each sample was around 30 mins which depended on the 2 theta and scanning step settings. The principle of XRD analysis is based on the Bragg's Law principle as shown in equation 3.1:

$$\lambda = 2d \sin \phi \quad (3.1)$$

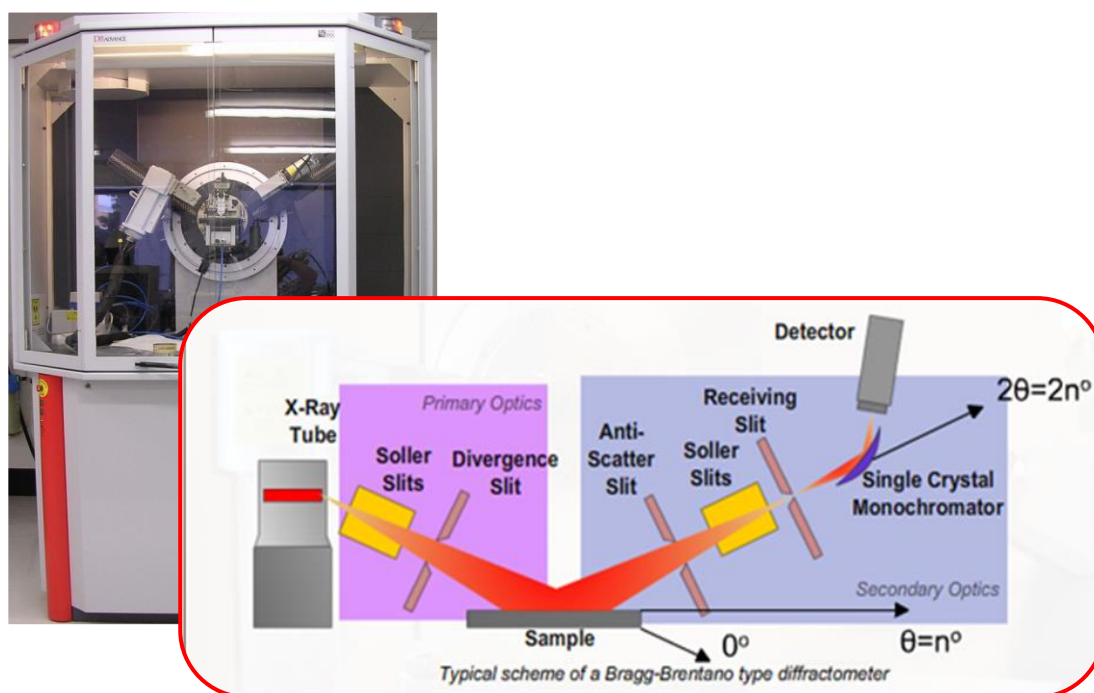


Figure 3-8 Bruker D8 X-Ray diffraction spectroscopy (Modified figure based on [9]).

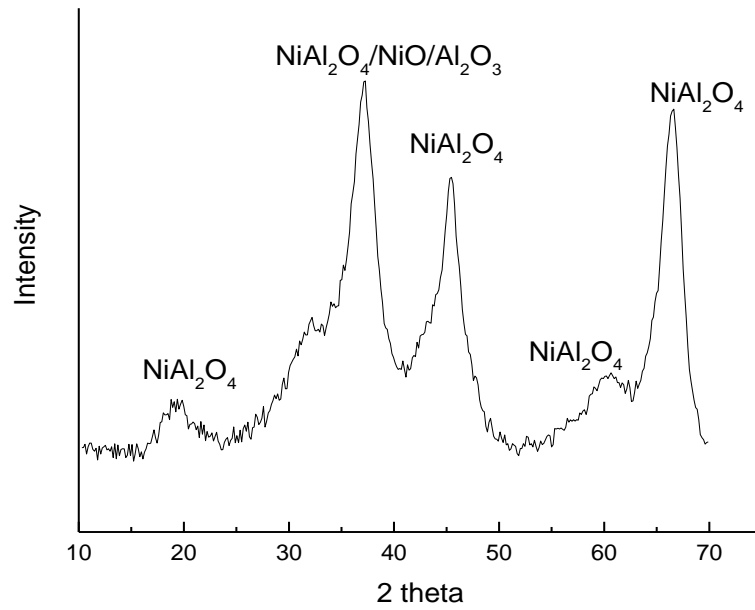


Figure 3-9 Typical XRD spectrum of fresh Ni/Al₂O₃ catalyst.

The particle sizes of crystals were calculated based on the Scherrer equation as shown in equation 3.2 [10]:

$$\tau = \frac{K\lambda}{\beta \cos\theta} \quad (3.2)$$

Where

τ = the mean size of the order domain;

K = a dimensionless shape factor which a typical value of 0.9;

λ = wavelength of X-Ray;

β = line boarding at half the maximum intensity;

θ = is the Bragg angle in degrees.

3.3.2 Porous catalysts characterization

The porous properties of fresh catalysts such as BET surface area and total pore volumes were determined by measuring the amounts of nitrogen adsorption and desorption isotherms from the catalyst surface at equilibrium vapour pressure by the static volumetric method. All of the catalysts were initially degassed before the nitrogen adsorption or desorption measurements to remove the moisture and impurities in the porous catalysts. After the degassing, the catalyst samples were placed in the Nova 2200e analyser from Quantachrome Corporation, US as shown in Figure 3-10 and subjected to nitrogen flow under different partial pressure at 77K. The amount of adsorbed adsorbate on the surface of the sample can be measured at equilibrium at constant temperature under a range of pressures. Also, the desorption isotherm can also be drawn based on the removed amount of nitrogen from the porous catalysts as the pressure decrease. In Figure 3-11 shows the example of adsorption and desorption isothermal plots of 20 wt. Fe/Ni/MCM-41 catalyst with Fe:Ni ratio at 1:1.



Figure 3-10 NOVA 2200e instrument used to characterize the porous properties of catalysts.

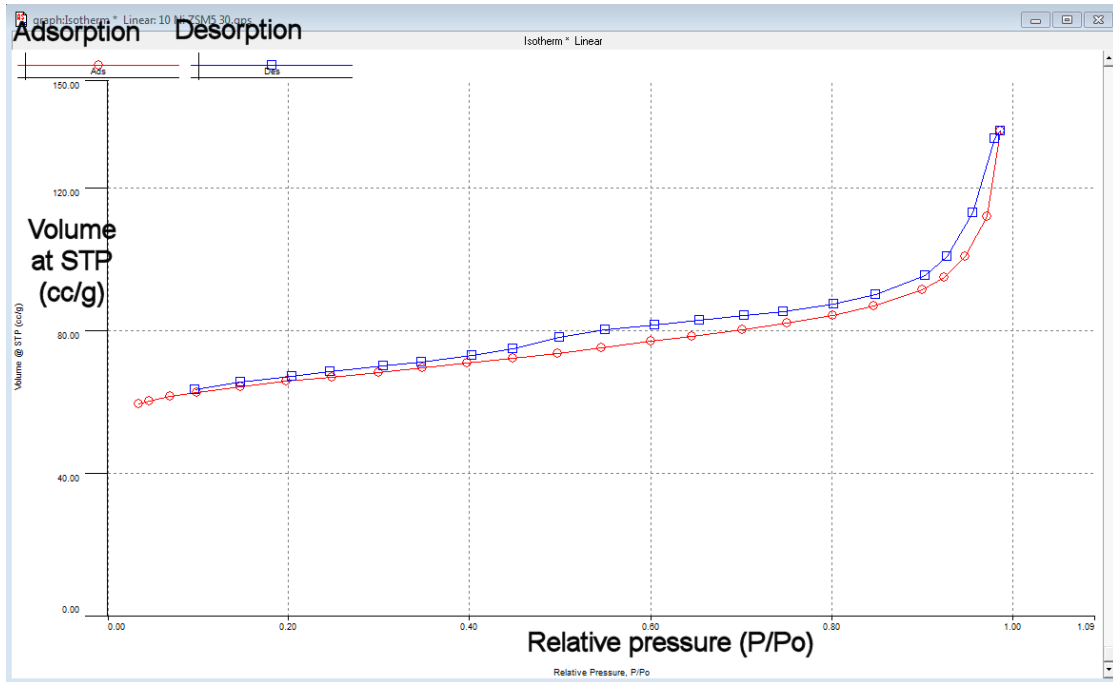


Figure 3-11 Example of the adsorption and desorption isothermal for 20 wt. % Fe/Ni/MCM-41 catalyst with Fe:Ni ratio at 1:1 by a NOVA 2200e instrument.

3.3.2.1 BET surface area

The surface area of the catalysts was derived by the Brunauer, Emmett and Teller (BET) method which has been reported as the most common method for determining the internal and external surface area of the mesoporous materials [11, 12]. The BET equation is described as following equations 3.3-3.9:

$$\frac{1}{v\left(\frac{P_0}{P}-1\right)} = \frac{1}{v_m \cdot C} + \frac{C-1}{v_m \cdot C} \times \frac{P}{P_0}$$

(3.3)

Where:

v = is the volume of adsorbed gas at a relative pressure P ;

P = is the partial pressure of nitrogen;

P_0 = is the saturation pressure at experimental temperature;

v_m = is the volume of adsorbed adsorbate at monolayer coverage;

C = is the BET constant which is related to the energy of the adsorption in the first adsorbed layer.

The most of solid materials adsorbate gas is limited to a relative pressure (P/P_0) region of 0.05 to 0.35. The volume adsorbed at monolayer coverage v_m can be calculated by taking the slope value and intercept of the BET plots based on the following equations:

$$\text{Slope} = \frac{C-1}{v_m \cdot C} \quad (3.4)$$

$$\text{Intercept} = \frac{1}{v_m \cdot C} \quad (3.5)$$

Therefore, the volume of adsorbate v_m can be calculated by combining equations 2.2 and 2.3 which

$$v_m = \frac{1}{\text{Slope} + \text{Intercept}} \quad (3.6)$$

The total surface area S_{total} of the porous catalysts can then be calculated by the following equations:

$$S_{total} = \frac{v_m \cdot N_a \cdot A}{V} \quad (3.7)$$

Where:

N_a = is the Avogadro's number ($6.023 \times 10^{23} \text{ mol}^{-1}$);

A = is the molecular cross sectional area of the adsorbate gas (m^2);

V = is the molar volume of adsorbate gas (m^3).

Nitrogen as the most common used adsorbate gas for surface area determination with molecular cross sectional area A is 0.162 nm^2 , where the BET surface area of the catalyst can be calculated based on the equation 3.8:

$$S_{BET} = \frac{S_{total}}{W} \quad (3.8)$$

Where:

W = is the weight of sample (g).

3.3.2.2 Total pore volume

The total pore volume of the mesoporous catalysts can be determined from nitrogen adsorption isotherms and calculated by equation 3.9. P/P_0 is 0.98 was used to estimate the total pore volume and that the pores were occupied by nitrogen:

$$V_{liquid} = \frac{V_{adsorbate} \cdot M}{V_{standard} \cdot \rho_{N_2}} \quad (3.9)$$

where:

V_{liquid} = is the total pore volume (cm^3g^{-1}) at standard temperature and pressure (STP);

$V_{adsorbate}$ = is the volume of adsorbed gas at P/P_0 is 0.98;

M = the molecular weight of nitrogen (28 g mole^{-1});

$V_{standard}$ = is the volume of 1 mole of nitrogen at STP ($22420 \text{ cm}^3 \text{ mole}^{-1}$);

ρ_{N_2} = is the liquid density of nitrogen (0.8081 g cm^{-3}).

3.3.3 Gas chromatography

The gaseous productions produced from pyrolysis-catalysis/catalytic reforming of tyres or plastics were analysed off-line with three separate Varian 3380 gas chromatographs (GC) which were fitted with different columns and detectors as shown in Figure 3-12. The GC used for permanent gases including H_2 , CO , O_2 and N_2 was fitted with a 2m long, 2mm diameter, 60-80mm mesh molecular sieve column and a thermal conductivity detector (TCD). The GC used for CO_2 analysis was a thermal conductivity detector. The packed molecular sieve column was 2 m long, 2 mm diameter and 80-100mm mesh. The carrier gas for both permanent gases and carbon dioxide analysis GC was argon. The GC used for hydrocarbons analysis which included C_1 - C_4 was fitted with an 80-100mm mesh Haysep molecular sieve column and flame ionization detector (FID). The carrier gas was nitrogen. The total analysis time for permanent gas is 11 mins, 7 mins for carbon dioxide and 21 mins for hydrocarbons.

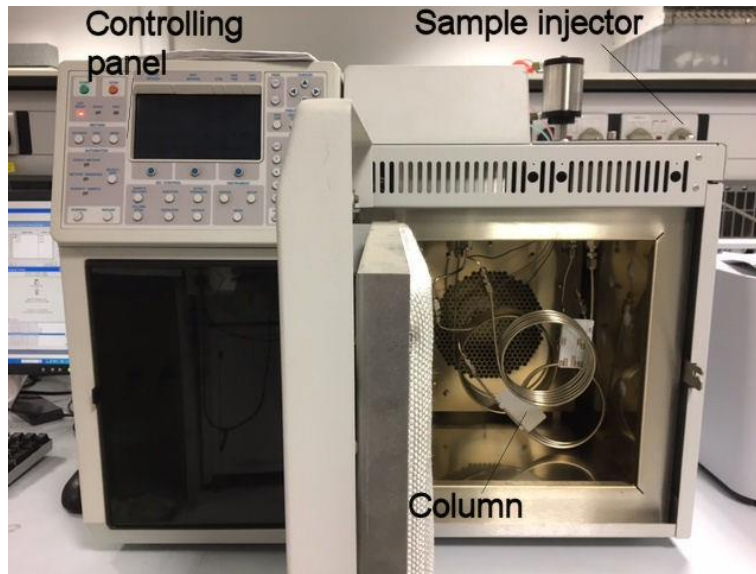
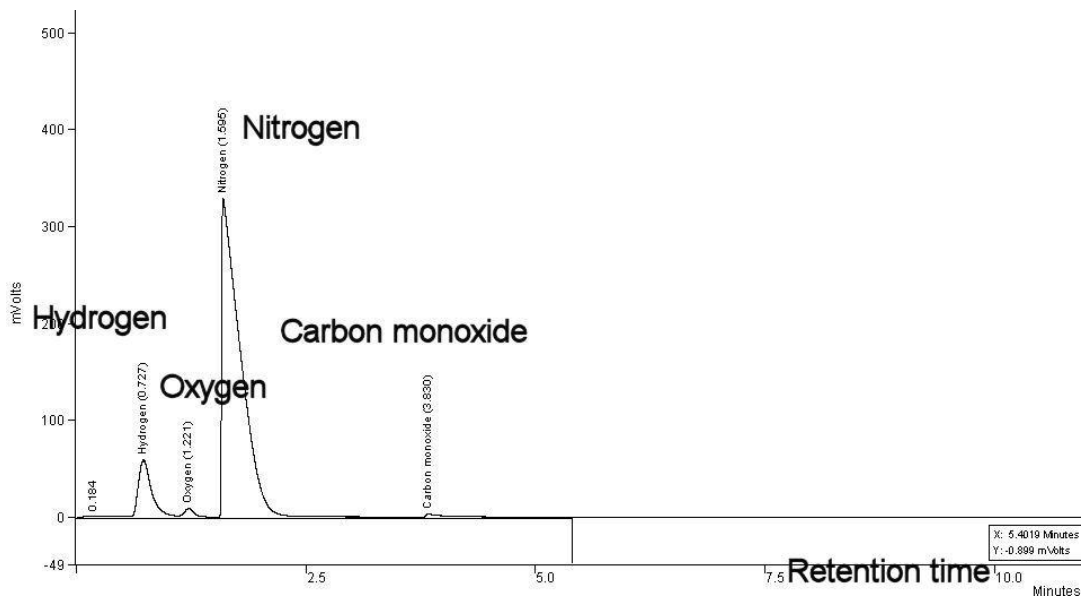
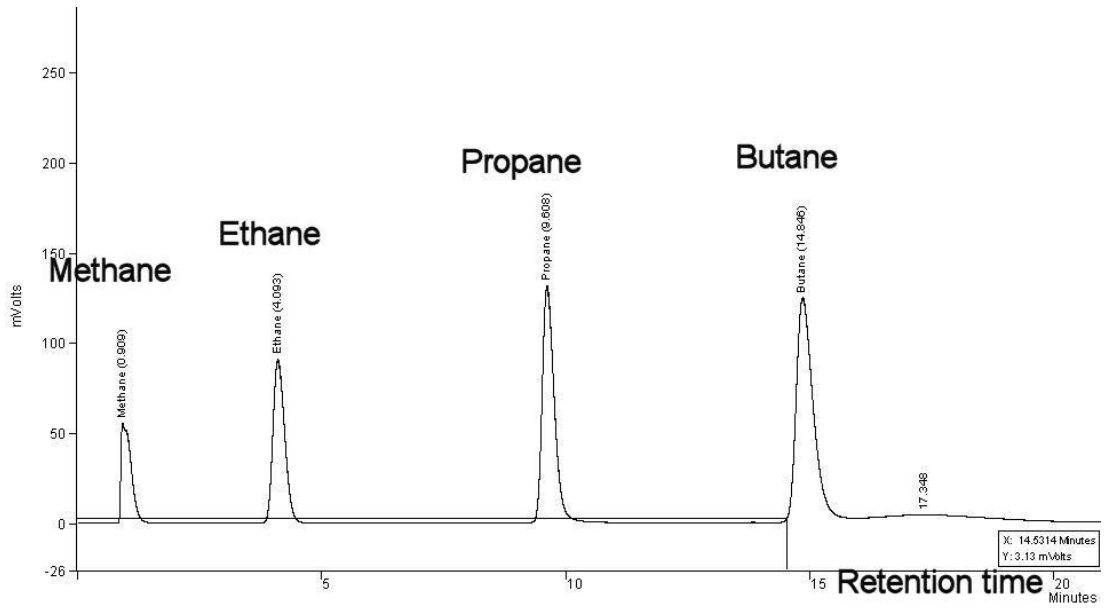


Figure 3-12 Varian 3380 gas chromatography

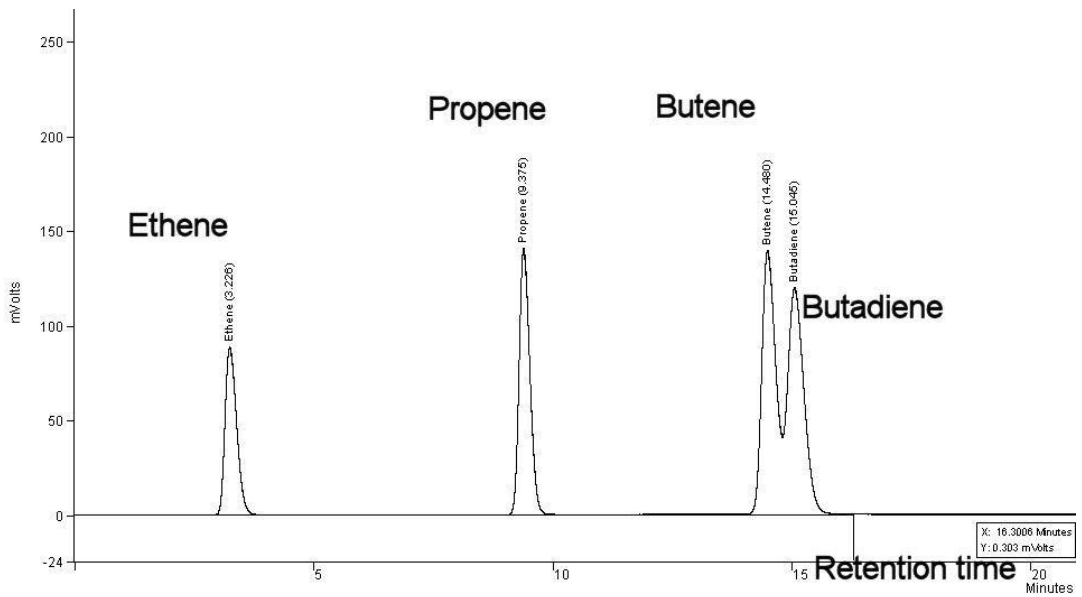
(a)



(b)



(c)



(d)

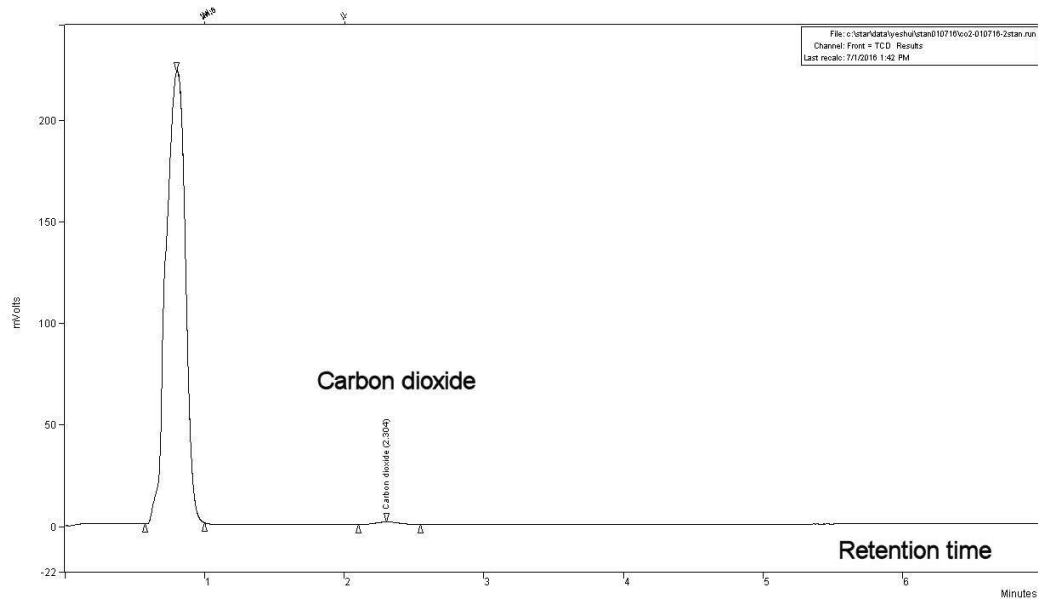


Figure 3-13 GC response peaks for standard gas (a) permanent gas chromatogram; (b) alkanes chromatogram; (c) alkenes chromatogram; (d) carbon dioxide chromatogram.

The standard gases used contained 1 vol.% of carbon monoxide, 1 vol.% of carbon dioxide, 1 vol.% of hydrogen, 1 vol.% of oxygen and balanced with nitrogen; standard alkanes including 1 vol.% of methane, 1 vol.% of ethane, 1 vol.% of propane, 1 vol.% of butane balanced with nitrogen; and alkenes including 1 vol.% of ethylene, 1 vol.% of propene, 1 vol.% of butane, 1 vol.% of butadiene and balanced with nitrogen were obtained from Scientific and Technical gases which were used as references to calculate the produced gas compositions. The calibration of the GC was performed regularly with standard gas to ensure the accuracy of the results. Example chromatograms of 1 ml of each type of standard gas (permanent gas, hydrocarbon gases and carbon dioxide) are shown in Figure 3-13 which also includes the retention time for each type of gas.

The corresponding peak areas of each standard gas component was obtained by the Varian Star software which was used as reference to calculate produced gas concentration based on equation 3.10:

$$C_{sample} = \frac{C_{standard} \times A_{sample}}{A_{standard}} \quad (3.10)$$

Where:

$C_{samples}$ = is the concentration of sample gas;

$C_{standard}$ = is the concentration of standard gas;

A_{sample} = is the peak area of sample gas obtained from GC;

$A_{standard}$ = is the peak area of standard gas obtained from GC.

Repeatability of the GC analyses of the same gas sample was taken to ensure the data validity. The repeat results obtained by both GC-FID and GC-TCD are shown in Table 3-4 that shows good repeatability of the gas concentrations with small standard deviation in a range between 0.10 to 1.17.

Table 3-4 Repeatability of the gas concentrations by GC-FID and GC-TCD (STDEV is standard deviation).

Gas concentrations (vol. %)	H ₂	CO	CH ₄	C ₂ -C ₄
Run 1	47.54	42.33	6.32	1.28
Run 2	47.22	42.69	6.28	1.28
Run 3	48.40	42.65	6.20	1.26
Run 4	45.99	42.87	6.49	1.30
Run 5	45.12	43.28	6.18	1.81
Run 6	44.63	43.44	6.34	1.31
Run 7	44.92	43.57	6.41	1.33
Run 8	45.91	43.09	6.27	1.28
Run 9	45.39	42.79	6.49	1.32
Mean	46.12	42.97	6.33	1.35
STDEV	1.17	0.36	0.10	0.15

Calculations for gas yield, H₂ yield, carbon yield and gaseous product calorific value:

$$RF = \frac{\text{Peak area}}{\text{Real concentration (vol\%)}} \quad (3.11)$$

$$\text{Concentration of sample} = \frac{\text{Sample area}}{\text{RF}} \quad (3.12)$$

$$\text{Volume of N}_2 = \text{Concentration of N}_2 \times \text{Total volume of gas} \quad (3.13)$$

$$\text{Total volume of gas} = \frac{\text{Volume of N}_2}{\text{Concentration of N}_2} = \frac{\text{Flow rate of N}_2 \times \text{Time}}{\text{Concentration of N}_2} \quad (3.14)$$

$$\begin{aligned} \text{NO. of moles} &= \frac{\text{Volume of sample}}{22.4L} \\ &= \frac{\text{Total volume of sample} \times \text{Concentration of volume}}{22.4L} \end{aligned} \quad (3.15)$$

$$\text{Mass} = \text{No. of moles} \times \text{molar mass} \quad (3.16)$$

$$\text{Mass balance} = \frac{\text{Mass of outlet}}{\text{Mass of inlet}} \times 100\% \quad (3.17)$$

$$\text{Gas yield per gram of sample (wt. \%)} = \frac{\text{Mass of gas yield}}{1g \text{ of sample}} \times 100\% \quad (3.18)$$

$$\text{H}_2 \text{ yield per gram of sample (mmol g}^{-1}\text{)} = \frac{\text{Molar mass} \times \text{Mole of H}_2}{1g \text{ of sample}} \quad (3.19)$$

$$\text{Liquid yield per gram of sample (wt. \%)} = \frac{\text{Mass of liquid yield}}{1g \text{ of sample}} \times 100\% \quad (3.20)$$

The calculated calorific value of the gas mixture produced during the pyrolysis catalysis/catalytic-gasification was estimated based on the volume fraction of each type of gas. The calorific value of the product gas was obtained by taking the calorific values of the individual gas components and multiplying their

corresponding mole fraction in the product gas. The sum obtained was then corrected for the compressibility of the mixture as set out in reported methods [13] and was calculated as follows.

The compressibility of the gas mixture is given by:

$$CV_m = x_1 \cdot CV_1 + x_2 \cdot CV_2 + \dots \quad (3.21)$$

Where:

x = is the mole fraction of each type of gas component

CV = is the calorific value of the each type of gas component

The compressibility factor is given by:

$$Z_m = 1 - (x_1 \cdot \sqrt{b_1} + x_2 \cdot \sqrt{b_2} + \dots)^2 + 5 \times 10^{-4} (2x_H - x_H^2) \quad (3.22)$$

Where:

b_1, b_2 is gas law derivations of the components (except H₂);

x is the mole fraction of the gas component;

x_H is the mole fraction of H₂ present in the mixture .

The corrected calorific value is given by:

$$CV = \frac{CV_m}{Z_m} \quad (3.23)$$

3.3.4 Thermal gravimetric analyser

3.3.4.1 Temperature programmed oxidation

The deposited carbons on the surface of the used catalysts were analysed through temperature programmed oxidation (TPO) and also the gravimetric analysis (TGA) of raw waste tyre rubbers were carried out using a Shimadzu thermal gravimetric analyser (TGA-50) as shown in Figure 3-14. Similar amounts (approximately 4-10 mg) of each reacted catalyst or raw sample was

placed in the sample crucible which was heated up to 800 °C at a ramp rate of 15 °C min⁻¹. For the TPO requires air flow rate at 50 ml min⁻¹ atmosphere and TGA requires nitrogen flow at 50 ml min⁻¹.

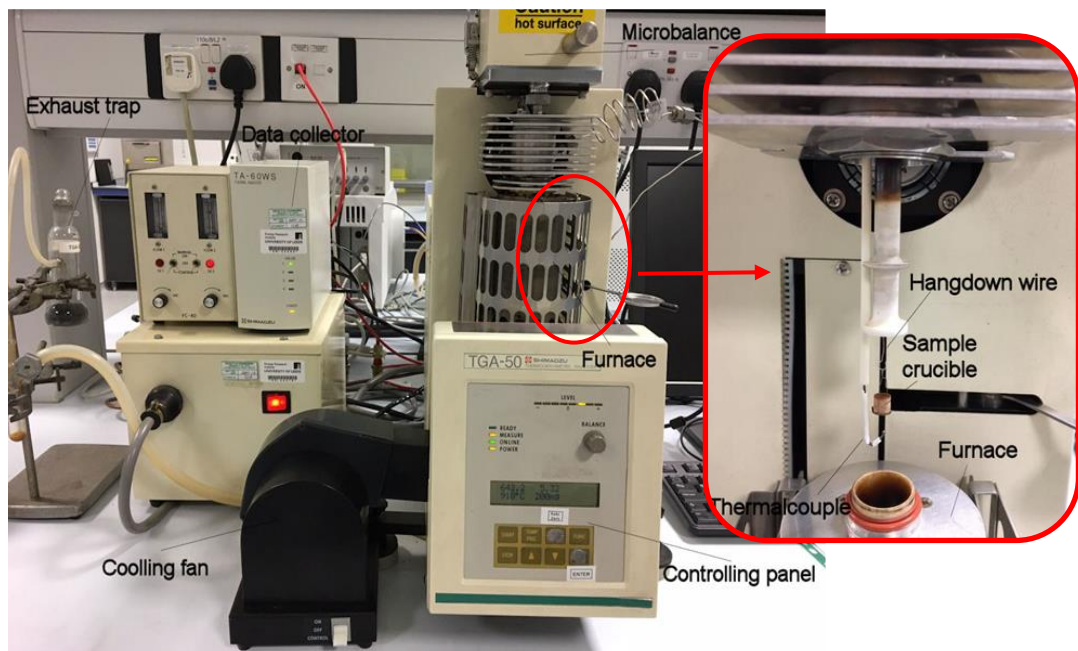


Figure 3-14 Shimadzu thermal gravimetric analyser (TGA-50).

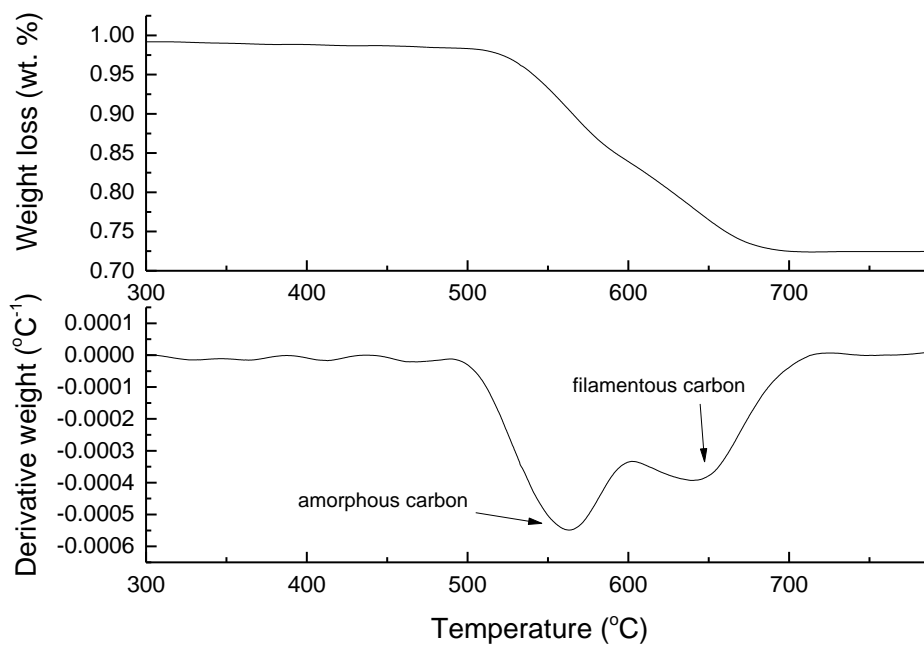


Figure 3-15 Typical TGA-TPO and DTG-TPO results of reacted Ni/Al₂O₃ catalyst.

Comparing the different oxidation characteristics between the reacted catalysts that were obtained from different experimental conditions, the results are able to identify the different phases of carbon deposition due to the different thermal stability of the different types of carbon depositions. Amorphous carbon is oxidized at lower temperature compared with the filamentous carbon since the filamentous carbon has a higher thermal stability [14-18]. A typical TPO and derivative thermograms are shown in Figure 3-15. The weight loss in the TPO thermogram is due to the oxidization of deposited carbon on the catalyst surface, the two peaks in the derivative thermogram at different temperature indicate the two types of carbon oxidized at different temperatures, where the peak at lower temperature indicates the oxidization of amorphous carbon and the peak at higher temperature indicates the oxidization of filamentous carbon.

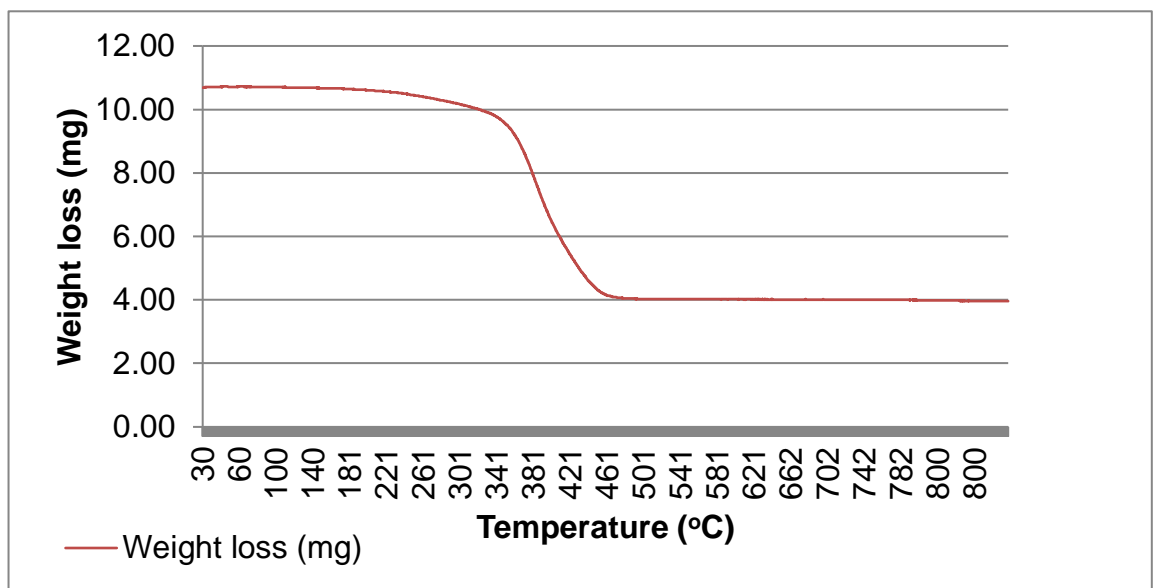


Figure 3-16 Thermal gravimetric analysis (TGA) of waste truck tyre.

Figure 3-16 shows the thermal gravimetric analysis of raw waste truck tyre sample. The truck tyre starts to decompose at a temperature around 300 °C

and the decomposition is finished at around 460 °C. The residue was constant at the temperature higher than 460 °C.

3.3.4.2 Temperature programmed reduction

Temperature programmed reduction (TPR) was carried out using a Stanton-Redcroft thermo gravimetric analyser (TGA) as shown in Figure 3-17. 10 mg fresh catalyst sample was placed in the TGA, and preheated to 150 °C at a heating rate of 20 °C min⁻¹ and hold for 30 min in the atmosphere of N₂ at a flow rate is 50 ml min⁻¹. After the sample was cooled down to room temperature, TPR was carried out with H₂ at a concentration of 5 vol.% (95% N₂) to 900 °C at a heating rate is 10 °C min⁻¹.

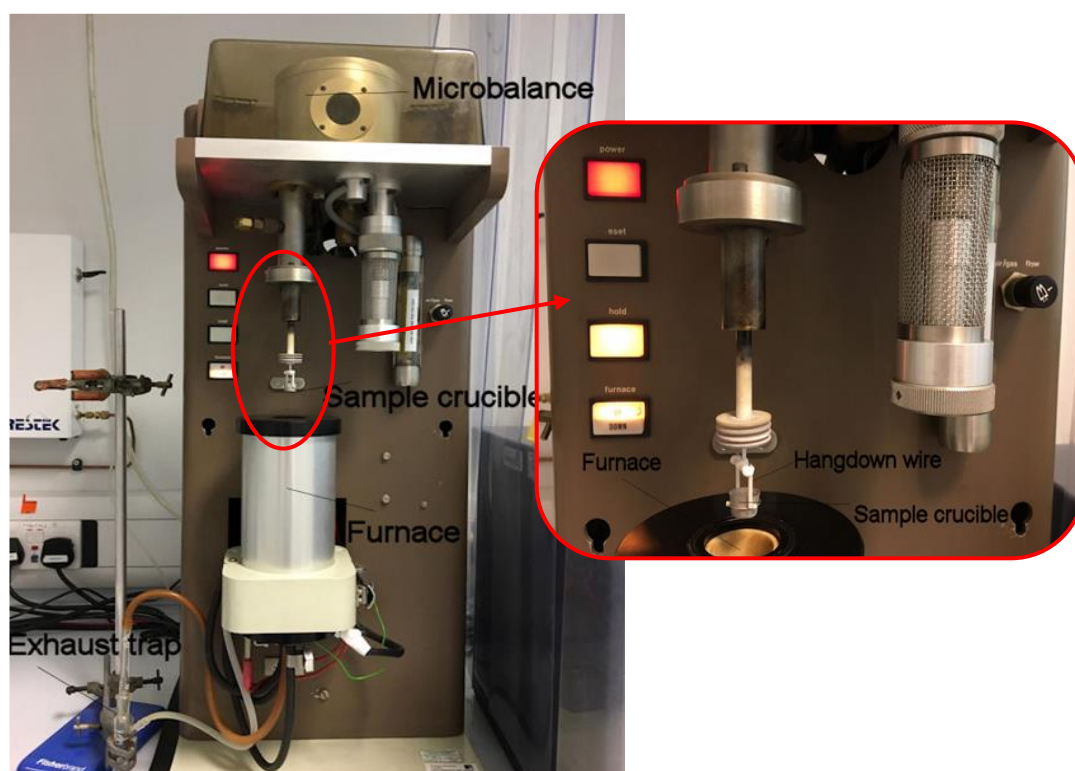


Figure 3-17 Stanton-Redcroft thermo gravimetric analyser

3.3.5 Scanning electron microscopy

A high resolution scanning electron microscope was used to characterize both the fresh and reacted catalysts, which is a widely applied technique for heterogeneous catalysts. The morphology, crystallites and surface texture of catalysts were characterized by a Hitachi SU8230 scanning electron microscope (SEM) as shown in Figure 3-18. The powdered sample was stuck on a specimen stub and taped with carbon film. All the specimens were coated with 10 nm of iridium/platinum to avoid negative charge. The catalyst samples on the specimen stub were placed in the working stage under vacuum conditions. The images were taken at a working distance around 3 mm and accelerating voltage at 2 KV. Figure 3-19 shows examples of SEM images of the fresh and reacted Fe/Ni/MCM-41 catalyst with Fe:Ni ratio of 05:15.

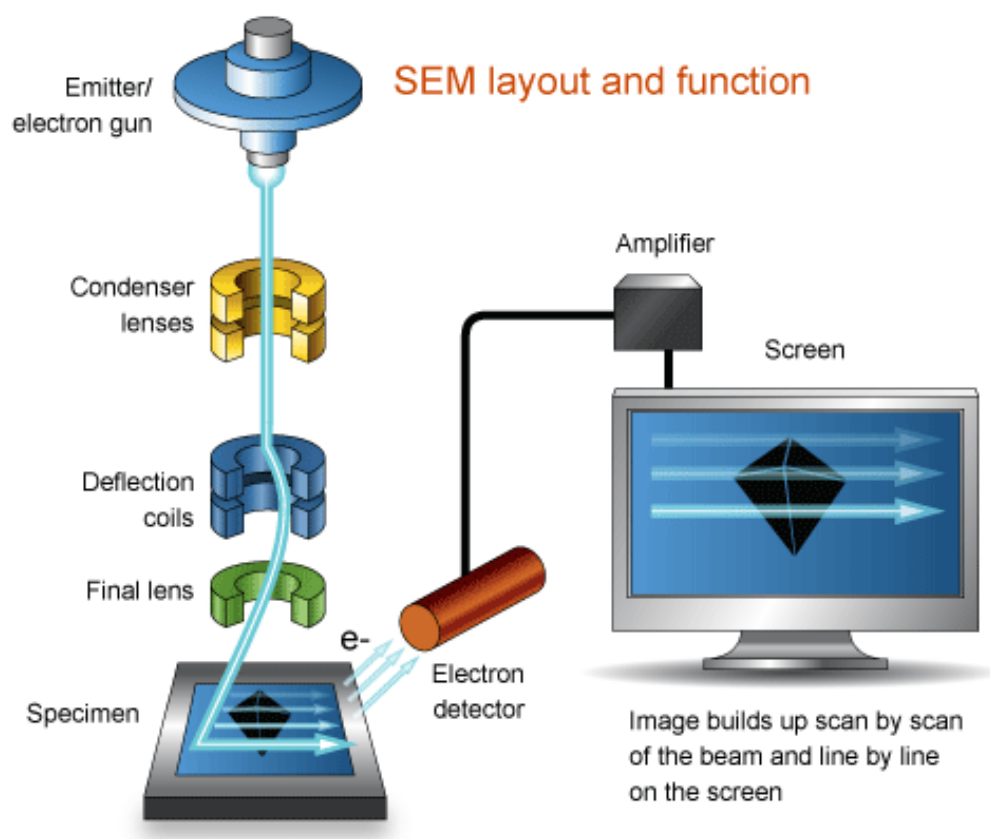


Figure 3-18 Hitachi SU8230 Scanning electron microscope [19].

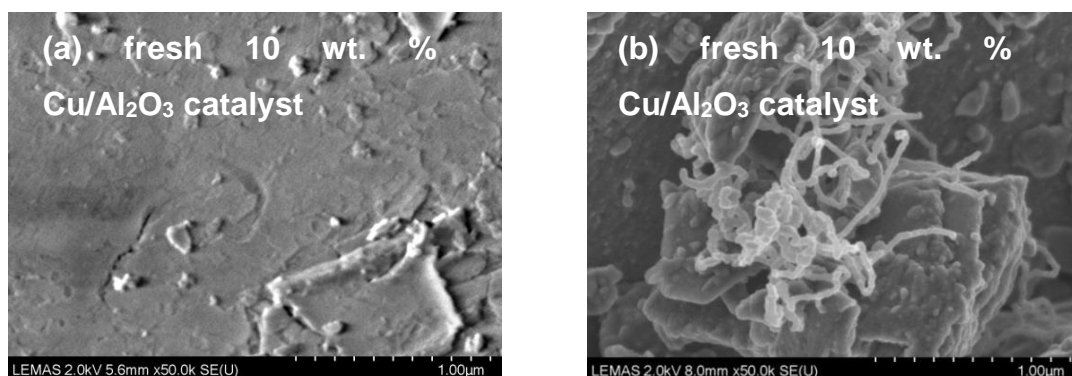


Figure 3-19 Sample of SEM images of (a) fresh 10 wt. % Cu/Al₂O₃ catalyst and (b) reacted catalyst with filamentous carbon production by pyrolysis-catalysis waste truck tyre.

3.3.6 Transmission electron microscopy with energy dispersive X-Ray analyser

The reacted catalysts were further analysed by a Tecnai TF20 transmission electron microscope (TEM) as shown in Figure 3-20 to observe the graphitic quality of the deposit carbon. TEM is similar to SEM and can be used to obtain higher magnification image which is very useful to identify the types of produced filamentous carbon based on the morphology. For example, solid carbon nanofibers can easily be distinguished from the hollow structure of carbon nanotubes. Figure 3-21 (a) shows an example of a TEM image of carbon nanotubes produced on the Fe/Ni/MCM-41 catalyst with a metal particle at the tip of the tube.

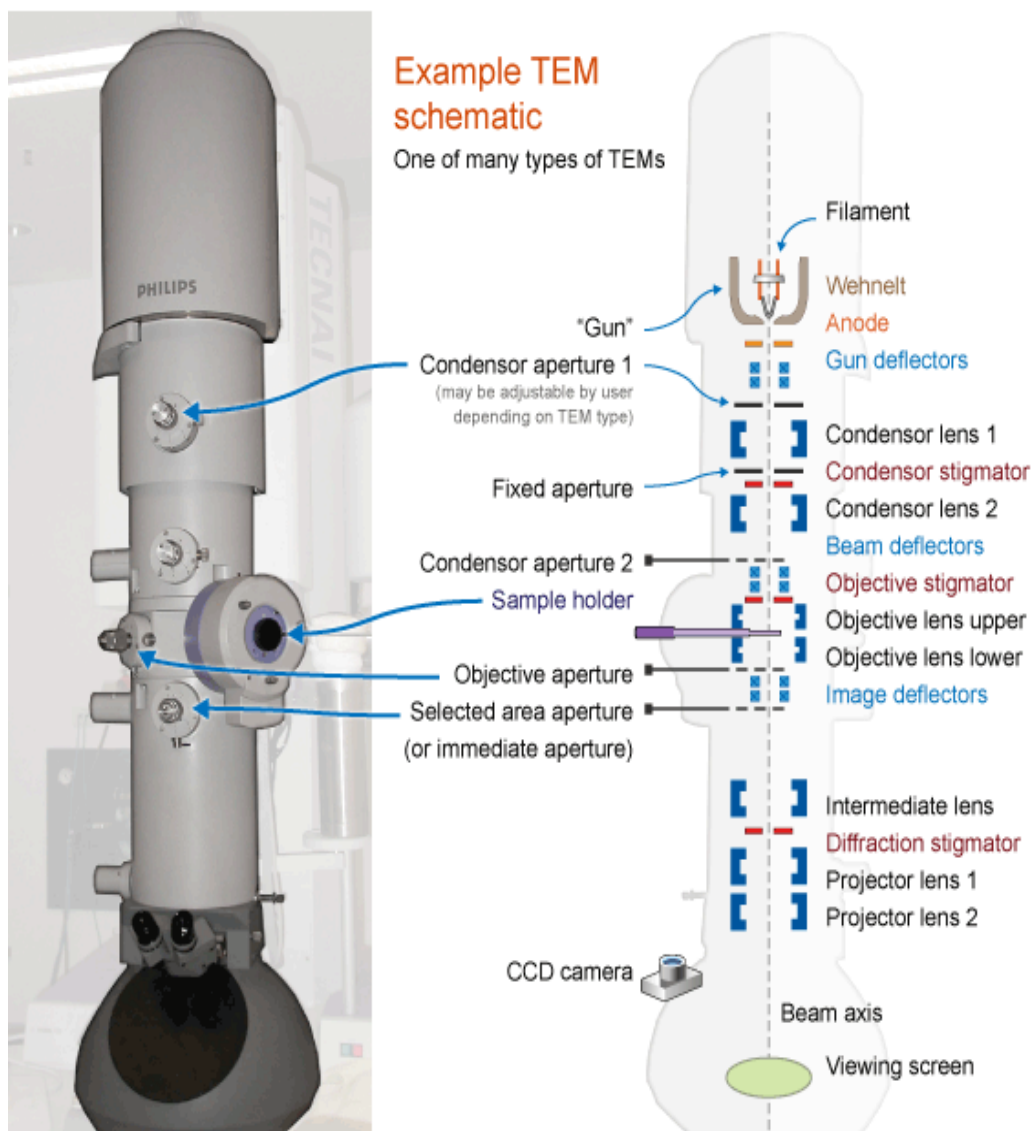


Figure 3-20 TECNAI TF20 Transmission electron microscopy (From TECNAI TF20 operation manual).

Energy dispersive X-Ray analysis (EDX) was subsequently carried out with TEM. The elements can be identified by the specific X-Ray spectra that produced by the interactions between the samples and electron beam. The EDX can be focused on a single particle or certain area, which can be used to identify the each type of element on anywhere of the catalyst. Figure 3-21 (b), (c) and (d) are the EDX mappings for carbon, nickel and iron of reacted Fe/Ni/MCM-41 (05:15) catalyst. From the mapping results, very useful information can be obtained, for example, identification of the metal particle at the tip of the carbon nanotube can be obtained which is a very advantageous

method for bimetallic catalysts study in pyrolysis catalysis/catalytic-gasification process.

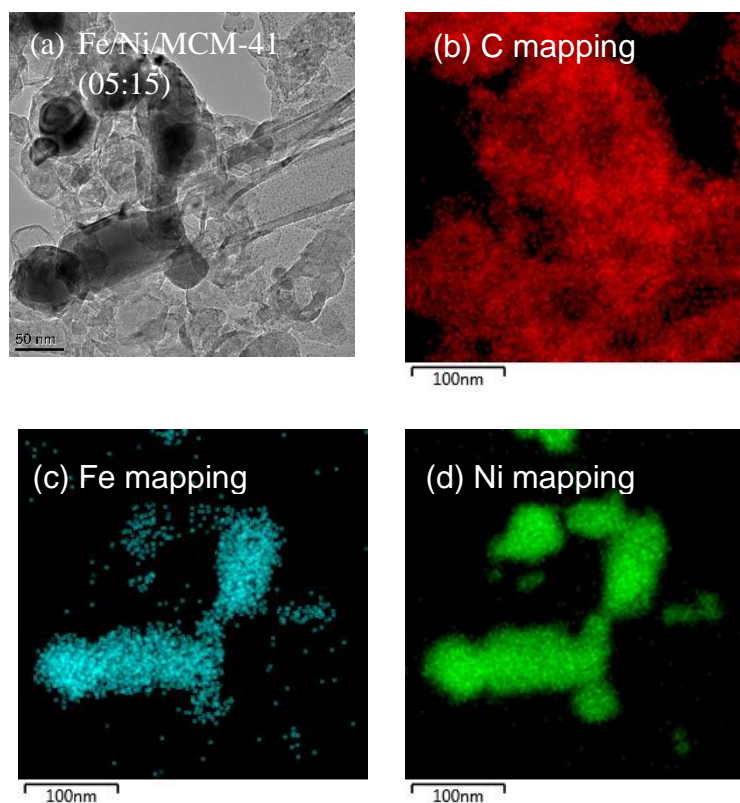


Figure 3-21 Samples of TEM and EDX mapping of reacted catalyst.

3.3.7 Raman analysis

A Renishaw Invia Raman spectroscope as shown in Figure 3-22 with a wavelength of 514 nm at Raman shifts between 100 and 3200 cm^{-1} was used to obtain Raman analysis results to indicate the degree of graphitization of the deposited carbon. Raman spectroscopy is one of the techniques used to characterize the structures of carbon materials, including the amorphous and/or graphitic carbons [20-24]. As shown in Figure 3-23 (a), the Raman spectrum in the wavelength range of 1000 to 2750 cm^{-1} is presented to indicate the carbon produced from pyrolysis-catalysis of waste tyre at 800 °C with 10 wt. % Ni/Al₂O₃ catalyst. Figure 3-23 (b) is the Raman spectrum of the carbon produced from waste truck tyre by pyrolysis-catalysis with 20 wt. Fe/MCM-41 catalysts at 800

°C. The D band indicates the disordered carbon, G band indicates the graphite carbon and G' band indicates the purity of CNTs as coupling the two photon elastic scattering process [21]. The baseline rise of the Raman spectrum in Figure 3-23 (b) is due to the resolution and the intensity of the peaks. When the resolution and the intensity are weak, the baseline will slope upwards and not be flat. When the resolution and the intensity is strong as shown in Figure 3-23 (a), a much flatter baseline can be generated.

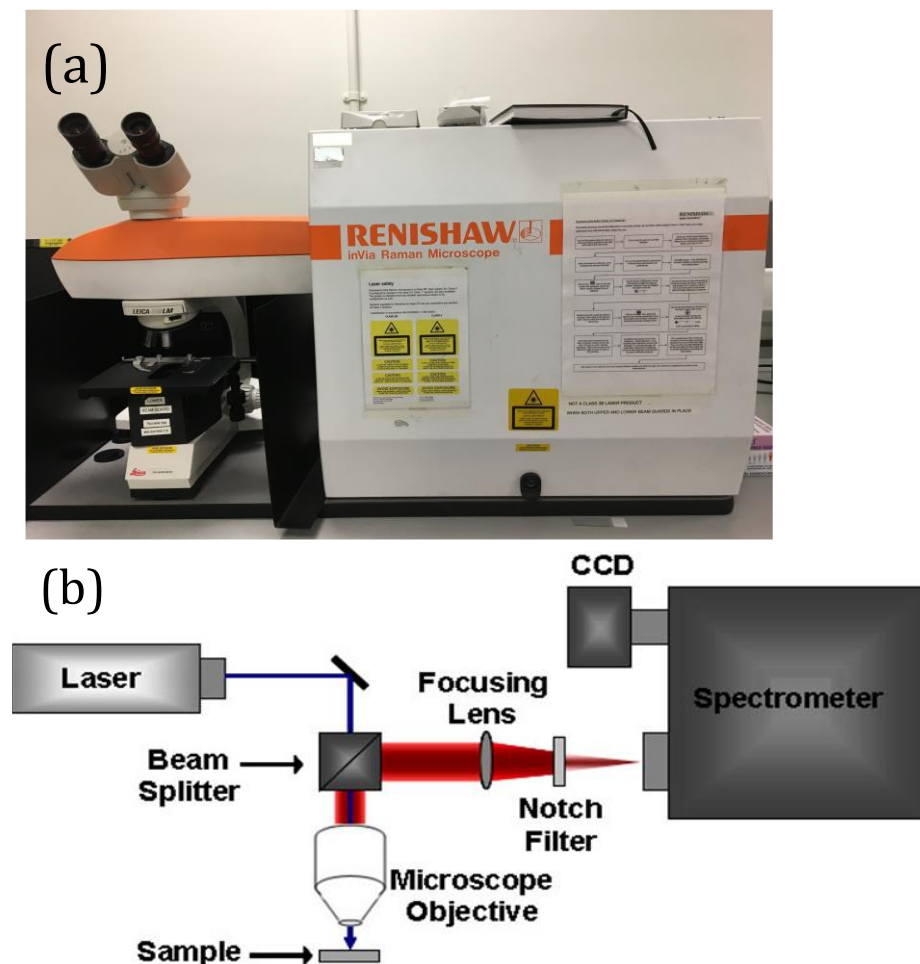
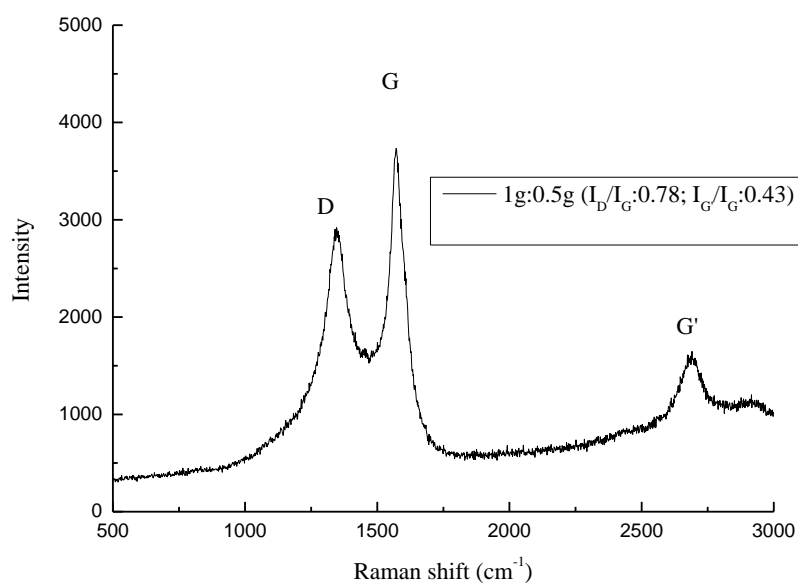
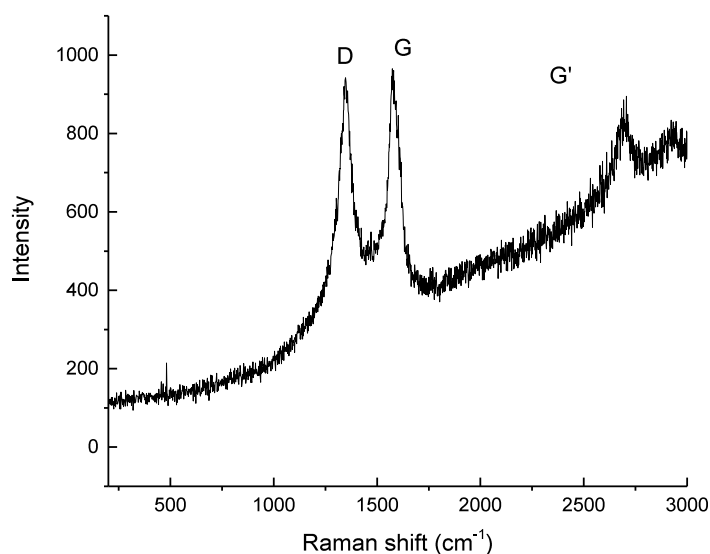


Figure 3-22 Renishaw InVia Raman spectroscopy [25].



(a)



(b)

Figure 3-23 (a) Example of Raman result for the reacted 10 wt. % Ni/Al₂O₃ catalyst after the pyrolysis-catalysis of waste tyre experiment at 800 °C; (b) example of Raman result for the reacted 20 wt.% Fe/MCM-41 catalyst after pyrolysis-catalytic reforming of simulated mixed waste plastics.

References

1. Krevelen, D.W.V., *Properties of Polymers: Their Correlation with Chemical Structure; their Numerical Estimation and Prediction from Additive Group Contributions*. Vol. 4th, completely rev.;4;4th;. 2009, NL: Elsevier Science.
2. Williams, P.T., *Pyrolysis of waste tyres: A review*. Waste Management, 2013. 33(8): p. 1714-1728.
3. Dai, X., et al., *Pyrolysis of waste tires in a circulating fluidized-bed reactor*. Energy, 2001. 26(4): p. 385-399.
4. Aylón, E., et al., *Valorisation of waste tyre by pyrolysis in a moving bed reactor*. Waste management, 2010. 30(7): p. 1220-1224.
5. Delgado, C., et al., *Assessment of the environmental advantages and drawbacks of existing and emerging polymers recovery processes*. JRC Institute for Prospective Technological Studies, 2007.
6. Acomb, J.C., et al., *The use of different metal catalysts for the simultaneous production of carbon nanotubes and hydrogen from pyrolysis of plastic feedstocks*. Applied Catalysis B: Environmental, 2016. 180: p. 497-510.
7. Cheng, C.-F., et al., *Optimal parameters for the synthesis of the mesoporous molecular sieve [Si]-MCM-41*. Journal of the Chemical Society, Faraday Transactions, 1997. 93(1): p. 193-197.
8. Seker, E., *The catalytic reforming of bio-ethanol over SiO₂ supported ZnO catalysts: The role of ZnO loading and the steam reforming of acetaldehyde*. International Journal of Hydrogen Energy, 2008. 33(8): p. 2044-2052.
9. University, Y. *XRD*. West Campus Materials Characterization Core 2017; Available from: <http://ywcmatsci.yale.edu/xrd>.
10. Patterson, A., *The Scherrer formula for X-ray particle size determination*. Physical review, 1939. 56(10): p. 978.
11. Brunauer, S., et al., *Adsorption of gases in multimolecular layers*. J. Am. Chem. Soc, 1938. 60(2): p. 309-319.
12. Bartholomew, C.H., et al., *Hydrogen production and synthesis gas reactions*. Fundamentals of Industrial Catalytic Processes, Second Edition, 2006: p. 339-486.
13. Rose, J.W., et al., *Technical Data on Fuel*. 1977: Scottish Academic Press.

14. Wu, C., et al., *Investigation of coke formation on Ni-Mg-Al catalyst for hydrogen production from the catalytic steam pyrolysis-gasification of polypropylene*. Applied Catalysis B: Environmental, 2010. 96(1–2): p. 198-207.
15. Zhang, Y., et al., *Pyrolysis-catalysis of waste plastic using a nickel-stainless steel mesh catalyst for high value carbon products*. Environmental Technology, 2017: p. 1-27.
16. Zhang, Y., et al., *Carbon nanotubes and hydrogen production from the pyrolysis catalysis or catalytic-steam reforming of waste tyres*. Journal of Analytical and Applied Pyrolysis, 2016.
17. Zhang, Y., et al., *Carbon nanotubes and hydrogen production from the pyrolysis catalysis or catalytic-steam reforming of waste tyres*. Journal of Analytical and Applied Pyrolysis, 2016. 122: p. 490-501.
18. Zhang, Y., et al., *High-value resource recovery products from waste tyres*. Proceedings of the Institution of Civil Engineers - Waste and Resource Management, 2016. 169(3): p. 137-145.
19. MyScope. *Layout, principles, Scanning electron microscopy in practice, SEM*. 2013; Available from: <http://www.ammrf.org.au/myscope/sem/practice/principles/layout.php>.
20. Fang, W., et al., *Ce-Ni mixed oxide as efficient catalyst for H₂ production and nanofibrous carbon material from ethanol in the presence of water*. RSC Advances, 2012. 2(25): p. 9626-9634.
21. Dresselhaus, M.S., et al., *Raman spectroscopy on isolated single wall carbon nanotubes*. Carbon, 2002. 40(12): p. 2043-2061.
22. Carrero, A., et al., *Effect of Mg and Ca addition on coke deposition over Cu–Ni/SiO₂ catalysts for ethanol steam reforming*. Chemical Engineering Journal, 2010. 163(3): p. 395-402.
23. DiLeo, R.A., et al., *Purity assessment of multiwalled carbon nanotubes by Raman spectroscopy*. Journal of Applied Physics, 2007. 101(6): p. 064307.
24. Ferrari, A.C., et al., *Raman spectroscopy of amorphous, nanostructured, diamond-like carbon, and nanodiamond*. Philosophical Transactions of the Royal Society of London A: Mathematical, Physical and Engineering Sciences, 2004. 362(1824): p. 2477-2512.
25. Barron, C.P.A.R. *Surface-Enhanced Raman Spectroscopy for the Study of Surface Chemistry*. April 2010 [cited 2010; Available from: <http://cnx.org/contents/-KGSWHOc@1/Surface-Enhanced-Raman-Spectro>.

Chapter 4. Investigation of different catalysts and process conditions for carbon nanotubes production and by-product hydrogen by pyrolysis-catalysis of waste tyres

In this section, different metal catalysts supported on the same alumina support (Ni/Al₂O₃, Co/Al₂O₃/ Fe/Al₂O₃ and Cu/Al₂O₃) have been firstly investigated to compare the effect of metals on the hydrogen and carbon nanotube production by pyrolysis-catalysis of waste tyres with a two-stage fixed-bed reactor (Chapter 3). The overall aim of this project is to produce hydrogen and CNTs from waste hydrocarbon by pyrolysis-catalysis/catalytic-reforming. Therefore, the investigation for section 4.1 was carried out without steam to demonstrate the base line conditions to determine the level of CNT production from waste tyre.

According to the results shown in section 4.1, the Ni/Al₂O₃ catalyst gave the best hydrogen and CNT production from the waste tyre pyrolysis-catalysis process. Therefore, Ni-based catalysts have been applied for all of the experiments carried out in section 4.2. The only variable is the support of the catalysts which were alumina-silica with different SiO₂:Al₂O₃ ratios. (3:5, 1:1, 3:2 and 2:1), which was aimed to investigate the effect of supports on hydrogen and CNT production from waste tyre by pyrolysis-catalysis.

Section 4.1 and 4.2 show the catalyst effect on CNT production has been investigated from the pyrolysis-catalysis of waste tyres. In section 4.2 the aim was to investigate the optimum conditions to co-produce hydrogen and CNTs. Three parameters were investigated which were water injection rate, catalysis/catalytic reforming temperature and sample to catalyst ratios.

4.1 Effect of different metals including Co, Fe, Ni and Cu with Al₂O₃ catalyst support

Catalysts play an important role in the waste tyres, plastics or biomass pyrolysis-catalysis process to enhance hydrogen production [1]. Many researchers have undertaken research on catalyst effects on hydrogen production from hydrocarbon thermal conversion processes, nickel-based catalysts are the most common catalysts used for hydrogen production from biomass or plastics by thermal processing because of the high thermal stability, selectivity etc. [1-3]. Sutton et al. summarized that the group 8 metals can catalyse the steam reforming or dry reforming reactions and Ni-based catalysts have been widely used in industry [4] which effectively increase the hydrogen and carbon monoxide contents of the production gas. Baker et al. have compared several different commercial Ni-based catalysts in a wood gasification process [5]. Wu et al. compared several different Ni-based catalysts with different supports and trimetal catalysts in polypropylene pyrolysis catalytic-gasification [1, 6]. Elbaba et al. investigated hydrogen production from waste tyre by pyrolysis catalytic-gasification in the presence of Ni/dolomite and Ni/cerium catalysts [7, 8].

Alkali metals are effective in eliminating tar formation or upgrading the gas products formed in the thermal chemical conversion of carbonaceous materials. Hauserman [9] investigated alkali catalysts for hydrogen production from coal or wood gasification. Sutton et al. [4] concluded that alkali carbonate increases the carbon conversion to gases from the condensable liquid from the gasification process.

Ni-, Fe- and Co-based catalysts have also been used for gasification of hydrocarbons [10]. Hernadi et al. [11] investigated Fe-based catalysts with different supports to produce carbon nanotubes via a chemical vapour deposition (CVD) method of different hydrocarbons, including acetylene, ethylene and propylene. They found that a Fe/silica catalyst showed the highest activity in carbon nanotubes formation compared with other types of catalysts, such as graphite, ZSM-5 and NaY. Co-based catalysts also been investigated to enhance the formation of CNTs in the hydrocarbon reforming process [12].

Qian et al. [12] compared Co- and Ni-based catalysts in a methane decomposition process to produce CNT productions in a fluidized bed reactor. Kong et al. [13] synthesised CNTs by CVD of methane in presence of different catalysts. They compared the effect of different metals (Fe-, Ni-, Co- and Fe/Co-based) and different supports (alumina and silica) on the CNTs formation. Nath et al. [14] synthesised bundles of aligned CNTs by acetylene pyrolysis in the presence of Fe- and Co- based catalysts.

Therefore, in section 4.1, Ni/Al₂O₃, Fe/Al₂O₃, Co/Al₂O₃ and Cu/Al₂O₃ catalysts have been chosen to investigate the metal effect on hydrogen and CNTs production in the waste tyre pyrolysis-catalysis process.

Experiments were carried out in a two-stage fixed-bed reactor in the presence of Co/Al₂O₃, Cu/Al₂O₃, Fe/Al₂O₃ and Ni/Al₂O₃ catalysts. The pyrolysis temperature and catalyst temperature were 600 °C and 800 °C, respectively. The sample to catalyst ratio was consistent throughout section 4.1 which was 1 g of waste truck tyres sample to 0.5 g of catalyst. No steam was introduced in the experiment, therefore the process system was pyrolysis-catalysis.

4.1.1 Characterisations of the fresh catalysts

4.1.1.1 Scanning electron microscopy (SEM)

Scanning electron microscopy (SEM) was used to examine the surface characteristics of the freshly prepared catalysts to determine any differences in surface morphology and structure of the Co/Al₂O₃, Cu/Al₂O₃, Fe/Al₂O₃ and Ni/Al₂O₃ catalysts. Scanning Electron Microscopy (SEM) images of the fresh catalysts used in the pyrolysis-catalytic gasification process are present in Figure 4-1. The SEM images show that the catalysts were composed by many irregular particles. The particles sizes for each catalyst are approximately 1 μm. The metal dispersion of Fe/Al₂O₃ catalysts seems very different from other catalysts. Figure 4-1 (b) shows that the alumina particles were well encased by iron oxide particles and the particles sizes are more homogenous. The active metal oxides particles of Co/Al₂O₃, Cu/Al₂O₃ and Ni/Al₂O₃ catalysts are more dispersive with irregular shapes compared with Fe/Al₂O₃.

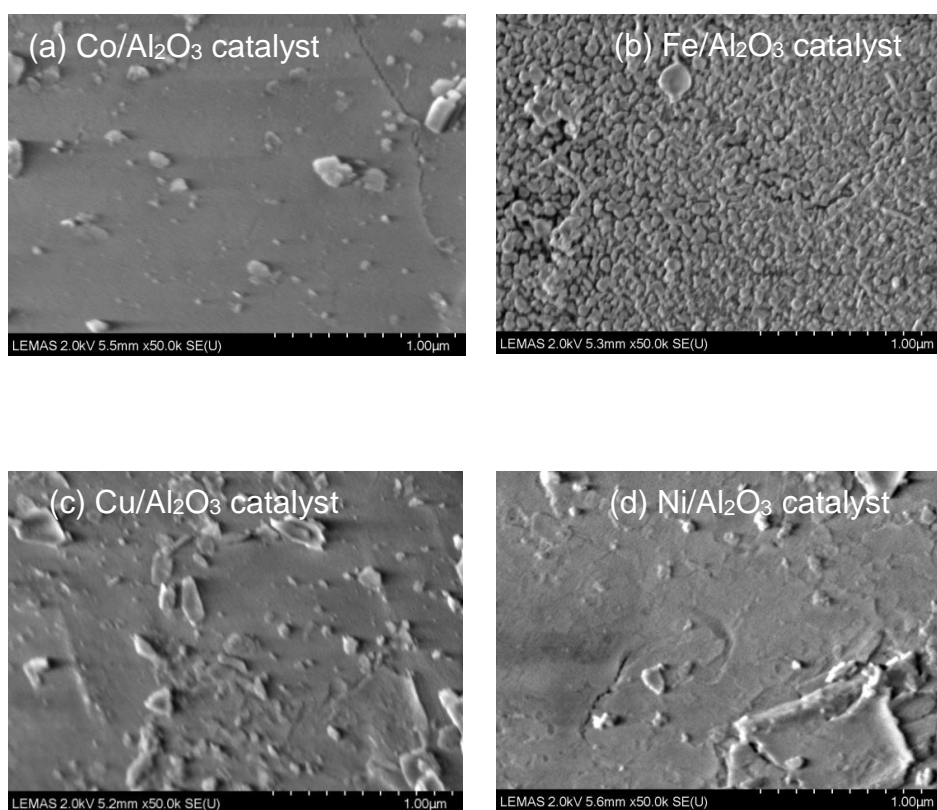


Figure 4-1 SEM images of the fresh Co/Al₂O₃, Cu/Al₂O₃, Fe/Al₂O₃ and Ni/Al₂O₃ catalysts before pyrolysis-catalysis.

4.1.1.2 Temperature programmed reduction (TPR) of the fresh catalysts

Temperature programmed reduction (TPR) analysis was used to characterize the most effective reduction condition of the fresh catalysts therefore to determine the exact type of metal oxides presented in the catalyst. The TPR results are shown in Figure 4-2. The Ni/Al₂O₃ catalyst has two main reduction peaks which occurred at around temperatures of 230 and 800 °C; these two reduction peaks can be assigned to the reduction of bulk NiO particles and Ni-Al spinel phases (NiAl₂O₄), respectively. The NiO and NiAl₂O₄ phases were reported by Wu et al. [6] and Clause et al. [15]. The reason for the first reduction peak at the relatively low reduction temperature of 230 °C may be because of the nature of the reduction of the nickel oxide species on the alumina support.

There are several reduction peaks for Fe/Al₂O₃ catalysts, which might be due to the reduction of Fe₂O₃ to Fe₃O₄, Fe₃O₄ to FeO, and FeO to Fe. The relatively

low temperature of reduction of iron oxide species has been attributed to the well dispersed nature of iron on the support [16]. Brown et al.[17] considered the reduction peak of Fe_3O_4 to FeO as partial reduction and re-oxidation. Wan et al. [18] described the reduction of Fe_2O_3 which ends at a FeO metastable phase rather than Fe which is easily oxides below 570°C .

Berry et al. [19] found the reductions of Fe_2O_3 to Fe occurs at around 440 and 640°C , which are similar to that found in Figure 4-2, where the reduction peaks occur at the temperatures of 460°C and 630°C . They also interpreted the reduction process to include the mixture of Fe^{3+} and Fe^{2+} to Fe^0 . The Fe-Al spinel phase has a reduction peak at a relatively high temperature which has been suggested as being to the strong interaction of Fe ions with the alumina support [17].

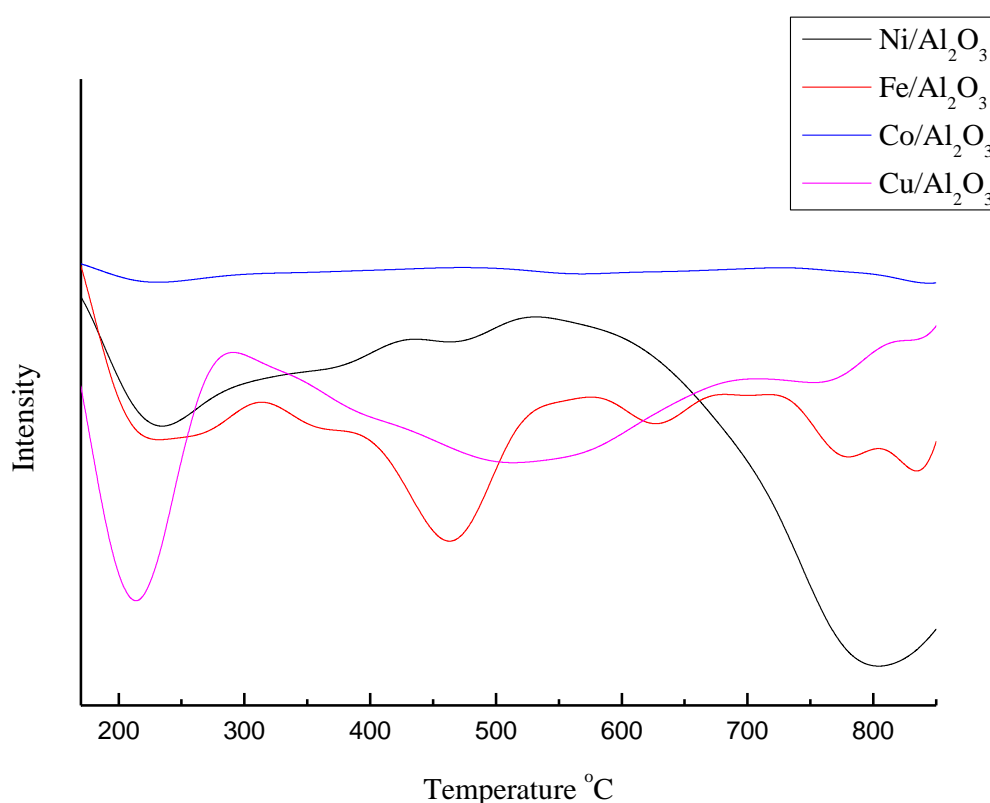


Figure 4-2 DTG-TPR results of the $\text{Co}/\text{Al}_2\text{O}_3$, $\text{Cu}/\text{Al}_2\text{O}_3$, $\text{Fe}/\text{Al}_2\text{O}_3$ and $\text{Ni}/\text{Al}_2\text{O}_3$ catalysts fresh catalysts

The Cu/Al₂O₃ catalyst has two main reduction stages with reduction peaks at temperatures of 210 and 300 °C. In addition, a broad slow reduction was observed for the TPR thermogram of the Cu/Al₂O₃ catalyst at temperatures between 300 and 700 °C. The first reduction peak indicates the reduction of CuO and the second reduction peak indicates the reduction of CuAl₂O₄ as suggested by Marino et al. [20] who investigated the reduction of CuO and CuAl₂O₄ phases present in a Cu/Al₂O₃ catalyst. For the Co/Al₂O₃ catalyst, it appears that this catalyst is hardly reduced under the TPR conditions used, suggesting that there are limited active Co sites in this catalyst. The result is similar to that reported by Chu et al.[21], they stated there were no Co₃O₄ component when they prepared a cobalt supporting alumina catalyst.

4.1.1.3 X-Ray diffraction (XRD) analysis of the Co/Al₂O₃, Cu/Al₂O₃, Fe/Al₂O₃ and Ni/Al₂O₃ catalysts.

X-ray diffraction (XRD) techniques can be used to identify the crystalline phases of the catalysts [22], the results for the Co/Al₂O₃, Cu/Al₂O₃, Fe/Al₂O₃ and Ni/Al₂O₃ catalysts are presented in Figure 4-3. A Fe₂O₃ phase was identified in the Fe/Al₂O₃ catalyst, NiAl₂O₄ and NiO phases were found in the Ni/Al₂O₃ catalyst, A CoAl₂O₄ spinel phase was identified in the Co/Al₂O₃ catalyst, and a CuAl₂O₄ phase was present in the Cu/Al₂O₃ catalyst. The oxide species Fe₂O₃, NiO and NiAl₂O₄, CoAl₂O₄ and CuAl₂O₄ will be transferred into active catalytic Fe, Ni, Co and Cu sites for hydrogen and carbon nanotube production in the pyrolysis-catalytic process, respectively, due to the reducing atmosphere generated in the process (CO and H₂) [23].

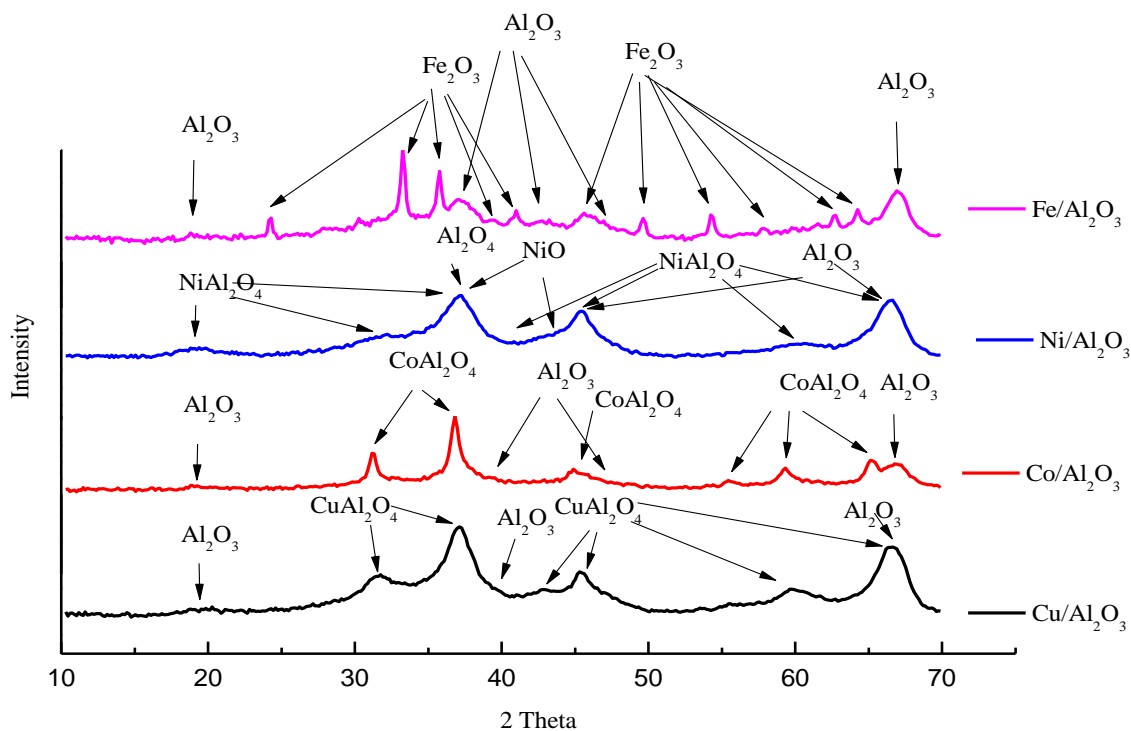


Figure 4-3 XRD analysis of the fresh Co/Al₂O₃, Cu/Al₂O₃, Fe/Al₂O₃ and Ni/Al₂O₃ catalysts.

4.1.2 Pyrolysis-catalysis of waste tyres: Mass balance and hydrogen production

Mass balance and gas concentrations derived from the pyrolysis-catalysis of waste tyres using the four different catalysts (Co/Al₂O₃, Cu/Al₂O₃, Fe/Al₂O₃ and Ni/Al₂O₃) are shown in In Table 4-1, for the investigated four catalysts, the gas yield ranking from the pyrolysis-catalysis process was Ni/Al₂O₃ >Cu/Al₂O₃>Fe/Al₂O₃>Co/Al₂O₃; The ranking of liquid yield in the catalysis process is Co/Al₂O₃>Ni/Al₂O₃>Cu/Al₂O₃>Fe/Al₂O₃; The residue yields for the different catalyst remained constant at around 38.00 wt.%, as expected, since the residue represents the pyrolysis char remaining in the pyrolysis reactor which would be unaffected by the catalysts.

Table 4-1. The product yields including gas, liquid and residue yields were calculated in relation to the mass of the waste tyres. The liquid and residue

yields were measured by weighing, and the carbon yield deposited on the catalyst was calculated by TGA-TPO from

Figure 4-4. Gas yield was calculated based on the gas concentration from the gas chromatography analysis of the individual gas species and their molecular mass.

In Table 4-1, for the investigated four catalysts, the gas yield ranking from the pyrolysis-catalysis process was Ni/Al₂O₃ >Cu/Al₂O₃>Fe/Al₂O₃>Co/Al₂O₃; The ranking of liquid yield in the catalysis process is Co/Al₂O₃>Ni/Al₂O₃>Cu/Al₂O₃>Fe/Al₂O₃; The residue yields for the different catalyst remained constant at around 38.00 wt.%, as expected, since the residue represents the pyrolysis char remaining in the pyrolysis reactor which would be unaffected by the catalysts.

Table 4-1 Mass balance and gas concentrations for the pyrolysis-catalysis of waste tyres.

	Sand	Fe/Al ₂ O ₃	Cu/Al ₂ O ₃	Co/Al ₂ O ₃	Ni/Al ₂ O ₃
Gas yield (wt.%)	30.26	22.07	30.40	24.76	34.60
Liquid yield (wt.%)	18.00	11.00	14.00	24.00	20.00
Residue (wt.%)	38.00	38.00	36.00	37.00	39.00
Hydrogen production (mmol g ⁻¹ tyre)	4.96	7.26	5.53	9.03	18.14
Carbon (wt.%)	-	14.00	14.00	8.00	12.00
Mass balance (wt.%)	86.26	92.43	94.40	93.76	105.60
Gas concentrations (vol.%)					
CO	3.04	7.83	3.30	12.80	16.06
H ₂	23.79	33.12	25.38	46.20	57.47
CH ₄	63.23	51.62	64.29	30.44	19.66
CO ₂	1.29	1.11	1.34	1.69	1.07
C ₂ -C ₄	8.65	6.31	5.68	8.88	4.40

In Table 4-1, for the investigated four catalysts, the gas yield ranking from the pyrolysis-catalysis process was $\text{Ni/Al}_2\text{O}_3 > \text{Cu/Al}_2\text{O}_3 > \text{Fe/Al}_2\text{O}_3 > \text{Co/Al}_2\text{O}_3$; The ranking of liquid yield in the catalysis process is $\text{Co/Al}_2\text{O}_3 > \text{Ni/Al}_2\text{O}_3 > \text{Cu/Al}_2\text{O}_3 > \text{Fe/Al}_2\text{O}_3$; The residue yields for the different catalyst remained constant at around 38.00 wt.%, as expected, since the residue represents the pyrolysis char remaining in the pyrolysis reactor which would be unaffected by the catalysts.

Table 4-1, shows that the gas yield increased from 30.26 wt.% to 34.60 wt.% with the introduction of the $\text{Ni/Al}_2\text{O}_3$ catalyst and the hydrogen yield increased from 4.96 wt.% to 18.14 wt.% with the $\text{Ni/Al}_2\text{O}_3$ catalyst. The liquid yield from waste tyre pyrolysis-catalysis was reduced from 18.0 wt.% to 11.0 wt.% with $\text{Fe/Al}_2\text{O}_3$ catalyst introduction.

The highest hydrogen production was 18.14 wt.% in the pyrolysis-catalysis process with the $\text{Ni/Al}_2\text{O}_3$ catalysts, and hydrogen yields were much less with the catalysts containing the other metals investigated, which were 9.03 wt.% with the $\text{Co/Al}_2\text{O}_3$ catalyst, 7.26 wt.% with the $\text{Fe/Al}_2\text{O}_3$ catalyst and 5.53 wt.% with the $\text{Cu/Al}_2\text{O}_3$ catalyst as shown in Table 4-1.

In this work, total carbon yield was calculated as the weight increase of the catalytic reactor tube divided by the weight of tyre sample. The ranking of carbon yield was 14 wt.% ($\text{Cu/Al}_2\text{O}_3$)= $\text{Fe/Al}_2\text{O}_3$ >12 wt.% ($\text{Ni/Al}_2\text{O}_3$)> 8 wt.% ($\text{Co/Al}_2\text{O}_3$). Carbon deposition formed in the pyrolysis-catalysis process using different catalysts will be further discussed.

Figure 4-4 shows the temperature programmed oxidation (TPO) results for the four used catalysts. For the used $\text{Cu/Al}_2\text{O}_3$ catalyst, there was a slight weight increase at around 400 °C, which is regarded as the oxidation of Cu metals to Cu oxides. The metal is produced during the initial pyrolysis-catalysis process step by reducing the copper oxides in the freshly prepared catalyst by reducing agents e.g. CO and H₂. The result is consistent with the temperature programmed reduction (TPR) analysis of the fresh $\text{Cu/Al}_2\text{O}_3$ catalyst (Figure 4-2), which shows the largest reduction peak at the lowest reduction temperature (~210 °C) compared with other catalysts.

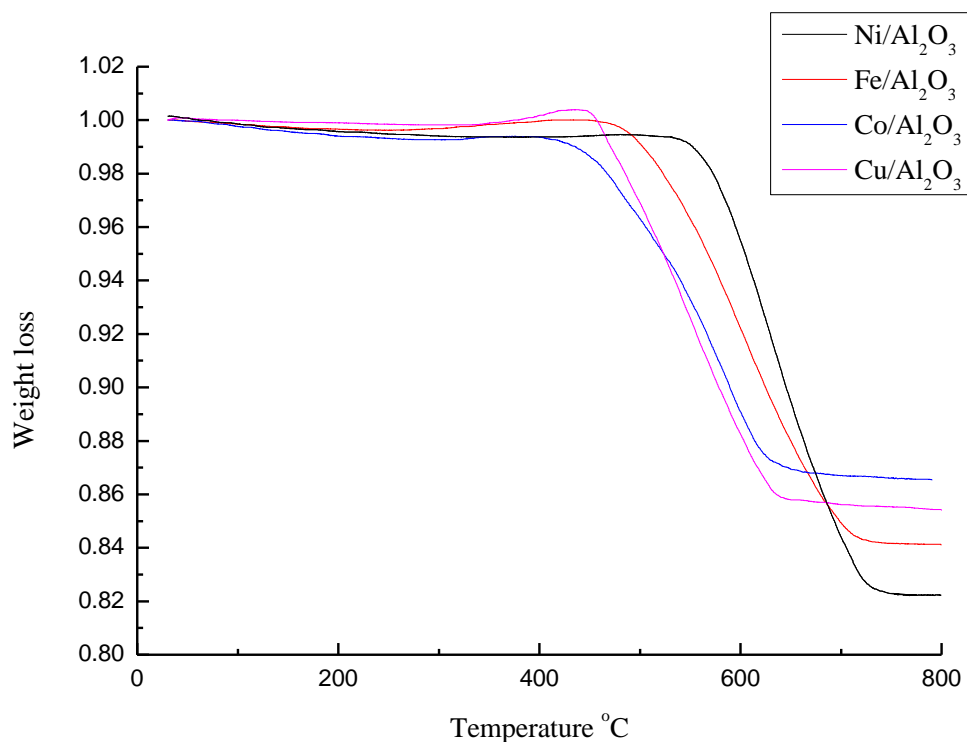


Figure 4-4 TPO results of different reacted catalysts from the pyrolysis-catalysis of waste tyre. (Catalyst temperature was 600 °C)

By calculation of the weight loss against the weight of used catalyst in the TPO experiments, the estimated carbon fraction is obtained regardless of the active metal reduction and oxidization. The TPO results shows that 13.44, 14.51, 15.86 and 17.78 wt.% of the weight of the reacted catalysts were ascribed to deposited carbon for the pyrolysis-catalysis process using the Co/Al₂O₃, Cu/Al₂O₃, Fe/Al₂O₃ and Ni/Al₂O₃ catalysts, respectively. The oxidation of the carbon starts from a temperature of around 550 °C which is assigned to the oxidation of amorphous carbons, while the oxidization at around 650 °C is assigned to the oxidation of filamentous carbons [15, 23, 24].

The derivative-TPO results (DTG-TPO) of the used Co/Al₂O₃, Fe/Al₂O₃, Cu/Al₂O₃ and Ni/Al₂O₃ catalysts are shown in Figure 4-5. The DTG-TPO results of the used Co/Al₂O₃ and Cu/Al₂O₃ catalysts show that two main oxidation peaks are observed indicating that there are two different types of carbons

formed on the catalyst. Two oxidation peaks (occurring at around temperatures of 500 and 600 °C) are obtained from the DTG-TPO results for both the Co/Al₂O₃ and Cu/Al₂O₃ catalysts; it is suggested both amorphous and filamentous carbons are formed using the Co/Al₂O₃ and Cu/Al₂O₃ catalysts during the pyrolysis-catalysis process. However, for the used Fe/Al₂O₃ and Ni/Al₂O₃ catalysts, there is only one peak (at a temperature of ~600 °C) identified in the DTG-TPO results, indicating that most of the carbon produced using the Fe/Al₂O₃ and Ni/Al₂O₃ catalysts are filamentous carbon. It is also shown that the highest temperature for carbon oxidation in the DTG-TPO results (Figure 4-5) is for the used Ni/Al₂O₃ catalyst. From the results, it is suggested that the Ni/Al₂O₃ catalyst produces carbon materials containing the largest fraction of filamentous carbons among the investigated catalysts.

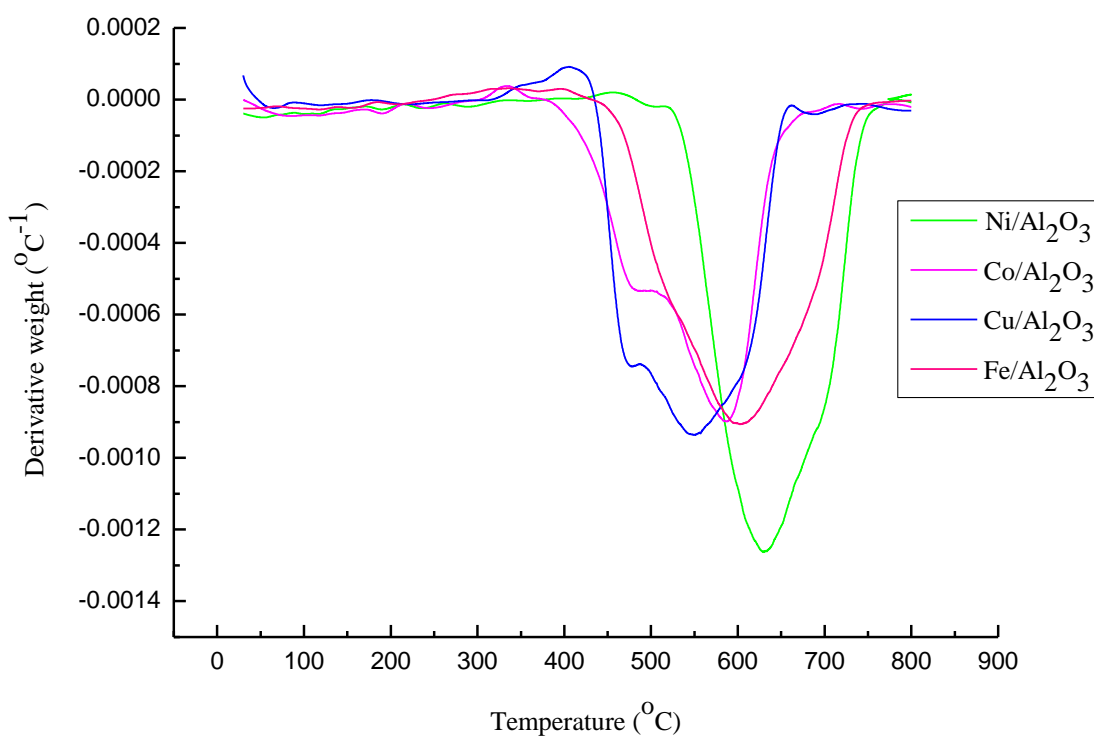


Figure 4-5 DTG-TPO results of different reacted catalysts from the pyrolysis-catalysis of waste tyre. (catalyst temperature was 600 °C

4.1.3 Carbon Nanotubes (CNTs) Production

4.1.3.1 SEM and TEM

Scanning electron microscopy (SEM) and transmission electron microscopy (TEM) were used for characterization of the catalysts used in the experiments and after the pyrolysis-catalysis process. As shown in Figure 4-6 (c,d), filamentous carbons were identified on the surface of the used Fe/Al₂O₃ and Ni/Al₂O₃ catalysts. The filamentous carbon produced on the surface of the used Ni/Al₂O₃ catalyst is relatively long (Figure 4-6 (d)) at around 1 cm compared with filamentous carbon formed using other catalysts that are in a few micrometres.

TEM results confirm that most of the filamentous carbons produced from the Ni/Al₂O₃ catalyst are multi walled carbon nanotubes (MWCNTs) (Figure 4-7 (c,d)). It is also shown that the Ni/Al₂O₃ catalyst produces CNTs that are relatively long and smooth; the SEM and TEM results are consistent with the TPO and DTG-TPO analysis (

Figure 4-4 and Figure 4-5) where carbons produced from the Ni/Al₂O₃ catalyst have the highest fraction of filamentous carbons.

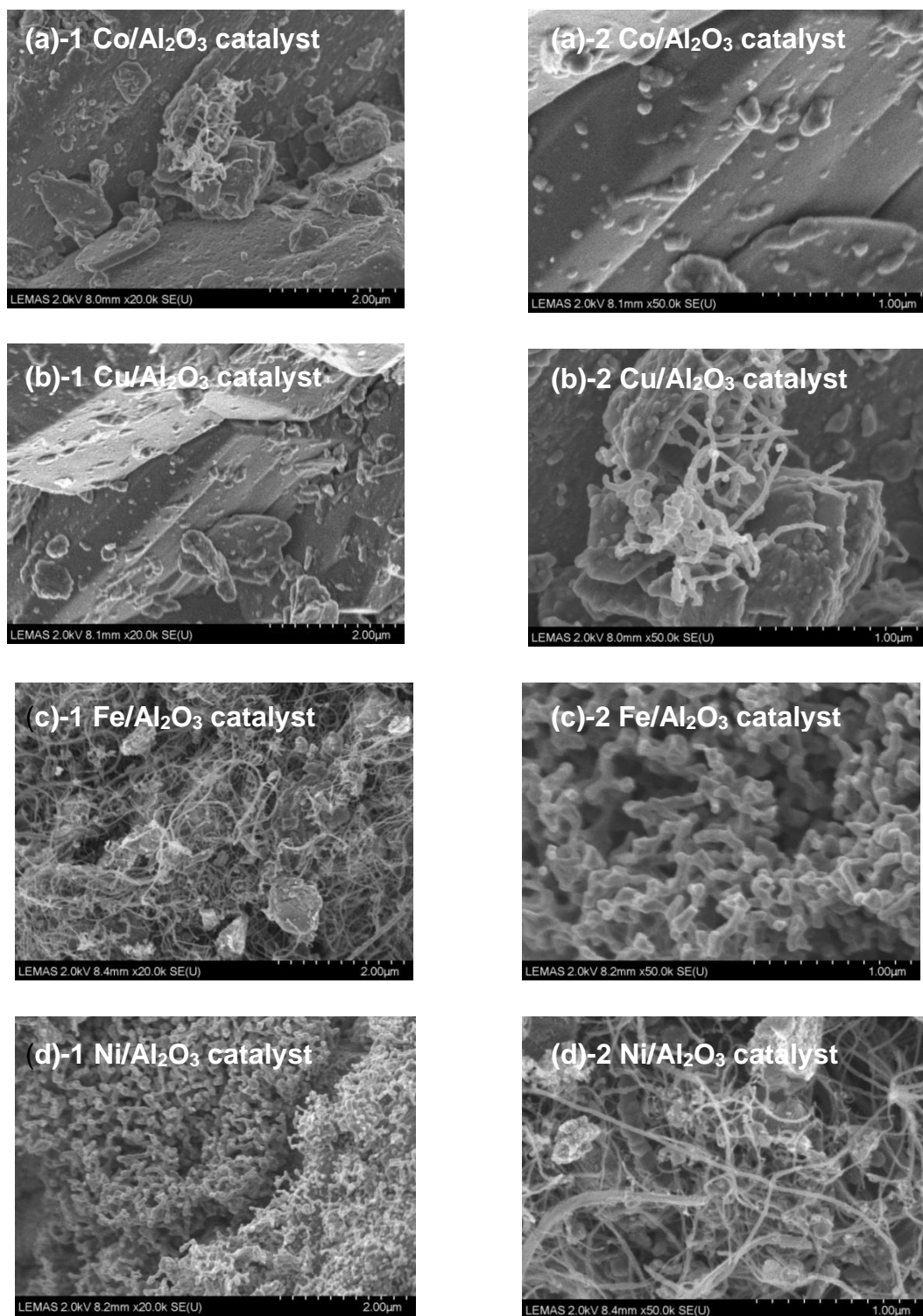


Figure 4-6 SEM analysis of the reacted Co/Al₂O₃, Cu/Al₂O₃, Fe/Al₂O₃ and Ni/Al₂O₃ catalysts after the pyrolysis-catalysis of waste tyre.

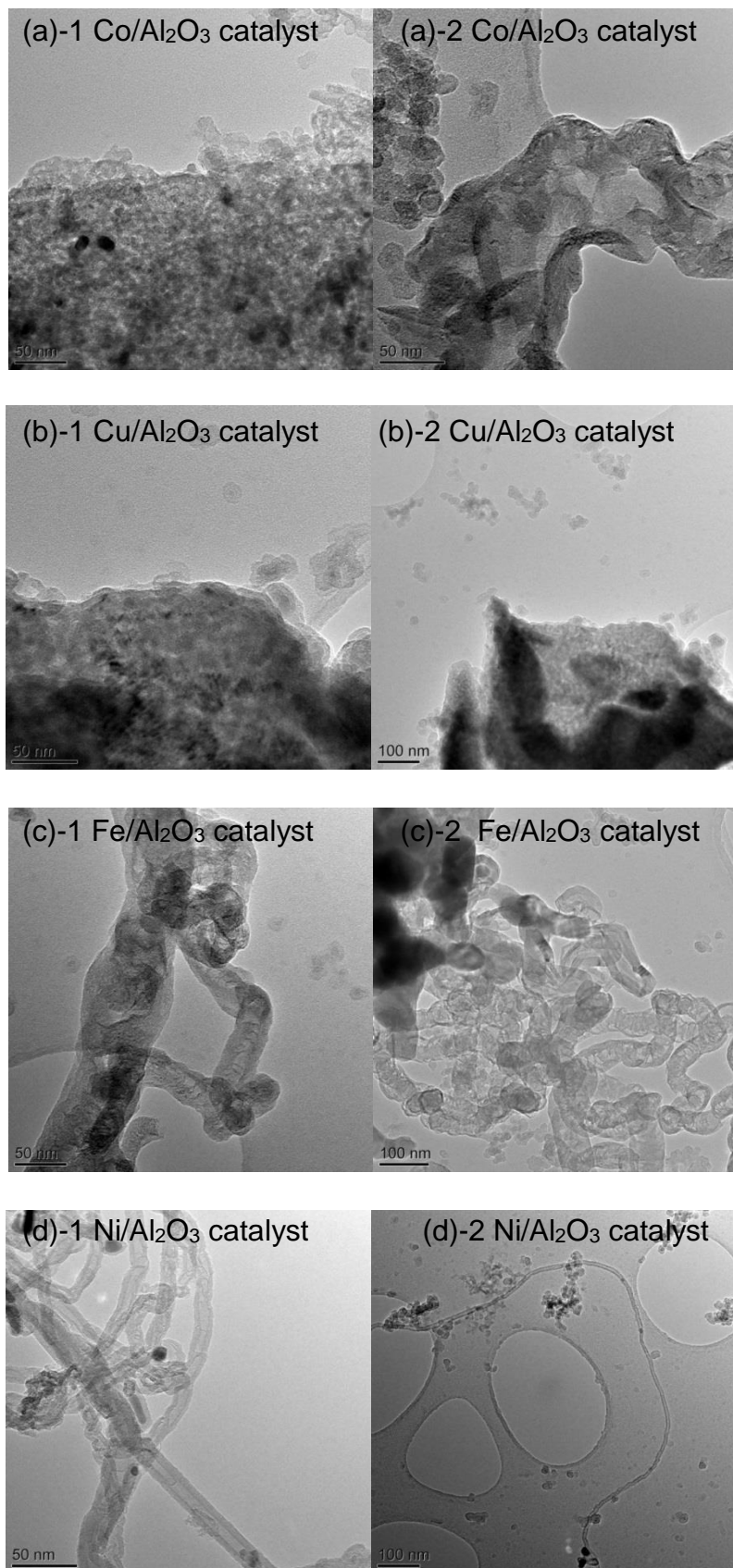


Figure 4-7 TEM analysis of the reacted Co/Al₂O₃, Cu/Al₂O₃, Fe/Al₂O₃ and Ni/Al₂O₃ catalysts derived from pyrolysis-catalysis of waste tyre

4.1.3.2 Raman Analysis

Raman spectroscopy analysis was used to characterize the carbons formed on the different catalysts produced from the pyrolysis-catalysis process for used tyres and the results are shown in

Figure 4-8. The D band at the Raman shift of around 1352 cm^{-1} indicates amorphous or disordered carbons. The G band at the Raman shift around 1587 cm^{-1} indicates a graphite carbon structure. The second order Raman spectrum G' at the Raman shift around 2709 cm^{-1} indicates the two photon elastic scattering process [25, 26].

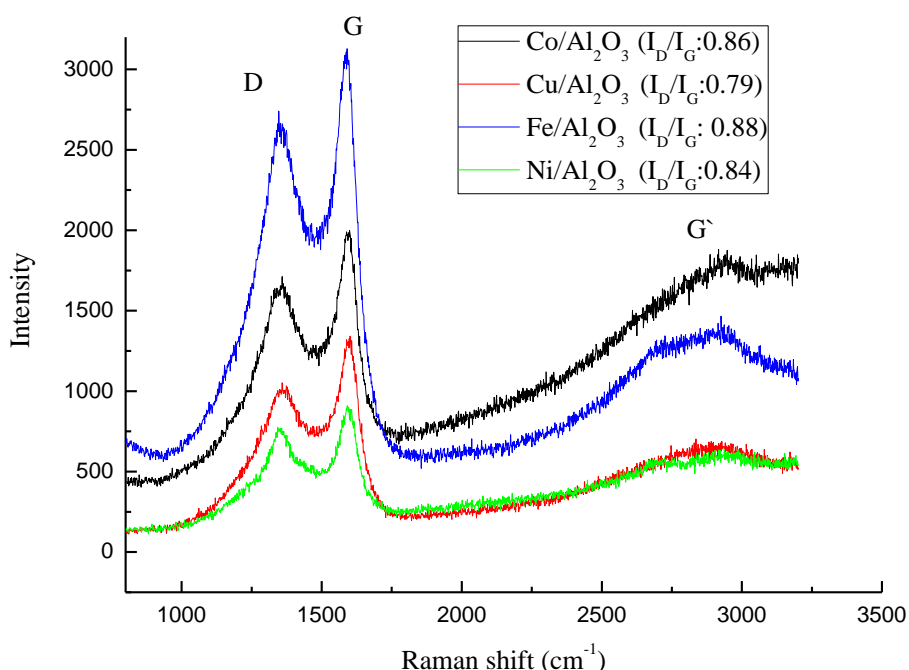


Figure 4-8 Raman analysis of the 4 reacted catalysts (Fe/Al₂O₃, Cu/Al₂O₃, Co/Al₂O₃, Ni/Al₂O₃)

The carbon materials produced in this work have similar Raman shift patterns compared with CNTs produced from other work and commercial CNTs [27-29]. To evaluate the degree of graphitization of CNTs in the waste tyre pyrolysis-catalysis process, the intensity of the D band (I_D) normalized to the intensity of the G band (I_G) which is the I_D/I_G ratio is used,

Figure 4-8 shows the I_D/I_G ratio for the carbons deposited on the different catalysts. The carbons from the Ni/Al_2O_3 catalyst show a relatively low I_D/I_G ratio compared with the other catalysts, indicating the carbons are less disordered and contain less amorphous carbons; the results are consistent with the TPO, SEM and TEM analysis, indicating that the Ni/Al_2O_3 catalyst is the best catalyst for CNTs production in terms of crystallization, smooth morphology and yield. The relatively low I_D/I_G ratio also indicates the relatively high quality of CNTs with less structural defects [27, 28, 30, 31].

4.1.4 Conclusion

In this section, four different kinds of catalysts (Co/Al_2O_3 , Cu/Al_2O_3 , Fe/Al_2O_3 and Ni/Al_2O_3) were investigated in the waste tyre pyrolysis-catalysis process to produce high-value carbon nanotubes (CNTs). The conclusions for this work are:

- 1) The highest carbon production was produced with the Ni/Al_2O_3 catalyst and most of the carbons are filamentous carbons which are mostly CNTs as shown by TPO and TEM data;
- 2) The Ni/Al_2O_3 catalyst also produced the best quality CNT production where SEM and TEM results show that the CNTs are relatively long, straight and additional Raman analysis shows that the CNTs are crystalline.

In addition, the amount of by-product hydrogen was also evaluated;

- 3) The presence of catalysts can boost the waste tyre pyrolysis-catalysis process to produce more hydrogen production. The Ni/Al_2O_3 catalyst produced the highest total gas yield and the highest H_2 production;

4.2 Effect of SiO₂:Al₂O₃ ratios of Ni/SiO₂/Al₂O₃ catalysts on the production of carbon nanotubes production and by-product hydrogen

Section 4.1 showed that the Ni/Al₂O₃ catalyst performed better in terms of yield and quality of CNTs from the pyrolysis-catalysis of waste tyres, Section 4.2 extends the work of Section 4.1 by investigating the influence of the type of support for nickel containing catalysts which enhance the production and quality of carbon nanotubes from the pyrolysis-catalysis of waste tyres. The influence of catalyst support as alumina-silica in terms of different Al₂O₃ to SiO₂ mole ratios of 3:5, 1:1, 3:2, 2:1 containing 20 wt.% Ni on the production of CNT's were investigated. In addition, the by-product production of hydrogen is also reported.

The two-stage pyrolysis-catalysis reactor system was used with pyrolysis of the tyres followed by catalytic reaction as described in Chapter 3. The final pyrolysis temperature used was 600 °C and the catalyst temperature was 800 °C. In each of the experiments, 1.0 g tyre sample and 0.5 g catalyst were used. The heating rate of the pyrolysis stage was 40 °C min⁻¹ to the final temperature of 600 °C and held at that temperature for 20 minutes. No steam was introduced to the experiments with different SiO₂:Al₂O₃ ratios catalysts.

4.2.1 Product yields and gas composition

4.2.1.1 Influence of SiO₂:Al₂O₃ ratio on the production of carbon nanotubes and by-product hydrogen

Table 4-2 shows the product yield from pyrolysis-catalysis of waste tyres with different 20 wt.% Ni/Al₂O₃/SiO₂ catalysts in relation to different Al₂O₃ to SiO₂ ratios. From Table 4-2 and Figure 4-9, it is shown that as the Al₂O₃ to SiO₂ ratio was increased, the hydrogen production increased to produce the highest amount of 13.96 mmol g⁻¹ hydrogen at the Al₂O₃:SiO₂ ratio of 1:1. At higher Al₂O₃:SiO₂ ratios the hydrogen production decreased. The calorific values of the produced gases did not change significantly by changing the Al₂O₃ to SiO₂ ratios, which were in the range of 18.67 to 20.67 MJ m⁻³.

Table 4-2 Product yields and gas concentrations from the pyrolysis-catalysis of waste tyres with a 20 wt. % Ni/Al₂O₃/SiO₂ catalyst with different Al₂O₃ to SiO₂ ratios (the yields were calculated based on the weight of feedstock).

Al ₂ O ₃ :SiO ₂ ratio	3:5	1:1	3:2	2:1
Gas yield (wt. %)	23.30	27.30	25.90	25.30
Liquid yield (wt. %)	14.00	13.00	15.00	17.00
Residue (wt. %)	39.00	36.00	39.00	39.00
Catalyst coke (wt. %)	18.00	19.00	14.00	13.00
Hydrogen production (mmol g ⁻¹ _{tyre})	11.50	14.00	12.00	12.00
CO production (mmol g ⁻¹ _{tyre})	2.40	3.30	2.60	2.30
Syngas production (mmol g ⁻¹ _{tyre})	13.90	17.30	14.60	14.30
Gas composition (vol. %)				
CO	11.60	13.30	11.90	10.70
H ₂	55.10	56.10	54.90	55.00
CH ₄	23.30	22.00	21.40	20.90
CO ₂	0.00	0.00	0.00	0.00
C ₂ -C ₄	4.80	4.50	6.00	4.60
Calorific value (MJ m ⁻³)	20.00	19.50	20.70	18.70

Also, the gas yield, catalyst carbon yield and hydrogen gas concentration were at the highest levels for the catalyst with an Al₂O₃ to SiO₂ ratio of 1:1, at 27.34 wt.%, 19.00 wt.% and 56.06 vol.% respectively. There was no significant difference in liquid yield between the different catalysts with different Al₂O₃ to SiO₂ ratios. However, the liquid yield increased slightly as the Al₂O₃:SiO₂ ratio increased, therefore, the catalyst coke formation was correspondingly decreased since the carbon formed as heavy hydrocarbon liquid instead of solid carbon formation. It can be concluded that the catalyst with an Al₂O₃:SiO₂ ratio

1:1 showed the best performance in terms of the gas yield and hydrogen production. Figure 4-9 shows that the increased content of Al₂O₃ in the 20 wt.% Ni/Al₂O₃/SiO₂ catalyst produced reduced amounts of catalyst carbon deposition, decreasing from ~18 to ~13 wt.%. Kukovecz et al. [32] found that the decrease of alumina content in Co/Al₂O₃/SiO₂ catalysts which was reduced from 80 to 20%, the carbon production increased from 30.1% to 68.5 % in experiments with acetylene to produce carbon nanotubes.

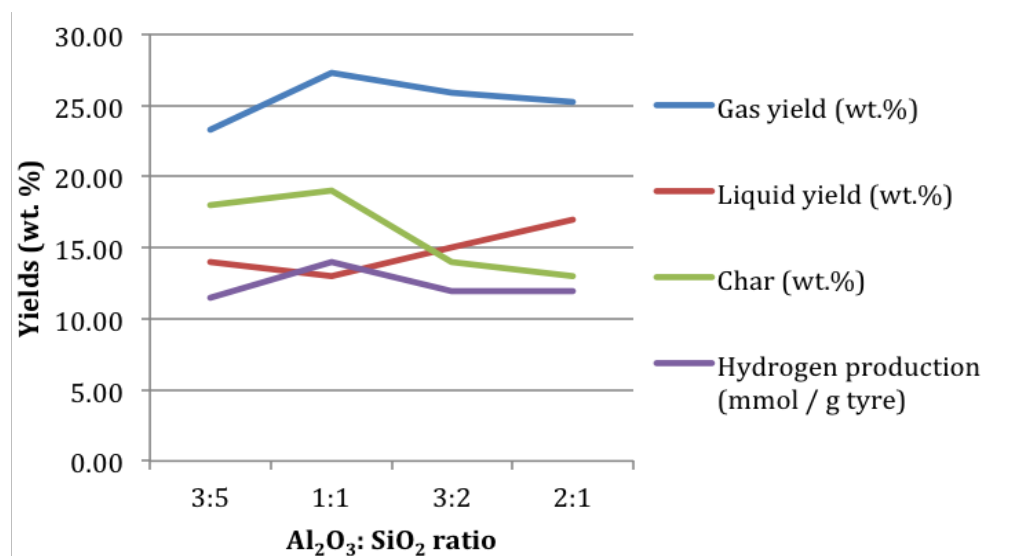


Figure 4-9 Product yields from the pyrolysis-catalysis of waste tyres with a 20 wt. % Ni/Al₂O₃/SiO₂ catalyst with different Al₂O₃ to SiO₂ ratios.

4.2.2 Characteristics of carbon production

4.2.2.1 Influences of different Al₂O₃ to SiO₂ ratios

The reacted Ni/Al₂O₃/SiO₂ catalysts with different Al₂O₃ to SiO₂ ratios have been further analysed by TGA-TPO. For this analysis the weight loss is mainly due to the oxidation of carbon production on the catalyst surface. Figure 4-10 shows the TGA-TPO and DTG-TPO results of the reacted catalysts. It can be observed that there are two peaks for all of the four different catalysts in the DTG-TPO figure. All of these four DTG-TPO curves show similar trends. There were no peaks below 500 °C for all of the catalyst, this could be because of the lack of formation of amorphous carbon on the catalyst surface, since such carbons are known to oxidise at lower temperature.

For example, Fang et al. [33] found that for DTG-TPO there was no peaks present under 400 °C. Musumeci et al. [34] have suggested that the amorphous carbons are easily oxidized from the surface of nickel based catalyst.

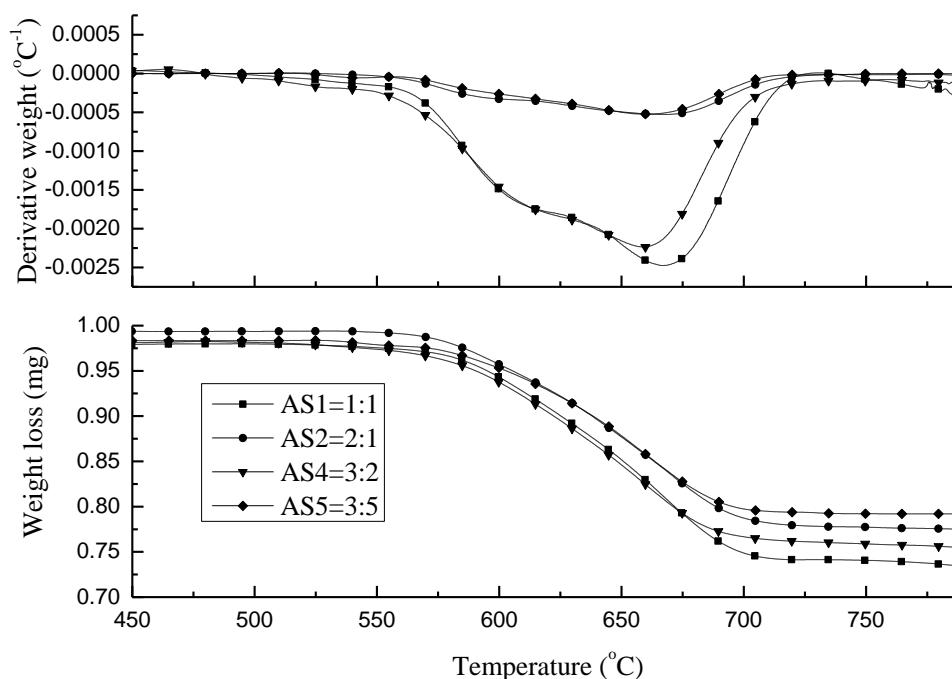


Figure 4-10 TGA-TPO and DTG-TPO analyses for reacted catalysts from the pyrolysis-catalysis of waste tyres with different alumina:silica ratios for 20 wt. % Ni/Al₂O₃/SiO₂ catalyst with different Al₂O₃ to SiO₂ ratios (AS1 = alumina:silica ratio is 1:1; AS2 = alumina:silica ratio is 2:1; AS4 = alumina:silica ratio is 3:2; AS5 = alumina:silica ratio is 3:5).

The oxidation peaks for all of the catalysts are presented at similar temperatures in which the first peak occurs at around 600°C and the second peak arises between 650°C and 675°C. The first peak indicates the oxidization of smaller sized filamentous carbon with less graphitization. The second oxidization peak indicates the oxidization of filamentous carbon that are of larger size and with a higher degree of graphitization. In addition, carbon nanotubes are reported to be oxidized at a high temperature above 600 °C by Wu et al. [35], and also Musumeci et al. [34] suggested that the more graphitic filamentous carbons are more stable and can only be oxidized at higher temperature with a sharp oxidation peak. Therefore, from the TPO results it can

be suggested that the carbon produced in these experiments may be filamentous type carbon with different degrees of graphitization. Examination of the corresponding SEM images in Figure 4-11 can also confirm that the carbon formed on the catalyst surface are filamentous carbons. The corresponding TEM images shown in Figure 4-12 also confirm that the filamentous carbons are mostly multi-walled carbon nanotubes (MWCNTs).

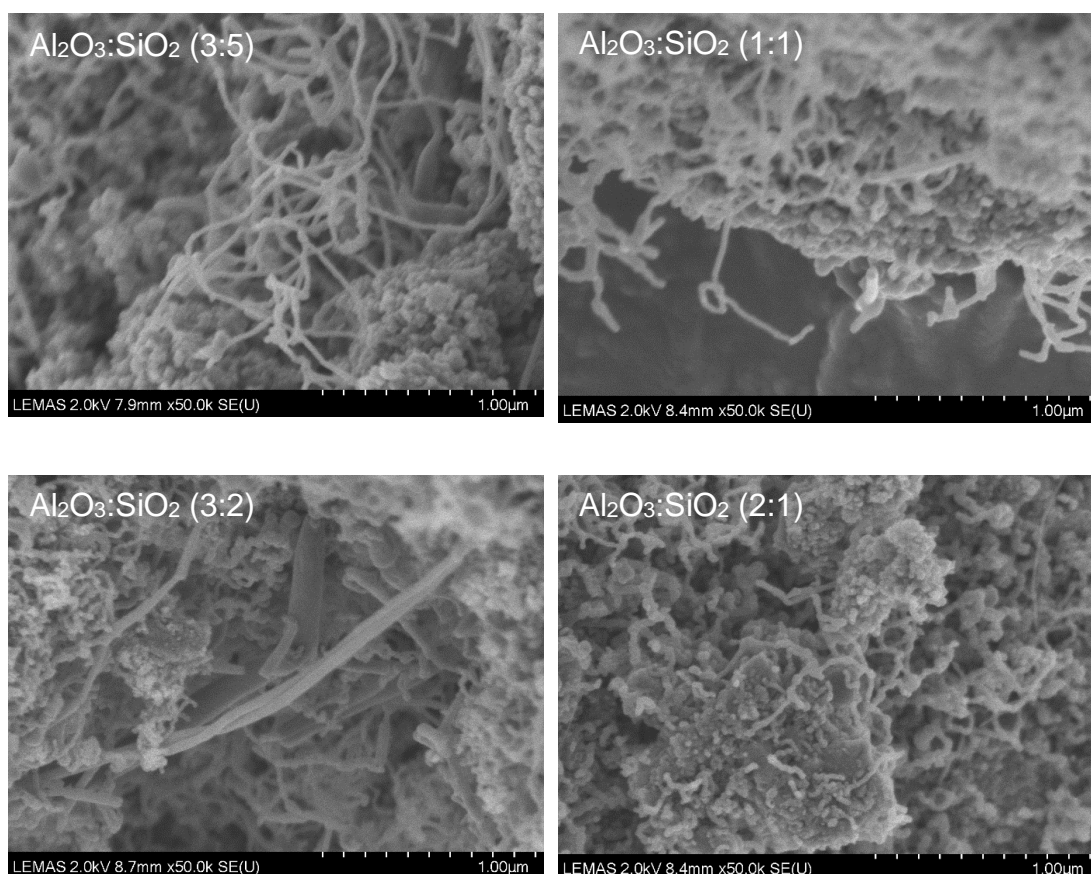


Figure 4-11 SEM images of reacted catalysts from the pyrolysis-catalysis of waste tyres with a 20 wt. % Ni/Al₂O₃/SiO₂ catalyst with different Al₂O₃ to SiO₂ ratios.

In Figure 4-10, the first oxidation peaks in the DTG-TPO curves for Al₂O₃ to SiO₂ ratios of 3:2 and 1:1 are produced at lower temperatures than the other two Al₂O₃ to SiO₂ ratios. This can be assigned to the diameters of the MWCNTs produced with Al₂O₃ to SiO₂ ratios at 3:2 and 1:1 catalysts which are smaller than the MWCNTs produced with the nickel catalysts with Al₂O₃ to SiO₂ ratios of 3:5 and 2:1 for the waste tyres pyrolysis-catalysis process. The TEM images in Figure 4-12 confirm the difference in diameters of the MWCNTs. The inner

diameters of the MWCNTs produced with catalysts with Al₂O₃ to SiO₂ ratios at 3:5, 1:1, 3:2 and 2:1 are approximately 36 nm, 18 nm, 11 nm (and 20 nm) and 25 nm, respectively.

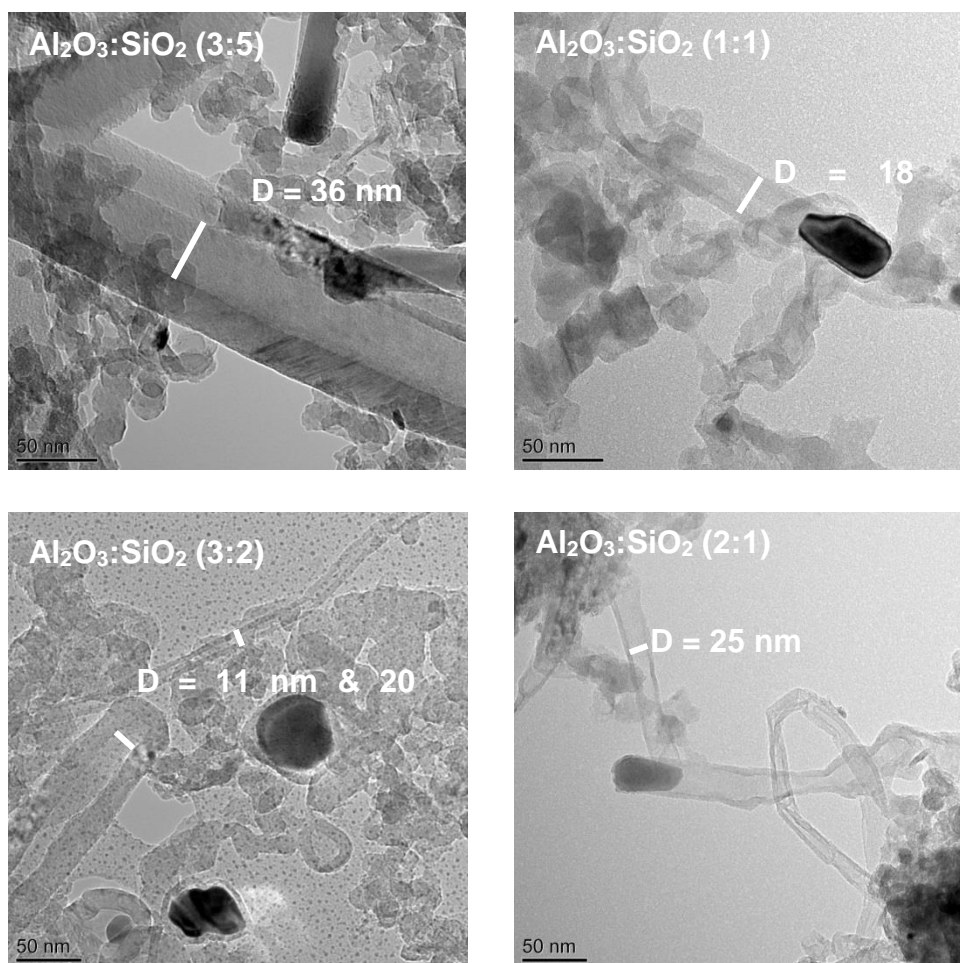


Figure 4-12 TEM images of reacted catalysts from the pyrolysis-catalysis of waste tyres with a 20 wt. % Ni/Al₂O₃/SiO₂ catalyst with different Al₂O₃ to SiO₂ ratios.

Fang et al. [33] suggested that smaller NiO and CeO₂ particles of the catalysts contribute to higher reactivity of the smaller size of filamentous carbon. They reported that the oxidization peak of smaller diameter filamentous carbons in TPO results was larger and shifted to lower temperature compared with the larger sized filamentous carbon. The largest inner diameter of CNTs was produced with the highest SiO₂ content (Al₂O₃:SiO₂ is 3:5) 20 wt. % Ni/Al₂O₃/SiO₂ catalyst. Kukoveca et al. [32] also found that increasing the amount of silica in the catalyst support slightly increased the thickness of the carbon nanotubes.

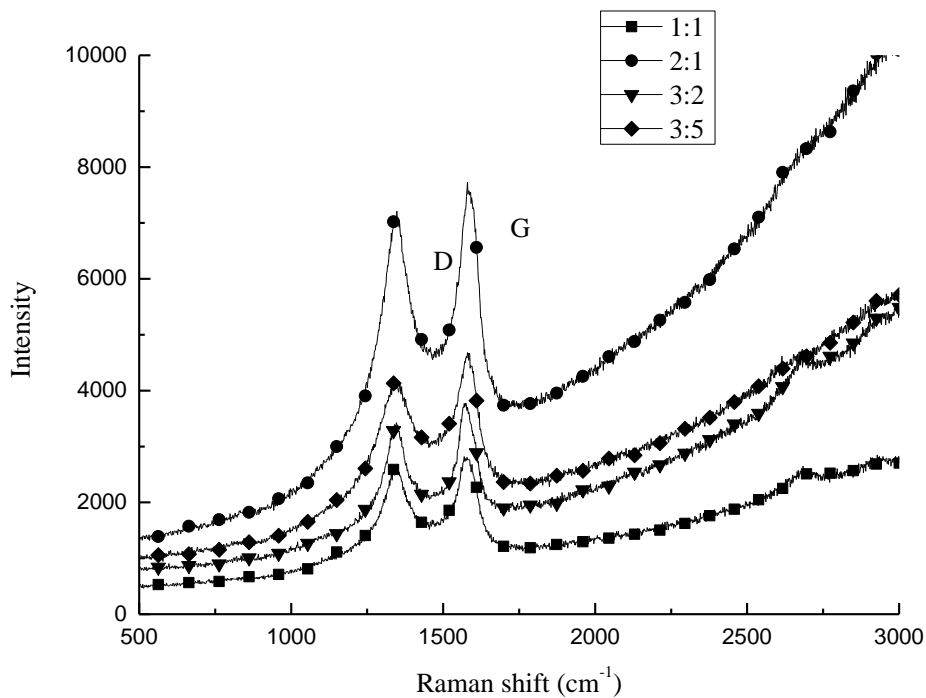


Figure 4-13 Raman analysis of reacted catalysts from the pyrolysis-catalysis of waste tyres with a 20 wt. % Ni/Al₂O₃/SiO₂ catalyst with different Al₂O₃ to SiO₂ ratios.

Raman spectroscopy analysis presented in Figure 4-13 was used to determine the degree of graphitization of the carbon deposited on the different Al₂O₃ to SiO₂ ratio supported nickel catalysts in the pyrolysis-catalysis of waste tyres process. The D band, which occurs at the Raman shift at around 1350 cm⁻¹, indicates the presence of amorphous carbons or disordered carbons; the G band, which occurs at the Raman shift around 1584 cm⁻¹, indicates a graphite carbon structure. The ratio of the intensity of the D band to the intensity of the G band (I_D/I_G) can help to evaluate the graphitization level of the produced CNTs [36]. The I_D/I_G ratios of catalysts with Al₂O₃ to SiO₂ ratios 3:5, 1:1, 3:2, 2:1 are 0.89, 0.93, 0.91, and 0.93 respectively. The lowest I_D/I_G ratio shows the highest graphitization of the carbon produced on the catalyst at Al₂O₃ to SiO₂ ratio was 3:5, suggesting that the CNTs produced have the highest crystallinity.

The amounts of the different types of carbon produced on the catalysts are shown in Figure 4-14. The results show that as the Al₂O₃:SiO₂ ratio was

increased from 3:5 to 2:1, the filamentous carbon production increased from 171.68 mg g⁻¹ waste tyre to 179.12 mg g⁻¹ at the ratios is 1:1 and then decreased to 124.40 mg g⁻¹. Therefore, it can be concluded that the nickel catalyst with a Al₂O₃:SiO₂ ratio of 1:1 gave the highest CNTs production, but the ratio at 3:5 gave the larger size of CNTs production with higher crystallinity. This could be because the synergetic effect between iron and nickel that could change the interaction between active metals and support.

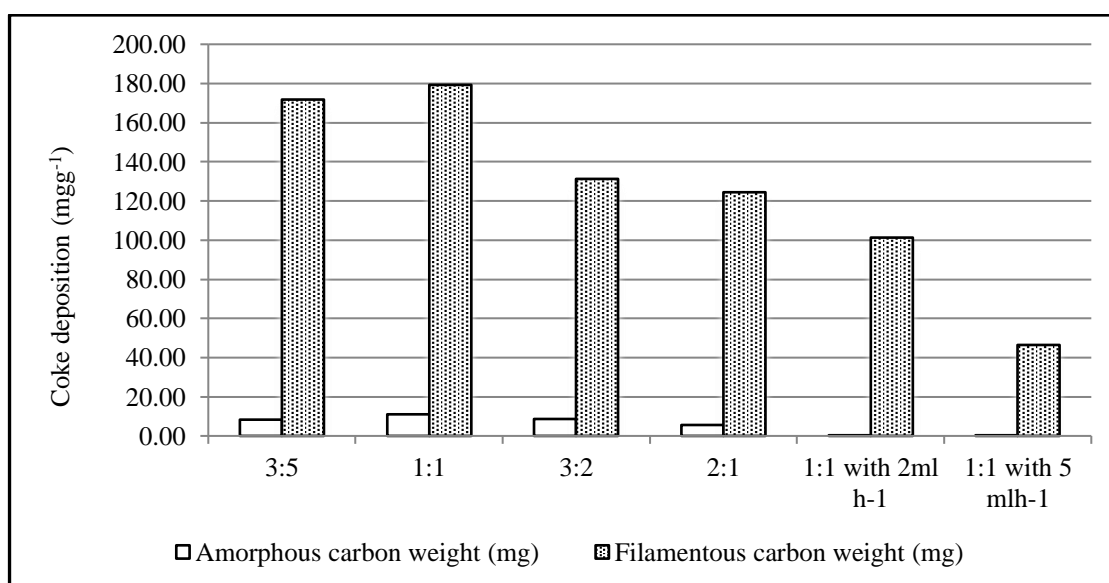


Figure 4-14 Proportions of amorphous and filamentous carbons produced from the pyrolysis-catalysis of waste tyres with a 20 wt. % Ni/Al₂O₃/SiO₂ catalyst with different Al₂O₃ to SiO₂ ratios.

4.2.3 Effect of catalyst temperature on carbon nanotube production and by-product hydrogen from the pyrolysis-catalysis of tyres

The influence of catalyst temperature for the pyrolysis-catalysis of waste tyres was investigated. The main purpose of this work was to maximise the production of carbon nanotubes formed on the surface of the Ni/Al₂O₃ catalyst in addition to monitoring the production of hydrogen. Therefore no steam input to the process was used.

Table 4-3 Product yield and gas concentrations from the pyrolysis-catalysis of tyres at different temperatures (700, 800 and 900 °C) with no water and tyre:catalyst ratio is 1:0.5.

Tyre+10 wt.% Ni/Al ₂ O ₃	Catalyst Temperature		
	700 °C	800°C	900°C
Gas yield (wt. %)	28.15	27.49	27.19
Oil yield (wt. %)	23.00	22.00	15.00
Char residue (wt. %)	39.00	37.00	40.00
Carbon (wt. %)	9.00	8.00	13.00
Mass balance (wt. %)	99.15	94.49	95.19
Hydrogen production (mmol g ⁻¹ tyre)	8.05	11.01	18.02
Gas concentrations (vol. %)			
CO	12.93	19.37	11.97
H ₂	43.05	49.64	63.56
CH ₄	22.12	23.36	17.81
CO ₂	0.00	0.00	0.00
C ₂ -C ₄	10.75	5.91	0.71

The catalyst temperature plays an important role in the waste tyre pyrolysis-catalysis process. Three different catalyst temperatures, 700, 800 and 900 °C, were investigated for the production of carbon nanotubes (CNTs) from the pyrolysis-catalysis of waste tyres. The catalyst mass used was fixed at 0.5 g of the 10 wt.% Ni/Al₂O₃ catalyst and 1.0 g of waste tyres were used in each experiment.

Table 4-3 shows the product yields from the pyrolysis catalysis of waste tyre in relation to catalyst temperature. As the catalyst temperature was increased from

700 to 900 °C, the gas yield was not significantly influenced by temperature, however, the oil yield decreased from 23 to 15 wt.% and carbon deposition increased significantly from 8.00 to 13.00 wt.%. As the catalysis temperature was increased from 700 to 900 °C, H₂ production increased from 8.05 mmol g⁻¹ tyre at 700 °C to 18.02 mmol g⁻¹ tyre at 900 °C. The concentration of H₂ in the product gas mix increased from 43.05 to 63.56 vol. %, with CH₄ concentration decreased from 22.12 to 17.81 vol.% and hydrocarbons C₂-C₄ markedly decreased in concentration.

Acomb et al. [37] investigated the influence of catalysis temperature on the production of carbon from the pyrolysis-catalysis of low density polyethylene and reported that more hydrogen and CNTs were produced as the temperature was increased. It was suggested that the polyethylene was initially degraded into lighter organic compounds, then dehydrogenated to produce solid carbon. Liu et al. [38] also found that increasing temperature improved both hydrogen and MWCNTs production from polypropylene by a catalytic pyrolysis process.

The aim of this section of the work was to maximise the production of CNTs. The composition of tyre pyrolysis oil plays an important role in CNTs production from the pyrolysis-catalysis process. Aromatic compounds such as benzene and toluene have been used as the source feedstock for CNTs synthesized by chemical vapor deposition [39-43]. In addition, more than 100 compounds have been identified in tyre pyrolysis oil, including aliphatic, aromatic, heteroatom and polar compounds [44]. Therefore, tyres pyrolysis oil which contains high concentration of aromatic compounds represents an effective feedstock for CNTs production.

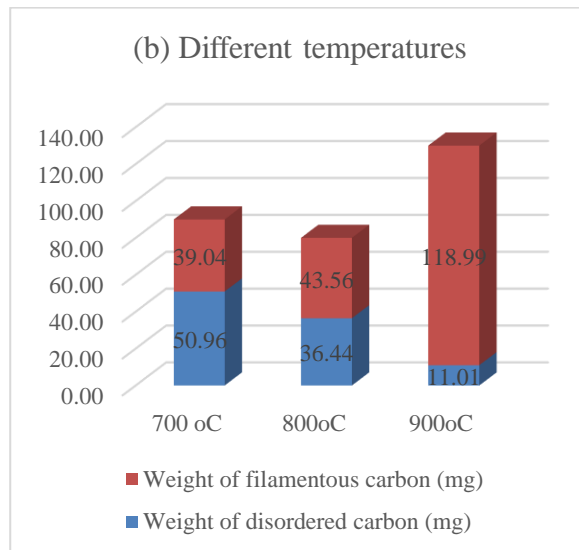
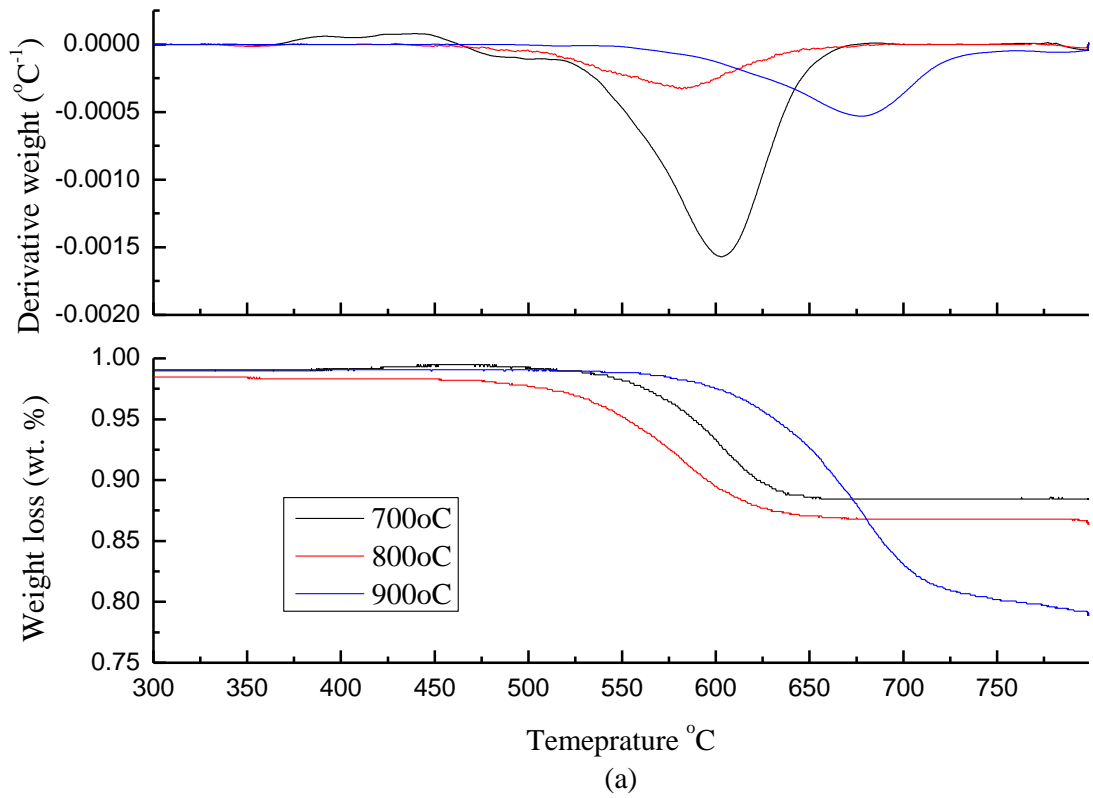


Figure 4-15 (a) TGA-TPO and DTG-TPO analysis results of the used catalysts; (b) Proportions of disordered and filamentous types of carbon formed from the pyrolysis-catalysis of tyres at different temperatures (700, 800 and 900 °C) with no water and tyre:catalyst ratio is 1:0.5.

The type of carbon formed on the catalyst was determined by TGA-TPO analysis. The carbon oxidation caused weight loss in the TGA and was assigned to the amorphous carbon oxidation at $< 600\text{ }^{\circ}\text{C}$ and the weight loss above $600\text{ }^{\circ}\text{C}$ was assigned to the oxidation of filamentous carbon [45, 46]. The weight loss shown in the TGA-TPO thermogram (Figure 4-15(a)) for the carbons formed at 700 and $800\text{ }^{\circ}\text{C}$ catalyst temperature represents oxidation of the carbon formed on the catalyst surface which occurred over a temperature range of 450 to $700\text{ }^{\circ}\text{C}$, which indicates the presence of both amorphous and filamentous carbon.

The DTG-TPO results in relation to the catalyst carbon produced at $900\text{ }^{\circ}\text{C}$ catalyst temperature suggest that the carbons were more filamentous in nature, oxidising at significantly higher temperature than the carbons produced on the catalyst surface for the catalysts used at 700 and $800\text{ }^{\circ}\text{C}$. The proportions of amorphous/disordered and filamentous carbons taken from the DTG-TPO data (Figure 4-15 (b)) suggest that the carbons were a mix of different types for the 700 and $800\text{ }^{\circ}\text{C}$ catalyst temperatures but at $900\text{ }^{\circ}\text{C}$ catalyst temperature the dominant carbon type formed was filamentous carbon. The total amount of carbon formation at 700 and $800\text{ }^{\circ}\text{C}$ were similar at 39.04 mg g^{-1} tyre and 43.56 mg g^{-1} respectively.. However, at the higher catalyst temperature of $900\text{ }^{\circ}\text{C}$, 118.99 mg g^{-1} tyre of filamentous carbon was produced.

Figure 4-16 shows SEM images of the deposited carbon on the surface of the catalysts and reveals the presence of filamentous carbon formation at the three catalysis temperatures for the tyre pyrolysis catalysis process. Figure 4-16 also shows the corresponding TEM images of the carbons deposited on the catalyst surface in relation to catalyst temperature. The presence of MWCNTs can be confirmed by the TEM images for the carbon formation at catalysis temperatures are 800 and $900\text{ }^{\circ}\text{C}$ but less so for the catalyst used at $700\text{ }^{\circ}\text{C}$. The carbons oxidised at higher temperature for the catalyst used at $900\text{ }^{\circ}\text{C}$ shown in Figure 4-16(a) may be attributed to MWCNTs as a particular type of filamentous carbon. Li et al. [47] have suggested that carbons oxidised at higher temperatures are MWCNTs because of the strong interaction between graphite layers in MWCNTs, resulting in higher thermal stability compared with amorphous /disordered carbon.

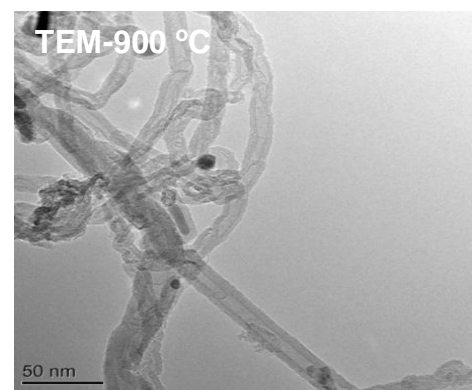
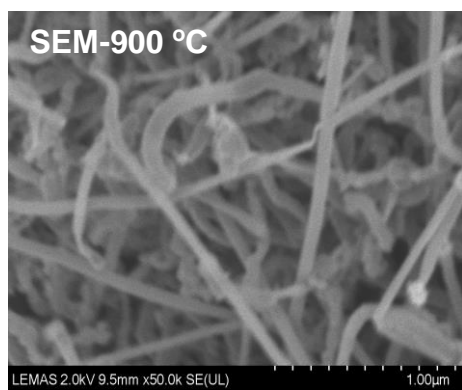
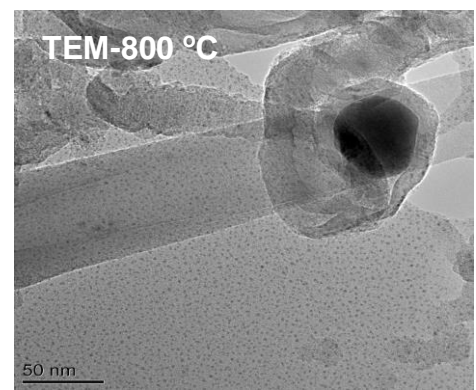
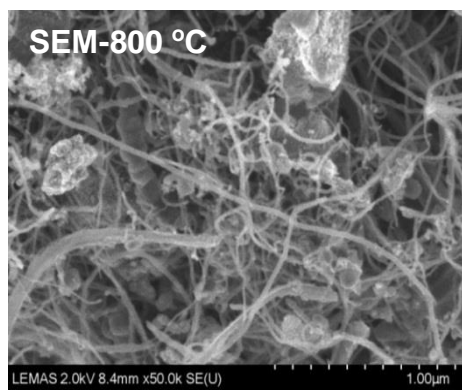
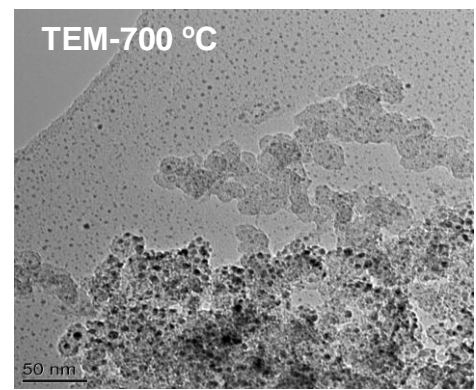
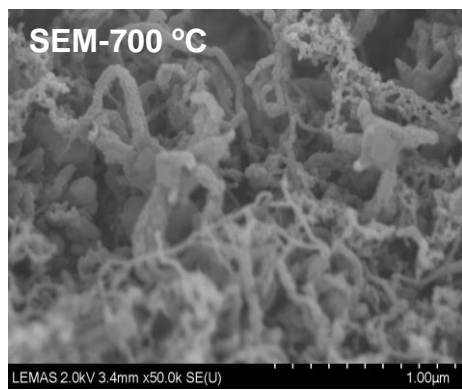


Figure 4-16 SEM and TEM images of the used catalysts from the pyrolysis-catalysis of tyres at different temperatures (700, 800 and 900 °C) with no water and tyre:catalyst ratio is 1:0.5.

The quality of the MWCNTs formed on the catalyst surface was further characterized by Raman spectroscopy as shown in Figure 4-17. The I_D/I_G ratios presented in Figure 4-17 were used to assess the quality of the CNTs formed at different catalysis temperatures derived from the waste tyre pyrolysis-catalysis process. The data show that raising the catalyst temperature from 700 to 900

°C leads to a decreasing trend of I_D/I_G ratios of 0.93, 0.85 and 0.78, which indicates that the degree of graphitization was increased. Also, the minimum I_D/I_G ratio 0.78 obtained at catalysis temperature 900 °C also indicate that the CNTs formed have fewer defects and higher crystallinity compared with the filamentous carbons formed at 700 and 800 °C [48].

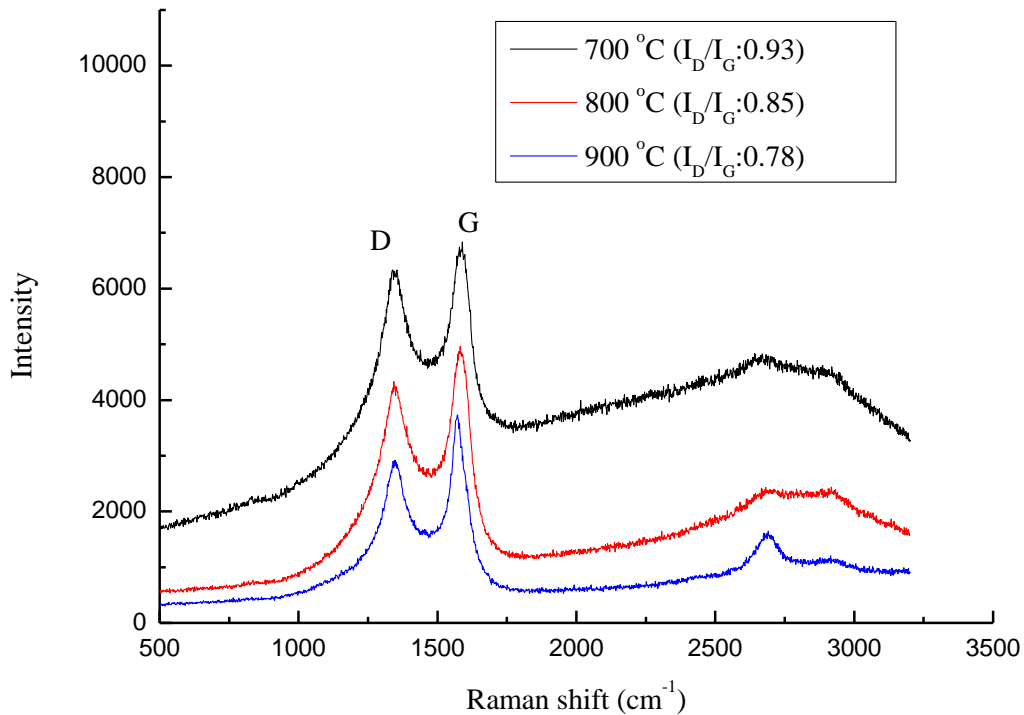


Figure 4-17 Raman analysis results of the used catalysts from the pyrolysis-catalysis of tyres at different temperatures (700, 800 and 900 °C) with no water and tyre:catalyst ratio is 1:0.5.

The results suggest that higher catalyst temperature dominates carbon formation because the hydrocarbons can break up easily to form H_2 and solid carbon. The results are consistent with other studies on different materials as carbon sources to produce CNTs [37, 40]. Acomb et al. [37] found similar results using low density polyethylene pyrolysis experiments to produce both hydrogen and carbon nanotubes. The C_2 - C_4 compositions reduced significantly from 45 to 17.5 vol.% as catalyst temperature was increased from 700 to 900 °C. Das et al. [40] showed that the CNTs yields linearly increased from 6 to 39 %

as temperature was increased from 600 to 800 °C when synthesising CNTs from aromatic hydrocarbons by chemical vapour deposition.

4.2.4 Effect of tyre:catalyst ratio on carbon nanotube production and by-product hydrogen from the pyrolysis catalysis of tyres

From the results obtained above, higher temperature promotes the formation of CNTs. Therefore, the influence of tyre:catalyst ratio was investigated to determine its influence on the formation of carbon (CNTs) formation on the catalyst surface using pyrolysis-catalysis conditions with a catalyst temperature of 900 °C. Tyre:catalyst ratios of 1:0.5, 1:1 and 1:2 were investigated. No steam was introduced into the process and 10 wt.% Ni/Al₂O₃ catalyst was used.

Table 4-4 Product yield and gas concentrations from the pyrolysis-catalysis of tyre at different tyre:catalyst ratios (1:0.5; 1:1; 1:2) with no water and 900°C .

Different tyre:catalyst ratio (g/g) at 900°C	1:0.5	1:1	1:2
Gas yield (wt. %)	27.19	33.78	27.40
Liquid yield (wt. %)	15.00	2.00	8.00
Residue (wt. %)	40.00	37.00	38.00
Carbon (wt. %)	13.00	27.00	22.00
Mass balance (wt. %)	95.19	99.78	95.40
Hydrogen production (mmol g ⁻¹ tyre)	18.02	25.64	27.41
Gas concentrations (vol. %)			
CO	11.97	20.61	18.18
H ₂	63.56	70.18	76.44
CH ₄	17.81	5.46	4.46
CO ₂	0.00	0.00	0.00
C ₂ -C ₄	0.71	1.76	0.09

The results in relation to product yields and gas compositions are shown in Table 4-4. The results show that the gas yield increased from 27.19 to 33.78 wt. %, then dropped to 27.4 wt. % as the tyre:catalyst ratio was decreased from 1:0.5 to 1:2 and reached a maximum at the tyre:catalyst ratio of 1:1. The oil yield also showed a minimum at the tyre:catalyst ratio of 1:1. Similarly, the maximum deposition of carbon occurred at the tyre:catalyst ratio of 1:1 at 27.0 wt.%. H₂ production increased from 18.02 to 27.41 mmol g⁻¹. The fraction of hydrogen in the gas also increased from 63.56 vol.% to 76.44 vol.% as the tyre:catalyst ratio was increased, with methane decreasing from 17.81 vol.% to 4.46 vol.%.

Figure 4-18 (a) shows the TGA-TPO and DTG-TPO oxidation peaks for the carbon deposits formed on the catalyst 201 at different tyre:catalyst ratios, which all occurred at 650 °C or above which indicates the oxidation of filamentous carbon. TPO results were used to calculate the proportions of amorphous/disordered and filamentous/CNTs carbons and the results are shown in Figure 4-18(b). The results show that at the tyre:catalyst ratio of 1:1, the highest yield of CNTs were produced at 201.5 mg g⁻¹ tyre.

Scanning electron microscope analysis of the carbon deposits on the catalyst at different tyre:catalyst ratios of 1:0.5, 1:1, 1:2, are shown in Figure 4-19. The presence of filamentous type carbons is clear, however, those produced at the tyre:catalyst ratio of 1:0.5 are longer and thinner than the shorter and wider carbon filaments observed at tyre:catalyst ratios of 1:1 and 1:2. Figure 4-19 also shows the corresponding TEM images of the deposited carbons in relation to tyre:catalyst ratio. The presence of MWCNTs can be identified at all tyre:catalyst ratios. However, the CNTs formed at the tyre:catalyst ratio of 1:0.5 were more ordered and straighter compared to the disordered and disjointed structures of the MWCNTs observed on the used catalysts from the experiments at tyre:catalyst ratios of 1:1 and 1:2.

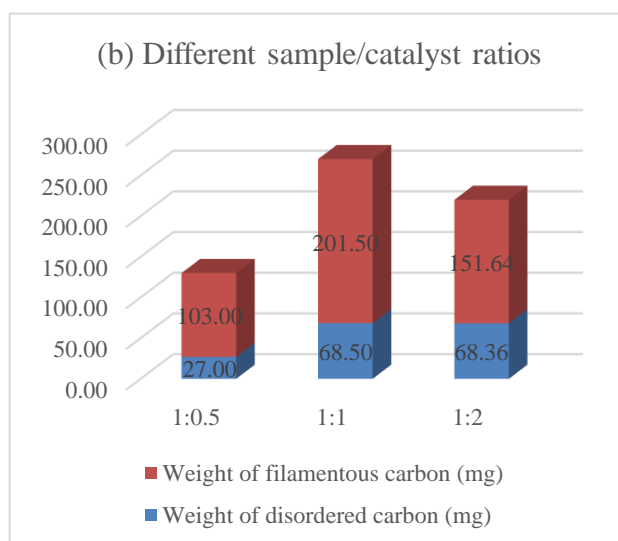
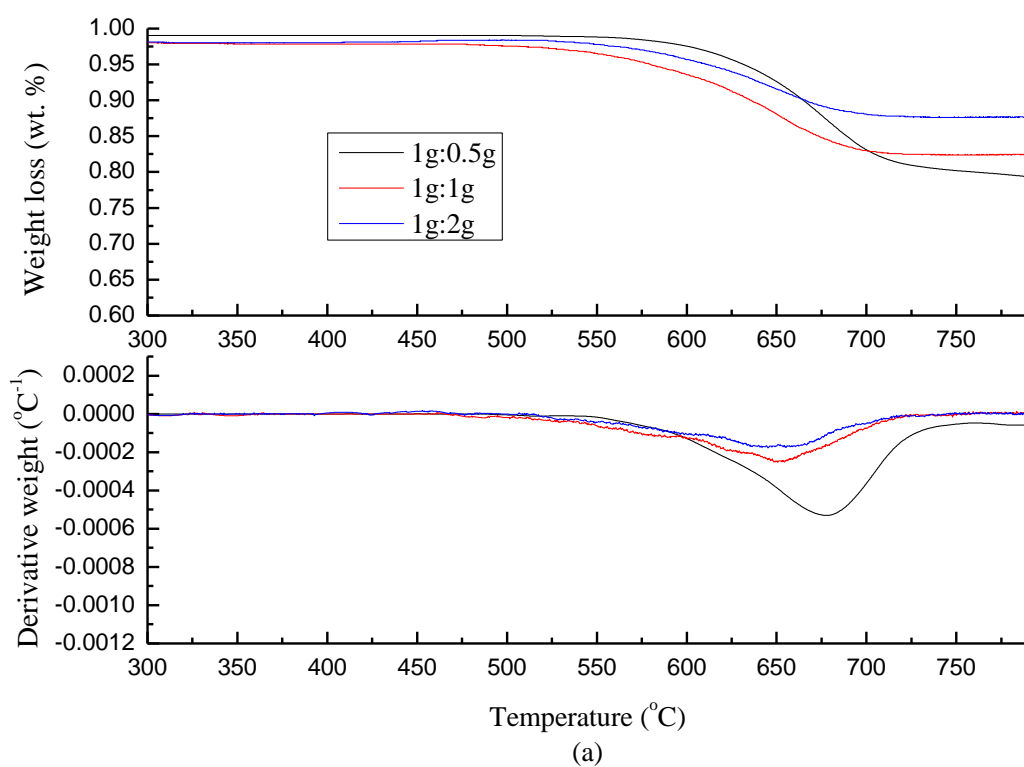


Figure 4-18 (a) TGA-TPO and DTG-TPO results of reacted catalysts; (b) Proportions of disordered and filamentous types of carbon formed from the pyrolysis-catalysis of tyres at different tyre:catalyst ratios (1:0.5; 1:1; 1:2) with no water and 900°C.

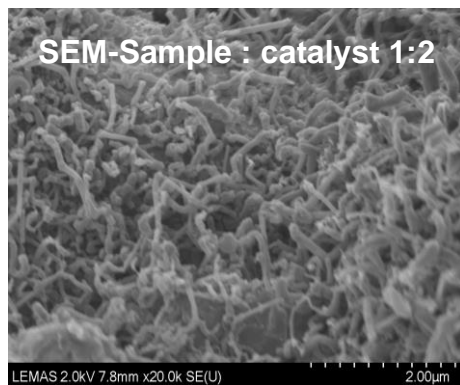
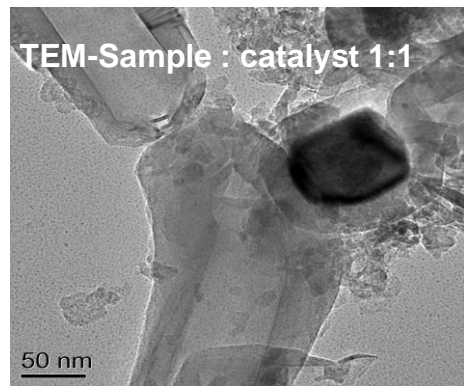
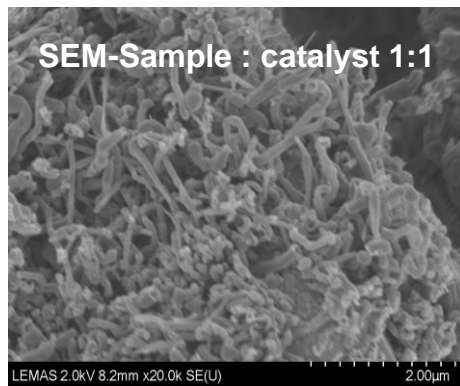
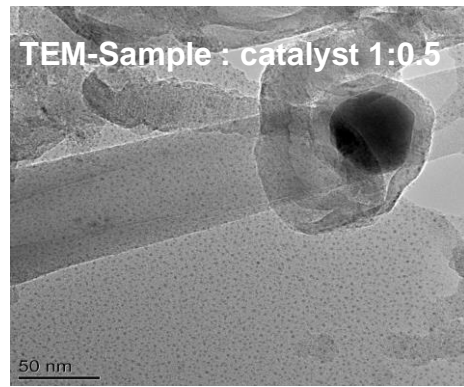
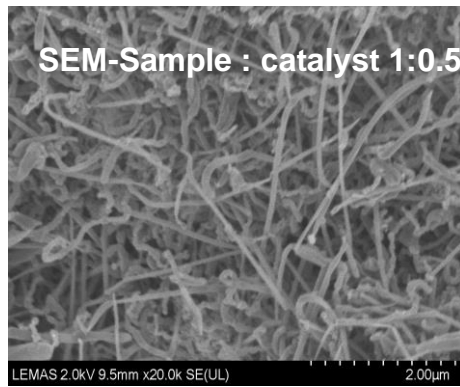


Figure 4-19 SEM and TEM images of reacted catalysts from the pyrolysis-catalysis of waste tyres at different tyre:catalyst ratios (1:0.5; 1:1; 1:2) with no water and 900°C .

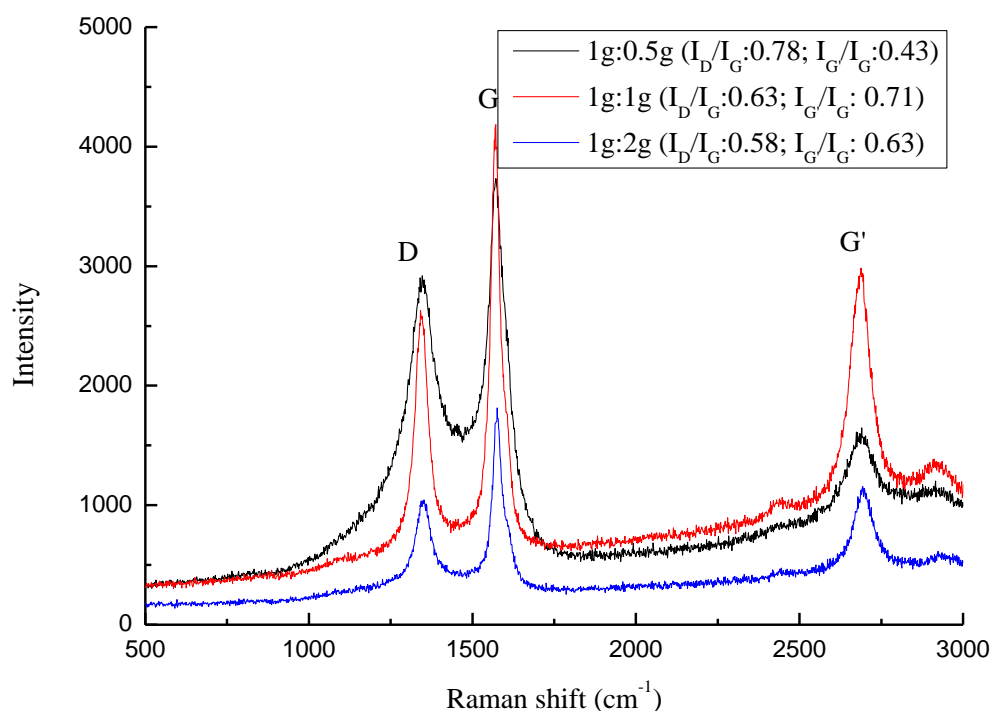


Figure 4-20 Raman analysis results of reacted catalysts from the pyrolysis-catalysis of tyre at different tyre:catalyst ratios (1:0.5; 1:1; 1:2) with no water and 900°C .

Raman spectroscopy was also used to characterize the CNTs formed at different tyre to catalyst ratios on the Ni/Al₂O₃ catalyst and the results are shown in Figure 4-20. There were three peaks in Raman shift. The peak occurred at 1375 cm⁻¹ wavelength for each sample corresponds to the D peak which is associated with disordered carbon which are the defects within the graphitic lattice. The G peaks occurred at 1600 cm⁻¹ and is associated with graphitic carbon. The G' peak which occurred at 2700 cm⁻¹ wavelength is associated with the purity of CNTs, which indicates the two photon elastic scattering process and mainly appears on ordered carbon [49].

I_D/I_G ratio may be assessed from the Raman data to evaluate the quality of the CNTs using the I_G'/I_G ratios which were calculated to identify the purity the CNTs produced. The catalyst carbon formed at the tyre:catalyst ratio of 1:0.5 had the highest I_D/I_G ratio 0.78 compared to 0.63 and 0.58 at tyre:catalyst ratio 1:1 and

1:2, respectively. This indicates the CNTs formed at the tyre:catalyst ratio of 1:0.5 represents more disordered carbon. Li et al. [47], reported that an increased tyre:catalyst ratio enhanced the carbon dissolving rate compared with the rates of carbon diffusing and precipitating, thus the formation of filamentous carbons were prohibited [47]. In addition, carbons formed on the catalyst at the ratio of 1:0.5 also showed the lowest I_G/I_G ratio of 0.43 which was significantly less than the ratios obtained at tyre:catalyst ratios of 1:1 and 1:2. The result indicates the CNTs formed at tyre:catalyst ratio 1:0.5 had the lowest purity and more defects. Considering both of I_D/I_G and I_G/I_G ratios, the tyre:catalyst ratio of 1:1 gave the best quality of CNTs. In addition, Table 3, showed that the tyre:catalyst ratio of 1:1, also produced the highest yield of CNTs at 201.5 mg g⁻¹ tyre (Figure 4-18(b)). This could be because the 1:0.5 ratio with less active metal sites as filamentous carbon growth tips, and the 1:2 ratio with much more active metal sites but less carbon source.

4.2.5 Conclusion

The production of high value carbon nanotubes (CNTs) from waste tyre by pyrolysis catalysis has been investigated using a two-stage fixed bed reactor. The influence of catalyst temperature and tyre:catalyst ratios on the production of CNTs by pyrolysis-catalysis were studied. The aim was to identify the optimum condition for CNTs production from waste tyres.

In this section, 20 wt.% Ni/Al₂O₃/SiO₂ catalysts with four different Al₂O₃ to SiO₂ mole ratios (3:5, 1:1, 3:2, 2:1) were studied for the pyrolysis catalysis of waste tyres for carbon production, particularly carbon nanotubes. In addition, the amount of by-product hydrogen was also determined. The catalyst with an Al₂O₃ to SiO₂ mole ratio 1:1 gave the highest gas yield (27.34 wt. %), the highest hydrogen production (13.96 mmol/g tyre) and highest syngas production (17.26 mmol/g tyre) when no steam was introduced to the system.

The catalyst with Al₂O₃ to SiO₂ mole ratio 3:5 showed a high quality of CNT production which were the highest in the degree of graphitization. But, the hydrogen production was only 11.47 mmol g⁻¹, which was lower than hydrogen production from the waste tyre in the presence of 20 wt. % Ni-based catalysts

with other Al₂O₃ to SiO₂ ratios. Therefore, the catalyst with the Al₂O₃ to SiO₂ ratio 1:1 gave the highest hydrogen production and simultaneously the highest filamentous carbon production that was 179.12 mg g⁻¹ of waste tyre of relatively high quality.

Pyrolysis-catalysis of waste tyres was further investigated to maximise the production of CNTs. The highest yield (118.99 mg g⁻¹ tyre) and quality of filamentous carbon was produced at 900 °C. The influence of tyre:catalyst ratio on CNTs production showed that a ratio of 1:1 gave the highest filamentous carbon production reaching a maximum of 201.5 mg g⁻¹ tyre compared to CNTs produced at 1:0.5 and 1:2.

4.3 Investigation of process conditions for the pyrolysis-catalysis/ catalytic reforming of waste truck tyres for hydrogen and by-product carbon nanotube productions with Ni/Al₂O₃ catalysts

In this section, different experimental process conditions including water injection rate, catalysis temperature and tyre to catalyst ratio were investigated, with the aim of improving hydrogen production from waste tyres by the catalytic steam reforming process. In addition, the influence of the process conditions on the production of by-product carbon nanotubes was also investigated. The two-stage pyrolysis-catalytic reactor system described in Chapter 3 was used and the influence of catalyst temperature (700, 800 and 900 °C), tyre:catalyst ratio (1:0.5, 1:1 and 1:2) and steam input (water injection 0, 2 and 5 ml h⁻¹) to the second catalyst stage were investigated. The catalyst used in most experiments was a Ni/Al₂O₃ catalyst, however, the influence of water injection rate for the nickel catalyst with a 1:1 Al₂O₃/SiO₂ ratio of 1:1 and 20 wt.% nickel was also investigated.

Pyrolysis-catalytic reforming experiments involved the input of steam (water injection via a syringe pump) and investigated the influence of steam input rate targeted at the production of increased levels of hydrogen.

4.3.1 Effect of water injection rate on pyrolysis-catalytic reforming

The main targeted product in this section was hydrogen. Consequently, the influence of steam addition to the two-stage pyrolysis-catalytic reforming system was investigated. Thereby, the reaction system comprised a pyrolysis-catalytic reforming process.

Table 4-5 Product yield and gas concentrations from the pyrolysis-catalytic reforming of tyres at different water injection rates (0,2 and 5 ml/h) at 800°C and tyre:catalyst ratio 1:0.5 (Reacted water was calculated based on the assumption that the oxygen source was only from injected water).

Tyre+10 wt. % Ni/Al ₂ O ₃ In relation to tyre & water (800 °C)	Water Input		
	No water	2ml h ⁻¹	5ml h ⁻¹
Gas yield (wt. %)	27.49	56.28	58.50
Oil yield (wt. %)	22.00	3.50	6.72
Residue of feedstock (wt. %)	37.00	27.08	25.50
Carbon (wt. %)	8.00	5.55	3.36
Mass balance (wt. %)	94.49	92.40	94.08
Hydrogen production (mmol g ⁻¹ tyre)	11.01	32.64	34.69
Gas concentrations (vol. %)			
CO	19.37	18.15	16.31
H ₂	49.64	56.74	57.06
CH ₄	23.36	9.80	9.61
CO ₂	0.00	12.19	14.24
C ₂ -C ₄	5.91	2.01	2.46
Reacted water (g)	None	0.44	0.49
In relation to tyre only			
Gas yield (wt. %)	27.49	81.06	87.17
Oil yield (wt. %)	22.00	5.03	10.01
Residue (wt. %)	37.00	39.00	38.00
Carbon (wt. %)	8.00	8.00	5.00
Mass balance (wt. %)	94.49	133.09	140.18

Table 4-5 shows the product yields from the pyrolysis-catalytic steam reforming of tyres at different water injection rates of 0, 2 and 5 ml h⁻¹. The results are presented as calculation of the yields in relation to mass of tyre and injected water, also calculated was the yield of products in relation to the mass of tyre sample only. The pyrolysis conditions were slow pyrolysis from ambient temperature to 600 °C, a catalyst reforming temperature of 800 °C and tyre:catalyst ratio of 1:0.5.

Table 4-5 shows that for the results in relation to the mass of tyre sample only, the introduction of steam produced an increase in gas yield to 87.17 wt.% at 5 ml h⁻¹ water injection rate compared to 27.49 in the absence of steam. Correspondingly, the oil yields decreased from 22 to 5.03 wt.% and then increased slightly to 10.01 wt.% as increasing amounts of water were introduced into the system. The pyrolysis residues remaining in the pyrolysis stage were all around 38.00 ± 1 wt. %, since the pyrolysis stage was the same for each experiment. The amount of reacted water calculated from the water injected versus the condensed water showed a slight increase from 0.44 to 0.49 ml as the injection rate increased from 2 – 5 ml h⁻¹.

The production of hydrogen shows a marked increase from 11.01 mmol g⁻¹ tyre in the absence of steam rising to 32.64 mmol g⁻¹ tyre at 2 ml h⁻¹ water injection rate and 34.69 mmol g⁻¹ tyre at 5 ml h⁻¹. The limited increment in H₂ production as the water injection rate was increased suggested that high levels of water injection could reverse the water gas shift reaction [50, 51]. The gas compositions at different water injection rates also shown in Table 4-5, shows that H₂ concentration increased from 49.64 vol.% in the absence of steam to 56.74 vol.% at 2 ml h⁻¹ and 57.06 vol.% at 5 ml h⁻¹. Hydrogen was produced from the injected steam which reacted with carbon to form hydrogen based on Equation 4.1 [39]:



The hydrocarbons concentration decreased with the steam addition, CH₄ decreased from 23.36 vol.% in the absence of steam to 9.61 vol.% at 5 ml h⁻¹

water injection rate and C₂-C₄ concentration decreased from 5.91 to 2.46 vol.%. It is suggested the hydrocarbon reforming with the introduction of steam results in increased H₂ production (Table 4-5) Equation 4.2 [39].



The CO concentration decreased from 19.37 to 16.31 vol.% and the CO₂ concentration increased from 0 to 14.24 vol.%. It was suggested that H₂O becomes involved in the water gas shift reaction producing decreased CO and increased CO₂ and H₂ [39] as shown in Equation 4.3.



Water introduction in the tyre pyrolysis-catalysis process had a very significant effect on catalyst carbon deposition. As Table 4-5 shows, the carbon production decreased in relation to the increase of water injection rates from 0 to 5 ml h⁻¹, with carbon decreasing from 8.0 to 3.36 wt. % in relation to the results in relation to the mass of tyre sample and water. The steam reacts with the carbon to produce CO and H₂ (Equation 4.1).

To characterize the carbon deposited on the catalyst surface, temperature programmed oxidation was used to identify the type of carbon such as amorphous/disordered and filamentous carbon/CNTs. This technique has been applied to characterize carbon type by many researchers [36, 51-54]. Figure 4-21 (a) illustrates the TGA-TPO and the derivative rate of weight loss in relation to temperature programmed oxidation (DTG-TPO) results of the carbon on the used 10% Ni/Al₂O₃ catalyst. The weight loss at oxidation temperatures higher than 600 °C indicates the oxidation of filamentous carbon and the weight loss occurred at <600 °C can be attributed to the oxidation of amorphous or disordered carbon [36, 37, 45]. Figure 4-21 (b) shows the proportions of disordered and filamentous carbons formed from pyrolysis-catalytic reforming of waste tyre at different water injection rates.

The proportions of both disordered/amorphous and filamentous carbon are presented in Figure 4-21(b) based on the DTG-TPO data. The filamentous carbon produced at a water injection rate 2 ml h⁻¹ produces the highest amount of filamentous carbon at 77.09 mg g⁻¹ tyre, which is higher than the filamentous

carbons produced without water introduction that is 43.56 mg g⁻¹ tyre. The higher water injection rate at 5 ml h⁻¹ hindered the filamentous carbon formation that was reduced to 47.92 mg g⁻¹. This is due to the carbon formation was further reacted with steam at high temperature.

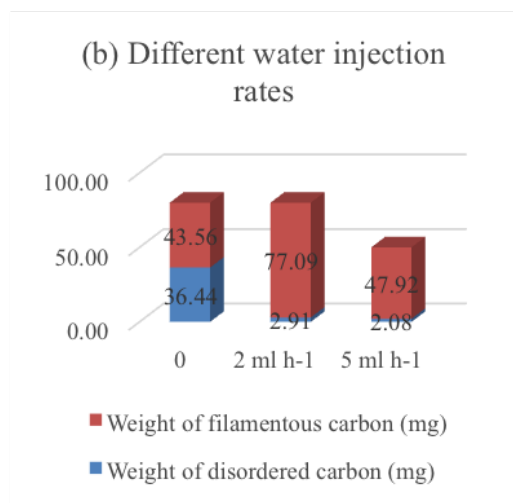
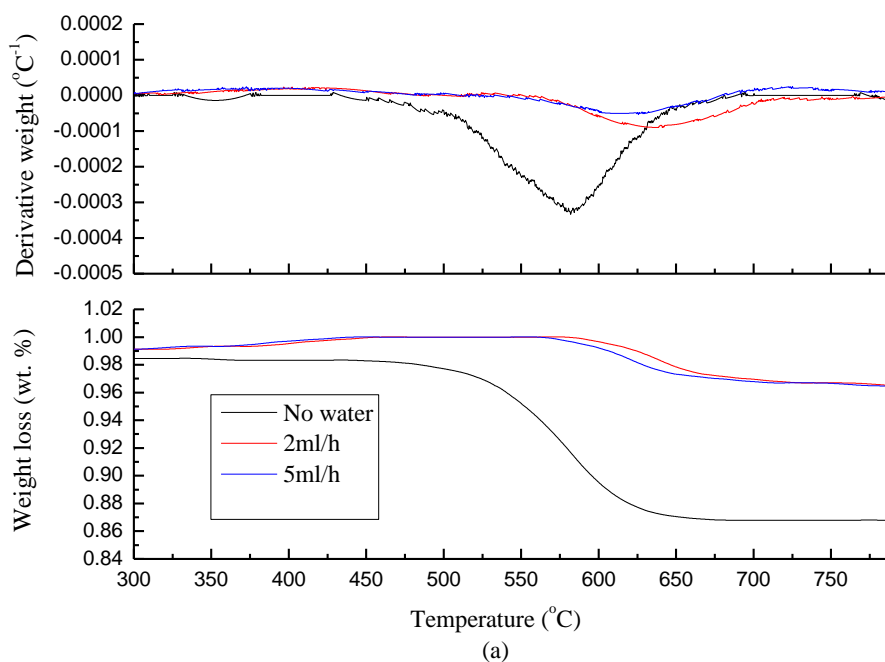


Figure 4-21 (a) TGA-TPO and DTG-TPO analysis results of the used catalysts from the pyrolysis-catalytic reforming of waste tyre at different water injection rates; (b) Proportions of disordered and filamentous types of carbon formed from the pyrolysis-catalytic reforming of tyres with different water injection rates (0, 2 and 5 ml h⁻¹) at 800 °C and tyre:catalyst ratio 1:0.5.

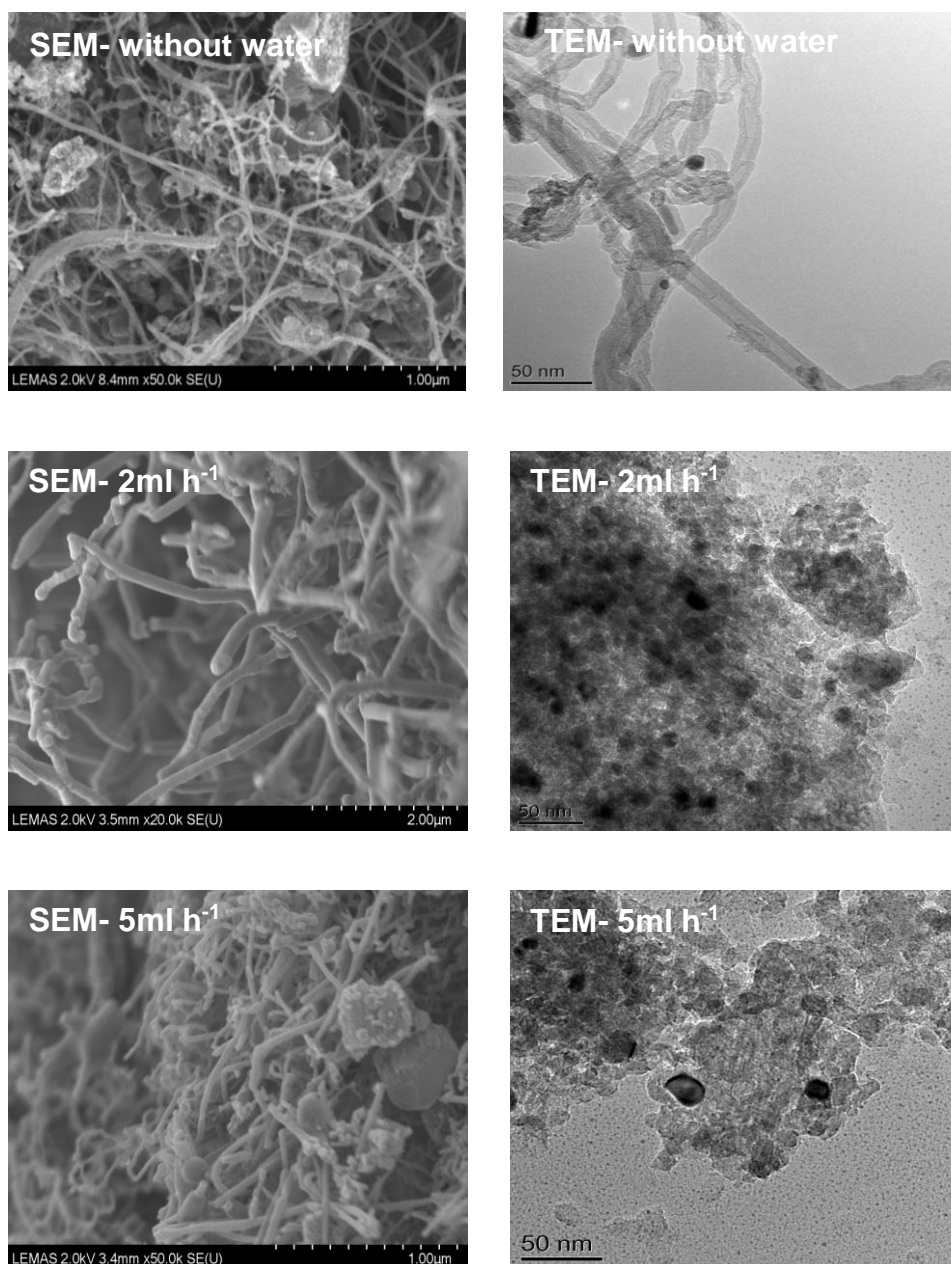


Figure 4-22 SEM and TEM images of the used catalysts from the pyrolysis-catalytic reforming of waste tyres at different water injection rates (0, 2 and 5 ml h⁻¹) at 800 °C and tyre:catalyst ratios 1:0.5.

The presence of filamentous carbon on the catalyst surface was shown by TPO, however, to further characterize the filamentous carbon, scanning and transmission electron microscopy (SEM and TEM) were used to identify the morphology of the carbons produced, in particular the presence of multi-walled

carbon nanotubes (MWCNTs) [35, 55-57]. SEM and TEM images of the carbon deposited on the used catalyst produced at different water injection rates are shown in Figure 4-22. From the SEM images the formation of considerable quantities of filamentous carbon could be identified regardless of water injection rate. In addition, the accompanying TEM images clearly show that the filamentous carbons formed in the absence of steam injection are long and straight MWCNTs. However, with the introduction of steam to the process, the filamentous carbon was largely degraded and few carbon nanotubes were detected.

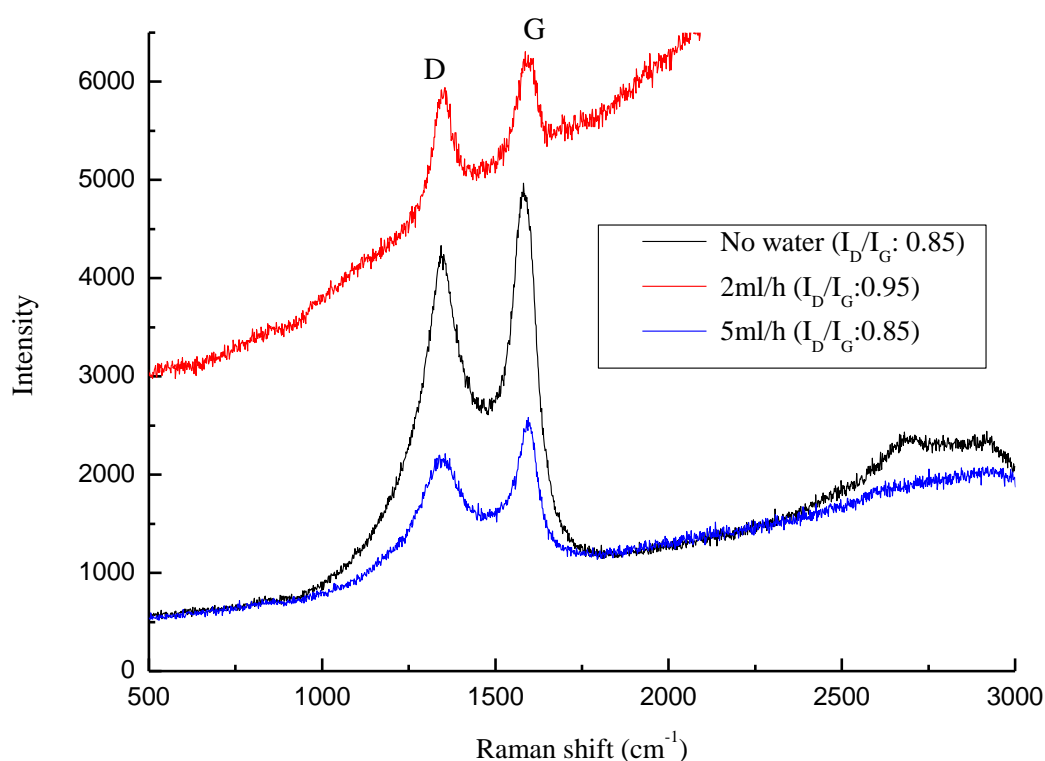


Figure 4-23 Raman analysis of the used catalysts from the pyrolysis-catalytic reforming of waste tyres at different water injection rates (0, 2 and 5 ml h⁻¹) at 800 °C and tyre:catalyst ratios 1:0.5.

Raman spectroscopy is commonly used to identify the quality of CNTs based on the intensity of D and G bands [36, 45, 58, 59], where the D band in Raman shift indicates amorphous or disordered carbon and the G band indicates

graphitic or filamentous carbon. The I_D/I_G ratios, intensity of D band nominalized intensity of G band, which indicates the degree of graphitization of CNTs produced from waste tyre pyrolysis-catalytic reforming at different water injection rates are shown in Figure 4-23. The I_D/I_G ratio for the CNTs produced without water present were close to that produced for commercial CNTs which is in the ranges of 0.63-1.5 [60].

According to the analyses above, the introduction of steam into the reactor system inhibited CNTs production in the waste tyre pyrolysis-catalysis process with more defects and less structured filamentous carbon being formed. The carbon production reduced with the increment of water injection rates from 2 to 5 ml h⁻¹, but not the expected MWCNTs production.

4.3.1.1 Influence of different water injection rates for the Al₂O₃ to SiO₂ ratio 1:1 nickel catalyst

In Section 4.2, the 20 wt. % nickel catalyst at a Al₂O₃ to SiO₂ ratio of 1:1 produced the highest yield of hydrogen in the pyrolysis-catalysis experiments. Therefore, further work was carried out to increase the production of hydrogen from the waste tyres by introducing steam (injected water) to the second stage to produce a pyrolysis-catalytic steam reforming process. Table 4-6 shows the product yields and gas compositions from waste tyre pyrolysis-catalytic steam reforming with 20 wt. % Ni/Al₂O₃/SiO₂ (1:1) catalyst at different water injection rates. The gas yields with water injection rate at 2 and 5 ml h⁻¹ were similar at 58.02 and 57.84 wt. % respectively, which are much higher than the experiments without water at only 27.34 wt. %.

The hydrogen production from the process shows a similar trend, at 13.96, 33.81 and 34.52 mmol g⁻¹ for the water injection rates of 0, 2 and 5 ml h⁻¹, respectively. These increases in gas and hydrogen yield are attributed to the reacted water since at a water injection rate of 5 ml h⁻¹ the reacted water was 0.5 g, whereas at 2 ml h⁻¹ the reacted water was 0.48 g. Table 3 also shows the calorific values of gas products. The results show that as the water injection rate was increased from 0 to 5 ml h⁻¹, there was decrease in the calorific value of the product gases, from 19.47 to 10.72 MJ m⁻³, due mainly to the decrease of the

methane and C₂ – C₄ hydrocarbons due to the catalytic steam reforming process of these hydrocarbons.

Table 4-6 Product yields and gas concentrations from the pyrolysis-steam reforming of waste tyres with a 20 wt. % Ni/Al₂O₃/SiO₂ catalyst with an Al₂O₃:SiO₂ ratio of 1:1 (Reacted water was calculated based on the assumption that the oxygen source was only from injected water).

Tyre + 20%Ni/Al ₂ O ₃ /SiO ₂			
In relation to sample & reacted water	No water	2ml h ⁻¹	5ml h ⁻¹
Gas yield (wt. %)	27.3	58.0	57.8
Oil yield (wt. %)	13.0	2.7	7.0
Residue (wt. %)	36.0	26.3	24.6
Catalyst coke (wt. %)	19.0	10.1	4.6
Mass balance (wt. %)	95.3	97.2	94.0
Hydrogen production (mmol g ⁻¹ _{tyre})	14.0	33.8	34.5
CO production (mmol g ⁻¹ _{tyre})	3.3	11.41	10.48
Syngas production (mmol g ⁻¹ _{tyre})	17.3	45.22	45.00
Gas concentrations (vol. %)			
CO	13.26	19.11	17.41
H ₂	56.06	56.65	57.33
CH ₄	22.01	8.43	8.52
CO ₂	0.00	12.80	14.58
C ₂ – C ₄	4.47	1.55	1.75
Reacted water (g)	None	0.48	0.50
In relation to sample only			
Gas yield (wt. %)	27.34	85.90	87.03
Oil yield (wt. %)	13.00	4.04	10.46
Residue (wt. %)	36.00	39.00	37.00
Catalyst coke (wt. %)	19.00	15.00	7.00
Mass balance (wt. %)	95.34	143.94	141.49
Calorific value (MJ m ⁻³)	19.47	13.31	10.72

Table 4-6 shows that the product oil and carbon deposition decreased as the amount of water injected into the second stage reforming process was increased. The results show the oil yields are 13.00, 2.73 and 6.95 wt. % at water injection rates of 0, 2 and 5 ml h⁻¹, respectively. It should be noted that Table 4-6 shows data calculated in relation to the amount of injected water and reacted water which shows that there was 36.00 wt.% of residue with no water added, with 2 and 5 ml h⁻¹ water injections, the pyrolysis residues decreased to 26.34 and 24.59 wt. %. However, determination of the pyrolysis residue in relation to tyre sample weight produced pyrolysis residue data that was very similar 37±2 wt. % (as was also shown in Table 4-2). Wu et al. [52] reported that increasing water flow rate contributes to a significant decrease of carbon deposition on the catalyst in their experiments in relation to hydrogen production from the pyrolysis-catalytic reforming of polypropylene.

Table 4-6 also shows that the CO concentration increased up to 19.11 and 17.41 vol. % from 13.26 vol. % with the introduction of water injection at the rates of 2 and 5 ml h⁻¹. The CO₂ concentration increased from 0 vol. % to 12.80 and 14.58 vol. % at water injection rates of 2 and 5 ml h⁻¹. The increase of water injection rate, produced a reduction in CH₄ and C₂-C₄ hydrocarbons through steam reforming reactions. The CH₄ concentration was 22.01 vol. % without water in the experiment, but decreased to 8.43 and 8.52 vol.% at water injection rates of 2 and 5 ml h⁻¹ and C₂-C₄ concentrations decreased from 4.47 vol.% at no water addition to 1.55 and 1.75 vol.% at water injection rates of 2 and 5 ml h⁻¹ respectively. Turn et al. [61] found similar results in their experiments for biomass where an increase of steam to biomass ratio, produced an increase in H₂ and CO₂ yields. Further increasing steam to the process to high levels can saturate the catalyst surface and reduce hydrogen production and also higher water inputs require more energy for steam generation [52].

4.3.1.2 Influences of different water injection rates on catalyst carbon deposition

Figure 4-24 shows the TPO and DTG-TPO results of the reacted catalysts from pyrolysis catalytic steam reforming of waste tyres with the 20 wt. % Al₂O₃/ SiO₂

catalyst with an Al_2O_3 to SiO_2 ratio of 1:1 at different water injection rates. The results show that the introduction of water leads to a significant decrease in the amount of carbon deposited on the catalyst. Filamentous carbons oxidized at high temperature were observed from the DTG-TPO results. SEM images in Figure 4-11 and Figure 4-24, confirm filamentous carbon formation.

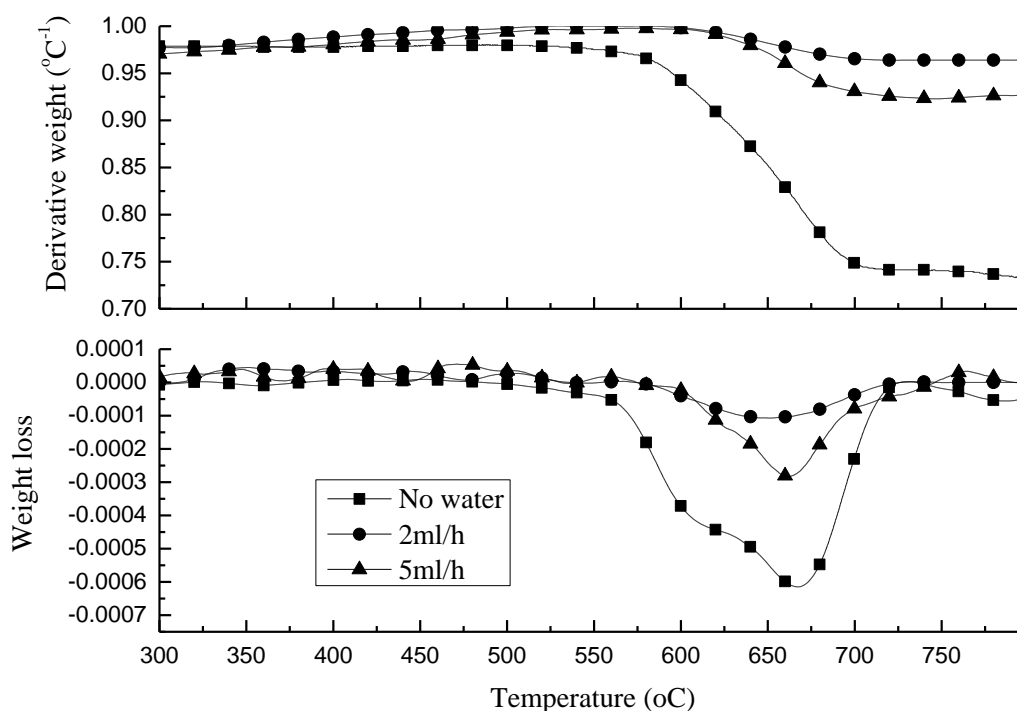


Figure 4-24 TGA-TPO and DTG-TPO results of reacted catalysts produced from the pyrolysis-catalytic reforming of waste tyres with a 20 wt. % $\text{Ni}/\text{Al}_2\text{O}_3/\text{SiO}_2$ catalyst with an $\text{Al}_2\text{O}_3:\text{SiO}_2$ ratio of 1:1.

Figure 4-25 shows that the filamentous carbon formed with the 20 wt. % $\text{Ni}/\text{Al}_2\text{O}_3/\text{SiO}_2$ catalyst (1:1 ratio) and different water injection rates are solid carbon fibres. Figure showed earlier that for the 1:1 ratio $\text{Al}_2\text{O}_3/\text{SiO}_2$ nickel catalyst in the absence of water (steam) input, the deposited carbons were MWCNTs. The Raman analysis in Figure 4-27, shows that for the I_D/I_G ratios for the deposited carbons for the experiments with 2 and 5 ml h^{-1} water injection rates are 0.87 and 0.90 which indicates the lower water injection rate contributes to higher graphitization of carbon formation.

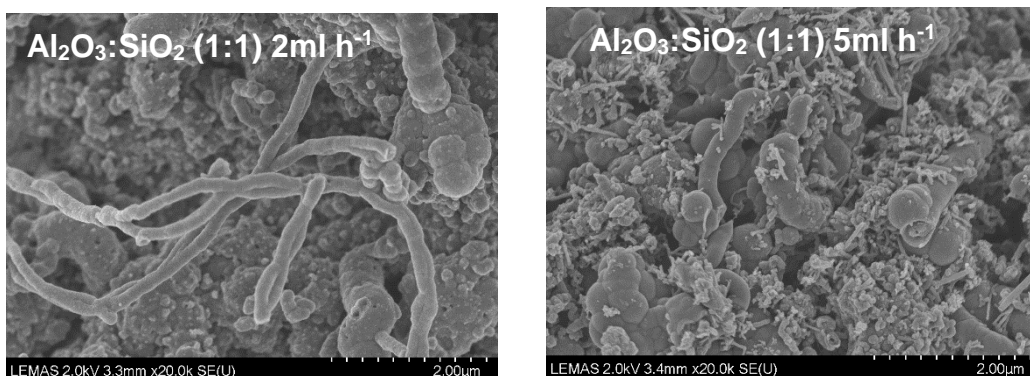


Figure 4-25 SEM images of reacted catalysts produced from the pyrolysis-catalytic reforming of waste tyres with a 20 wt. % Ni/Al₂O₃/SiO₂ catalyst with an Al₂O₃:SiO₂ ratio of 1:1.

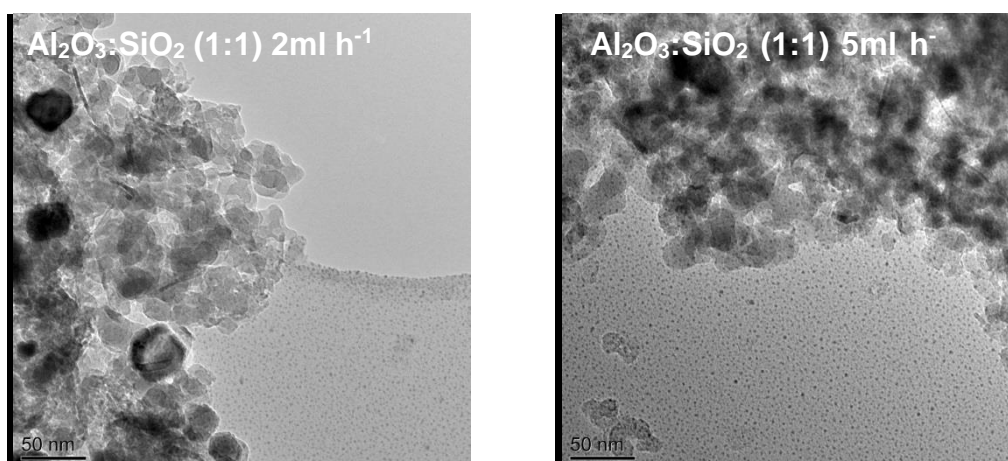


Figure 4-26 TEM images of reacted catalysts produced from the pyrolysis-catalytic reforming of waste tyres with a 20 wt. % Ni/Al₂O₃/SiO₂ catalyst with an Al₂O₃:SiO₂ ratio of 1:1.

Figure 4-14 clearly shows that when water was introduced into the waste tyres pyrolysis catalytic- reforming process, less filamentous carbon was produced and less carbon produced. As the water injection rate was increased from 0 to 5 ml h⁻¹, the amount of filamentous carbon production decreased from 179.12 to 46.33 ml h⁻¹. Also, the amorphous carbon production decreased simultaneously. Therefore, the water introduction inhibited the carbon production in the waste

tyres pyrolysis-catalytic reforming process and also inhibited filamentous carbon production.

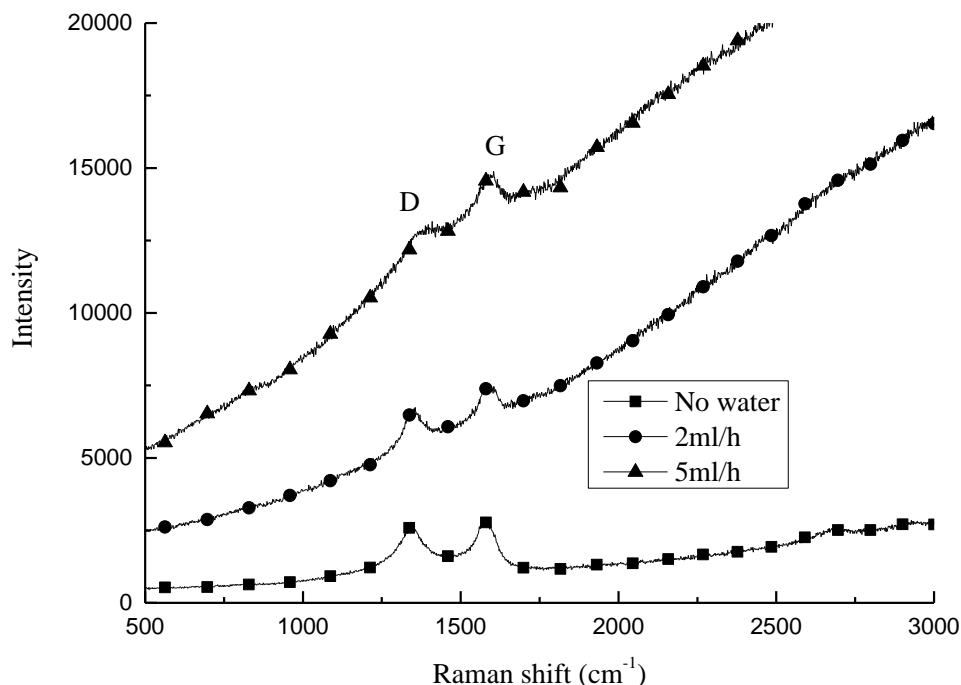


Figure 4-27 Raman analyses reacted catalysts produced from the pyrolysis-catalytic reforming of waste tyres with a 20 wt. % Ni/Al₂O₃/SiO₂ catalyst with an Al₂O₃:SiO₂ ratio of 1:1.

Water (steam) introduction to the waste tyre pyrolysis-catalysis process resulted in catalytic steam reforming and the production of hydrogen, reaching a maximum of 34.69 mmol g⁻¹ tyre and a gas composition consisting of 57.06 vol.% H₂, 16.31 vol.% CO, 14.24 vol.% CO₂ and 9.61 vol.% CH₄. In addition, introducing steam to the process reduced the formation of carbon on the catalyst from 8.0 (no water) to 3.36 wt.%.

4.4 Conclusions for hydrogen production from waste tyres by pyrolysis-catalytic reforming

The introduction of steam to the process to produce pyrolysis-catalytic steam

reforming of the waste tyres at different water injection rates was also investigated to determine the influence on both hydrogen and carbon production. The results show that more water addition to the experiments promotes higher hydrogen production but restricts CNTs production. The more water injection would be favorable for more hydrogen production, but there should be an optimized water injection rate with the highest hydrogen production without saturating the catalyst. Furthermore, the water introduction inhibited the filamentous carbon production. As the water injection rate was increased from 0 to 5 ml h⁻¹, the carbon production decreased from 19 to 4.65 wt. % and the filamentous carbon production decreased from 164 to 45 mg g⁻¹. Nevertheless, the filamentous carbons formed in waste tyre pyrolysis-catalytic reforming with water introduction are mostly solid carbon fibers and not carbon nanotubes.

The production of high value carbon nanotubes (CNTs) and hydrogen from waste tyre by pyrolysis catalysis and pyrolysis catalytic steam reforming has been investigated using a two-stage fixed bed reactor. The influence of different water injection rates on the production of hydrogen using pyrolysis-catalytic steam reforming were studied. The influence of catalyst temperature and tyre:catalyst ratios on the production of CNTs by pyrolysis-catalysis were also studied. The aim was to identify the optimum condition for hydrogen and CNTs production from waste tyres.

Water (steam) introduction to the waste tyre pyrolysis-catalysis process resulted in catalytic steam reforming and the production of hydrogen, reaching a maximum of 34.69 mmol g⁻¹ tyre and a gas composition consisting of 57.06 vol.% H₂, 16.31 vol.% CO, 14.24 vol.% CO₂ and 9.61 vol.% CH₄. In addition, introducing steam to the process reduced the formation of carbon on the catalyst from 8.0 (no water) to 3.36 wt.%.

Pyrolysis-catalysis of waste tyres was further investigated to maximise the production of CNTs, therefore no steam was added to the process. The highest yield (118.99 mg g⁻¹ tyre) and quality of filamentous carbon was produced at 900 °C. The influence of tyre:catalyst ratio on CNTs production showed that a

ratio of 1:1 gave the highest filamentous carbon production reaching a maximum of 201.5 mg g⁻¹ tyre compared to CNTs produced at 1:0.5 and 1:2.

For the co-production of hydrogen and CNTs, a catalyst temperature of 900 °C and tyre:catalyst ratio of 1:1 without steam addition produced the high yields of H₂ and filamentous carbons and thereby carbon nanotubes.

Reference

1. Wu, C., **et al.**, *Hydrogen production by steam gasification of polypropylene with various nickel catalysts*. Applied Catalysis B: Environmental, 2009. **87**(3): p. 152-161.
2. Lakhapatri, S.L., **et al.**, *Analysis of catalyst deactivation during steam reforming of jet fuel on Ni-(PdRh)/ γ -Al₂O₃ catalyst*. Applied Catalysis A: General, 2011. **405**(1–2): p. 149-159.
3. Wu, C., **et al.**, *Pyrolysis–gasification of plastics, mixed plastics and real-world plastic waste with and without Ni–Mg–Al catalyst*. Fuel, 2010. **89**(10): p. 3022-3032.
4. Sutton, D., B., **et al.**, *Review of literature on catalysts for biomass gasification*. Fuel Processing Technology, 2001. **73**(3): p. 155-173.
5. Baker, E.G., **et al.**, *Steam gasification of biomass with nickel secondary catalysts*. Industrial & Engineering Chemistry Research, 1987. **26**(7): p. 1335-1339.
6. Wu, C., **et al.**, *Investigation of Ni-Al, Ni-Mg-Al and Ni-Cu-Al catalyst for hydrogen production from pyrolysis–gasification of polypropylene*. Applied Catalysis B: Environmental, 2009. **90**(1–2): p. 147-156.
7. Elbaba, I.F., **et al.**, *High yield hydrogen from the pyrolysis–catalytic gasification of waste tyres with a nickel/dolomite catalyst*. Fuel, 2013. **106**(0): p. 528-536.
8. Elbaba, I.F., **et al.**, *Hydrogen production from the pyrolysis–gasification of waste tyres with a nickel/cerium catalyst*. International Journal of Hydrogen Energy, 2011. **36**(11): p. 6628-6637.
9. Hauserman, W.B., *High-yield hydrogen production by catalytic gasification of coal or biomass*. International journal of hydrogen energy, 1994. **19**(5): p. 413-419.
10. Kumar, M., **et al.**, *Chemical vapor deposition of carbon nanotubes: a review on growth mechanism and mass production*. Journal of nanoscience and nanotechnology, 2010. **10**(6): p. 3739-3758.
11. Hernadi, K., **et al.**, *Fe-catalyzed carbon nanotube formation*. Carbon, 1996. **34**(10): p. 1249-1257.

12. Qian, W., et al., *Enhanced production of carbon nanotubes: combination of catalyst reduction and methane decomposition*. Applied Catalysis A: General, 2004. **258**(1): p. 121-124.
13. Kong, J., et al., *Chemical vapor deposition of methane for single-walled carbon nanotubes*. Chemical Physics Letters, 1998. **292**(4–6): p. 567-574.
14. Nath, M., et al., *Production of bundles of aligned carbon and carbon–nitrogen nanotubes by the pyrolysis of precursors on silica-supported iron and cobalt catalysts*. Chemical Physics Letters, 2000. **322**(5): p. 333-340.
15. Clause, O., et al., *Preparation and thermal reactivity of nickel/chromium and nickel/aluminium hydrotalcite-type precursors*. Applied Catalysis, 1991. **73**(2): p. 217-236.
16. Bukur, D.B., et al., *Activation Studies with a Precipitated Iron Catalyst for Fischer-Tropsch Synthesis: I. Characterization Studies*. Journal of Catalysis, 1995. **155**(2): p. 353-365.
17. Brown, R., et al., *Temperature programmed reduction of alumina-supported iron, cobalt and nickel bimetallic catalysts*. Applied Catalysis, 1982. **3**(2): p. 177-186.
18. Wan, H.-J., et al., *Study on Fe–Al₂O₃ interaction over precipitated iron catalyst for Fischer–Tropsch synthesis*. Catalysis Communications, 2007. **8**(10): p. 1538-1545.
19. Berry, F.J., et al., *Microwave heating during catalyst preparation: influence on the hydrodechlorination activity of alumina-supported palladium–iron bimetallic catalysts*. Applied Catalysis A: General, 2000. **204**(2): p. 191-201.
20. Mariño, F.J., et al., *Hydrogen from steam reforming of ethanol. characterization and performance of copper-nickel supported catalysts*. International Journal of Hydrogen Energy, 1998. **23**(12): p. 1095-1101.
21. Chu, W., et al., *Cobalt species in promoted cobalt alumina-supported Fischer–Tropsch catalysts*. Journal of Catalysis, 2007. **252**(2): p. 215-230.
22. Ebshish, A., et al., *Review of hydrogen production via glycerol reforming*. Proceedings of the Institution of Mechanical Engineers, Part A: Journal of Power and Energy, 2012. **226**(8): p. 1060-1075.
23. Wu, C., et al., *Processing Real-World Waste Plastics by Pyrolysis-Reforming for Hydrogen and High-Value Carbon Nanotubes*. Environmental Science & Technology, 2013. **48**(1): p. 819-826.

24. Wu, C., et al., *Sustainable processing of waste plastics to produce high yield hydrogen-rich synthesis gas and high quality carbon nanotubes*. RSC Advances, 2012. **2**(10): p. 4045-4047.
25. Wu, C., et al., *Renewable hydrogen and carbon nanotubes from biodiesel waste glycerol*. Scientific reports, 2013. **3**.
26. Dresselhaus, M.S., et al., *Raman spectroscopy on isolated single wall carbon nanotubes*. Carbon, 2002. **40**(12): p. 2043-2061.
27. Popovska, N., et al., *Catalytic growth of carbon nanotubes on zeolite supported iron, ruthenium and iron/ruthenium nanoparticles by chemical vapor deposition in a fluidized bed reactor*. Powder Technology, 2011. **207**(1–3): p. 17-25.
28. Weizhong, Q., et al., *Production of carbon nanotubes in a packed bed and a fluidized bed*. AIChE Journal, 2003. **49**(3): p. 619-625.
29. See, C.H., et al., *Process Parameter Interaction Effects during Carbon Nanotube Synthesis in Fluidized Beds*. Industrial & Engineering Chemistry Research, 2008. **47**(20): p. 7686-7692.
30. Triantafyllidis, K.S., et al., *Formation of carbon nanotubes on iron/cobalt oxides supported on zeolite-Y: Effect of zeolite textural properties and particle morphology*. Microporous and Mesoporous Materials, 2008. **110**(1): p. 128-140.
31. Porwal, D., et al., *Investigation of the synthesis strategy of CNTs from CCVD by thermal analysis*. Thermochimica Acta, 2007. **463**(1–2): p. 53-59.
32. Kukovecz, A., et al., *Catalytic synthesis of carbon nanotubes over Co, Fe and Ni containing conventional and sol-gel silica-aluminas*. Physical Chemistry Chemical Physics, 2000. **2**(13): p. 3071-3076.
33. Fang, W., et al., *Ce-Ni mixed oxide as efficient catalyst for H₂ production and nanofibrous carbon material from ethanol in the presence of water*. RSC Advances, 2012. **2**(25): p. 9626-9634.
34. Musumeci, A., et al., *Thermal decomposition and electron microscopy studies of single-walled carbon nanotubes*. Journal of thermal analysis and calorimetry, 2007. **88**(3): p. 885-891.
35. Wu, C., et al., *Investigation of coke formation on Ni-Mg-Al catalyst for hydrogen production from the catalytic steam pyrolysis-gasification of polypropylene*. Applied Catalysis B: Environmental, 2010. **96**(1–2): p. 198-207.
36. Zhang, Y., et al., *Pyrolysis-Catalytic Reforming/Gasification of Waste Tires for Production of Carbon Nanotubes and Hydrogen*. Energy & Fuels, 2015. **29**(5): p. 3328-3334.

37. Acomb, J.C., **et al.**, *Effect of growth temperature and feedstock:catalyst ratio on the production of carbon nanotubes and hydrogen from the pyrolysis of waste plastics*. Journal of Analytical and Applied Pyrolysis, 2015. **113**: p. 231-238.
38. Liu, J., et al., *Catalytic pyrolysis of polypropylene to synthesize carbon nanotubes and hydrogen through a two-stage process*. Polymer degradation and stability, 2011. **96**(10): p. 1711-1719.
39. Elbaba, I.F., **et al.**, *Two stage pyrolysis-catalytic gasification of waste tyres: Influence of process parameters*. Applied Catalysis B: Environmental, 2012. **125**(0): p. 136-143.
40. Das, N., et al., *The effect of feedstock and process conditions on the synthesis of high purity CNTs from aromatic hydrocarbons*. Carbon, 2006. **44**(11): p. 2236-2245.
41. Andrews, R., et al., *Multiwall Carbon Nanotubes: Synthesis and Application*. Accounts of Chemical Research, 2002. **35**(12): p. 1008-1017.
42. Andrews, R., et al., *Continuous production of aligned carbon nanotubes: a step closer to commercial realization*. Chemical Physics Letters, 1999. **303**(5): p. 467-474.
43. Lee, D.C., **et al.**, *Carbon nanotube synthesis in supercritical toluene*. Journal of the American Chemical Society, 2004. **126**(15): p. 4951-4957.
44. Kumar¹, A., **et al.**, *Hydrogen production from steam reforming of bioethanol using Cu/Ni/K γ -Al₂O₃ catalysts. Effect of Ni*. International Journal of Environmental Research and Development, 2014. **4**(3): p. 203-212.
45. Zhang, Y., et al., *High-value resource recovery products from waste tyres*. Proceedings of the Institution of Civil Engineers - Waste and Resource Management, 2016. **169**(3): p. 137-145.
46. Wu, C., **et al.**, *Pyrolysis–gasification of post-consumer municipal solid plastic waste for hydrogen production*. International Journal of Hydrogen Energy, 2010. **35**(3): p. 949-957.
47. Li, W., **et al.**, *Effect of temperature on growth and structure of carbon nanotubes by chemical vapor deposition*. Applied Physics A, 2002. **74**(3): p. 397-402.
48. S. Karthikeyan, P.M., *Carbon Nanotubes from Unconventional Resources: Part A: Entangled Multi-Walled Carbon Nanotubes and Part B: Vertically-Aligned Carbon Nanotubes*, in *Syntheses and Applications of Carbon Nanotubes and Their Composites*, D.S. Suzuki, Editor 2013, InTec: Croatia.

49. DiLeo, R.A., **et al.**, Raffaele, *Purity assessment of multiwalled carbon nanotubes by Raman spectroscopy*. Journal of Applied Physics, 2007. **101**(6): p. 064307.
50. Alvarez, J., et al., *Hydrogen production from biomass and plastic mixtures by pyrolysis-gasification*. International Journal of Hydrogen Energy, 2014. **39**(21): p. 10883-10891.
51. Li, J., et al., *Hydrogen-rich gas production by steam gasification of palm oil wastes over supported tri-metallic catalyst*. International Journal of Hydrogen Energy, 2009. **34**(22): p. 9108-9115.
52. Wu, C., **et al.**, *Hydrogen Production from the Pyrolysis- Gasification of Polypropylene: Influence of Steam Flow Rate, Carrier Gas Flow Rate and Gasification Temperature*. Energy & Fuels, 2009. **23**(10): p. 5055-5061.
53. Wu, C., et al., *Renewable hydrogen and carbon nanotubes from biodiesel waste glycerol*. Scientific Reports, 2013. **3**: p. 2742.
54. Yang, R.-X., **et al.**, *Effects of Nickel Species on Ni/Al₂O₃ Catalysts in Carbon Nanotube and Hydrogen Production by Waste Plastic Gasification: Bench- and Pilot-Scale Tests*. Energy & Fuels, 2015. **29**(12): p. 8178-8187.
55. Malaibari, Z.O., et al., *Performance characteristics of Mo-Ni/Al₂O₃ catalysts in LPG oxidative steam reforming for hydrogen production*. International Journal of Hydrogen Energy, 2014. **39**(19): p. 10061-10073.
56. Theofanidis, S.A., et al., *Carbon gasification from Fe-Ni catalysts after methane dry reforming*. Applied Catalysis B: Environmental, 2016. **185**: p. 42-55.
57. Djaidja, A., et al., *Study of Ni-M/MgO and Ni-M-Mg/Al (M= Fe or Cu) catalysts in the CH₄-CO₂ and CH₄-H₂O reforming*. International Journal of Hydrogen Energy, 2015. **40**(14): p. 4989-4995.
58. Song, Y.-Q., **et al.**, *Effects of preparation methods of ZrO₂ support on catalytic performances of Ni/ZrO₂ catalysts in methane partial oxidation to syngas*. Applied Catalysis A: General, 2008. **337**(1): p. 19-28.
59. Wang, K., et al., *High - performance two - ply yarn supercapacitors based on carbon nanotubes and polyaniline nanowire arrays*. Advanced materials, 2013. **25**(10): p. 1494-1498.
60. Afkhami, A., et al., *Surface decoration of multi-walled carbon nanotubes modified carbon paste electrode with gold nanoparticles for electro-oxidation and sensitive determination of nitrite*. Biosensors and Bioelectronics, 2014. **51**: p. 379-385.

61. Turn, S., et al., *An experimental investigation of hydrogen production from biomass gasification*. International Journal of Hydrogen Energy, 1998. **23**(8): p. 641-648.

Chapter 5. Influence of different rubbers and tyre pyrolysis oil compounds on hydrogen and carbon nanotube production

This chapter concentrates on the factors which influence mainly the production of carbon nanotubes (CNTs) from the pyrolysis-catalysis process. Therefore, no steam was introduced in the experiments. However, the effect on hydrogen production as a by-product was also reported.

Section 5.1 concerns the investigation of three types of rubbers (butadiene rubber, styrene-butadiene rubber and nature rubber) which are the main components of real world tyres and two types of waste tyres (truck tyre and car tyre), which aims to better understand the process. Also, examining individual rubber components used in tyre manufacture to determine the influence on the CNTs and hydrogen production.

In section 5.2, five types of model compounds (aliphatic: hexadecane, decane; sing-ring aromatic: styrene; polycyclic aromatics: naphthalene and phenanthrene) found in tyre pyrolysis oil have been investigated, which aim to determine which type of model compounds are more dominant to both CNTs and hydrogen production from the pyrolysis-catalysis process.

This chapter is more concentrated on the in depth investigation of the mechanism for CNTs and hydrogen productions from waste tyre pyrolysis-catalysis, which is also continues the study of the previous chapter.

5.1 Pyrolysis catalysis of butadiene rubber (BR), Styrene butadiene rubber (SBR), natural rubber (NR), waste car tyre and waste truck tyre

Chapter 4 reported on a process that enables the production of high value carbon nanotubes (CNTs) and hydrogen-rich syngas from the two-stage pyrolysis-catalysis of waste tyres. The first stage pyrolysed the tyres at a

temperature of 600 °C and catalysis of the derived pyrolysis gases took place in the second stage catalytic reactor at 800 °C, using a nickel-alumina catalyst. In this section, three of the main rubber elastomers used in tyre manufacture, polybutadiene rubber (BR), styrene-butadiene rubber (SBR) and natural rubber (NR), were also investigated to further understand the process.

In this section, we report on the pyrolysis-catalysis of the main rubbers used in tyre manufacture with the aim of determining the yield and composition of multi walled carbon nanotubes (MWCNTs). In addition, also reported is the production of the product syngas, with an emphasis on hydrogen. Waste truck tyres and car tyres were also used as the feedstock for comparison with the tyre elastomers and the catalyst used was a Ni-alumina catalyst.

5.1.1 Characterisation of the Feedstock Rubber Samples

The thermal degradation of the rubber samples were characterised using thermogravimetric analysis (TGA). In addition, the tyre samples used in Chapter 4 were also characterised by TGA for comparison with the tyre elastomers.

Figure 5-1 shows the resultant thermograms and shows that the main decomposition for natural rubber occurs at a peak temperature of 385 °C; for styrene-butadiene rubber, the main decomposition peaks at 360 °C; and for polybutadiene rubber at a temperature of 475 °C. The three rubbers also showed much smaller weight loss at higher temperature for the natural rubber and lower temperature for the styrene-butadiene and polybutadiene rubbers.

Kandasamy and Gokalp [1] reported slightly different maximum thermal degradation temperatures of 375 °C, 445 °C and 465 °C for natural rubber, styrene-butadiene and polybutadiene rubbers respectively, probably due to minor differences in the rubber compositions. Tamura and Murakami [2] proposed that the reason for natural rubber decomposition at relatively low temperature is because of the formation of volatile isoprene and dipentene produced from depolymerisation of the rubber by β -scission at double bonds.

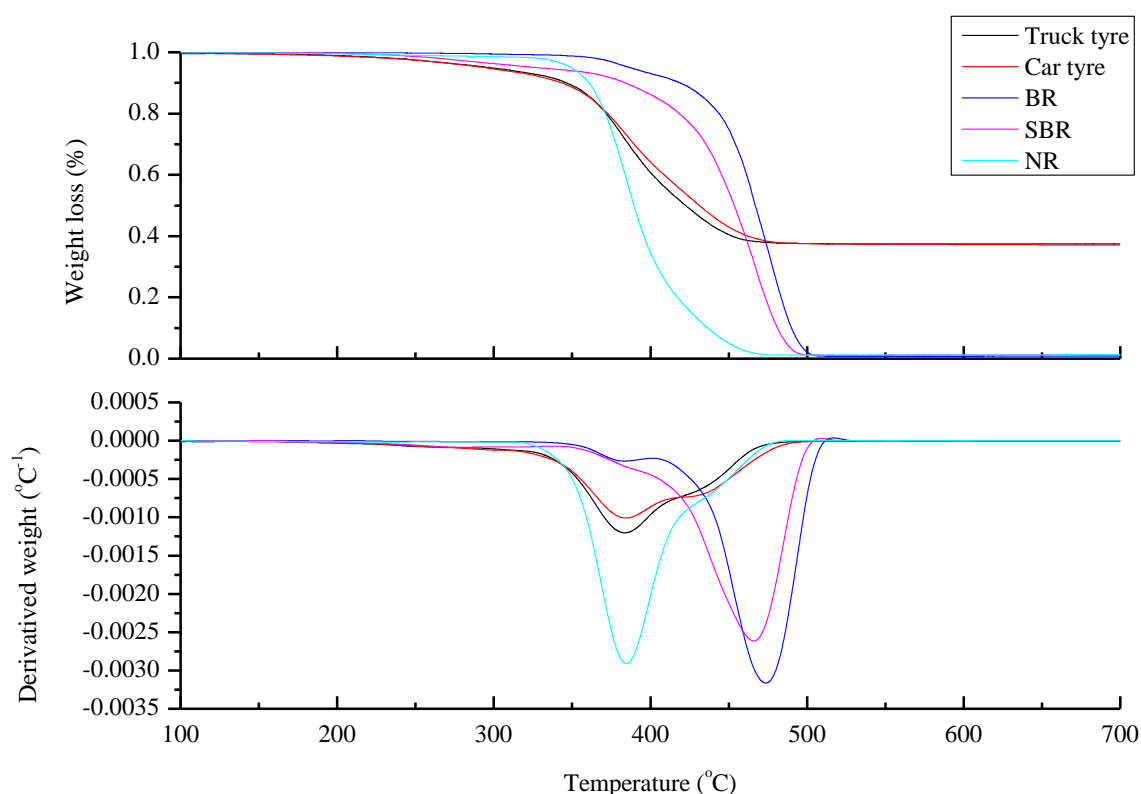


Figure 5-1 TGA and DTG analysis results of the feedstock truck tyre, car tyre, poly-butadiene rubber (BR), styrene-butadiene rubber (SBR) and natural rubber (NR).

Erdogen et al. [3] identified that initial products from thermal degradation of styrene-butadiene rubber were butadiene fragments derived from the butadiene element of the copolymer at lower temperature, and the styrene elements of the co-polymer were degraded at higher temperature to form styrene or benzene. Schwartz and Brazier [4] proposed the degradation of polybutadiene with a first stage decomposition via depolymerisation of the rubber to produce mainly butadiene and dipentene. The second decomposition peak is assigned as the decomposition of the residues formed in the first stage by cyclisation and cross-linking to form a complex mixture of hydrocarbons.

Figure 5-1 also shows the TGA thermograms for the waste car and truck tyres (Described in Chapter 3), which indicate two decomposition peak temperatures. The data suggests that the lower temperature weight loss peak at a

temperature of 385 °C may be ascribed to the thermal decomposition of natural rubber and the higher weight loss temperature peaking at ~430 °C may be ascribed to the thermal decomposition of styrene-butadiene and polybutadiene rubber. However, the interpretation of weight loss is more complicated, since a typical automotive tyre can be composed of up to 30 different synthetic rubbers and 8 different kinds of natural rubber [5]. Sulkowski et al. [6], have also suggested that the two temperature weight loss regimes for waste tyres is due to the thermal decomposition of the different rubber components in tyres. In addition, Seidelt et al. [7] have reported a third lower temperature weight loss which they attributed to the volatilization of the additives used in tyre manufacture, including hydrocarbon oils, moisture, plasticizers and other additives.

5.1.2 Product yields from pyrolysis-catalysis of tyres and rubbers

Pyrolysis-catalysis of the tyre rubber samples in the presence of the Ni/Al₂O₃ catalyst was carried out in the two-stage reactor system. In addition, the pyrolysis-catalysis of waste car and truck tyres was also undertaken for comparison with the tyre rubbers. The results for product yield and gas composition are shown in Table 5-1. The comparison of car tyre and truck tyre at a tyre:catalyst ratio of 1:0.5 showed small differences in product yield, for example, the gas yield from the pyrolysis-catalysis of car tyres was 30.2 wt.% and 27.5 wt.% for truck tyres. Also, the residual char residue left in the pyrolysis reactor after reaction differed, producing 40 wt.% for the waste car tyre and 37 wt.% for the waste truck tyre. These differences were most probably due to the different rubbers and formulations used to produce the tyres.

The char being produced from pyrolysis polymerisation reactions of the heavy hydrocarbon species, but also the char is derived from the carbon black which can be typically 22 wt.% of the tyre. Of more significance was the difference between the two tyre samples in terms of the carbon deposition, which represented carbon deposited mainly on the catalyst and also some on the walls of the catalytic reactor. For the truck tyre, this was 8 wt.%, but for the car tyre was 3 wt.%, again, probably representing different formulations of each tyre

sample. Table 5-1 also shows the influence of increasing the tyre:catalyst ratio on the product yield, with higher amounts of catalyst producing greater conversion of the tyre rubber to carbon deposits, rising from 8.0 wt.% at 1:0.5 tyre:catalyst ratio to 13.0 – 14.0 wt.% at higher ratios.

Table 5-1 Product yield and gas concentrations from the pyrolysis-catalysis of truck tyre, car tyre, poly-butadiene rubber (BR), styrene-butadiene rubber (SBR) and natural rubber (NR).

Feedstock	Truck tyre	Truck tyre	Truck tyre	Car tyre	BR	SBR	NR
Tyre: Catalyst Ratio	1:0.5	1:1	1:2	1:0.5	1:0.5	1:0.5	1:0.5
Product yield							
Gas yield (wt.%)	27.5	29.7	29.5	30.2	41.3	39.3	52.8
Liquid yield (wt.%)	22.0	12.0	14.0	21.0	23.0	17.0	17.0
Char residue (wt.%)	37.0	38.0	38.0	40.0	2.0	1.0	0.0
Carbon deposits (wt.%)	8.0	14.0	13.0	3.0	36.0	40.0	36.0
Hydrogen production (mmol g ⁻¹ tyre/rubber)	11.0	16.7	21.8	12.0	16.3	16.8	25.0
Gas concentrations (vol.%)							
CO	19.4	16.0	18.9	27.1	4.8	4.6	8.9
H ₂	49.6	60.0	68.3	53.8	46.8	47.1	51.8
CH ₄	23.4	15.7	9.4	5.8	35.4	40.6	31.8
CO ₂	0.0	0.0	0.0	0.0	0.2	0.2	0.5
C ₂ -C ₄	5.9	6.4	3.4	10.7	7.6	6.2	5.3
Calorific Value (MJ m ⁻³)	20.9	19.3	16.4	18.8	24.4	25.5	22.8

Analysis of the gas composition (Table 5-1) showed the gas product from the pyrolysis-catalysis of waste tyres was mainly carbon monoxide, hydrogen and methane. Hydrogen yield was high, producing 49.6 vol.% for the waste truck tyre and 53.8 vol.% for the waste car tyre. The hydrogen yield in terms of the mass of tyres was similar for the two tyres at 11.0 – 12.0 mmol g⁻¹ tyre. Increasing the amount of catalyst relative to the amount of tyre resulted in a large increase in hydrogen production from 11.0 mmol g⁻¹ tyre at a tyre:catalyst ratio of 1:0.5 to 21.8 mmol g⁻¹ tyre at a tyre:catalyst ratio of 1:2. The hydrogen gas concentration correspondingly increased to 68.3 vol.%. Table 5-1 also shows the calculated calorific value (CV) of the product gases. The CV of the gases produced from the tyres was between 16.4 and 20.9 MJ m⁻³, depending on process conditions, which is sufficient to provide the energy requirements for the pyrolysis-catalysis process. Considering also, that the total gas yield was between 27.5 and 30.2 wt.% of tyre, the gas could also be exported off-site.

Pyrolysis-catalysis of the three rubber samples is also shown in Table 5-1 where the product yields show a much higher conversion to gas and catalyst carbon deposits with low char formation. The highest gas yield was from natural rubber at 52.8 wt.% and was largely composed of hydrogen and methane, giving a rubber conversion to hydrogen of 25.0 mmol g⁻¹ polybutadiene. The total gas yields from the two synthetic rubbers was much lower at ~40 wt.% and hydrogen concentration in the product gas was ~47 vol.% with a hydrogen yield in terms of mass of rubber at ~16.5 mmol g⁻¹ rubber for both polybutadiene and styrene-butadiene rubber. The carbon deposits formed with the pyrolysis-catalysis of the three rubber samples were very high at 36 wt.%, 40 wt.% and 36.wt% for the polybutadiene rubber, styrene-butadiene rubber and natural rubber respectively.

Overall, the pyrolysis-catalysis of waste tyres has shown a high conversion of the tyre rubber to gas which is largely composed of hydrogen at around 50 vol.%, the remaining gases are combustible methane and carbon monoxide, producing a product gas with a high calorific value of between 16.4 and 20.9 MJ m⁻³. The three rubber samples investigated, polybutadiene rubber, styrene-butadiene rubber and natural rubber, all have a major contribution to the total

gas yield produced and also hydrogen yield. The product gas can be used as process fuel and/or exported off-site.

5.1.3 Carbon formation

Table 5-1 shows that carbon formation on the catalyst (carbon deposits) for the catalyst used in the pyrolysis-catalysis of waste tyre samples was significant, being up to 14 wt.% depending on process conditions. The rubber samples produced a major contribution to the carbon deposits on the catalyst with between 36 and 40 wt.%. Consequently, the individual rubber formulation in the tyre produces the carbon deposition on the catalyst during the pyrolysis-catalysis process. Normally high catalyst coke formation is deemed as a major problem to the catalytic process since the active metal sites of the catalyst become blocked and hence the catalyst becomes deactivated. Therefore, detailed characterisation of the catalyst coke deposits formed during pyrolysis-catalysis of the waste tyres and rubber samples with the Ni/Al₂O₃ catalyst was carried out. Figure 5-2 shows the temperature programmed oxidation (TPO) results for the catalyst carbon deposits used with the waste car tyre, waste truck tyre, and the polybutadiene, styrene-butadiene and natural rubbers. Figure 5-2 shows that the main weight loss of the reacted catalysts resulting from carbon oxidation occurred between temperatures of 450 and 600 °C and was assigned to the oxidation of amorphous carbon and the oxidation that occurred after a temperature of 600 °C was assigned to the oxidation of filamentous/whisker type carbon [8, 9].

Figure 5-2 indicates that the used catalysts for waste car tyre and waste truck tyre display one oxidation temperature peak and the catalysts used with polybutadiene rubber, styrene-butadiene rubber and natural rubber have two oxidation temperature peaks. The oxidation peak of the catalyst coke deposits for the car tyre pyrolysis-catalysis occurred at a lower temperature (585 °C) compared to the catalyst coke from the waste truck tyre (615 °C) suggesting that the coke deposits were a mixture of amorphous and graphitic type carbons, but amorphous dominating for the car tyre and more graphitic filamentous carbons produced with the truck tyre reaction. The TPO thermograms for the

rubber samples show that polybutadiene rubber and styrene-butadiene rubber show two temperature peaks, but the largest is at the lower temperature range, below 600 °C indicating a dominance of amorphous carbon, but also significant graphitic type carbons indicated by carbon oxidation at around 650 °C. In contrast, the natural rubber sample produced mainly graphitic carbons (oxidising at ~650 °C) and less amorphous carbon (oxidising at 580 °C). The proportions of amorphous and graphitic type carbons have been estimated from the TPO thermograms shown in Figure 5-2 and the results are shown in Figure 5-3.

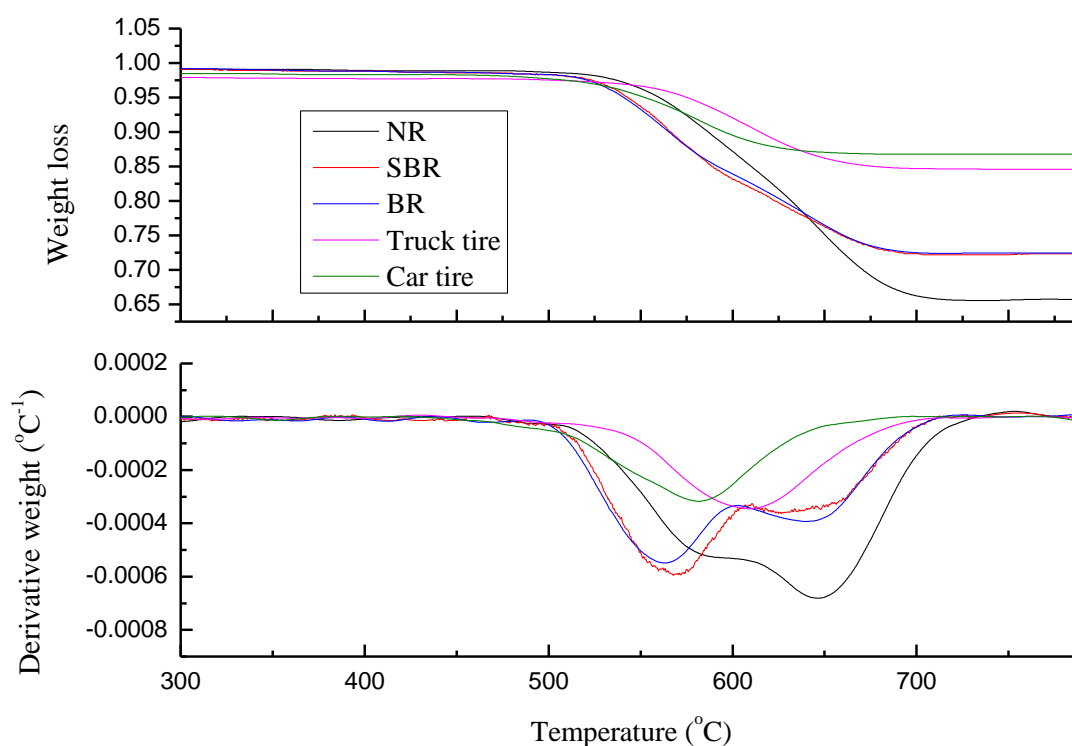


Figure 5-2 TGA-TPO and DTG-TPO results of the used catalysts from the pyrolysis-catalysis of truck tyre, car tyre, poly-butadiene rubber (BR), styrene-butadiene rubber (SBR) and natural rubber (NR)

The deposits of carbon formed on the Ni/Al₂O₃ catalyst during pyrolysis-catalysis of the tyres/rubbers were examined using scanning electron microscopy and transmission electron microscopy (Figure 5-4). The catalytic deposited carbons produced with the pyrolysis-catalysis of the three rubber

samples all show the presence of filamentous or whisker type carbons [10] These appear as entangled string-like filaments of the TEM micrographs reveals that the vast majority of these filamentous carbons are in fact hollow nano-sized filaments, i.e. carbon nanotubes. Figure 5-4 also shows that the carbon deposited on the catalyst used for the pyrolysis-catalysis of the truck tyres also shows this entangled nanotube structure.

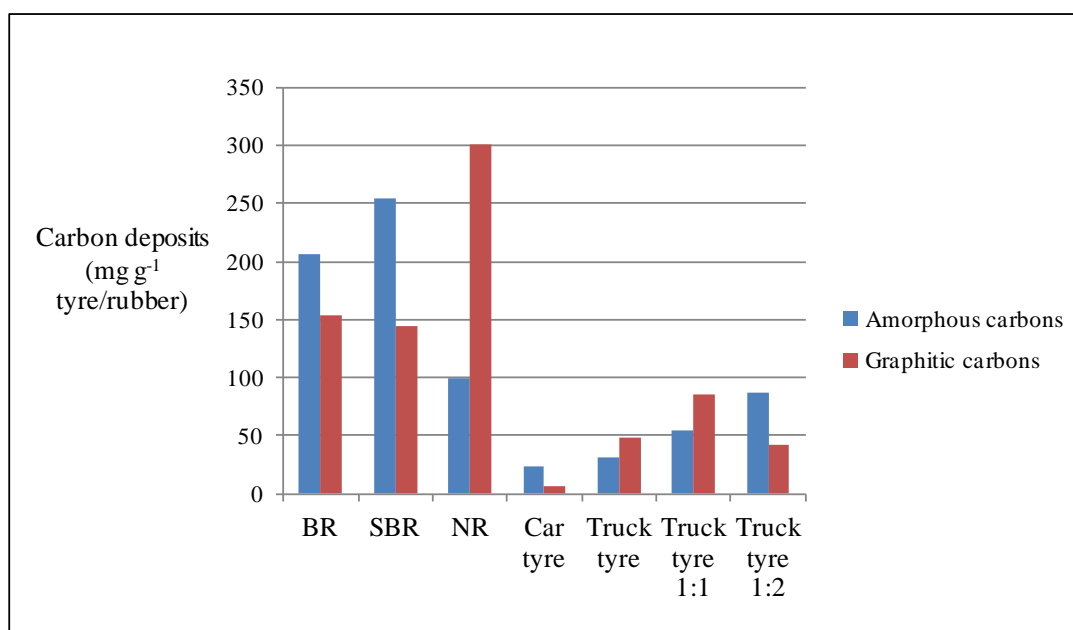


Figure 5-3 Proportion of amorphous and graphitic type carbons formed from the pyrolysis-catalysis of truck tyre, car tyre, poly-butadiene rubber (BR), styrene-butadiene rubber (SBR) and natural rubber (NR).

However, the car tyre showed a poorer development of the carbon nanotubes, as also shown in Figure 5-2 and Figure 5-3 where a more amorphous type of catalyst carbon deposition was indicated. Most probably due to the higher nature rubber content of car tyre and additive formulation of the car tyre compared to the truck tyre. Carbon nanotubes have several different structures, including for example, straight, coiled, waved, branched, and entangled carbon nanotubes [11-13]. Entangled carbon nanotubes as shown in Figure 5-4 have been proposed for use in water and air purification applications [12, 13].

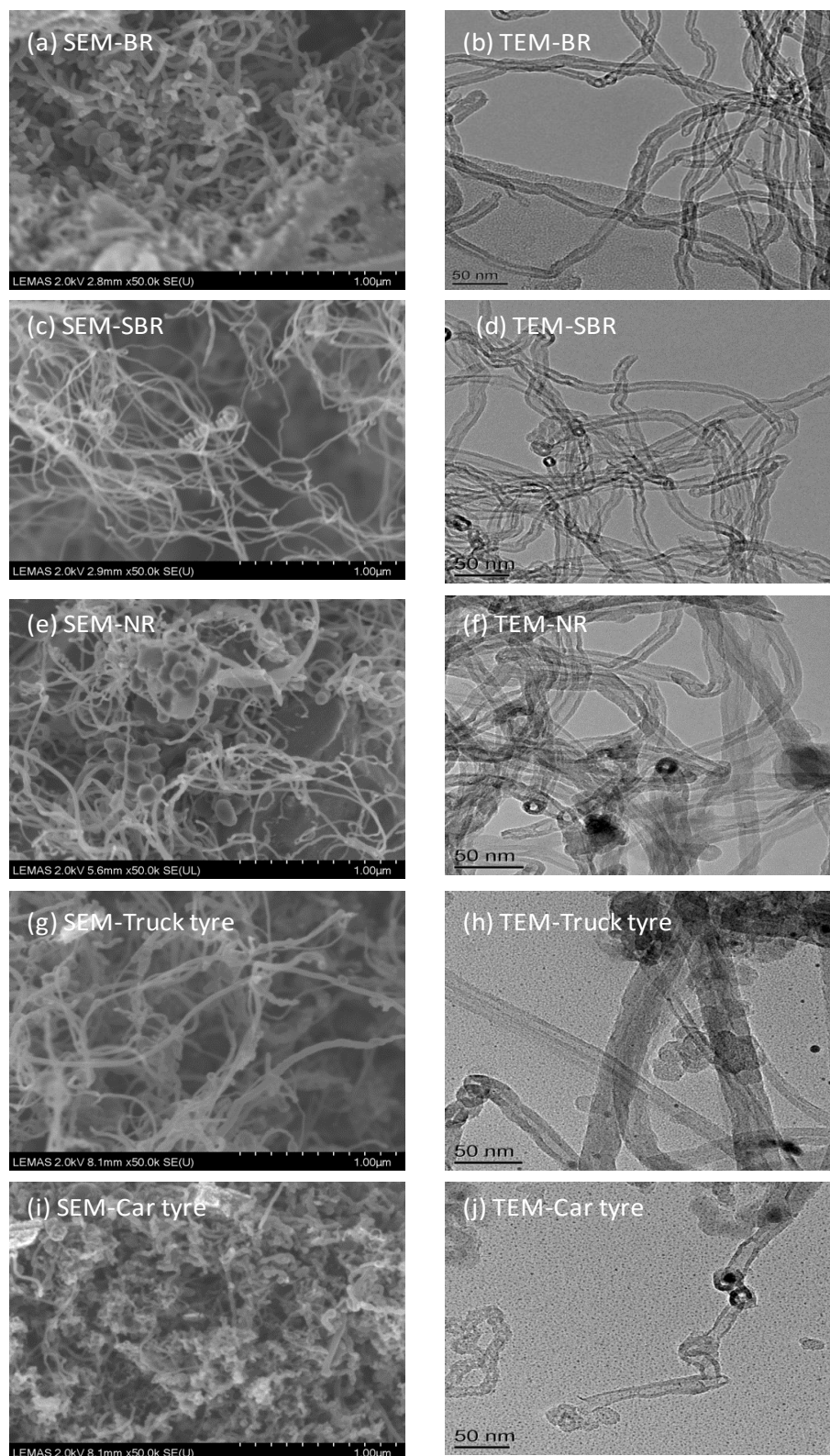


Figure 5-4 SEM and TEM images of the carbon deposited on the catalyst from the pyrolysis-catalysis of truck tyre, car tyre, poly-butadiene rubber (BR), styrene-butadiene rubber (SBR) and natural rubber (NR).

In relation to the TPO results shown in Figure 5-2, Li.et al. [14] have also suggested that the weight loss in relation to carbon oxidation at temperatures <600 °C may also be due to oxidation of single-walled carbon nanotubes as they are less thermally stable compared to multi-walled carbon nanotubes; stability arising from the strong interaction between graphite layers in multi-walled carbon nanotubes. The TEM micrographs in Figure 5-4, show there are carbon nanotubes with different diameters, where thinner walled carbon nanotubes may be thermally less stable than thicker walled nanotubes.

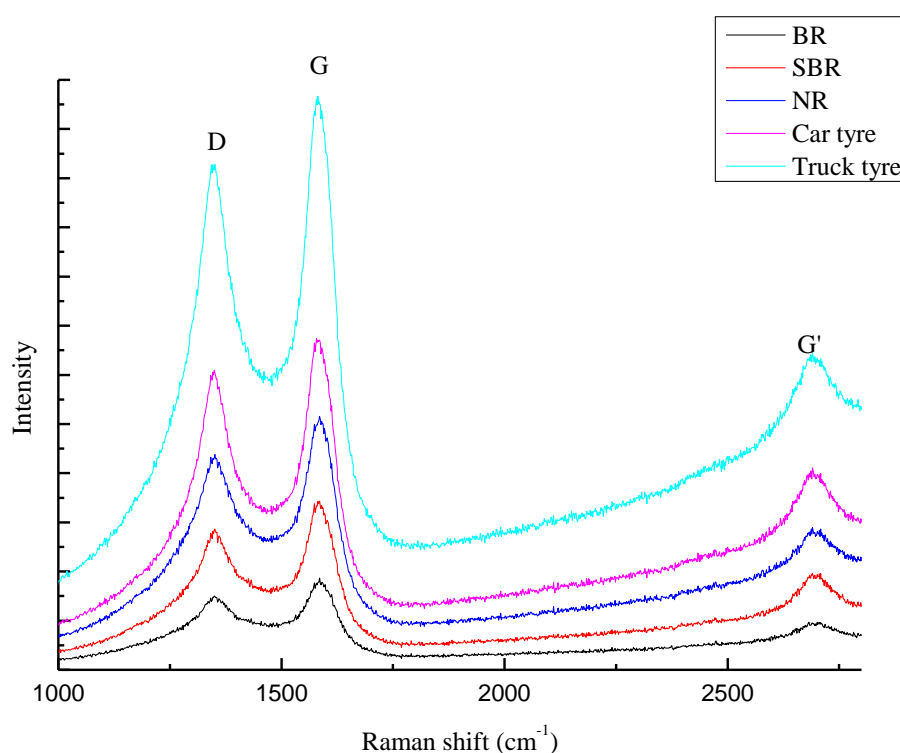


Figure 5-5 Raman analysis of the carbon deposited on the catalyst from the pyrolysis-catalysis of truck tyre, car tyre, poly-butadiene rubber (BR), styrene-butadiene rubber (SBR) and natural rubber (NR)

Raman spectroscopy analysis was used to further characterise the quality of carbon nanotubes, the results are shown in Figure 5-5. The two main spectral peaks for the carbon deposits occur at ~1580 cm⁻¹ and 1350 cm⁻¹. The ~1580 cm⁻¹ peak is designated the G peak and represents the resonance peak of graphitic carbon indicating a well crystallised carbon structure and the peak at

$\sim 1350\text{ cm}^{-1}$ designated as the D peak is the scattering peak of disordered carbon indicating defects in the graphitic crystalline structure or amorphous carbon [13, 15]. The intensity (I) of each peak and the ratio of the two peak intensities I_D/I_G is used to determine the degree of crystallisation of the carbon structure, with a higher I_D/I_G ratio indicating higher quality in regard to carbon nanotubes. A G' peak is also obtained at Raman shifts around 2709 cm^{-1} and is a further indication of CNT purity. The intensity of the D band (I_D) normalized to the intensity of the G band (I_G) (I_D/I_G) and intensity ratio of G' to G ($I_{G'}/I_G$) was used to evaluate the quality of the carbon nanotubes.

The I_D/I_G and $I_{G'}/I_G$ values for the carbons produced with natural rubber, polybutadiene rubber and styrene butadiene rubber showed no significant differences being 0.83 ± 0.01 for the I_D/I_G value and 0.54 ± 0.02 for the $I_{G'}/I_G$ values. The Raman spectra for the carbon derived from the waste tyres were similar to each other with a small increase in both I_D/I_G and $I_{G'}/I_G$ values at 0.89 ± 0.01 and 0.57 ± 0.02 respectively. The data confirm that the carbons deposited on the catalyst during the pyrolysis-catalysis of the waste tyres and rubber samples contained both amorphous and carbon nanotubes and also indicated by the TGA results (Figure 5-2) and TEM micrographs (Figure 5-4).

5.1.4 Conclusions

The pyrolysis-catalysis of the three main rubbers used in the manufacture of automotive tyres has been investigated using a $\text{Ni}/\text{Al}_2\text{O}_3$ catalyst to investigate the production of carbon nanotubes. In addition, the results were compared with the production of hydrogen and carbon nanotubes from waste car and truck tyres. The main conclusions were:

The pyrolysis-catalysis process produced significant deposition of carbon onto the catalyst. Examination of the carbon using transmission electron microscopy supported by temperature programmed oxidation and Raman spectroscopy showed that the carbons produced from both waste tyres and the rubber samples were carbon nanotubes of diameters between 5-10 nm and lengths of several microns. The maximum deposition of carbon was found with the waste truck tyre at $\sim 13\text{ wt.}\%$ of tyre. However, for the rubber samples, polybutadiene,

styrene-butadiene and natural rubber, the carbon desposition was between 26.0 and 40.0 wt.%.

In addition, the highest yield of gas was obtained from the pyrolysis-catalysis of waste truck tyres at 29.5 wt% of tyre feedstock at a tyre:catalyst ratio of 1:2. The gas was composed of ~70 vol.% of hydrogen with the other main gases being carbon monoxide and methane, giving a product gas with a calorific value of 16.4 MJ m⁻³. The conversion of the tyre rubber to hydrogen was 13 mmol H₂ g⁻¹ tyre. For the rubber samples, natural rubber produced the largest gas yield at 52.8 wt% of natural rubber feedstock and the highest conversion to hydrogen, yielding 25 mmol H₂ g⁻¹ rubber.

5.2 Investigation of tyre oil compounds on hydrogen and carbon nanotube production

Pyrolysis-catalysis of five typical tyre pyrolysis oil model compounds (hexadecane, decane, styrene, naphthalene and phenanthrene) in the presence of 10% wt. Ni/Al₂O₃ catalyst have been investigated to determine their influence on the production of carbon nanotubes. The compounds chosen to investigate represent typical aliphatic and aromatic compounds detected in tyre pyrolysis oil. Chapter 2 showed that the yield and structure of carbon materials such as carbon nanotubes are related to the chemical structure of precursor oil compounds used in production. For example, aromatic compounds promote solid carbon formation including multi-walled carbon nanotubes. In addition, solid carbon nanofibers can be formed from polyaromatic compounds, which have very similar morphology as carbon nanotubes based on scanning electron microscopy images. Therefore in this section, several tyre model compounds typically found in tyre pyrolysis oils were investigated to determine their influence on the formation of carbon nanotubes. Such compounds would enter the second stage catalytic process in the two-stage pyrolysis-catalysis process used in this work. Thereby using model tyre pyrolysis oil compounds helps to better understand the multi-walled carbon nanotubes formation mechanism in waste tyre pyrolysis-catalysis process.

In addition, two commercial carbon nanofibers and MWCNTs purchased from Sigma-Aldrich were also been analysed to compare the quality of carbon produced from pyrolysis-catalysis process. This work seeks to also investigate the production of a hydrogen-rich syngas that could be used for process fuel.

The different types of model compounds were placed in the sample crucible during the experiments. Exactly 0.5 g of the 10 wt.% Ni/Al₂O₃ catalyst was placed in the catalysis stage which was then pre-heated to the temperature of 800 °C and the pyrolysis stage was heated to 600 °C with the heating rate of 40 °C min⁻¹ constantly. The weight of each type of model compound added to the first stage was calculated based on the carbon content of each gram of waste truck tyre (81.16 wt.% carbon content per gram of waste truck tyre mentioned in chapter 3). Therefore the weight of each model compound had the same amount of carbon content of 0.8116 g regardless of hydrogen content. The calculation procedure of model compounds weights are explained below:

Weight of decane (g) was calculated by using per gram of truck tyre equivalent carbon 0.8116 g divide the molecular weight ratio of carbon content of decane to decane, that the decane amount was 0.9624 g; Weight of hexadecane (g) was calculated by using per gram of truck tyre equivalent carbon 0.8116 g divide the molecular weight ratio of carbon content of hexadecane to hexadecane, that the amount of hexadecane was 0.9572 g; Weight of styrene (g) was calculated by using per gram of truck tyre equivalent carbon 0.8116 g divide the molecular weight ratio of carbon content of styrene to styrene, that the styrene amount was 0.8805 g; Weight of naphthalene (g) was calculated by using per gram of truck tyre equivalent carbon 0.8116 g divide the molecular weight ratio of carbon content of naphthalene to naphthalene, that the naphthalene amount was 0.8668 g; Weight of phenanthrene (g) was calculated by using per gram of truck tyre equivalent carbon 0.8116 g divide the molecular weight ratio of carbon content of phenanthrene to phenanthrene, that the phenanthrene amount was 0.8610 g.

The gaseous carbon conversion (wt.%) was calculated by using total carbon contents of each hydrocarbon gas product divide the total carbon content of the model compound and then multiply 100 %.

5.2.1 Carbon production and characterisation

Table 5-2 shows the amount of carbon formed from the pyrolysis-catalysis of the tyre pyrolysis oil model compounds using the two-stage pyrolysis-catalysis reactor system. Table 5-2 shows that the aromatic and polyaromatic model compounds produced higher carbon formation e.g. for styrene 0.4g per gram of truck tyre equivalent carbon, was produced, naphthalene produced 0.28 g per gram of truck tyre equivalent tyre and phenanthrene produced 0.29 g per gram of truck tyre equivalent of solid carbon. This carbon formation was significantly higher than that produced from the aliphatic hydrocarbon model compounds from hexadecane and decane which were 0.06 and 0.2 g g⁻¹, respectively.

Table 5-2 Carbon formation from the pyrolysis-catalysis of tyre pyrolysis oil model compounds

	aliphatic	Aliphatic	sing ring	Polyaro matic	polyaromatic
10% Ni/Al ₂ O ₃	hexadecane C ₁₆ H ₃₄	decane C ₁₀ H ₂₂	styrene C ₈ H ₈	naphthalene C ₁₀ H ₈	phenanthrene C ₁₄ H ₁₀
Carbon production (g per gram of tyre equivalent carbon)	0.06	0.20	0.40	0.28	0.29
Gaseous carbon conversion (%)	42.6 0	37.65	6.59	1.22	0.17

5.2.1.1 Thermogravimetric analysis (TGA) of reacted catalysts with carbon deposition

Figure 5-6 shows the thermogravimetric analysis of reacted catalysts with carbon deposition from different tyre oil model compound by pyrolysis-catalysis process, which aim to compare the thermal stability of carbon produced from

different tyre pyrolysis oil model compound. The weight loss in Figure 5-6 indicates the oxidation of carbon formed on the catalyst surface. The oxidation of carbon produced from different model compounds are in the temperature range of 450 to 750 °C as shown in Figure 5-7 which indicates the carbon formed consist of different degrees of graphitization, such as disordered/amorphous type carbons which oxidise at lower temperature compared to graphitic/filamentous carbon which oxidise at higher temperature. The carbon with a high degree of graphitization would have a high thermal stability that was decomposed at higher temperature compared with the less graphitized carbon [16, 17]. Carbon oxidized below 600 °C can be assumed as the decomposition of amorphous carbon and the carbon oxidized above 600 °C could be assumed as filamentous carbon [18-21].

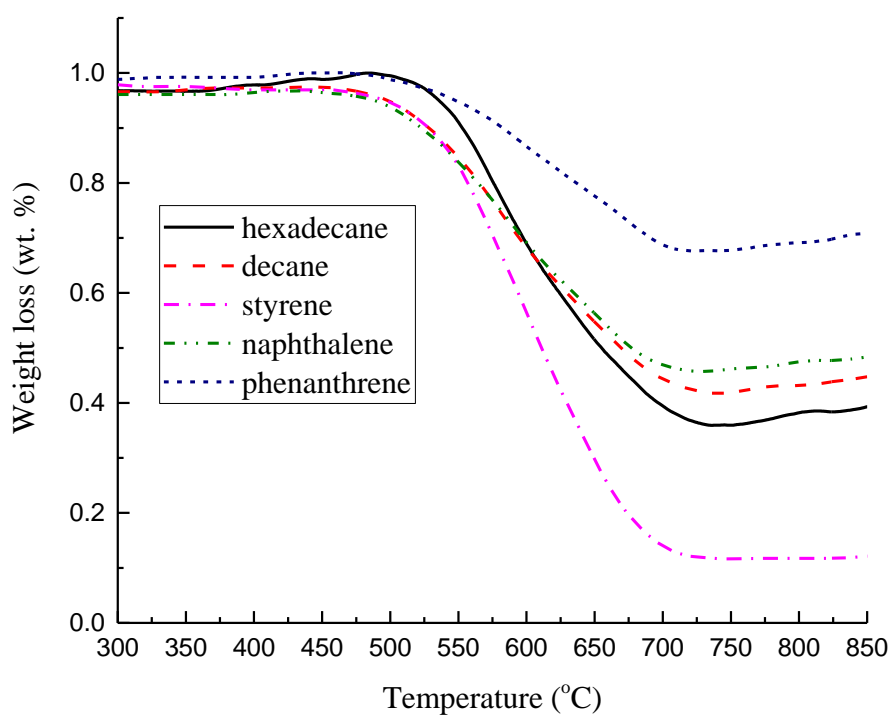


Figure 5-6 TGA-TPO results of reacted catalysts produced from pyrolysis catalysis of tyre oil model compounds.

Based on the weight loss from the TPO results, the amount of amorphous and filamentous carbon production can be estimated. The proportions of amorphous and filamentous carbon produced from the different tyre pyrolysis oil model compounds are shown in Figure 5-8. The figure shows that the cyclic aromatic hydrocarbons are dominant for solid carbon formation compared with the aliphatic model compounds and also for filamentous carbon formation. The filamentous carbon produced from styrene, naphthalene and phenanthrene were 174.19, 104.53 and 149.14 mg per gram of tyre equivalent carbon that are higher than the filamentous carbon produced from aliphatic hydrocarbons (hexadecane and decane) that are 32.94 and 12.08 mg per gram of tyre equivalent carbon, respectively.

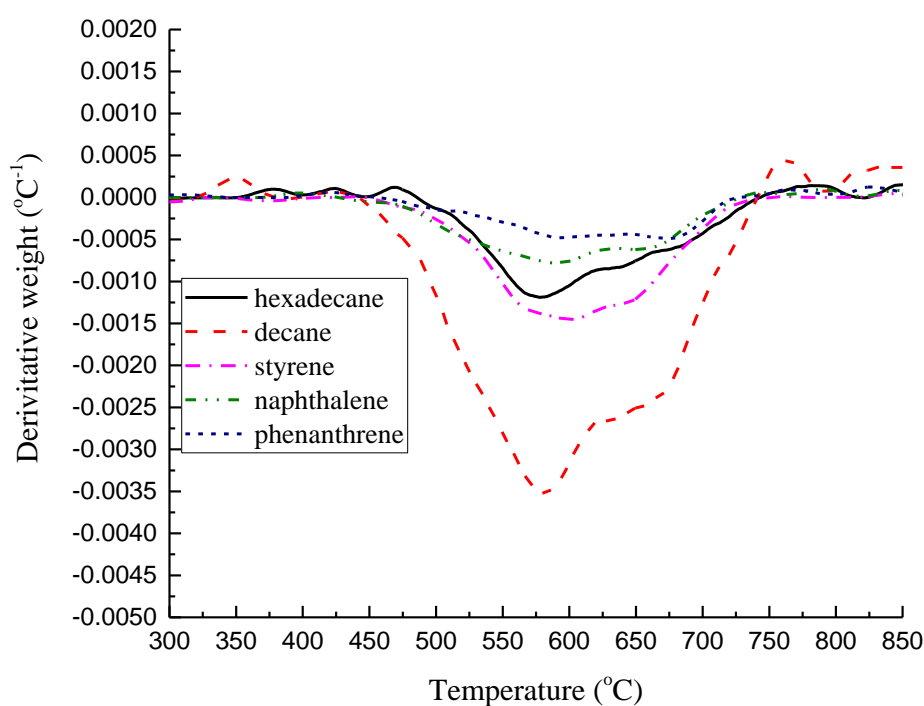


Figure 5-7 DTG-TPO results of reacted catalysts produced from pyrolysis catalysis of tyre oil model compounds.

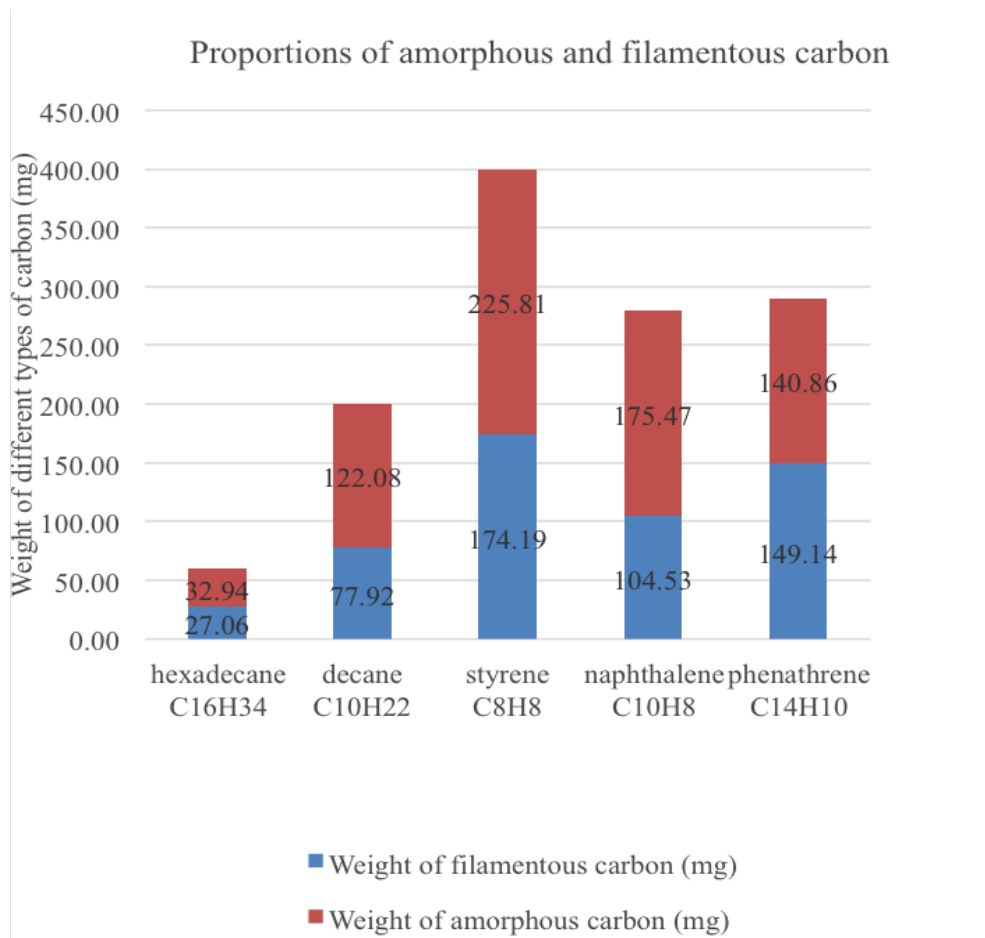


Figure 5-8 Proportions of disordered and filamentous types of carbon formed from pyrolysis of tyre oil model compounds.

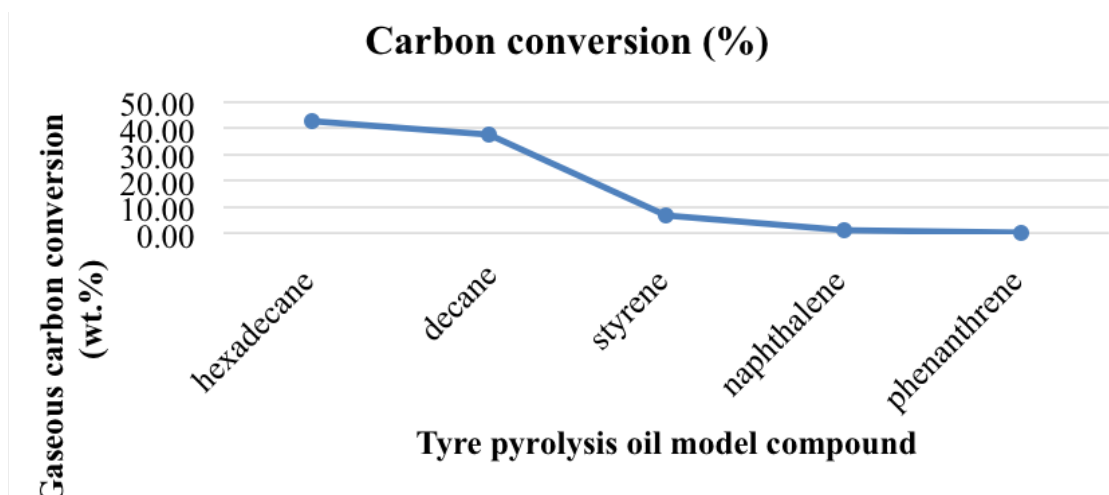
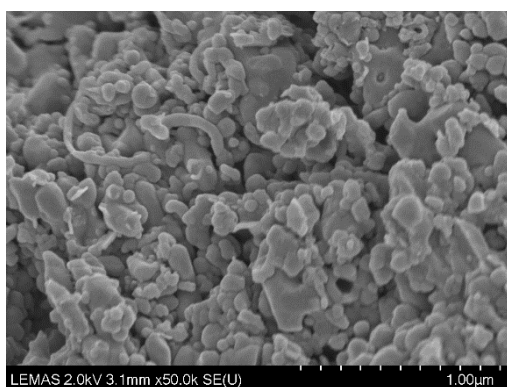


Figure 5-9 Gaseous carbon conversion

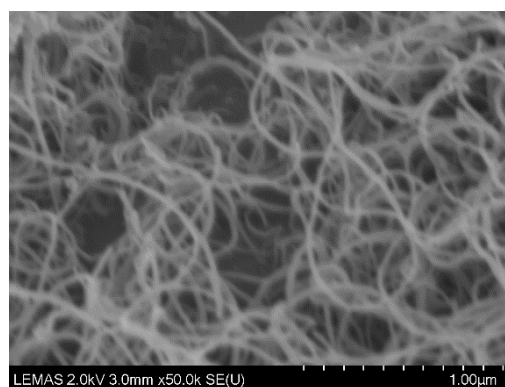
5.2.1.2 SEM and transmission electron microscopy (TEM) analysis of carbon produced from different tyre pyrolysis oil model compounds by pyrolysis-catalysis.

Figure 5-10 shows the scanning electron microscope (SEM) micrographs of carbon formed from five different types of tyre pyrolysis oil model compounds by the pyrolysis-catalysis process. The filamentous carbon formation from the different types of tyre pyrolysis oil model compounds can be seen in the SEM images as shown in Figure 5-10. The SEM images support the results obtained from TPO suggesting significant formation of filamentous carbons. The corresponding TEM images of the carbon formed on the catalyst with the model compounds is shown in Figure 5-11. The TEM images show that decane, styrene, naphthalene and phenanthrene produced MWCNTs with longer tube length and smooth walls. Kumar and Ando [22] reported that the molecular structure of the precursors used for the production of carbon nanotubes by chemical vapour deposition (CVD) directly affected the morphology of the growth of CNTs. Linear hydrocarbons (such as methane, ethylene, and acetylene) produce hollow CNTs since the linear hydrocarbons are thermally decomposed into atomic carbons or linear dimer or trimer carbon.

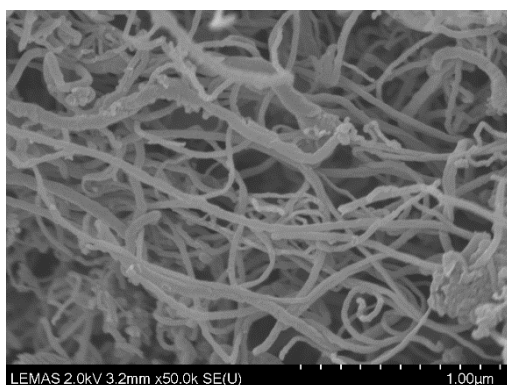
Cyclic hydrocarbons (such as benzene, xylene, cyclohexane, and fullerene) produce more curved CNTs [22-24]. The authors also reported that the relatively low temperature in the range of 600 to 900 °C is generally favoured for multi-walled CNTs (MWCNTs) production and single walled CNTs (SWCNTs) are formed at higher temperature between 900 to 1200 °C by CVD. This could explain why no SWCNTs could be detected on the catalysts used in the pyrolysis-catalysis of tyre oil model compounds. Chung and Jou [25] suggested that aliphatic olefins tend to produce long length CNTs during the pyrolysis of polyethylene and polypropylene in the presence of catalyst; whereas aromatic hydrocarbons facilitate the formation of CNTs with thicker walls through secondary pyrolytic deposition.



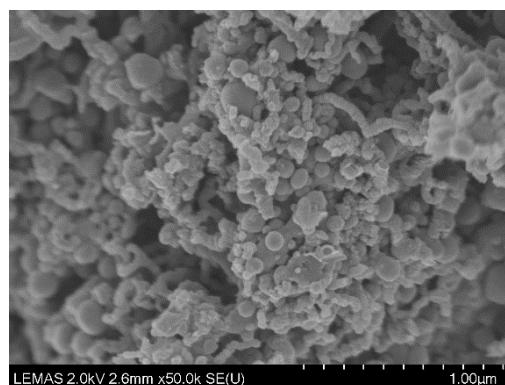
(a) hexadecane



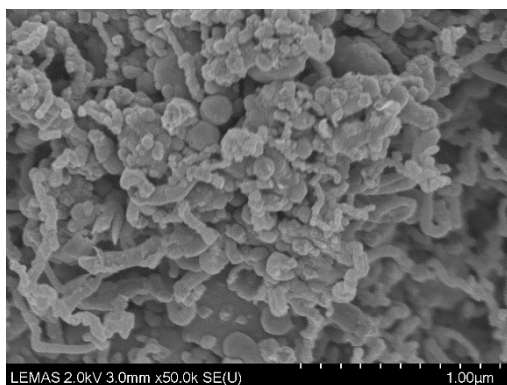
(b) decane



(c) styrene



(d) naphthalene



(e) phenanthrene

Figure 5-10 SEM images of reacted catalysts produced from pyrolysis catalysis of tyre oil model compounds.

Simultaneously, solid carbon fibres formed from naphthalene are also shown in TEM images in Figure 5-11(d)(e). The formation of solid carbon nanofibers has been reported in the carbon nanotube synthesis process by many researchers

[26-28]. Mori and Suzuki [26] proposed that carbon nanofibers consist of several graphitic basal planes in carbon nanofibers synthesis by plasma-enhanced chemical vapour deposition. They reported that the carbon nanotubes consist of graphitic basal planes parallel to the fibre axis with a holey structure; or if the basal planes are perpendicular to the fibre axis this leads to a platelet structure of carbon nanofibers which are not hollow. Yoon et al. [27] also proposed a conceptual model to define the structures of carbon nanofibers synthesised by catalytically growth including the platelet type which indicates the formation of solid carbon nanofibers, herringbone and tubular type carbon nanofibers. According to SEM, TEM, STM and XRD observations.

Yoon et al. [27] suggested that carbon nanofibers are commonly formed with sub-structures, which are carbon nano-rods and carbon nano-plates. Carbon nano-rods are a carbon cluster of graphene layers with unique diameter and various lengths, and carbon nano-plates are several graphene stacks that could be formed by association of carbon nano-rods. The faceted catalyst particle will dominate the order and arrangement of carbon nano-rods or carbon nano-plates to finally form the carbon nanofibers in platelet, herringbone or tubular types. The conceptual model has also been supported by Rodriguez et al. [28], suggesting that the anisotropic alignment of graphene layers dominate carbon nanofibers with diverse geometric structures, including platelet, herringbone and tubular carbon nanofibers which all depend on the directions of alignment and fiber axis.

The mechanism of carbon nanofibers growth by catalytic decompose of hydrocarbons has been studied by many researchers [29-32]. The possible routes include carbon precursor disassociation where the hydrocarbon molecules decompose on the free-metal surface and form carbon atoms. Alternatively, the mechanism involves hydrogen molecular desorption; diffusion of carbon atoms and nucleation whereby the carbon atoms precipitate as graphite on the metal surface [31]. Oberlin et al. [29] and Yang et al. [30] proposed that carbon atom diffusion occurred on the catalytic metal particle surface which could explain the formation of hollow carbon nanofibers formation. Snoeck et al. [32] summarized a concise model to explain a full or holey carbon nanofibers formation mechanism. They proposed that full fibers formed when

carbon atoms have reached the entire catalytic metal particle-support interface via diffusion, which is because the low temperature leads to low nucleation. As the temperature increases, the nucleation can be promoted before the metal-support interface is fully attached with carbon atoms, whereas the holey carbon fibers formed as the nucleation starts at the interface among the metal/support/gas phases [33].

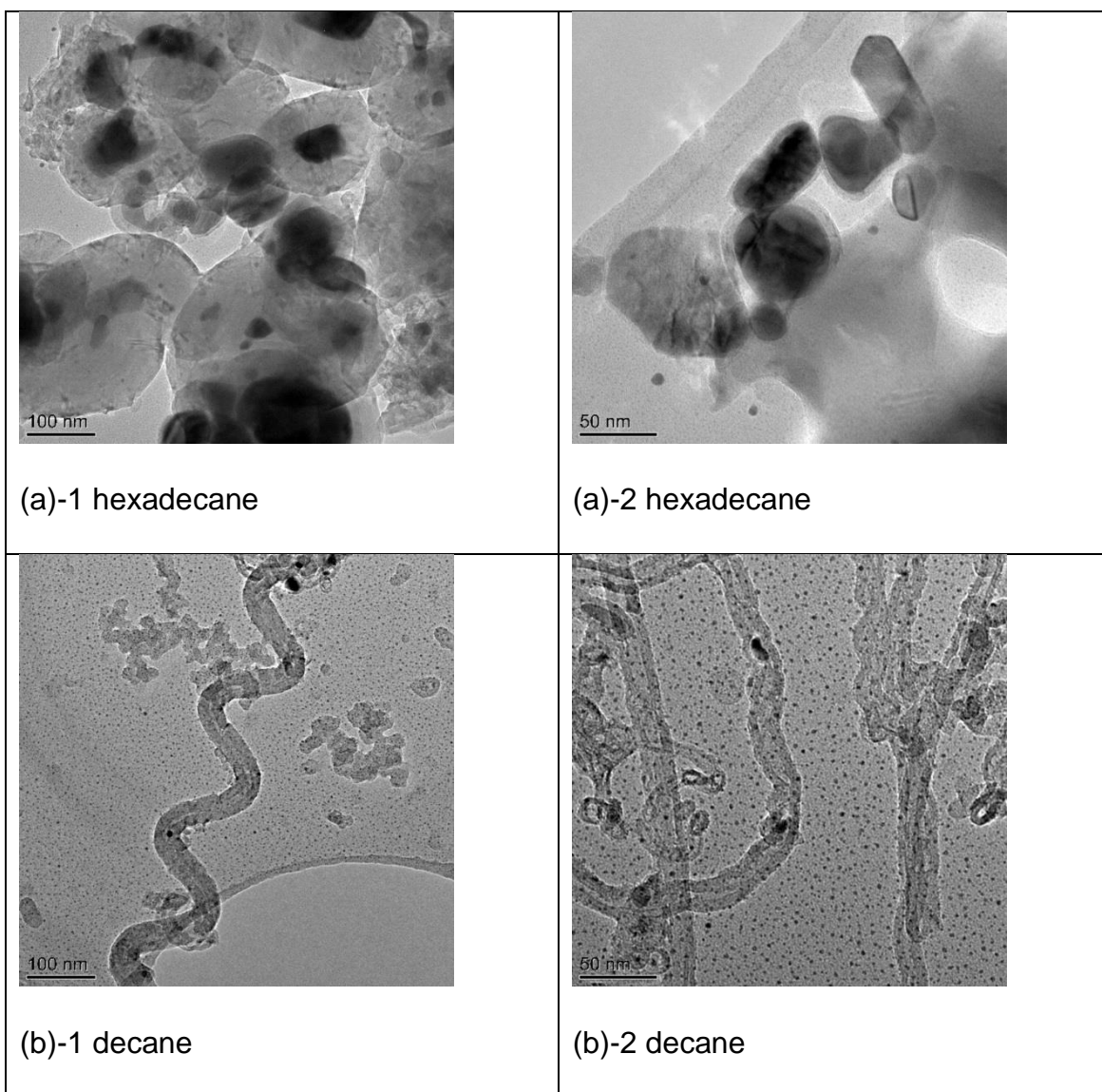
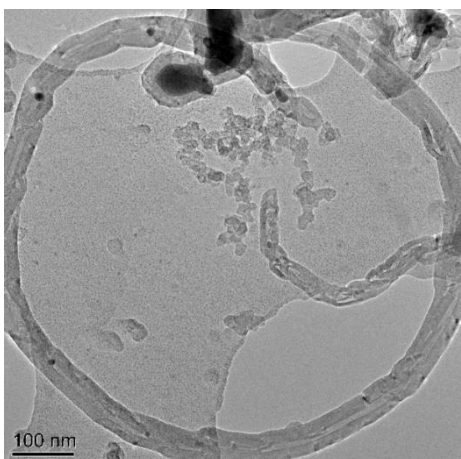
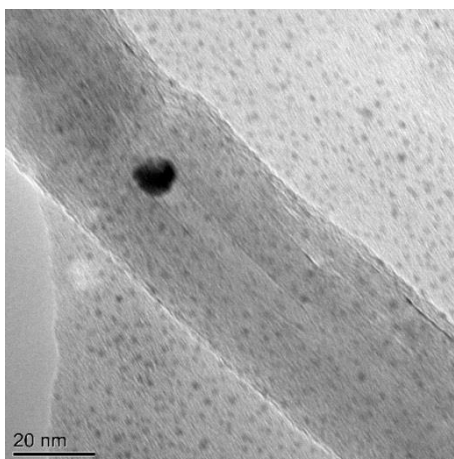


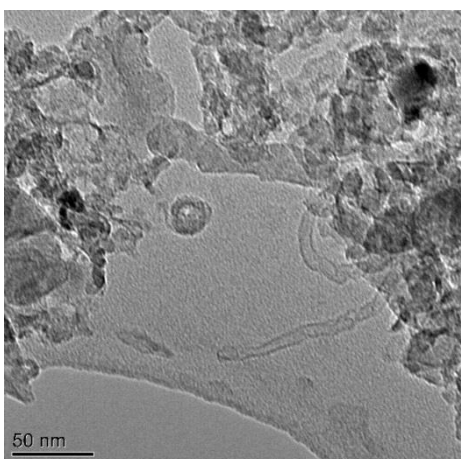
Figure 5-11 TEM images of reacted catalysts produced from pyrolysis tyre oil model compounds.



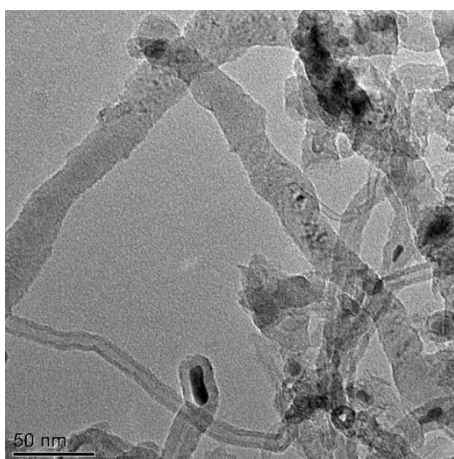
(c)-1 styrene



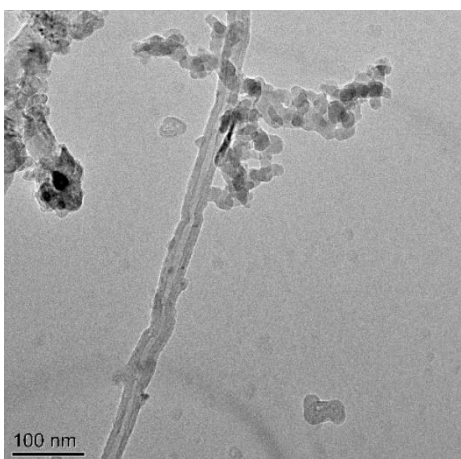
(c)-2 styrene



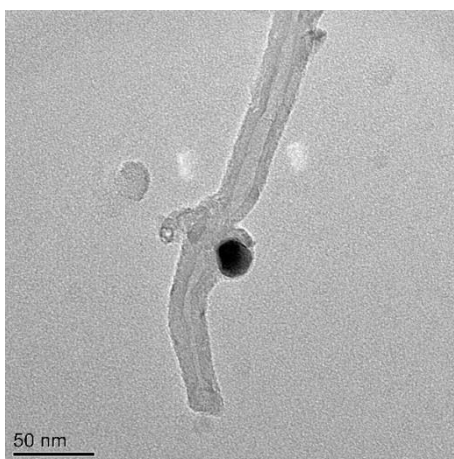
(d)-1 naphthalene



(d)-2 naphthalene

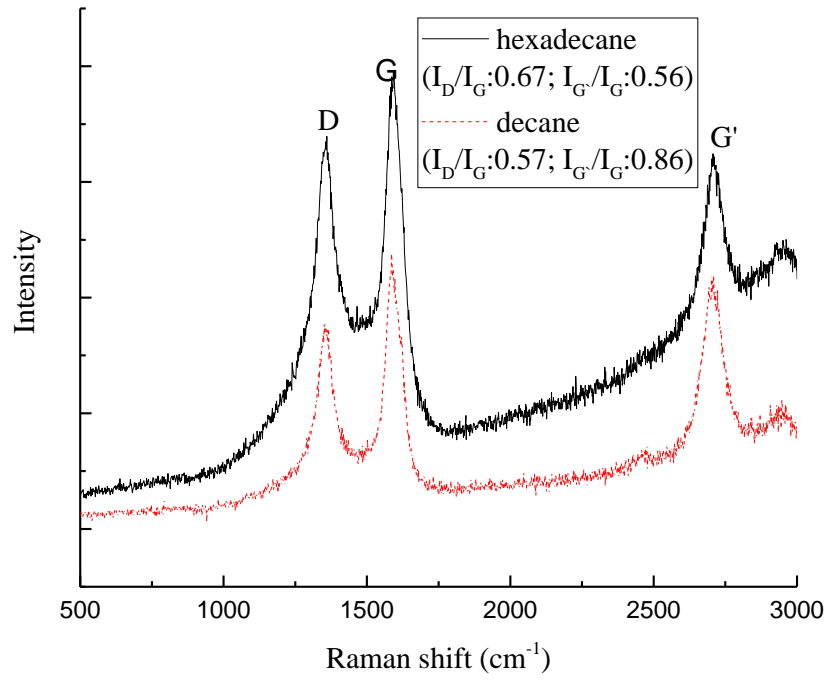


(e)-1 phenanthrene

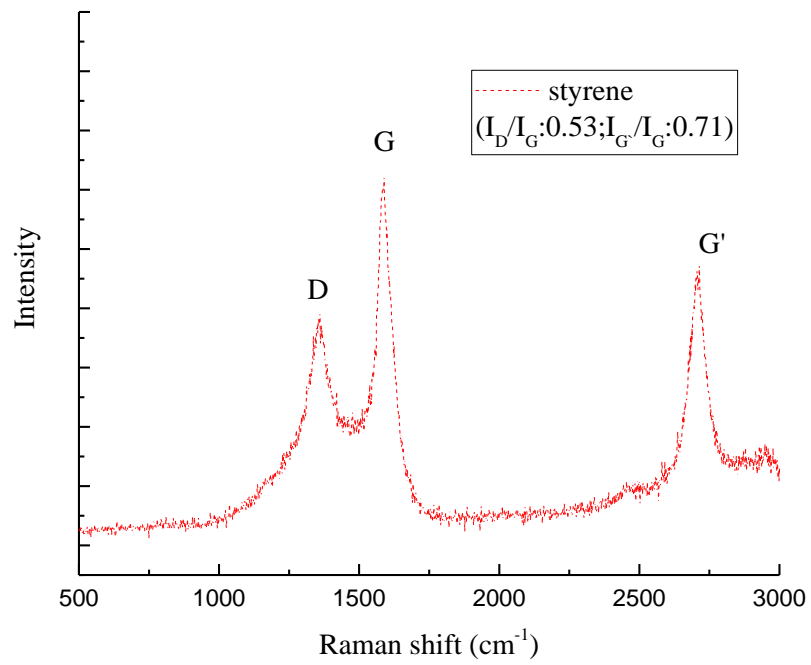


(e)-2 phenanthrene

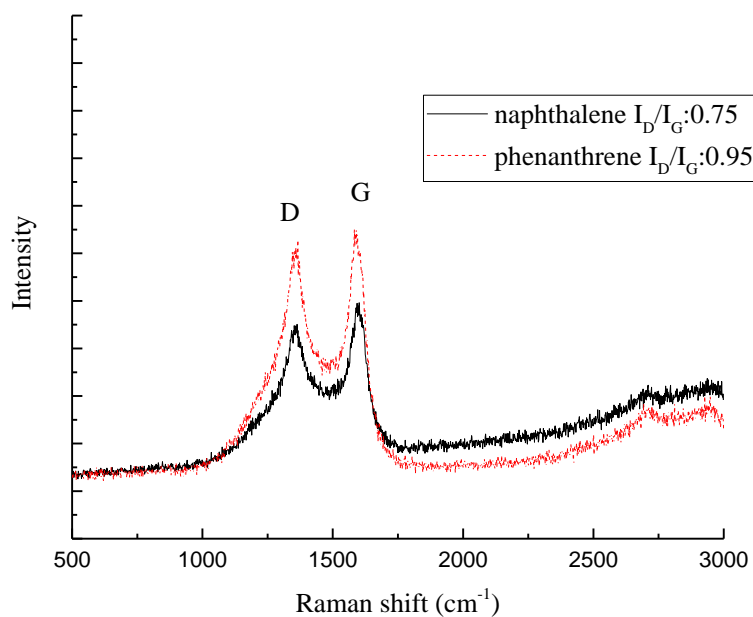
Figure 5-11 TEM images of reacted catalysts produced from pyrolysis tyre oil model compounds.



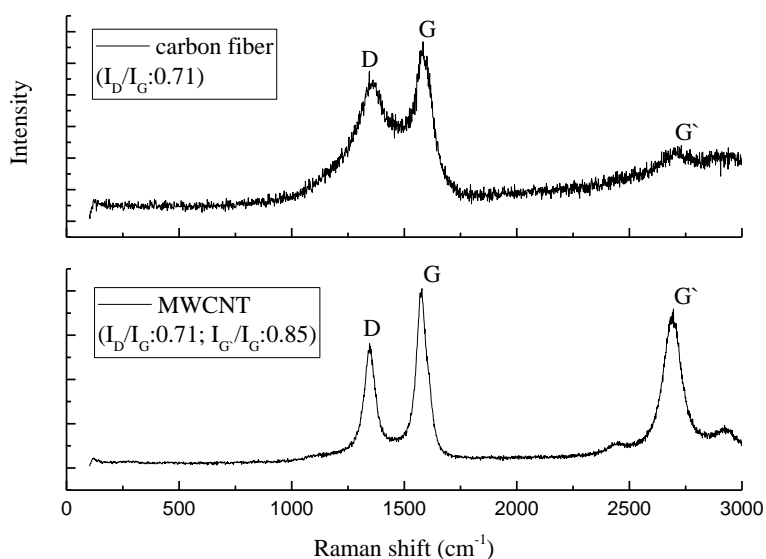
(a)



(b)



(c)



(d)

Figure 5-12 (a) Raman results of reacted catalysts produced from pyrolysis-catalysis of aliphatic tyre oil model compounds (hexadecane and decane); (b) single ring aromatic tyre oil model compounds (styrene); (c) polyaromatic tyre oil model compounds (naphthalene and phenanthrene); (d) commercial carbon nanofibers and multi-walled carbon nanotubes.

The quality of carbon produced on the catalyst from the five tyre pyrolysis oil model compounds by pyrolysis-catalysis can be further analysed by Raman spectroscopy. The Raman spectra of the product carbons in a wavelength range of 500 to 3000 cm^{-1} are shown in Figure 5-12. Carbon is normally formed as hybridizations including sp^1 , sp^2 and sp^3 , the different carbon allotropes either contain pure hybridizations or as a mixture. Carbon nanotubes, carbon nano-ribbons and amorphous carbon all contain different proportions of sp^2 and sp^3 [34]. The D band evident at the Raman shift at 1300 cm^{-1} indicates disordered carbon or amorphous carbon (such as sp^3 bonding carbon or broken sp^2 bonding carbon) [35]. The G band evident at 1550 cm^{-1} indicates the graphitized or filamentous structure of carbon (commonly for sp^2 carbon). The G' band occurred at wavelength 2700 cm^{-1} in the Raman shift indicates the defects in the graphitic crystallinity of carbon produced from different model compounds which can be used to estimate the purity of carbon production [35-37]. All sp^2 carbon materials have G' peaks in the Raman spectrum which is strongly dependent on the electronic and/or photon structure of graphene.

The intensity of the D band normalized to the intensity of the G band (I_D/I_G) can be used to determine the graphitization level of carbon. As Figure 5-12(a)(b)(c) shows, the carbon produced from the polyaromatic model compounds had relatively high I_D/I_G ratios, i.e. naphthalene and phenanthrene were 0.75 and 0.95, respectively. The aliphatic and single ring aromatic tyre oil model compounds had relatively low ratios, the ratio for hexadecane was 0.67, decane is 0.57 and styrene product carbon produced an I_D/I_G ratio of 0.53. The ratios indicate the carbon produced from hexadecane, decane and styrene had a high degree of graphitization compared with the carbon produced from naphthalene and phenanthrene by pyrolysis-catalysis process. Figure 5-12(d) shows the Raman shift of commercial carbon nanofibers and MWCNTs for comparison. The I_D/I_G ratio of carbon nanofibers was 0.71 and the ratio of the commercial MWCNTs sample was also 0.71. This is in the range of the reported typical ratios of MWCNTs which is between 0.63-1.5 [38]. The I_D/I_G ratios of carbon produced from the five tyre pyrolysis oil model compounds are close to the ratios of commercial carbon nanofibers and MWCNTs as shown in Figure

5-12(d). The data also indicates that the graphitization of the produced carbon is close to the commercial standard.

The intensity of the G' band normalized to the intensity of the G band ($I_{G'}/I_G$) can be used to estimate the purity of the carbon produced. The $I_{G'}/I_G$ ratio of carbon produced from hexadecane has the lowest ratio at 0.56 which suggests that the carbon produced had more defects and low purity compared with the carbon produced from decane and styrene. This is because the G' band arises from the two-photon scattering elastic process which indicates the long-range order of the sample. The less intensity of the G' band indicates the samples are less ordered such as containing a high amount of impurities which is not allowing for the coupling effect for the two-photon process [35, 36]. The $I_{G'}/I_G$ ratios of carbon produced from decane and styrene were 0.86 and 0.71 which are close to the ratio of commercial MWCNTs at 0.85 as shown in Figure 5-12(d). The results also support the suggestion that the carbon produced from decane and styrene can achieve that of the commercial MWCNTs quality. Figure 5-12(c) shows that the carbon produced from naphthalene and phenanthrene have no significant G' peaks that are similar to the commercial carbon nanofibers shown in Figure 5-12(d). The TEM images in Figure 5-12(d) and (e) also show that there are carbon nanofibers in addition to the MWCNTs.

5.2.2 Gas compositions

Table 5-3 illustrates the gas concentrations and weights from pyrolysis catalysis of five tyre oil model compounds. The results show the aliphatic model compounds are in favour of higher gaseous carbon conversion compared with aromatic model compounds, 31.74 vol. % and 25.75 vol. % of CH₄ were produced from hexadecane and decane, respectively; hexadecane and decane also produced high concentrations of C₂-C₄ which were 32.06 and 28.77 vol. %, respectively. Styrene produced much less hydrocarbons compared with aliphatic model compounds i.e. 7.75 vol. % of CH₄ and 5.92 vol. % of C₂-C₄. The polycyclic aromatic hydrocarbons (PAHs) produced low amounts of hydrocarbons, i.e. 1.87 and 1.94 vol. % of CH₄ were produced from naphthalene and phenanthrene, and 4.25 vol. % of C₂-C₄ were produced from

naphthalene. None of the C₂-C₄ hydrocarbons were found from phenanthrene. These results suggest that the molecular structures of the different model compounds influenced the gas composition produced from the pyrolysis-catalysis process. The straight chain aliphatic model compounds hexadecane and decane are easy to break down to lighter hydrocarbons corresponding with high gaseous carbon conversion rates that are 42.60 and 37.65%, respectively. The cyclic aromatic hydrocarbons favour hydrogen production instead of hydrocarbon gases and are also associated with very low gaseous carbon conversion rates, i.e. 6.59 % for styrene, 1.22 % for naphthalene and 0.17 % for phenanthrene.

Table 5-3 Gas concentrations and weights from pyrolysis catalysis of tyre oil model compounds

	aliphatic	aliphatic	ring	Polyaromatic	polyaromatic
10% Ni/Al ₂ O ₃	hexadecane C ₁₆ H ₃₄	decane C ₁₀ H ₂₂	styrene C ₈ H ₈	naphthalene C ₁₀ H ₈	phenanthrene C ₁₄ H ₁₀
Gas concentration (vol. %)					
H ₂	36.20	45.48	86.33	93.88	98.06
CH ₄	31.74	25.75	7.75	1.87	1.94
C ₂ -C ₄	32.06	28.77	5.92	4.25	0.00
Weight (mg per gram of tyre equivalent carbon)					
H ₂	21.13	26.51	38.82	8.86	11.48
CH ₄	147.43	119.46	27.74	1.40	1.81
C ₂ -C ₄	273.59	248.70	38.46	10.77	0.00

5.2.3 Conclusion

In summary, this work is focused on the dependence of the formation of filamentous carbon on the chemical structures of tyre pyrolysis oil model compounds, especially for multi-walled carbon nanotubes. The aliphatic model compounds (hexadecane and decane) favour gaseous hydrocarbons formation instead of solid carbon formation in the waste tyre pyrolysis-catalysis process. Aromatic compounds (styrene, naphthalene and phenanthrene) would dominate

the production of filamentous carbon compared to the aliphatic compounds (hexadecane and decane). However, the chemical structure of decane with shorter linear structure compared with hexadecane favours a higher quantity of filamentous carbon formation that is mostly multi-walled carbon nanotubes. The aromatic model compounds favour solid carbon formation where the majority of carbon formation is filamentous carbon. Comparing the sing ring aromatic model compound, the polyaromatic compounds produce more solid carbon nanofibers formation.

Reference

1. Kandasamy, J., **et al.**, *Pyrolysis, Combustion, and Steam Gasification of Various Types of Scrap Tires for Energy Recovery*. Energy & Fuels, 2015. **29**(1): p. 346-354.
2. Tamura, S., **et al.**, *Chemorheology of crosslinked polyisoprene/poly(butadiene co-styrene) blends*. Journal of Applied Polymer Science, 1987. **33**(5): p. 1663-1674.
3. Erdoğan, M., **et al.**, *Evolved gas analysis of pyrolysis products from some rubbers by mass spectrometry*. European Polymer Journal, 1991. **27**(4–5): p. 413-417.
4. Schwartz, N.V., **et al.**, *Observations on the thermogravimetric oxidation of carbon blacks in vulcanizates*. Thermochemica Acta, 1978. **26**(1–3): p. 349-359.
5. Evans, A.E.a.R., *The Composition of a Tyre: Typical Components*, 2006, The Waste & Resource Action Programme: Banbury.
6. Sulkowski, W.W.D., **et al.**, *Thermogravimetric study of rubber waste-polyurethane composites*. Journal of Thermal Analysis & Calorimetry, 2004. **Vol. 78** ,(Issue 3): p. p905.
7. Seidelt, S., **et al.**, *Description of tire pyrolysis by thermal degradation behaviour of main components*. Journal of Analytical and Applied Pyrolysis, 2006. **75**(1): p. 11-18.
8. Wu, C., **et al.**, *Processing Real-World Waste Plastics by Pyrolysis-Reforming for Hydrogen and High-Value Carbon Nanotubes*. Environmental Science & Technology, 2013. **48**(1): p. 819-826.
9. Wu, C., **et al.**, *Pyrolysis–gasification of post-consumer municipal solid plastic waste for hydrogen production*. International Journal of Hydrogen Energy, 2010. **35**(3): p. 949-957.
10. Sehested, J., *Four challenges for nickel steam-reforming catalysts*. Catalysis Today, 2006. **111**(1–2): p. 103-110.
11. Zhang, M., **et al.**, *Carbon nanotube in different shapes*. Materials today, 2009. **12**(6): p. 12-18.
12. Sears, K., **et al.**, *Recent developments in carbon nanotube membranes for water purification and gas separation*. Materials, 2010. **3**(1): p. 127-149.
13. S. Karthikeyan, P.M., *Carbon Nanotubes from Unconventional Resources: Part A: Entangled Multi-Walled Carbon Nanotubes and Part*

B: Vertically-Aligned Carbon Nanotubes, in *Syntheses and Applications of Carbon Nanotubes and Their Composites*, D.S. Suzuki, Editor 2013, InTec: Croatia.

14. Li, Q., et al., *Effect of hydrocarbons precursors on the formation of carbon nanotubes in chemical vapor deposition*. Carbon, 2004. **42**(4): p. 829-835.
15. Yang, Z., et al., *Coupled process of plastics pyrolysis and chemical vapor deposition for controllable synthesis of vertically aligned carbon nanotube arrays*. Applied Physics A: Materials Science & Processing, 2010. **100**(2): p. 533-540.
16. Zhang, Y., et al., *Carbon nanotubes and hydrogen production from the pyrolysis catalysis or catalytic-steam reforming of waste tyres*. Journal of Analytical and Applied Pyrolysis, 2016.
17. Kukovitskii, E.F., et al., *Carbon nanotubes of polyethylene*. Chemical Physics Letters, 1997. **266**(3–4): p. 323-328.
18. Zhang, Y., et al., *Pyrolysis–Catalytic Reforming/Gasification of Waste Tires for Production of Carbon Nanotubes and Hydrogen*. Energy & Fuels, 2015. **29**(5): p. 3328-3334.
19. Yang, R.-X., et al., *Effects of Nickel Species on Ni/Al₂O₃ Catalysts in Carbon Nanotube and Hydrogen Production by Waste Plastic Gasification: Bench- and Pilot-Scale Tests*. Energy & Fuels, 2015. **29**(12): p. 8178-8187.
20. Wu, C., et al., *Hydrogen Production from the Pyrolysis– Gasification of Polypropylene: Influence of Steam Flow Rate, Carrier Gas Flow Rate and Gasification Temperature*. Energy & Fuels, 2009. **23**(10): p. 5055-5061.
21. Zhang, Y., et al., *Pyrolysis-catalysis of waste plastic using a nickel-stainless steel mesh catalyst for high value carbon products*. Environmental Technology, 2017: p. 1-27.
22. Kumar, M., et al., *Chemical vapor deposition of carbon nanotubes: a review on growth mechanism and mass production*. Journal of nanoscience and nanotechnology, 2010. **10**(6): p. 3739-3758.
23. Morjan, R.E., et al., *Growth of carbon nanotubes from C₆₀*. Applied Physics A, 2004. **78**(3): p. 253-261.
24. Nerushev, O.A., et al., *Particle size dependence and model for iron-catalyzed growth of carbon nanotubes by thermal chemical vapor deposition*. Journal of Applied Physics, 2003. **93**(7): p. 4185-4190.

25. Chung, Y.-H., **et al.**, *Carbon nanotubes from catalytic pyrolysis of polypropylene*. *Materials chemistry and physics*, 2005. **92**(1): p. 256-259.
26. Mori, S., **et al.**, *Non-Catalytic, Low-Temperature Synthesis of Carbon Nanofibers by Plasma-Enhanced Chemical Vapor Deposition*. *Nanofibers*. 2010.
27. Yoon, S.-H., **et al.**, *A conceptual model for the structure of catalytically grown carbon nano-fibers*. *Carbon*, 2005. **43**(9): p. 1828-1838.
28. Rodriguez, N.M., **et al.**, *Catalytic engineering of carbon nanostructures*. *Langmuir*, 1995. **11**(10): p. 3862-3866.
29. Oberlin, A., **et al.**, *Filamentous growth of carbon through benzene decomposition*. *Journal of crystal growth*, 1976. **32**(3): p. 335-349.
30. Yang, R.T., **et al.**, *Mechanism of carbon filament growth on metal catalysts*. *Journal of Catalysis*, 1989. **115**(1): p. 52-64.
31. De Jong, K.P., **et al.**, *Carbon Nanofibers: Catalytic Synthesis and Applications*. *Catalysis Reviews*, 2000. **42**(4): p. 481-510.
32. Snoeck, J.-W., **et al.**, *Filamentous carbon formation and gasification: thermodynamics, driving force, nucleation, and steady-state growth*. *Journal of Catalysis*, 1997. **169**(1): p. 240-249.
33. Tracz, E., **et al.**, *High-resolution electron microscopy study of the carbon deposit morphology on nickel catalysts*. *Applied catalysis*, 1990. **66**(1): p. 133-147.
34. Somani, P.R., **et al.**, *Importance of transmission electron microscopy for carbon nanomaterials research*. *Modern Research and Educational Topics in Microscopy*, 2007. **3**: p. 634-42.
35. DiLeo, R.A., **et al.**, *Purity assessment of multiwalled carbon nanotubes by Raman spectroscopy*. *Journal of Applied Physics*, 2007. **101**(6): p. 064307.
36. Dresselhaus, M.S., **et al.**, *Raman spectroscopy on isolated single wall carbon nanotubes*. *Carbon*, 2002. **40**(12): p. 2043-2061.
37. Wu, C., **et al.**, *Renewable hydrogen and carbon nanotubes from biodiesel waste glycerol*. *Scientific Reports*, 2013. **3**: p. 2742.
38. Wu, C., **et al.**, *Sustainable processing of waste plastics to produce high yield hydrogen-rich synthesis gas and high quality carbon nanotubes*. *RSC Advances*, 2012. **2**(10): p. 4045-4047.

Chapter 6. Pyrolysis-catalysis/catalytic reforming of plastics for hydrogen and carbon nanotubes production

In previous chapters the research focused on hydrogen and carbon nanotubes production from waste tyres. In this chapter, plastics have been investigated for hydrogen and carbon nanotube production either by pyrolysis-catalysis or pyrolysis-catalytic reforming. The nickel loading on a stainless steel mesh catalyst has firstly been introduced in the pyrolysis-catalysis of HDPE for carbon nanotube and by-product hydrogen production. A simulated mixture of waste plastics and seven real world waste plastics were further investigated in the pyrolysis-catalytic reforming process mainly for hydrogen production along with the production of value added filamentous carbon especially carbon nanotubes. Bimetallic catalysts with different Fe:Ni ratios supported by mesoporous MCM-41 have been introduced in the waste plastics pyrolysis-catalytic reforming process and the influence of Fe:Ni ratio investigated.

6.1 Investigation of carbon nanotubes production from high density polypropylene (HDPE) with nickel loading on a stainless steel (NiSS) catalyst

In this section, multi-walled carbon nanotubes (MWCNTs) have been produced from waste highdensity polyethylene (HDPE) using a two-stage pyrolysis-catalysisprocessdiscussed in chapter 3. The catalyst was a stainless steel mesh loaded with nickel. The catalysis temperature and plastic to catalyst ratio were investigated to determine the influence on carbon nanotube production. The HDPE sample was placed in the first stage pyrolysis reactor and pyrolysed at a heating rate of $40\text{ }^{\circ}\text{C min}^{-1}$ to a final pyrolysis temperature of $500\text{ }^{\circ}\text{C}$. The second stage catalytic reactor was pre-heated to $800\text{ }^{\circ}\text{C}$ and contained the nickel loaded stainless steel mesh catalyst. To investigate the influence of catalyst temperatures, temperatures of 700 , 800 and $900\text{ }^{\circ}\text{C}$ were chosen where the plastic to catalyst ratio was 2:1. In addition, a plastic to catalyst ratio of 4:1 was investigated at a temperature of $900\text{ }^{\circ}\text{C}$. The sample to catalyst ratio

at 2:1 is 2 grams of plastics sample with 1 g of NiSS catalyst; the sample to catalyst ratio at 4:1 is 4 g of plastic sample with 1 g of NiSS catalyst.

6.1.1 Catalyst characterisation

The freshly prepared nickel-loaded stainless steel catalyst was examined using scanning electron microscopy and the results are shown in Figure 6-1.

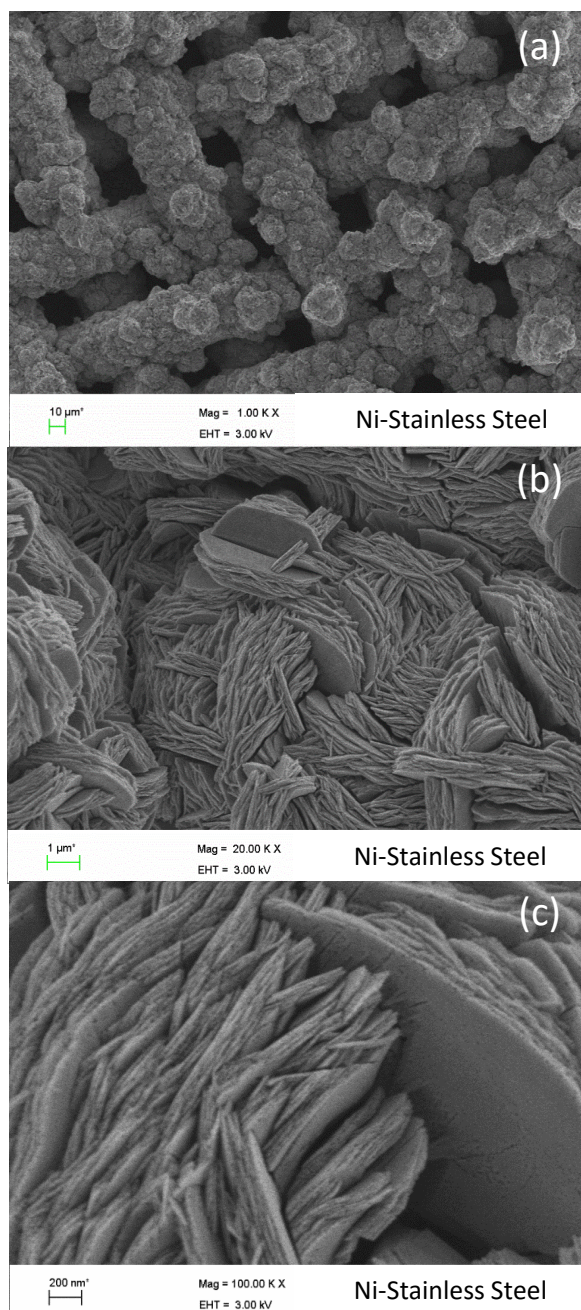


Figure 6-1 Scanning electron micrograph of the prepared nickel-loaded stainless steel mesh catalyst.

Figure 6-1(a) shows the low magnification image of the catalyst where the interlocking grid wires of the stainless steel mesh can be clearly seen. Figure 6-1(b) and (c) show higher magnification micrograms of the wire mesh surface showing a crystalline structure. Figure 6-2 shows an X-ray diffraction pattern of the freshly prepared nickel-loaded stainless steel catalyst indicating the presence of NiO, NiO/FeNi, FeNi and NiO peaks. During the pyrolysis of high density polyethylene, reducing gases including hydrogen and carbon monoxide are produced which serve to reduce the catalyst and produce nickel and nickel-iron phases.

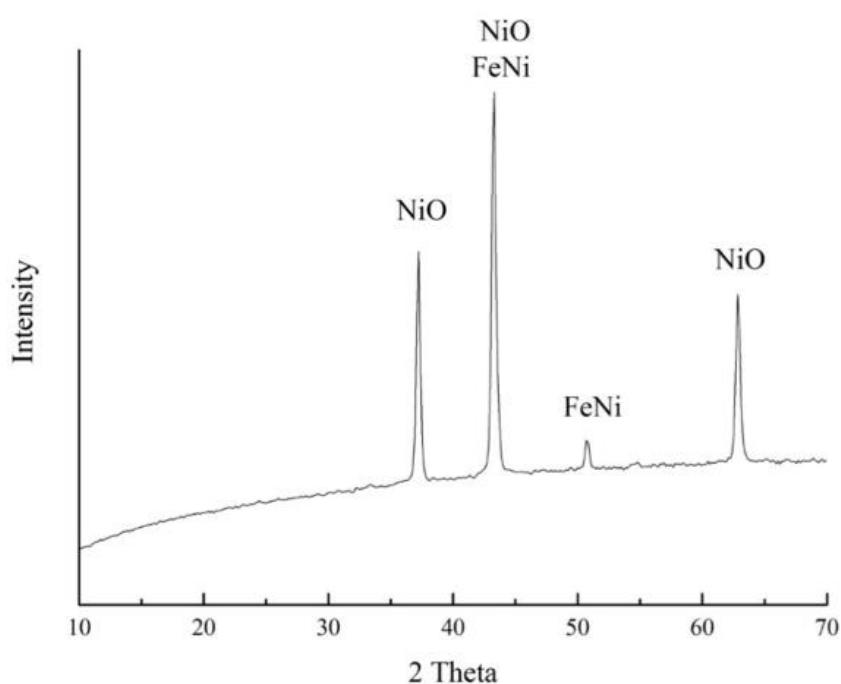


Figure 6-2 X-ray diffraction analysis of the prepared nickel-loaded stainless steel mesh catalyst

6.1.2 Product yield

Table 6-1 shows the product yield and gas composition for the pyrolysis-catalysis of high density polyethylene (HDPE) in the presence of the nickel-stainless steel catalyst in relation to catalyst temperature and also plastic to catalyst ratio. The results show that there was little influence of catalyst temperature on the yield of gas at each plastic to catalyst ratio, however, the liquid product yield showed a significant reduction from 17.00 wt.% at 700 °C to

10.50 wt.% at 900 °C catalyst temperature. Importantly, the carbon deposited on the nickel loaded stainless steel mesh catalyst showed an increase in yield from 32.50 wt.% to 38.00 wt.%.

Table 6-1 Mass balance and gas concentrations for the pyrolysis-catalysis of high density polyethylene (HDPE) in relation to catalyst temperature and different plastic to catalyst ratio.

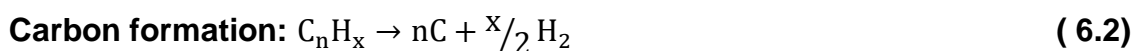
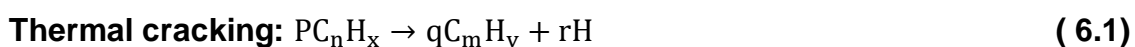
HDPE weight (g)	2	2	2	4
Temperature (°C)	700	800	900	900
Sample to catalyst ratio	2:1	2:1	2:1	4:1
Gas yield (wt. %)	50.44	51.99	51.13	62.62
Liquid yield (wt. %)	17.00	14.00	10.50	9.75
Residue yield (wt. %)	0.50	0.50	0.50	0.50
Carbon yield (wt. %)	32.50	34.00	38.00	25.75
Mass balance (wt. %)	100.44	100.49	100.13	98.87
Gas concentration (Vol. %)				
CO	0.78	1.82	3.02	2.23
H ₂	50.51	44.95	51.03	35.59
O ₂	0.28	0.43	0.62	0.85
CO ₂	0.26	0.33	0.33	0.21
CH ₄	21.48	32.57	32.08	37.99
C ₂ -C ₄	26.69	19.90	12.92	23.13

The residue yield in Table 6-1 refers to the mass of pyrolysis char in the pyrolysis reactor after the experiments, which was negligible at ~0.5 wt.%. Table 6-1 also shows the influence of increasing the plastic to catalyst ratio from 2:1 to 4:1 at a nickel-stainless steel mesh catalyst temperature of 900 °C. The results show that increasing the plastic to catalyst ratio increased the gas yield from ~51 wt.% to 62.62 wt.%, while the carbon deposition reduced from 38.00 to

25.75 wt.%. The liquid yield was largely unaffected by change in plastic to catalyst ratio.

Table 6-1 also shows the composition of the product gases in relation to the nickel-stainless steel mesh catalyst temperature and plastic to catalyst ratio. The main gases produced during the pyrolysis-catalysis of the HDPE were hydrogen, carbon monoxide, methane and C₂ – C₄ hydrocarbons. The gas product therefore has a significant calorific value which could be used as process fuel for the system. The increase of catalysis temperature from 700 to 900 °C increased the concentration of CO concentration from 0.78 to 3.02 Vol. and the concentration of hydrogen was the highest at 51.03 vol. %, when the catalyst temperature was at 900 °C.

The concentration of hydrocarbon gases (C₂-C₄) decreased from 26.69 to 12.92 wt. % as the catalysis temperature was increased from 700 to 900 °C. The decomposition of plastics to form gas products and solid carbon were described as the following reactions [1]:



During the pyrolysis-catalysis of plastics, the polyalkene plastic was initially degraded into smaller organic compounds, then these compounds were dehydrogenated to produce carbon products and gaseous products [2]. The product oils and gases which are generated from the pyrolysis of the HDPE and which pass over the stainless steel mesh catalyst have been analysed before and shown to be largely aliphatic in composition[3-5]. The gases produced are mainly methane, ethane, propane, propene, butane and butene, with lower concentrations of hydrogen and carbon monoxide [4].

Depending on the plastic pyrolysis conditions and the condensation temperature and system design, the product oil can be an oil or wax-like product. The wax when analysed by high temperature gas chromatography was formed to consist of alkane, alkene and alkadiene hydrocarbons in the range up to C₆₀ and the oils typically have a hydrocarbon range up to C₄₀ with a peak at C₂₀[5]. However, much higher molecular weight hydrocarbons can be detected

using size exclusion chromatography [3, 4]. Therefore, the thermal degradation of the HDPE via a random scission mechanism [5] might be expected to produce a wide range of aliphatic hydrocarbon gases, oils and waxes and polymer fragments from light gases up to heavy molecular weight species which then pass over the stainless steel mesh catalyst, cracking the pyrolysis gases and also depositing carbon nanotubes.

It is suggested that a higher reforming temperature promoted the secondary reactions in the polypropylene pyrolysis-catalysis process resulting in the enhancement of hydrogen and CO production [5, 6]. When the sample to catalyst ratio was increased from 2:1 to 4:1 at 900 °C catalyst temperature, H₂ concentration decreased from 51.03 to 35.59 vol.%, CO concentration decreased from 3.02 to 2.23 vol. % and hydrocarbon gases concentration increased from 12.92 to 23.13 vol.%.

6.1.3 Carbon production and characterization

The carbon deposited on the nickel loaded catalyst was collected by shaking the reacted NiSS catalyst which separated the carbon from the mesh. The collected carbon was characterised by several techniques. Thermogravimetric analysis (TGA) using temperature programmed oxidation (TPO) of the collected carbon deposits was carried out and the results are shown Figure 6-3. TGA-TPO characterisation enables the oxidation of the carbon in an air atmosphere in relation to a temperature controlled fixed heating rate. The different type of carbon deposit oxidise at different temperatures, for example disordered/amorphous carbon oxidise at lower temperatures than graphitic, filamentous type carbons[7] .

It was assumed the weight loss which occurred after 600 °C oxidation temperature was assigned as filamentous carbon, the weight loss that occurred before 600 °C was assigned as the oxidation of amorphous type carbon[6, 8, 9]. Based on the differentiation of the two types of carbon deposited on the nickel-stainless steel mesh catalysts using the data from Figure 6-3, the mass of filamentous and amorphous carbons were calculated by the weight loss from TPO results, which are shown in Figure 6-4. The weight of filamentous carbon

increased from 316.35 mg g⁻¹ plastic at 700 °C catalyst temperature to 374.06 mg g⁻¹ at 900 °C catalyst temperature. It is suggested that more heavy hydrocarbons were decomposed into light hydrocarbons when the catalysis temperature was increased; these produced light hydrocarbons that are suggested to provide more carbon sources for the formation of filamentous carbons. It is consistent with the changes of C₂-C₄ gaseous production shown in Table 6-1, when the catalysis temperature was increased from 700 to 900 °C, C₂-C₄ hydrocarbon concentrations decreased from 26.69 to 12.92 vol.%. Li et al.[10] reported that an increase of temperature from 600 to 900 °C promoted the production of CNTs.

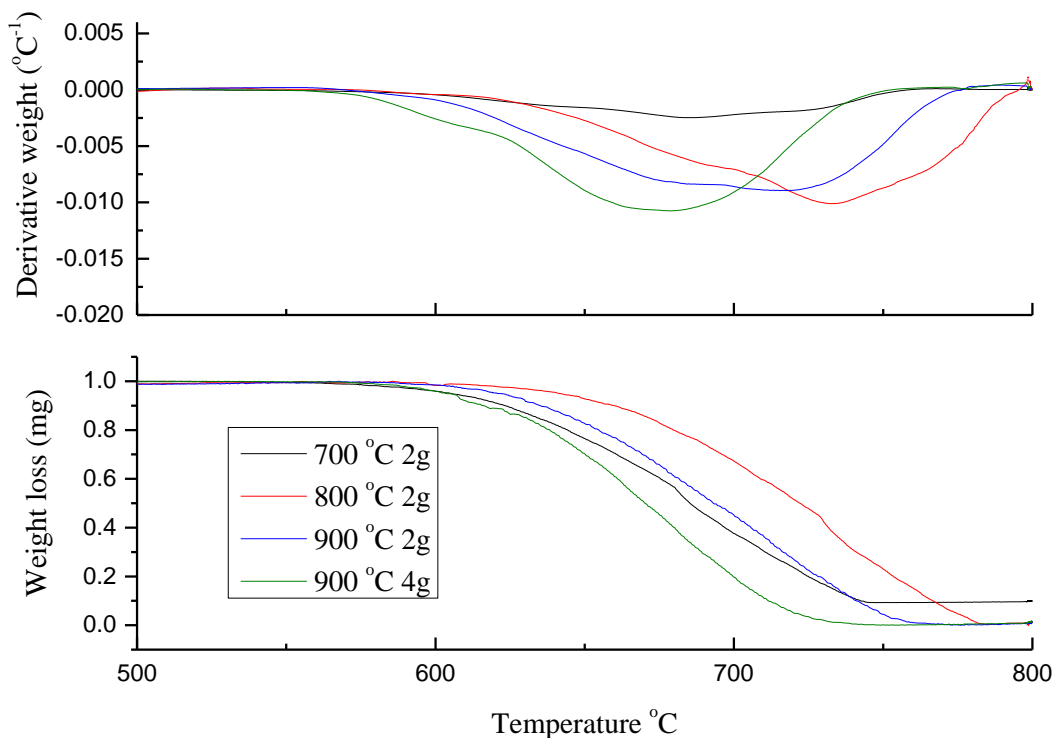


Figure 6-3 TGA-TPO and DTG-TPO results of the deposited carbon in relation to catalyst temperatures and different plastic to catalyst ratios.

Fang et al. [11] reported that the oxidation peak of filamentous carbons with smaller diameters occurred at lower temperatures during TGA-TPO analysis compared with oxidation of filamentous carbons with larger diameters which

occurred at higher oxidation temperatures. In addition, Li et al. [12] differentiated between the TGA-TPO characterisation of single walled carbon nanotubes and multi-walled carbon nanotubes, where the single-walled CNTs were oxidised at lower oxidation temperatures compared to multi-walled CNTs which oxidised at higher temperatures. They suggested that the oxidation of MWCNTs occurred at higher temperature because of strong interaction between graphite layers in the MWCNTs, which stabilised the structure of MWCNTs indicating higher thermal stability compared with single-wall CNTs. Consequently, the TGA-TPO data might indicate that the carbon oxidation at higher temperature corresponds to filamentous carbons, including multi-walled carbon nanotubes.

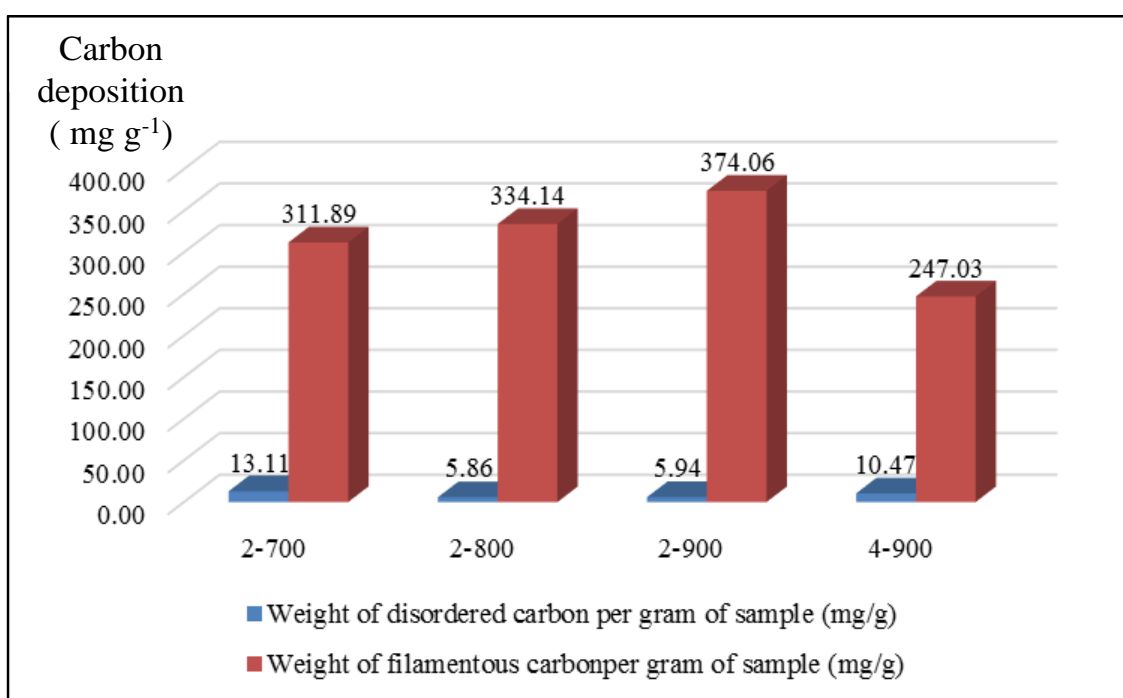


Figure 6-4 Proportions of disordered carbon and filamentous carbon produced from HDPE by pyrolysis-catalysis with the nickel-stainless steel mesh catalyst (The X-axis indicates the reaction temperature and amount of feedstock, for example 2-700 indicates the feedstock amount is 2 g and reaction temperature was 700 °C).

Increasing the plastic to catalyst ratio from 2:1 to 4:1 resulted in a decrease in filamentous carbon deposition from 374.06 to 247.03 mg g⁻¹ plastic. Li et al.[10, 12] reported that an increased sample to catalyst ratio enhanced the carbon

dissolving rate into the metal particles of the catalyst compared with the rates of carbon diffusing and precipitating, thus the formation of filamentous carbons were prohibited [10].

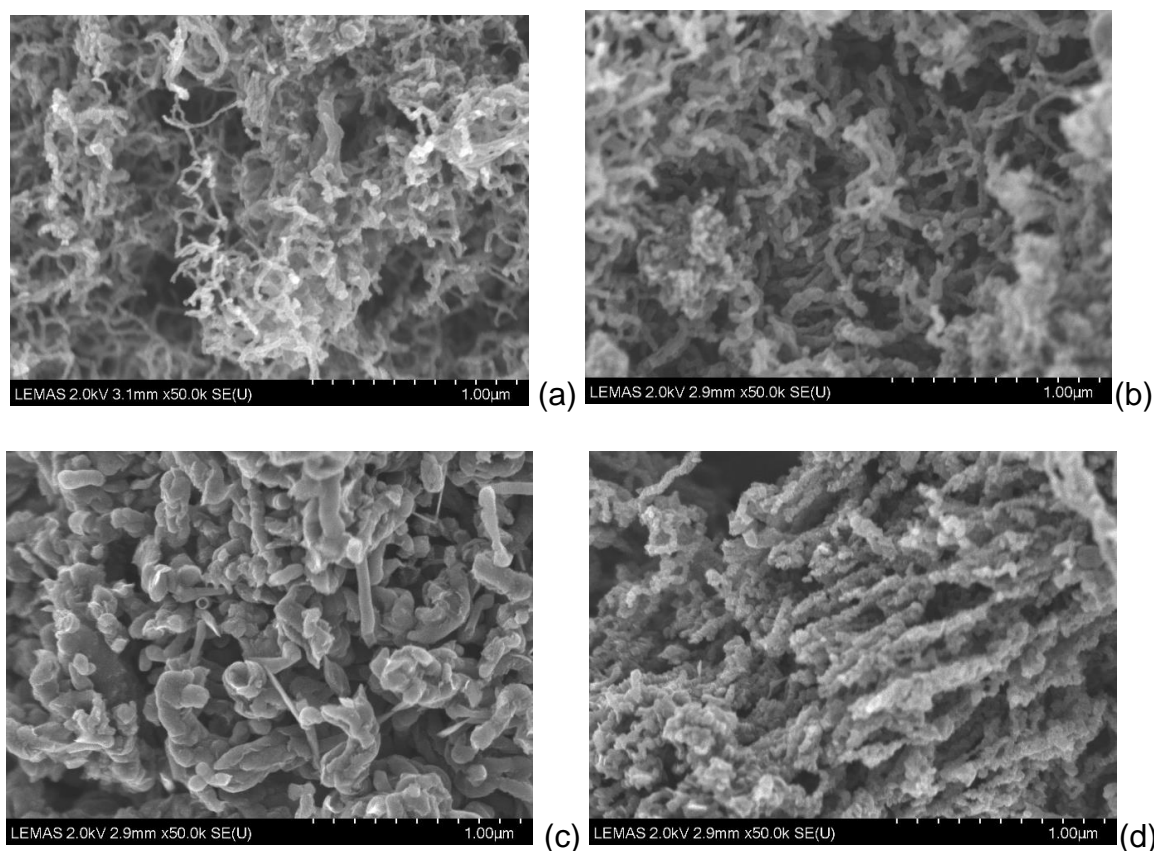


Figure 6-5 SEM results of different amounts of HDPE at different temperatures (a) 700 °C with 2g; (b) 800 °C with 2g; (c) 900 °C with 2g; (d) 900 °C with 4g.

Figure 6-5(a), (b) and (c) shows the SEM micrographs of the carbons formed on the reacted nickel-stainless steel mesh catalyst. It is clear that the diameters of filamentous carbons formed at the catalysis temperature at 700 °C are smaller than the filamentous carbons formed at higher catalyst temperature when the sample to catalyst ratio was 2:1. Figure 6-6(a) and (b) (TEM analysis) confirm the presence of MWCNTs as the type of carbon deposited on the nickel-stainless steel mesh catalyst. The carbon nanotubes were typically 10 – 20 nm diameter and more than 1 μm in length. Kumar and Ando [13] reported an increase of diameters of CNTs with the increase of reaction temperature with a chemical vapour deposition process using pure hydrocarbon as feedstock.

However, Gong et al. [14] pointed out the mechanism of CNTs growth from polyalkene plastics is different from using pure hydrocarbon gas, because of complicated products which are produced from such polymers including gas, liquid and semi-liquid products. The authors proposed that there were synergistic reactions between light hydrocarbons and aromatic compounds.

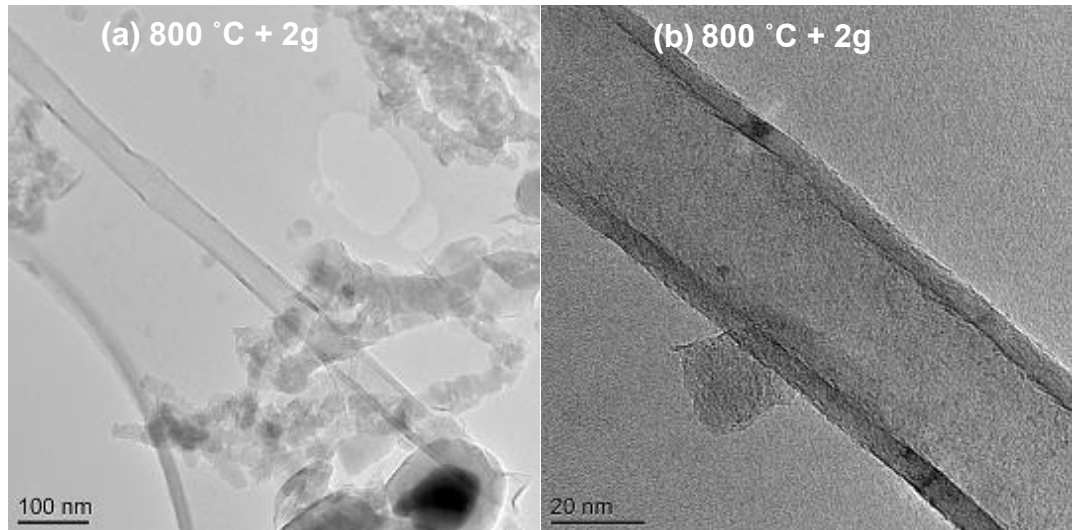


Figure 6-6 TEM results of the selected catalyst tested at 800 °C

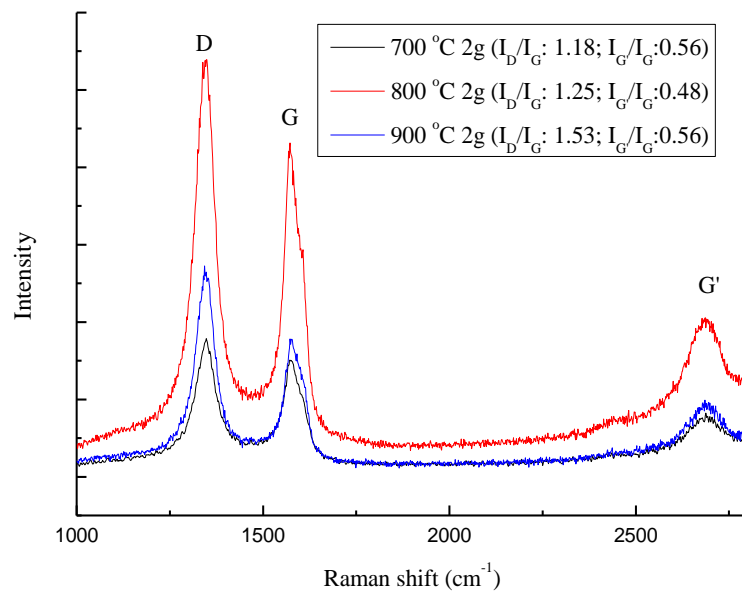


Figure 6-7 Raman analyses of carbon deposited on the wire mesh catalyst for the pyrolysis-catalysis of waste high density polyethylene in relation to temperature

Raman spectroscopy is one of the powerful techniques to characterize the structures of carbon materials, including the amorphous and/or graphitic carbons [11, 15-18]. As shown in Figure 6-7, the Raman spectra in the wavelength range of 1000 to 2750 cm^{-1} are presented to compare the CNTs produced at different catalysis temperature when the sample to catalyst ratio was 2:1. The D band centred at 1300 cm^{-1} indicates an amorphous or disordered carbon structure. The G band centred at 1550 cm^{-1} indicates filamentous or ordered carbons that correspond to the tangential vibrations of the graphite carbons. The G' band in the Raman shift at a wavelength around 2700 cm^{-1} indicates the purity of CNTs as coupling the two photon elastic scattering process [15, 19]. The graphitization of carbon production can be evaluated by the I_D/I_G ratio that is the intensity of the D band nominalized to the G band. The I_D/I_G ratios of the carbons produced at different catalysis temperatures are displayed in Figure 6-7 and are 1.18, 1.25 and 1.53 for the carbons produced at catalysis temperatures of 700, 800 and 900 °C respectively. The results show the graphitization of CNTs production produced from HDPE by pyrolysis-catalysis with the nickel-stainless steel mesh catalysts are close to those of commercial MWCNTs which is between 0.63-1.5 [20].

The $I_{G'}/I_G$ ratio indicates the purity of CNTs production, as the G' band in Raman shift mainly appears on ordered carbon which indicates defects in the graphitic crystallinity of the carbon [15, 17]. Dileo et al. [17] assessed the purity of MWCNTs synthesised by chemical vapour deposition method at different conditions with Raman Spectroscopy. They reported that the intensity of the G' band was increased when the mass fraction of MWCNTs was reduced. When a catalysis temperature of 800 °C was used for CNTs production, the $I_{G'}/I_G$ ratio was the lowest at 0.48 indicating the carbons have the highest purity of CNTs compared with the carbons produced at 700 and 900 °C.

Overall, this work has shown that large yields of graphitic, long, carbon nanotubes can be produced from the two-stage pyrolysis-catalysis of high density polyethylene. Around half of the filamentous carbon produced was carbon nanotubes based on the 24 different sites of TEM images in Figure 6-8. The carbon nanotubes have relatively small diameters (10 – 20 nm) and are

several microns in length. The use of the nickel-loaded stainless steel mesh enables the carbon nanotubes deposition on the catalyst during the reaction to be easily physically removed from the mesh more easily, which aids catalyst re-use and carbon nanotube utilisation.

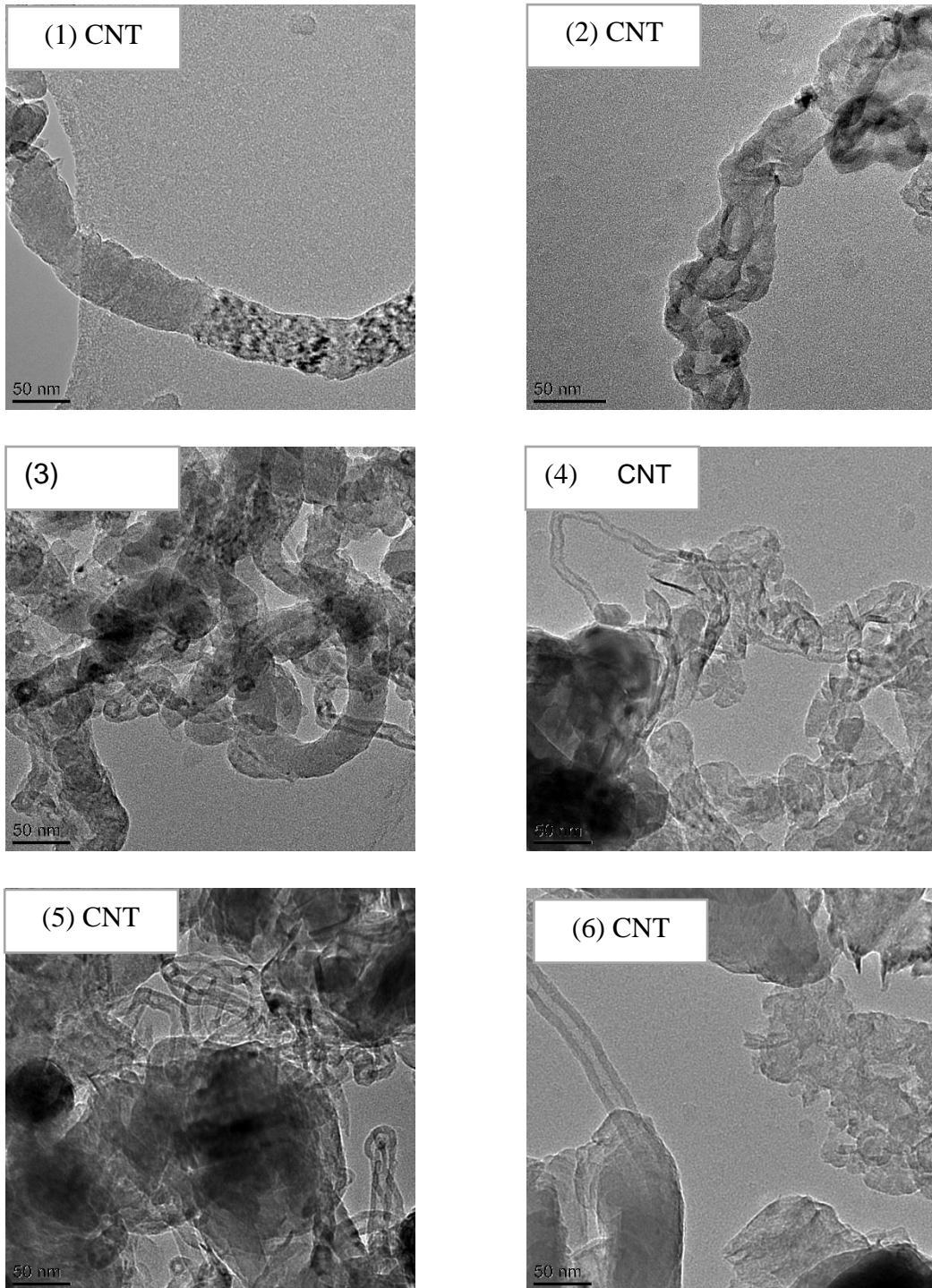


Figure 6-8 Carbon nanotubes amount estimation by TEM images

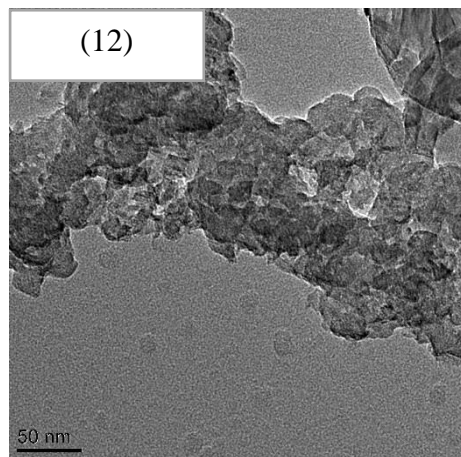
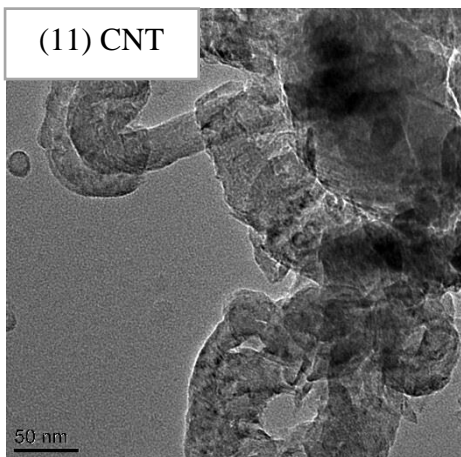
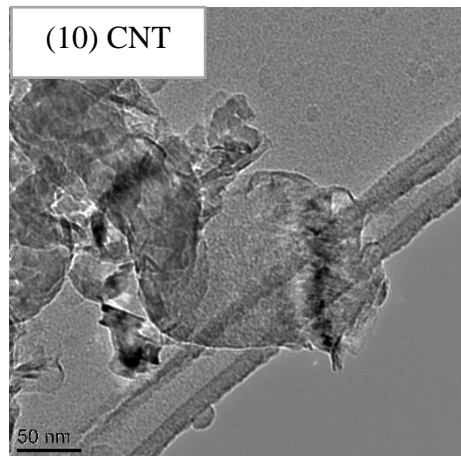
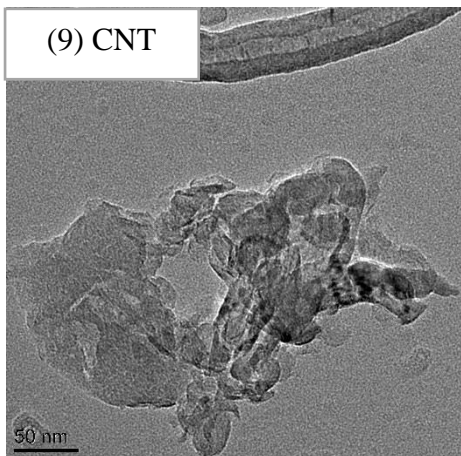
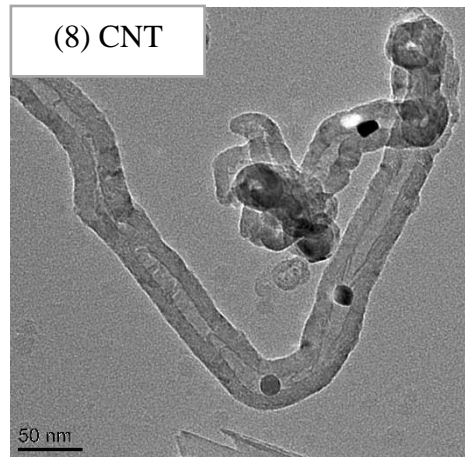
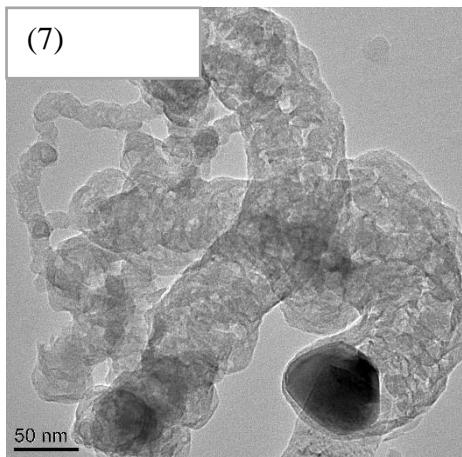


Figure 6-8 Carbon nanotubes amount estimation by TEM images

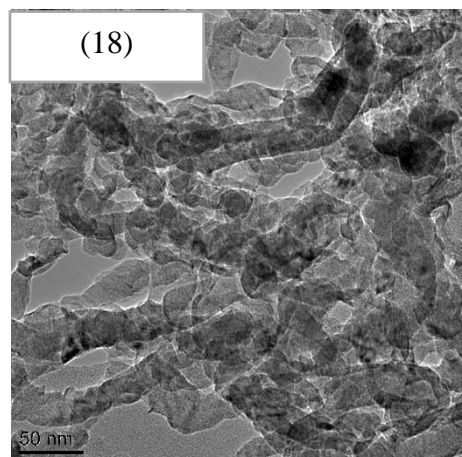
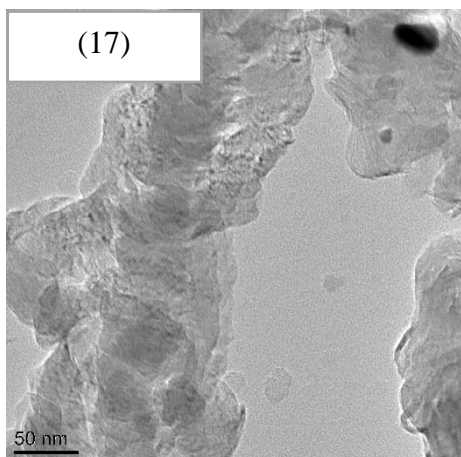
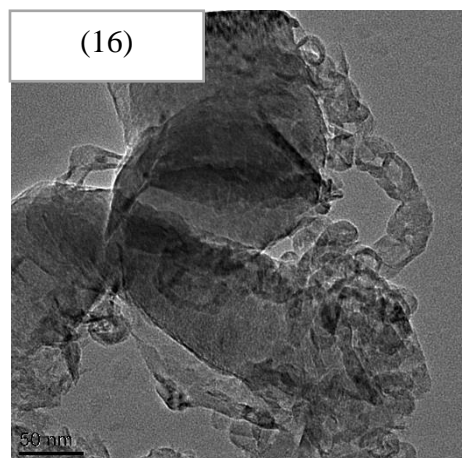
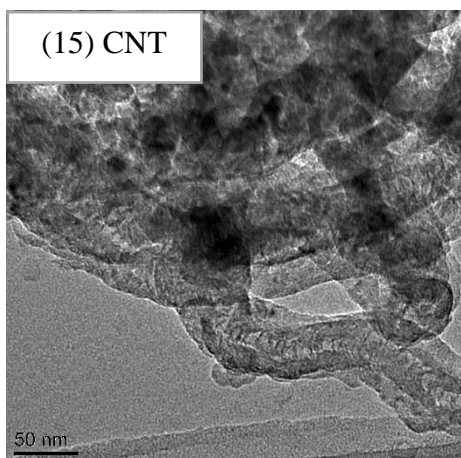
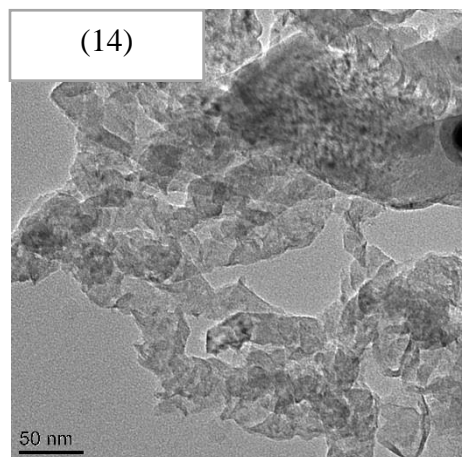
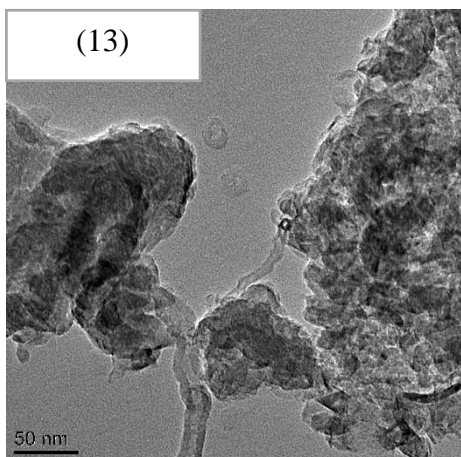


Figure 6-8 Carbon nanotubes amount estimation by TEM images

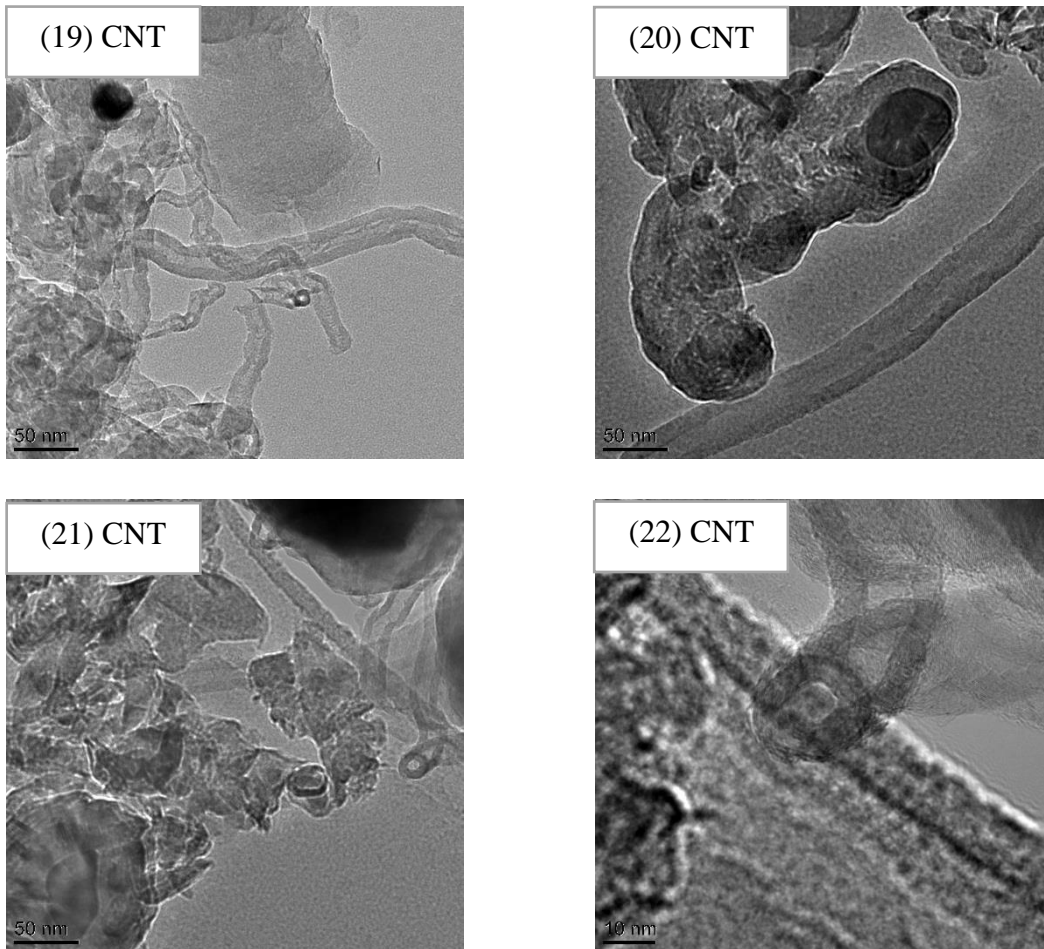


Figure 6-8 Carbon nanotubes amount estimation by TEM images

6.1.4 Conclusion

In this section, different catalysis temperatures (700, 800 and 900 °C), and different sample to catalyst ratios (2:1 and 4:1) were investigated for the pyrolysis-catalysis of high density polyethylene for the production of carbon nanotubes. The catalyst consisted of a stainless steel mesh which had been loaded with nickel to produce a nickel-stainless steel catalyst. Carbon was deposited during the process of pyrolysis-catalysis of the high density polyethylene. The influence of catalyst temperature was to produce increasing deposits of carbon on the mesh catalyst from 32.5 wt.% at 700 °C catalyst temperature to 38.0 wt.% at 900 °C. Using a higher plastic to catalyst feed ratio resulted in a reduction in catalyst carbon deposition. The carbon was easily

removable from the stainless steel mesh catalyst and were characterised by a number of techniques. Electron microscopy (SEM and TEM) examination of the carbon revealed that the carbon consisted of mainly filamentous carbons, which were mostly multi-walled carbon nanotubes. Raman spectroscopy showed that the quality of the carbon nanotubes was influenced by process conditions. Optimal conditions for the production of high yields of high carbon nanotubes was 800 °C nickel-stainless steel mesh catalyst temperature and plastic to catalyst ratio of 1:2, where yields were more than 0.3 g filamentous/carbon nanotubes type carbons for each gram of plastic feedstock.

6.2 Hydrogen and carbon nanotubes productions from waste plastics waste with Fe/Ni/MCM41 catalysts by pyrolysis-catalytic reforming

In this section, iron and nickel bimetallic catalysts have been investigated using the two-stage fixed-bed reactor detailed in Chapter 3, to determine how the Fe to Ni ratios on MCM-41 supported catalysts would affect hydrogen production from simulated mixed waste plastics (SMWP) by the two-stage pyrolysis-catalytic reforming process. The novelty of this work in this section is using mesoporous MCM-41 as catalysts support and the most popular catalyst metals iron and nickel alloy were introduced in the work to produce hydrogen from SMWP via pyrolysis-catalytic reforming process. The pyrolysis temperature was 500 °C at 40 °C min⁻¹ heating rate and catalytic reforming was at 800 °C. Sample to catalyst ratio 4:1 was applied in this section of research. Steam was introduced into the process by controlling the water injection rate at 2ml h⁻¹ at the inlet of reforming stage. Different Fe:Ni ratios (00:20, 05:15, 10:10, 05:15, 20:00) have been investigated in the process, to identify the catalyst which produced the highest hydrogen production.

6.2.1 Characterisation of fresh catalysts

The properties of the fresh catalysts were determined to characterise the effects of iron addition into the nickel based MCM-41 supported catalysts. The fresh

catalysts were characterized by a series of techniques; X-Ray diffraction (XRD) of the fresh catalysts was undertaken to confirm the metal phase structures and the surface area, total pore volumes and average pore radius were calculated based on BET nitrogen adsorption. The surface morphology of fresh catalysts was observed by scanning electron microscopy (SEM).

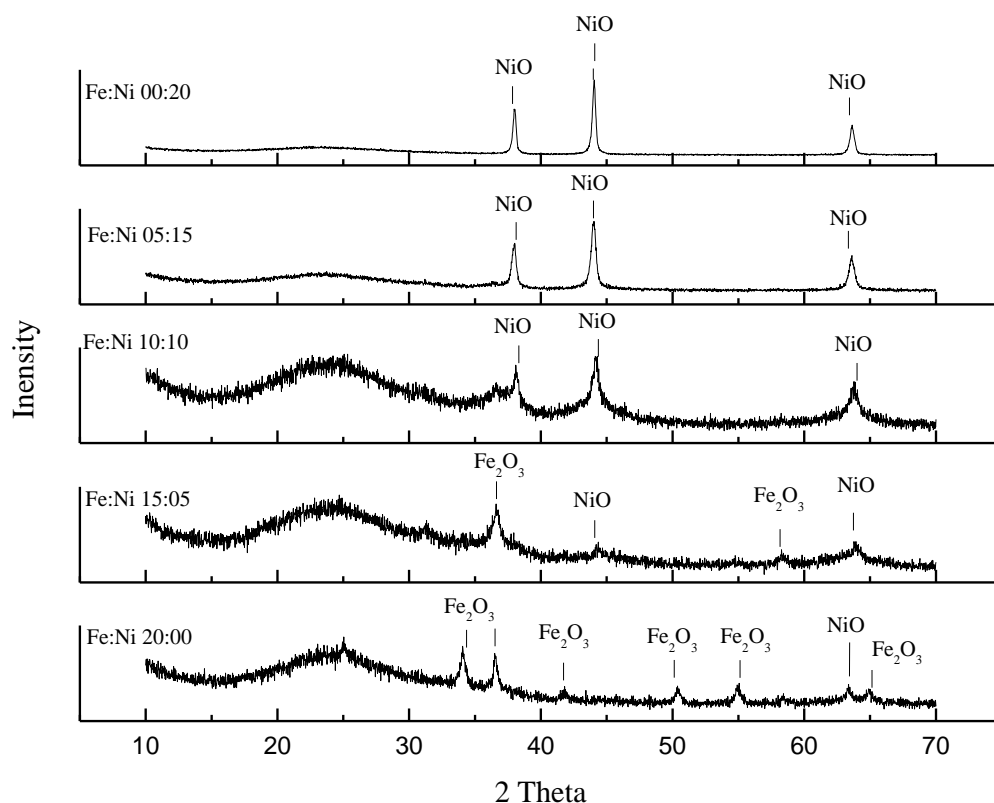


Figure 6-9 XRD analysis of fresh Fe/Ni/MCM-41 catalysts with different Fe:Ni ratios (00:20, 05:15, 10:10, 15:05, 20:00)

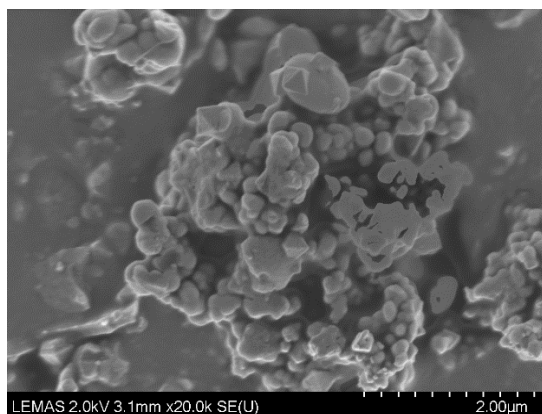
Figure 6-9 shows the XRD spectra of the fresh catalysts. As would be expected, the NiO phase was only observed for the fresh (00:20) Fe/Ni/MCM-41 catalyst, i.e. where no elemental Fe was present and the Fe₂O₃ phase was only observed for (20:00) Fe/Ni/MCM-41 catalyst, i.e. where no elemental Ni was present. However, when the bi-metallic catalysts were analysed, both NiO and Fe₂O₃ phases were observed for the fresh (05:15, 10:10, 15:05) Fe/Ni/MCM-41 catalysts. In Figure 6-9, it can be seen that the signal intensity of the NiO phases decreased and the intensity of the Fe₂O₃ phases increased

corresponding to the Fe:Ni ratio. The catalyst with only Fe loading, showed that the presence of more Fe₂O₃ phases were observed in the XRD spectra. Figure 6-9 shows that the metals in the Fe/Ni/MCM41 catalysts were oxides which will become reduced to the Ni and Fe metal by the reducing gases produced from the pyrolysis-catalytic reforming process, such as H₂ and CO [21]. The broad signal between 20° to 30° shown in Figure 6-9 is caused by the amorphous silica structure of the MCM-41. Figure 6-11 shows that the metals in the Fe/Ni/MCM-41 catalysts were oxides which will become reduced to the Ni and Fe metal by the reducing gases produced from the pyrolysis-catalytic reforming process, such as H₂ and CO [21].

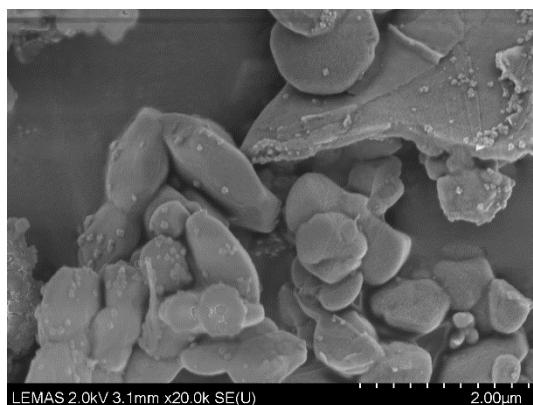
Table 6-2 BET surface area, pore volume and average pore radius of Fe/Ni/MCM-41 catalysts with different Fe:Ni ratios (00:20, 05:15, 10:10, 15:05, 20:00).

Fe:Ni (wt.%)	Surface area (m ² g ⁻¹)	Total pore volume (cm ³ g ⁻¹)	Average pore radius (nm)
00:20	826.29	6.42	1.55
05:15	776.86	6.01	1.55
10:10	801.90	6.31	1.57
15:05	781.23	6.28	1.61
20:00	799.71	6.29	1.57

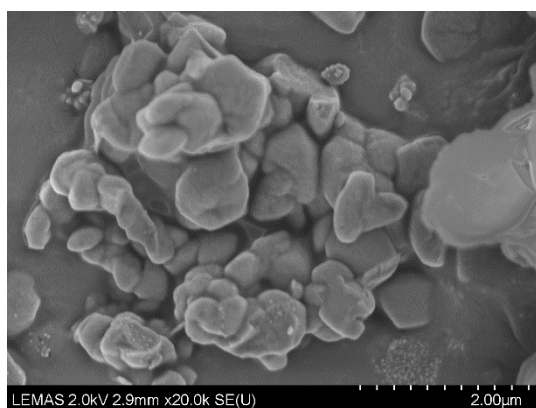
The surface area, total pore volumes and average pore radius were determined by N₂ adsorption and desorption isotherms. Table 6-2 shows that the catalysts all had a surface area of ~800 m² g⁻¹. There appeared to be no significant effects of the amount of iron addition to the catalyst in terms of surface area, pore volume or pore radius of the catalysts. This could be because the pore blockage caused by the metal iron and nickel oxides were at a similar level since the total metal loadings for each Fe:Ni ratio were maintained at 20 wt.% for each catalyst. The morphology of the fresh Fe/Ni/MCM-41 catalysts with different Fe to Ni ratios were determined by SEM and representative micrographs are shown in Figure 6-10. The fresh catalyst particles exhibited a fairly uniform particle size of between 0.5 μm – 1 μm.



(a)



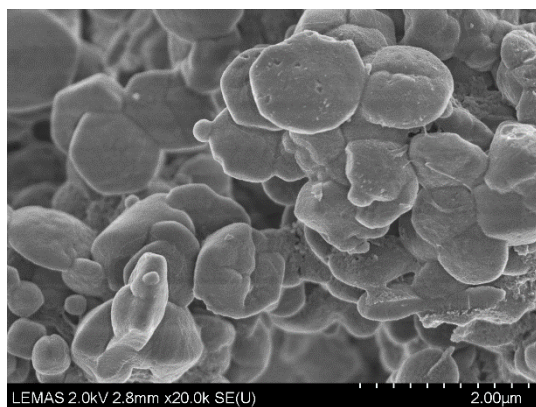
(b)



(c)



(d)



(e)

Figure 6-10 SEM fresh Fe/Ni/MCM-41 catalysts with different Fe:Ni ratios include (a) 00:20, (b) 05:15, (c) 10:10, (d) 15:05, (e) 20:00.

6.2.2 The effect of Fe:Ni ratio on gaseous products

The MCM-41 supported catalysts with different Fe:Ni ratios were used in the pyrolysis-catalytic reforming process with the simulated mixed waste plastics (SMWP) in terms of determining the influence of Fe:Ni ratio on hydrogen production.

Figure 6-11 shows the XRD spectra for the used Fe/Ni/MCM-41 catalysts after the pyrolysis-catalytic steam reforming process of the waste plastics mixture. The results confirm that the catalysts were reduced from the metal oxides to the elemental metal within the initial stages of the process by the product H₂ and CO produced during the process [21].

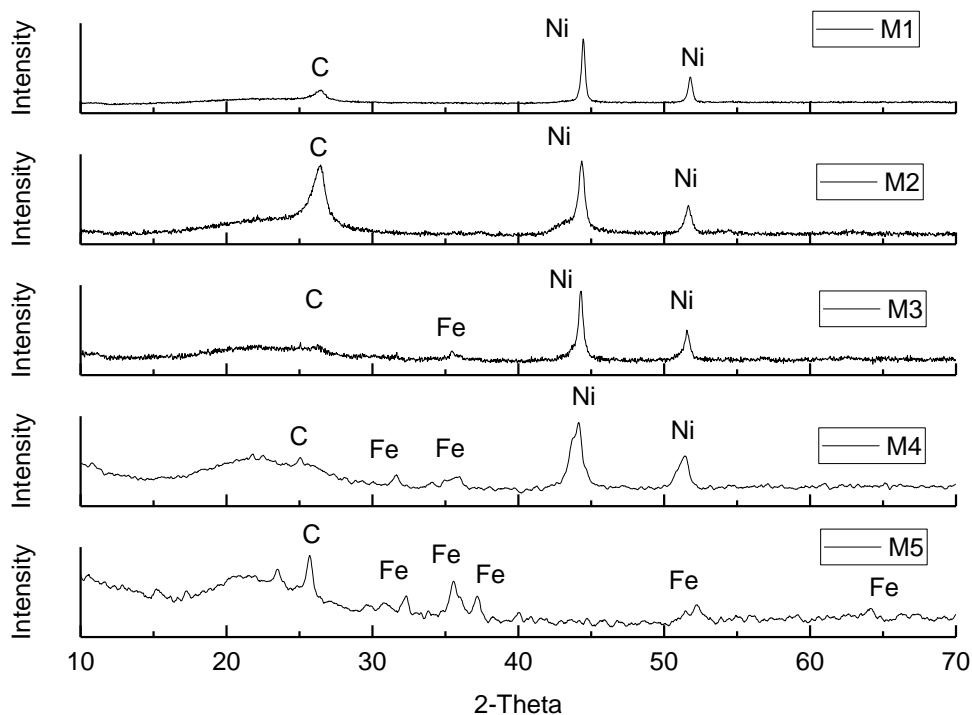


Figure 6-11 XRD analysis of the used Fe/Ni/MCM-41 catalysts from the pyrolysis-catalytic reforming of simulated mixed waste plastics with different Fe:Ni ratios (00:20, 05:15, 10:10, 15:05, 20:00).

The results are shown about product yields and gas compositions in Table 6-3. The gas yield in Table 6-3 is expressed in terms of mass of plastic feedstock only. In addition, the gas yield is also expressed as the yield in relation to the

mass of plastics and reacted water. The mass closure for all the experiments was between 94 wt.% and 99 wt.% when all reactants were taken into account.

Table 6-3 Product yields and gas concentrations from pyrolysis-catalytic reforming of simulated mixed waste plastics (SMWP) with Fe/Ni/MCM-41 catalysts with different Fe:Ni ratios (00:20, 05:15, 10:10, 15:05, 20:00).

SMWP +Fe/Ni/MCM-41(%)	00:20	05:15	10:10	15:05	20:00
Gas yield (wt.%)	50.74	43.16	63.10	66.07	43.45
Liquid yield (wt.%)	35.15	45.42	28.74	27.84	44.88
Residue yield (wt.%)	0.68	0.64	1.01	1.08	0.73
Carbon deposition (wt.%)	7.26	6.18	2.43	3.78	4.88
Mass balance (wt.%)	93.82	95.40	95.29	98.77	93.94
Carbon deposition (g)	0.32	0.29	0.12	0.14	0.20
Hydrogen production (mmol g ⁻¹ Mixed plastics)	30.49	29.89	46.06	30.94	18.05
Gas concentration (Vol.%)					
CO	19.29	13.19	32.23	27.63	17.31
H ₂	45.03	46.53	46.73	43.13	37.16
O ₂	0.49	1.76	0.00	1.72	0.00
CO ₂	3.37	3.04	1.93	2.49	3.43
CH ₄	8.89	10.06	6.23	7.29	12.45
C ₂ -C ₄	22.93	25.42	12.88	17.74	29.65

Table 6-3 shows that the gas yield in relation to the mass of plastics and reacted water for the nickel only (00:20) Fe/Ni/MCM-41 catalyst was 84.9 wt.% and for the iron only (20:00) Fe/Ni/MCM-41 catalyst the gas yield was 73.5 wt%. In terms of hydrogen the production was 30.5 mm g⁻¹_{plastic} and 18.1 mm g⁻¹_{plastic} for the Ni only (00:20) Fe/Ni/MCM-41 and Fe only (20:00) Fe/Ni/MCM-41 catalysts respectively. Nickel is reported to be more dominant for hydrogen production compared with iron, due to the higher catalytic activity of nickel-based catalysts [22]. The results are consistent with our previous research with

waste tyres as the feedstock, where a Ni/Al₂O₃ catalyst produced higher gas and hydrogen compared with a Fe/Al₂O₃ catalyst in a pyrolysis catalytic-gasification process[23].

However, for the 10:10 Fe:Ni MCM-41 catalyst, the gas yield (in relation to plastics and reacted water) was significantly higher than would be expected from a merely additive effect, being 95.0 wt% gas yield. In addition, the (10:10) Fe/Ni/MCM-41 catalyst produced the highest hydrogen production at 46.1 mm g⁻¹_{plastic} and highest CO production at 31.8 mm g⁻¹_{plastic}. The syngas (H₂ + CO) production from the pyrolysis-catalytic steam reforming of the mixed plastics was enhanced with the introduction of the Fe:Ni catalyst, particularly with the (10:10) Fe/Ni/MCM-41 catalyst producing 77.8 mmol_{gas} g⁻¹_{plastic}.

The results suggest a synergistic effect of the nickel and iron, which enhances the catalytic activity towards total gas yield and hydrogen production. The results suggest a synergistic effect of the nickel and iron which enhances the catalytic activity by increasing the metal dispersion and reduction temperature towards total gas yield and hydrogen production [24]. Zhang et al.[24] reported that metal dispersion had been improved by the synergy of Ni-Co as bimetallic catalysts. Becerra et al. [25] found that the number of surface metal atoms was significantly increased and consequently increased catalytic activity for a Ru-Ni bimetallic catalyst for carbon dioxide reforming of methane. Rynkowski et al. [26] also reported that the Ni-Pt bimetallic catalysts promote the metal dispersion on the catalyst, which is one of the most important factors which affects the catalysts activity.

It is also noteworthy that the lowest catalyst carbon deposition also occurred with the (10:10) Fe/Ni/MCM-41 catalyst at 6.0 wt.%. At different Fe:Ni ratios, there was less of a synergistic effect, with the (05:15) Fe/Ni/MCM-41 catalyst producing a lower gas yield and hydrogen production. The (15:05) Fe/Ni/MCM-41 catalyst showed an improved gas yield at 86.0 wt.% and higher hydrogen production at 30.9 mm g⁻¹_{plastic}, but the yields were lower than the Fe:Ni 10:10 catalyst.

The relative volumetric gas compositions are also shown in Table 6-3. The gas product consisted of mainly hydrogen and carbon monoxide, methane and C₂ -

C₄ hydrocarbons, with lower concentrations of carbon dioxide. The highest CO yield (32.2 vol.%) occurred with the (10:10) Fe/Ni/MCM-41 catalyst which also produced the highest hydrogen yield (46.7 vol.%) and the lowest CO₂ (1.9 vol.%), CH₄ (6.2 vol.%) and C₂ — C₄ (12.9 vol.%) yields. Hydrogen and carbon monoxide produced from the simulated mixture of waste plastics by pyrolysis-catalytic steam reforming are based on the following equations [27]:



The maximum yield of syngas (hydrogen and carbon monoxide) produced was 78.9 vol.% with the (10:10) Fe/Ni/MCM-41 catalyst which promotes the conversion of the hydrocarbons to produce more CO and H₂ based on equation 6.3-6.6. The CO may be involved in the water gas shift reaction (equation 2) producing more hydrogen, catalysed by the presence of the Fe in the catalyst [28].

6.2.3 Effect of Fe:Ni ratios on catalyst deactivation/carbon deposition

The carbon produced from the pyrolysis-catalytic steam reforming of the simulated mixed waste plastics (SMWP) process can encapsulate the active metal sites of the catalyst that will result in catalyst deactivation [29]. The conversion efficiency of the plastics in the catalytic steam reforming process could consequently decrease by catalyst deactivation depending on the amount of carbon deposited, but also the type of carbon deposited [29, 30]. Different types of carbon may form on the catalyst, including encapsulating carbons which lead to catalyst deactivation and/or filamentous type carbons which have a lesser deactivation effect on the catalyst [29]. Therefore, the properties of the deposited carbon on the catalyst were analysed by a series of analyses; temperature programmed oxidation (TPO) was used to identify the type of carbon deposition; scanning electron microscopy (SEM) and transmission

electron microscopy (TEM) were used to characterize the morphology of carbon deposition.

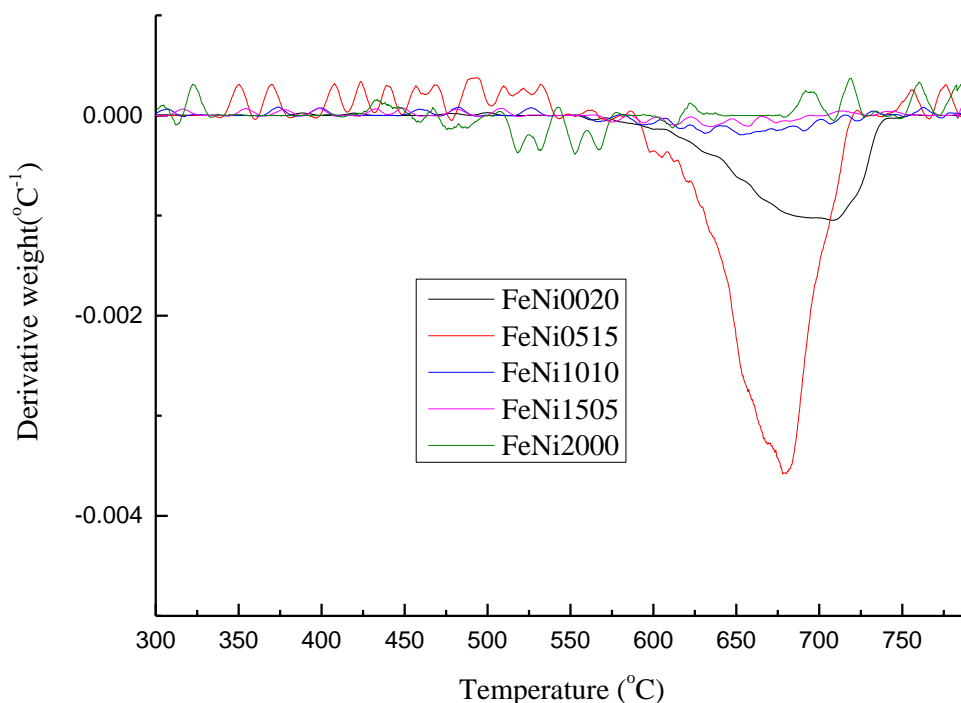


Figure 6-12 DTG-TPO results of the used catalysts from the pyrolysis-catalytic reforming of simulate mixed waste plastics (SMWP) with Fe/Ni/MCM-41 catalysts with different Fe:Ni ratios (00:20, 05:15, 10:10, 15:05, 20:00).

Table 6-3 shows that the Fe:Ni ratio influenced the amount of carbon deposited on the catalysts, with the lowest at the Fe:Ni ratio of 10:10 (6.0 wt.%) and the highest with the Ni only catalyst (Fe:Ni ratio 00:20) at 16.0 wt.% deposited carbon. This could be caused by the synergistic effect between iron and nickel metals which improves the carbon formation resistance due to the strong metal-support interaction.

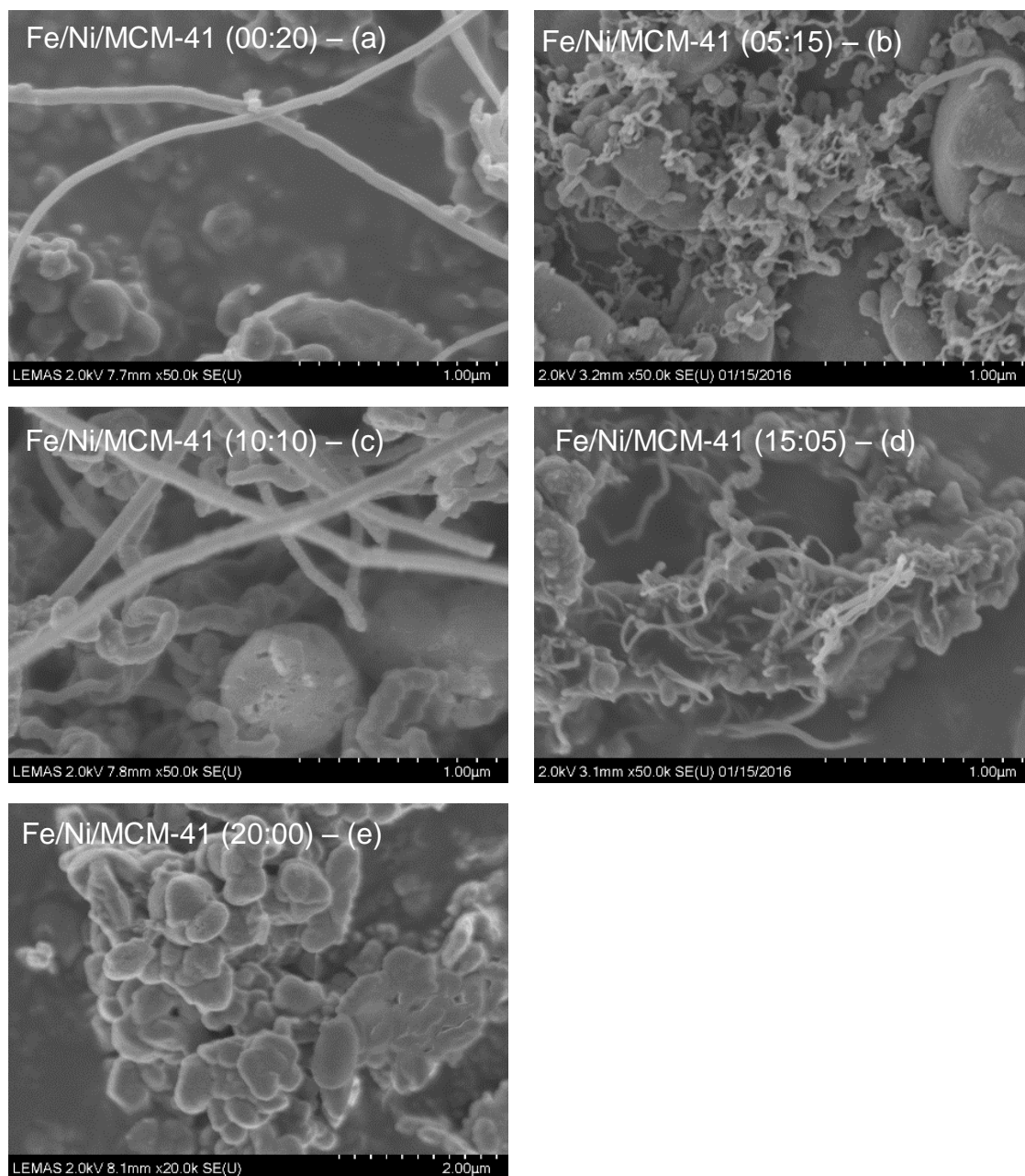


Figure 6-13 SEM images of the used catalysts from the pyrolysis-catalytic reforming of simulated mixed waste plastics (SMWP) with Fe/Ni/MCM-41 catalysts with different Fe:Ni ratios (00:20, 05:15, 10:10, 15:05, 20:00).

Temperature programmed oxidation (TPO) of the carbon deposits showed that for the catalyst that contained some nickel (05:15, 10:10, 15:05 and 20:00), the oxidation of the carbon occurred at temperatures of over 670 °C which indicates that most of the carbon deposited was filamentous carbon[31]. However, for the Fe only catalyst (20:00 Fe/Ni/MCM-41), the oxidation of carbon occurred at

less than 550 °C, indicating that the carbon deposited was mainly amorphous carbon.

Scanning electron microscopy (SEM) analysis was also carried out to characterise the carbons deposited on the catalyst. Figure 6-13 shows the SEM micrographs for the Fe:Ni MCM-41 catalysts after pyrolysis-catalytic steam reforming of the waste plastics. The SEM images for the reacted (00:20, 05:15, 10:10, 15:05) Fe/Ni/MCM-41 catalysts show the presence of filamentous carbon. However, the carbon produced with the Fe only catalyst (20:00, Fe/Ni/MCM-4) showed few filamentous carbons, indicating that the deposited carbon was the amorphous type.

Transmission electron microscopy with energy dispersive X-ray spectroscopy (TEM- EDXS) elemental mapping was carried out on the reacted bimetallic catalysts (containing both Fe and Ni), to determine the carbon, iron and nickel locations on the catalyst. The specific TEM images for the different catalysts (05:15, 10:10, 15:05, Fe-Ni-MCM-41) coupled with carbon, nickel and iron mapping are shown in Figure 6-14 and Figure 6-15.

Figure 6-14(a) shows the TEM micrograph of the carbon deposits from the 05:15 Fe/Ni/MCM-41 catalyst from pyrolysis-catalytic steam reforming of the waste plastics. The carbon mapping shows that the carbon is distributed throughout and the TEM image for all of the particles shown. However, Fe and Ni mapping of the same micrograph image show that the darker particles shown in the TEM image are composed of both Fe and Ni. Therefore the Fe:Ni catalysts are acting as bifunctional catalyst and the Fe and Ni are not present as separate particles.

The TEM images of the metal particles shown in Figure 6-14(a), (b) and (c) show that the particle size ranges from 5 nm to larger than 50 nm. The carbon deposits on all of the catalysts consisted of solid carbon and hollow carbon filaments, for example Figure 6-14(b) and (c) for the used 10:10, 15:05, Fe-Ni-MCM-41 catalysts shows the presence of hollow carbon filaments. In addition, Figure 6-14(b) and (c) shows that the metal particle is located within the hollow filament or at the tip or base of the carbon filament.

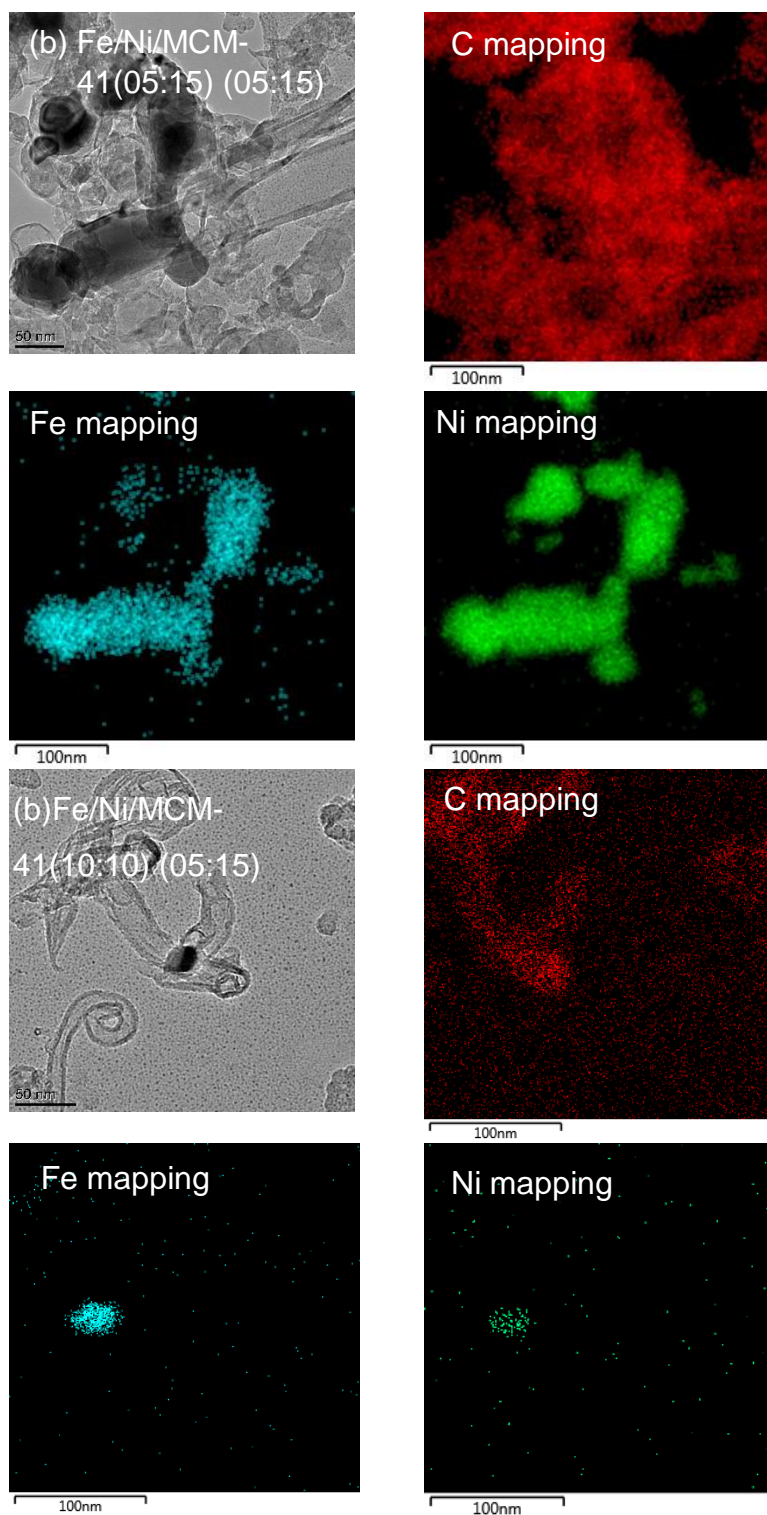


Figure 6-14 Transmission electron microscopy with energy dispersive X-ray spectroscopy (TEM-EDXS) elemental mapping analysis of C, Fe and Ni for reacted (05:15, 10:10, 15:05) Fe/Ni/MCM-41 catalysts

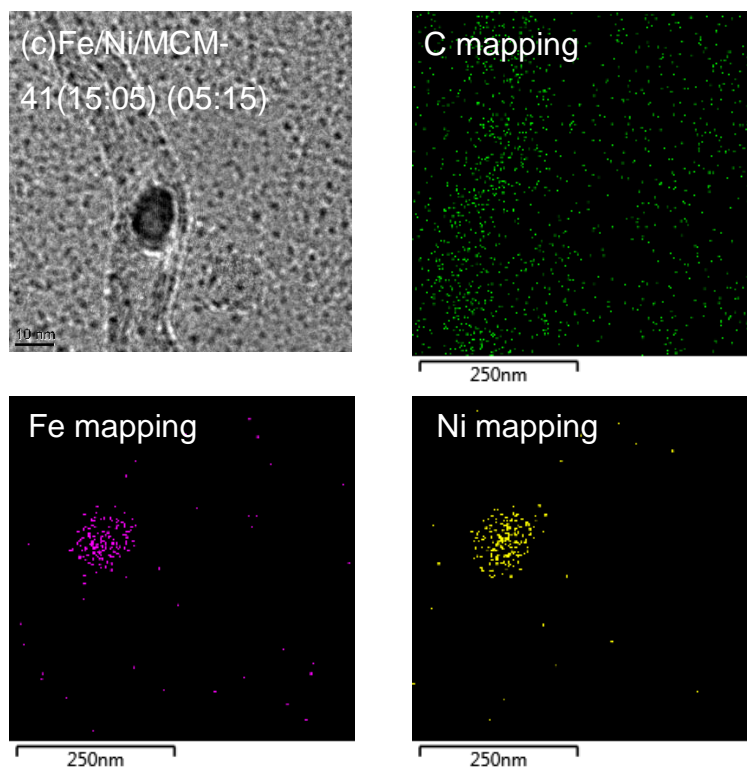


Figure 6-14 Transmission electron microscopy with energy dispersive X-ray spectroscopy (TEM-EDXS) elemental mapping analysis of C, Fe and Ni for reacted (05:15, 10:10, 15:05) Fe/Ni/MCM-41 catalysts.

There have been several reports suggesting the growth mechanism of the carbon filaments involving interaction of the catalyst support and the metal [29, 30, 32-36]. It is suggested that the interaction of the hydrocarbons derived from pyrolysis saturates the bimetallic Fe and Ni particles with carbon species such as metal carbides or reactive carbons [30, 32-34, 36]. The carbon species dissolve and diffuse into the bimetal particles and then precipitate to grow filaments away from the catalyst surface, or grow between the metal and support to lift the metal particle with the filament formation [36]. Whether the carbon filaments grow from the metal particle on the surface or lift the metal particle away from the surface depends on the strength of metal-support interaction [35].

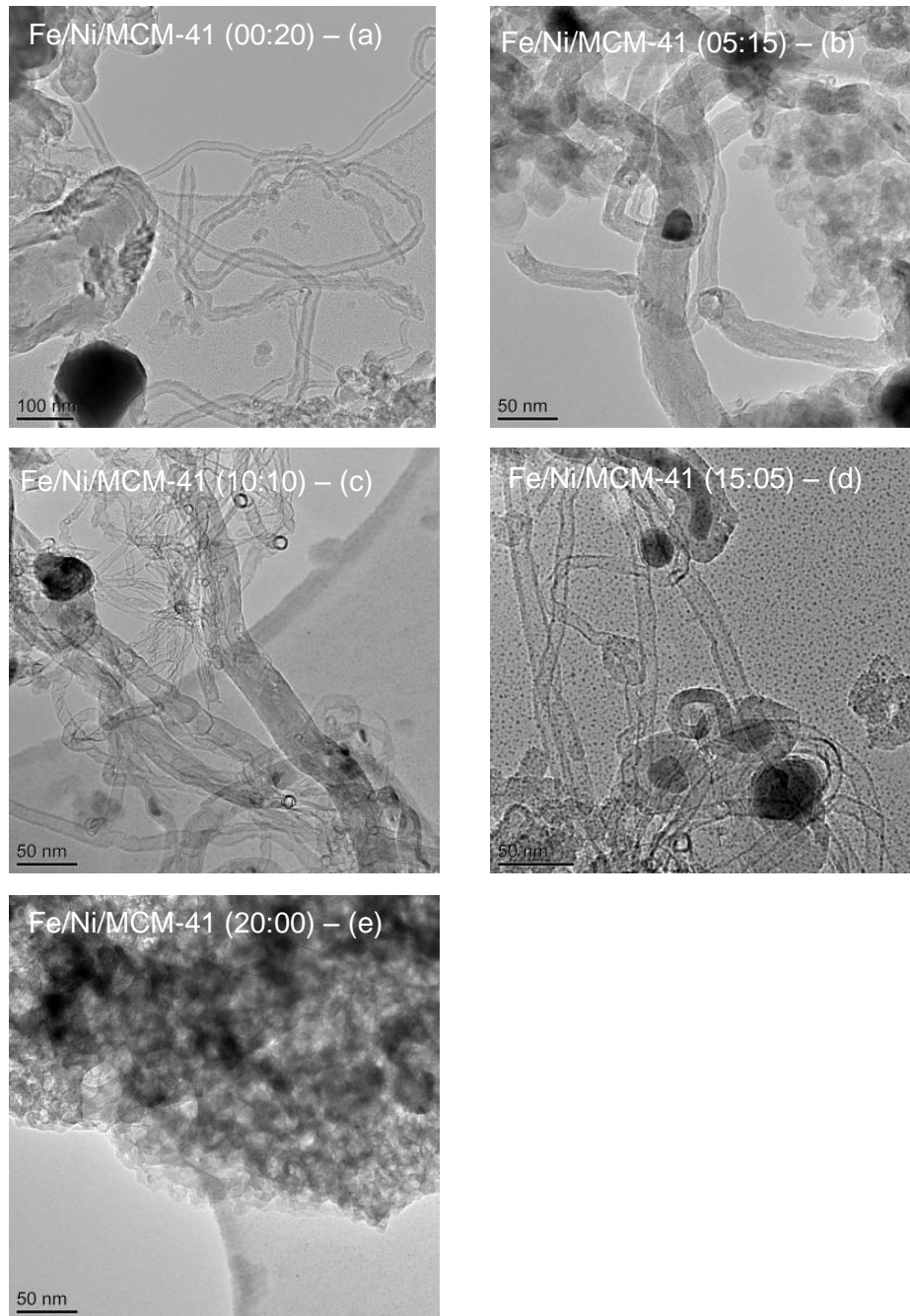


Figure 6-15 TEM images of the used catalysts from the pyrolysis-catalytic reforming of simulated mixed waste plastics (SMWP) with Fe/Ni/MCM-41 catalysts with different Fe:Ni ratios include (a) 00:20, (b) 05:15, (c) 10:10, (d) 15:05, (e) 20:00).

The results have shown that a syngas ($H_2 + CO$) with enhanced concentrations of hydrogen can be produced from waste plastics using a two-stage pyrolysis-catalytic steam reforming process using Fe-Ni-MCM-41 catalysts. Manipulating the Fe:Ni ratio can significantly raise the production of hydrogen and carbon

monoxide from the plastics, with the 10:10 Fe:Ni ratio producing the greatest effect. The Fe and Ni in the catalyst produced a synergistic enhancement of both H₂ and CO, compared to the Fe only and Ni only MCM-41 catalysts. For example, for the Fe only catalyst the H₂ production was 18.1 mmol g⁻¹_{plastic} and CO was 8.4 mmol g⁻¹_{plastic} for the Ni only catalyst H₂ production was 30.5 mmol g⁻¹_{plastic} and CO was 13.1 mmol g⁻¹_{plastic}. The calculated calorific value of the product gases was between 20.83 and 31.8 MJ m³, depending on Fe:Ni ratio, representing a useful product fuel gas. The highest calorific value of the product gas was for the Fe only catalyst at 31.8 MJ m³ due to the high content of C₁ - C₄ gases produced.

6.2.4 Conclusion

Waste plastics have been processed using a two-stage, pyrolysis-catalytic steam reforming process system to produce a hydrogen enhanced syngas using various Fe:Ni ratios supported on MCM-41 catalysts. The iron and nickel bimetallic catalysts promoted the formation of hydrogen and carbon monoxide. A synergistic effect of the iron and nickel was observed, particularly for the (10:10) Fe-Ni/MCM-41 catalyst where the highest gas yield (95 wt.%), H₂ obtained (46.1 mmol g⁻¹_{plastic}) and CO production (31.8 mmol g⁻¹_{plastic}) was shown. The product syngas contained high volumetric concentrations of hydrogen and carbon monoxide with lower concentrations of C₁ — C₄ hydrocarbons and CO₂. For example, the (10:10) Fe/Ni/MCM-41 catalyst produced a gas containing of 46.7 Vol.% hydrogen, 32.2 Vol.% carbon monoxide, 6.2 Vol.% methane, 12.9 Vol.% C₁ — C₄ and 1.9 Vol.% carbon dioxide. The process also resulted in significant deposition of carbon on the catalysts with the (10:10) Fe/Ni/MCM-41 catalyst producing the lowest carbon deposition (6 wt.%), while the nickel only (00:20) Fe/Ni/MCM-41 catalyst producing 16 wt.% carbon depositions and the iron only (20:00) Fe/Ni/MCM-41 catalyst produced 10.0 wt.% carbon deposition. Transmission electron microscopy with energy dispersive X-ray spectroscopy (TEM-EDXS) elemental mapping of the used catalyst showed that the iron/nickel metal particles promoted the growth of the carbon deposits as carbon solid and hollow filaments.

6.3 Hydrogen produced from different waste plastics with Fe/Ni/MCM-41 (10:10) catalyst by pyrolysis-catalytic reforming process.

In this section, seven different real world waste plastics and simulated mixed waste plastics have been investigated for hydrogen production by pyrolysis-catalytic reforming. The same two-stage fixed-bed reactor described in Chapter 3 was used for this section of experiments. The real world waste plastics were agricultural mixed plastics, plastics from detergent containers, plastics from vehicle fuel tank, plastics from mineral water containers, plastics from motor oil flasks, plastics from household food packaging and plastics from building reconstruction. The simulated mixed waste plastics is same as the feedstock used in section 6.2. This section is a continuation of the study of section 6.2, such that the Fe/Ni/MCM-41 catalyst used in this section is the Fe:Ni ratio 10:10 which presented the best performance on gas yield in the simulated mixed waste plastics pyrolysis-catalytic reforming process.

In this section, the only variable was the type of feedstock, 2 g of each type of real world waste plastics sample was placed in the first stage of the reactor the same amount of 0.5 g of Fe/Ni/MCM-41 catalyst with Fe to Ni ratio 10:10 for each experiment was placed in the second stage of the reactor. The water injection rate was 2 g h⁻¹, heating rate was 40 °C min⁻¹ and reforming temperature was 800 °C for all experiments.

6.3.1 Mass balance and gaseous products

The largest gas yields were obtained from the simulated mixed waste plastics and agricultural plastics by the pyrolysis-catalytic reforming process are 67.03 and 60.73 wt. % respectively as shown in Table 6-4. Gas yields from other types of plastics are generally in a lower range between 37.55 to 50.44 wt.%. The residues after the reaction are a very small amount for example, mineral water containers and food package plastics with relatively high residues are 5.29 and 3.68 wt. %.

Table 6-4 Product yields and gas concentrations from the pyrolysis-catalytic reforming of different waste plastics(Feedstock to catalysts ratio at 4:1, reforming temperature at 800 °C, heating rate at 50 °C min⁻¹, water injection rate 2 g h⁻¹ and Fe-Ni/MCM-41 catalysts with Fe to Ni ratio at 10:10)

In relation to sample & liquid								
Plastics+Fe/Ni/MCM-41(%)	Simulated waste plastics	Agricultural plastics	Detergent containers	Vehicle fuel tank plastics	Mineral water containers	Motor oil flasks	Food package	Building re-construction
Gas yield (wt.%)	67.03	60.73	47.99	50.44	37.55	42.92	39.82	55.87
Liquid yield (wt.%)	23.06	27.21	39.80	41.72	51.59	43.55	41.38	29.85
Residue yield (wt.%)	0.75	1.16	0.74	0.00	5.29	0.49	3.68	2.39
Carbon yield (wt.%)	3.01	1.16	5.90	0.84	0.13	7.06	5.98	5.37
Mass balance (wt.%)	93.85	90.27	94.43	93.00	97.17	94.01	90.85	93.49
Hydrogen production (mmol g ⁻¹ plastics)	44.11	55.99	32.61	44.45	18.94	35.96	28.00	22.66
Gas concentration (Vol.%)								
CO	32.67	28.92	20.62	27.92	36.92	20.58	19.36	21.13
H ₂	49.62	55.19	48.63	51.38	40.59	53.60	47.40	42.12
O ₂	0.40	0.00	0.85	0.38	2.95	0.00	1.04	18.40
CO ₂	2.21	1.80	3.03	1.93	13.05	2.72	1.86	2.02
CH ₄	7.35	9.57	14.04	10.19	5.38	13.31	15.07	8.69
C ₂ -C ₄	7.75	4.51	12.84	8.20	1.10	9.80	15.27	7.64
Calorific value (MJ m ⁻³)	18.36	16.81	22.28	19.21	12.13	20.60	24.06	16.64

Even though the previous research has shown that water introduction prohibited carbon formation in the pyrolysis-catalysis/catalytic reforming process [37], there was still considerable amounts of carbon production from some of the waste plastic samples, such as detergent containers which gave 5.90 wt. %, motor oil flasks gave 7.06 wt. %, food package gave 5.98 wt. % and building re-construction plastics gave 5.37 wt. % of carbon yield. The weight loss shown by the TGA-TPO results as shown in Figure 6-16 are also consistent with the carbon yields shown in Table 6-4, in that detergent container plastics, motor oil flasks, food package and building re-construction plastics gave significant amounts of carbon yield even in the presence of water/steam.

As shown in Table 6-4, hydrogen concentrations were produced in similar amounts at around 50 vol. % from the different real-world waste plastics. Nevertheless, hydrogen production from the different waste plastic samples showed some differences, for example, agricultural plastics gave the highest hydrogen production at 55.09 mmol g⁻¹ of plastics feedstock, simulated mixed waste plastics and vehicle fuel tank plastics gave relatively high hydrogen production at 44.11 and 44.45 mmol g⁻¹ of plastics feedstock respectively. Furthermore, methane and other hydrocarbons were also produced in similar amounts. Methane concentration achieved the highest concentration at 15.07 vol. % from household food package plastics that was more than twice that obtained compared with the lowest methane yield from mineral water container at 5.38 vol. %. The C₂-C₄ hydrocarbon concentration produced from mineral water containers gave the lowest concentration at 1.10 vol. % which was lower than the concentration produced from household food package.

Table 6-4 also shows the calorific values of the product gas produced from the different waste plastics. The calorific value of the product gas is influenced by the types of plastics. The gas produced from household food package waste plastic has the highest calorific value at 24.06 MJ m⁻³ and the gas produced from mineral water container has the lowest calorific value at 12.13 MJ m⁻³. The product gas with calorific values around 20 MJ m⁻³ can provide sufficient energy for the pyrolysis-catalytic reforming process [38].

6.3.2 Carbon deposition

The carbon deposition on the catalyst was only very small amounts as shown in Table 6-4. But it is necessary to further analysis the characteristics of the carbon produced from different real world waste plastics by pyrolysis-catalytic reforming process as high value filamentous carbon especially carbon nanotubes, were produced from the simulated waste plastics (as discussed in section 6.2). Temperature programmed oxidation and scanning electron microscopy were carried out to identify the types of carbon deposited on the catalysts and the results are presented in Figure 6-16, Figure 6-17 and Figure 6-18.

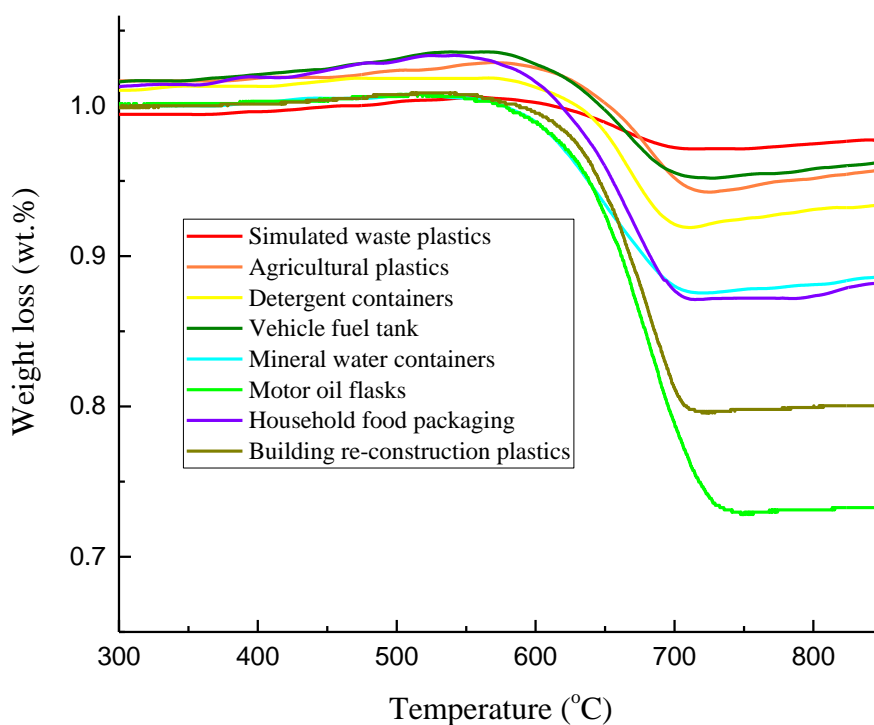


Figure 6-16 TGA-TPO analysis results of the used catalysts from the pyrolysis-catalytic reforming of different waste plastics.

From the weight loss profiles shown by the TGA-TPO results shown in Figure 6-16 and the carbon yields shown in Table 6-4, there were significant amounts of carbon produced from the different types of waste plastics via the pyrolysis-

catalytic reforming process. As the differential weight loss peaks shown in Figure 6-17 were all above 650 °C the results indicate that most of carbon produced from different waste plastics showed high thermal stability and high graphitization which also indicates that the carbon was more of the filamentous type carbon. The SEM images shown in Figure 6-18 also indicate the presence of filamentous carbons that were produced from the processing of the different real world waste plastics. Except for the carbon produced from the motor oil flasks plastics and building re-construction plastics, the filamentous carbon produced from other waste plastics were more homogenous and relatively longer.

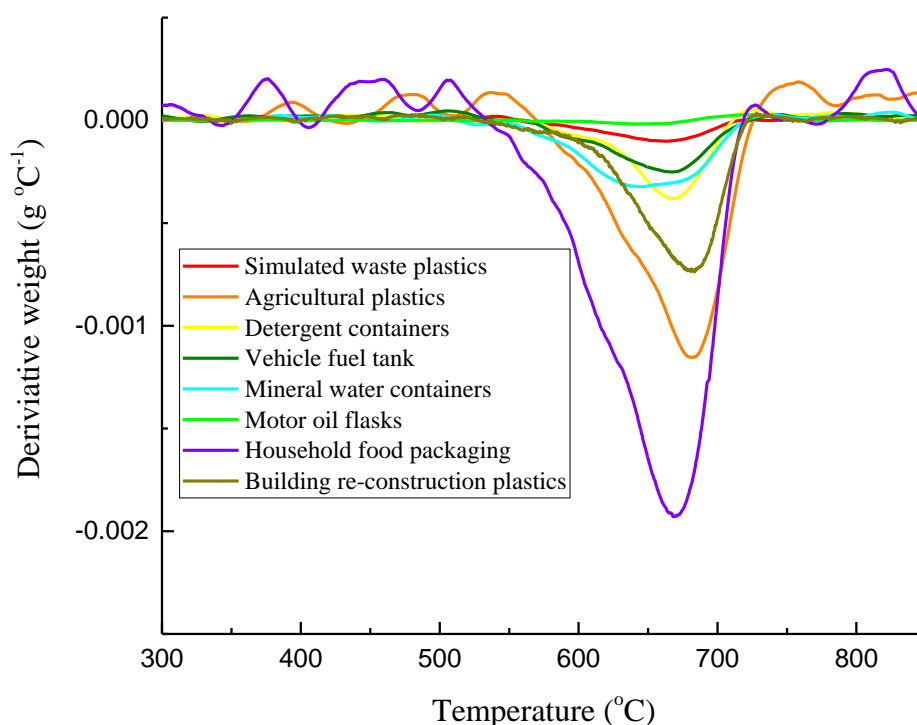


Figure 6-17 DTG-TPO analysis results of the used catalysts from the pyrolysis-catalytic reforming of different waste plastics (Feedstock to catalysts ratio at 4:1, reforming temperature at 800 °C, heating rate at 50 °C min⁻¹, water injection rate 2 g h⁻¹ and Fe-Ni/MCM-41 catalysts with Fe to Ni ratio at 10:10).

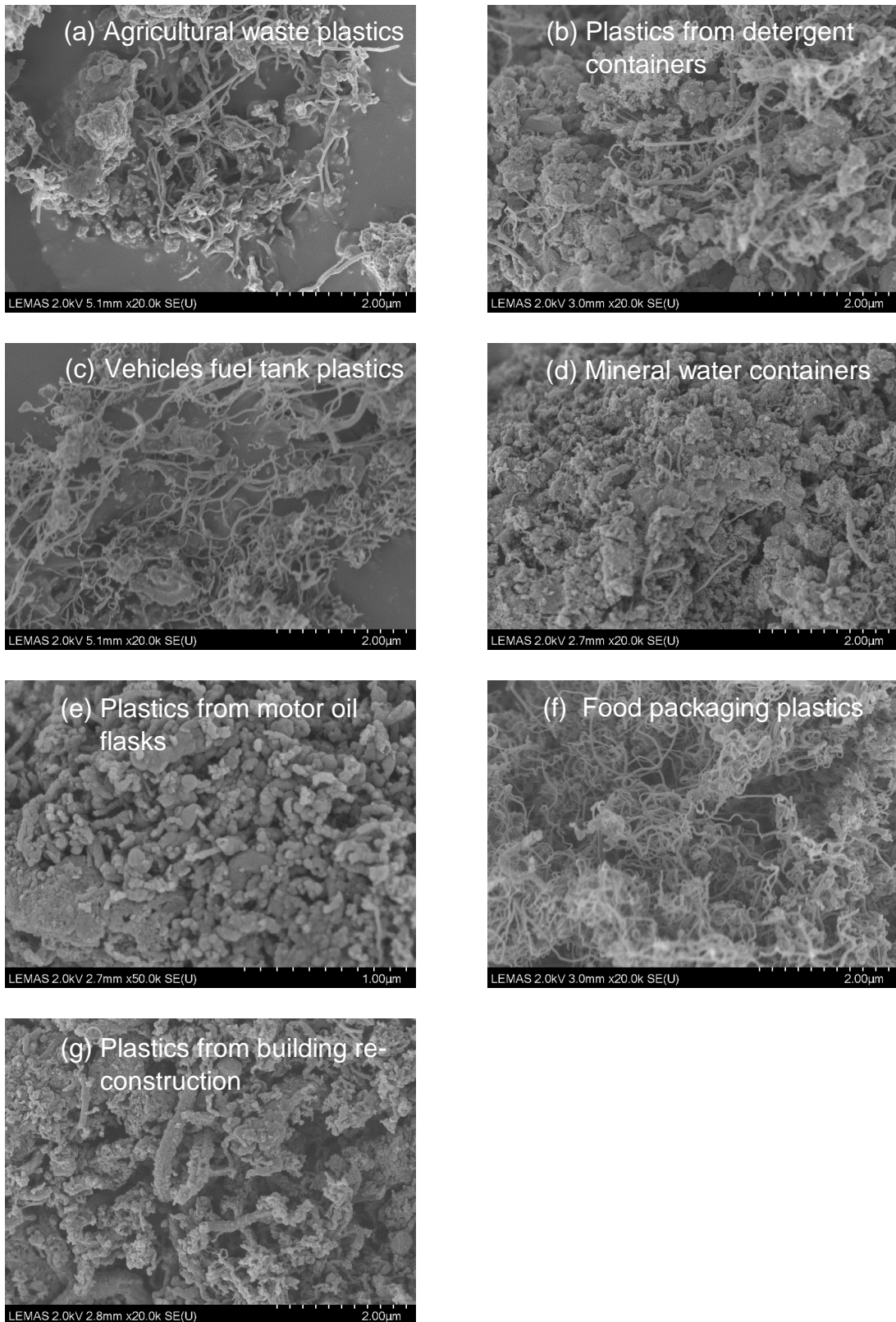


Figure 6-18 SEM images of reacted catalysts from the pyrolysis-catalytic reforming of different waste plastics.

6.3.3 Conclusion

The different types of real world waste plastics (agricultural mixed plastics, plastics from detergent containers, plastics from vehicle fuel tank, plastics from mineral water containers, plastics from motor oil flasks, plastics from household food packaging and plastics from building re-construction) have been investigated by pyrolysis-catalytic reforming with Fe/Ni/MCM-41 (Fe:Ni=10:10) catalyst for hydrogen and CNT production. The results show that there were large differences in gas yields between the different plastic feedstock. Agricultural waste plastics, plastics from vehicle fuel tanks and plastics from building re-construction are more dominant towards gas yields which were 60.73, 50.44 and 55.87 wt.%, respectively. The hydrogen production produced from building re-construction plastics and mineral water containers were much smaller than the production from other plastic samples, which were between 22.66 and 18.94 mmol per gram of plastics. The calorific values of the produced gases from different plastic samples were in the range of 12.13 - 24.06 MJ m⁻³. Hydrocarbons produced from detergent containers and household food package were relatively high in concentration corresponding with higher calorific value of the produced gases, which were 22.28 and 24.06 MJ m⁻³. The filamentous carbon has also been produced from most of the plastic samples, which can be a value added by-product from the waste plastics pyrolysis-catalytic reforming process.

Overall, the agricultural plastics, plastics from vehicles fuel tanks and motor oil flasks are good for hydrogen production. Agricultural plastics, vehicles fuel tank and plastics from food package are good for both quantity and quality of CNTs formation. In terms of hydrogen and CNTs productions, agricultural plastics and vehicles fuel tank plastics are good for both hydrogen production and simultaneously with high quality and amount of CNTs productions.

References

1. Kaewpengkrow, P., et al., *Pyrolysis and gasification of landfilled plastic wastes with Ni– Mg– La/Al₂O₃ catalyst*. Environmental Technology, 2012. **33**(22): p. 2489-2495.
2. Acomb, J.C., et al., *Effect of growth temperature and feedstock:catalyst ratio on the production of carbon nanotubes and hydrogen from the pyrolysis of waste plastics*. Journal of Analytical and Applied Pyrolysis, 2015. **113**: p. 231-238.
3. Williams, P.T., et al., *Interaction of plastics in mixed-plastics pyrolysis*. Energy & Fuels, 1999. **13**(1): p. 188-196.
4. Williams, E.A., et al., *The pyrolysis of individual plastics and a plastic mixture in a fixed bed reactor*. Journal of Chemical Technology and Biotechnology, 1997. **70**(1): p. 9-20.
5. Scheirs, J., et al., *Feedstock recycling and pyrolysis of waste plastics: converting waste plastics into diesel and other fuels*. 2006: J. Wiley & Sons.
6. Wu, C., et al., *Hydrogen Production from the Pyrolysis– Gasification of Polypropylene: Influence of Steam Flow Rate, Carrier Gas Flow Rate and Gasification Temperature*. Energy & Fuels, 2009. **23**(10): p. 5055-5061.
7. Kukovitskii, E.F., et al., *Carbon nanotubes of polyethylene*. Chemical Physics Letters, 1997. **266**(3–4): p. 323-328.
8. Yang, R.-X., et al., *Effects of Nickel Species on Ni/Al₂O₃ Catalysts in Carbon Nanotube and Hydrogen Production by Waste Plastic Gasification: Bench- and Pilot-Scale Tests*. Energy & Fuels, 2015. **29**(12): p. 8178-8187.
9. Amadou, J., et al., *Synthesis of a carbon nanotube monolith with controlled macroscopic shape*. Carbon, 2006. **44**(12): p. 2587-2589.
10. Li, W., et al., *Effect of temperature on growth and structure of carbon nanotubes by chemical vapor deposition*. Applied Physics A, 2002. **74**(3): p. 397-402.
11. Fang, W., et al., *Ce-Ni mixed oxide as efficient catalyst for H₂ production and nanofibrous carbon material from ethanol in the presence of water*. RSC Advances, 2012. **2**(25): p. 9626-9634.
12. Li, Q., et al., *Effect of hydrocarbons precursors on the formation of carbon nanotubes in chemical vapor deposition*. Carbon, 2004. **42**(4): p. 829-835.

13. Kumar, M., et al., *Chemical vapor deposition of carbon nanotubes: a review on growth mechanism and mass production*. Journal of nanoscience and nanotechnology, 2010. **10**(6): p. 3739-3758.
14. Gong, J., et al., *Catalytic carbonization of polypropylene by the combined catalysis of activated carbon with Ni₂O₃ into carbon nanotubes and its mechanism*. Applied Catalysis A: General, 2012. **449**: p. 112-120.
15. Dresselhaus, M.S., et al., *Raman spectroscopy on isolated single wall carbon nanotubes*. Carbon, 2002. **40**(12): p. 2043-2061.
16. Carrero, A., et al., *Effect of Mg and Ca addition on coke deposition over Cu–Ni/SiO₂ catalysts for ethanol steam reforming*. Chemical Engineering Journal, 2010. **163**(3): p. 395-402.
17. DiLeo, R.A., et al., *Purity assessment of multiwalled carbon nanotubes by Raman spectroscopy*. Journal of Applied Physics, 2007. **101**(6): p. 064307.
18. Ferrari, A.C., et al., *Raman spectroscopy of amorphous, nanostructured, diamond-like carbon, and nanodiamond*. Philosophical Transactions of the Royal Society of London A: Mathematical, Physical and Engineering Sciences, 2004. **362**(1824): p. 2477-2512.
19. Wu, C., et al., *Renewable hydrogen and carbon nanotubes from biodiesel waste glycerol*. Scientific Reports, 2013. **3**: p. 2742.
20. Wu, C., et al., *Sustainable processing of waste plastics to produce high yield hydrogen-rich synthesis gas and high quality carbon nanotubes*. RSC Advances, 2012. **2**(10): p. 4045-4047.
21. Gao, N., et al., *Steam reforming of biomass tar for hydrogen production over NiO/ceramic foam catalyst*. International Journal of Hydrogen Energy, 2015. **40**(25): p. 7983-7990.
22. Dong, L., et al., *Development of Fe-Promoted Ni–Al Catalysts for Hydrogen Production from Gasification of Wood Sawdust*. Energy & Fuels, 2016. **31**(3): p. 2118-2127.
23. Zhang, Y., et al., *Pyrolysis–Catalytic Reforming/Gasification of Waste Tires for Production of Carbon Nanotubes and Hydrogen*. Energy & Fuels, 2015. **29**(5): p. 3328-3334.
24. Zhang, J., et al., *Development of stable bimetallic catalysts for carbon dioxide reforming of methane*. Journal of Catalysis, 2007. **249**(2): p. 300-310.

25. Becerra, A., et al., *Promoting effects of rhodium on supported nickel catalysts in the dry reforming of methane*. Boletín de la Sociedad Chilena de Química, 2002. **47**(4): p. 385-392.
26. Rynkowski, J., et al., *Temperature-programmed reduction of alumina-supported Ni–Pt systems*. Journal of the Chemical Society, Faraday Transactions, 1995. **91**(19): p. 3481-3484.
27. Wu, C., et al., *Effect of Ni Particle Location within the Mesoporous MCM-41 Support for Hydrogen Production from the Catalytic Gasification of Biomass*. ACS Sustainable Chemistry & Engineering, 2013. **1**(9): p. 1083-1091.
28. Auprêtre, F., et al., *Bio-ethanol catalytic steam reforming over supported metal catalysts*. Catalysis Communications, 2002. **3**(6): p. 263-267.
29. Wu, C., et al., *Investigation of coke formation on Ni-Mg-Al catalyst for hydrogen production from the catalytic steam pyrolysis-gasification of polypropylene*. Applied Catalysis B: Environmental, 2010. **96**(1–2): p. 198-207.
30. Sutton, D., et al., *Review of literature on catalysts for biomass gasification*. Fuel Processing Technology, 2001. **73**(3): p. 155-173.
31. Wu, C., et al., *Investigation of coke formation on Ni-Mg-Al catalyst for hydrogen production from the catalytic steam pyrolysis-gasification of polypropylene*. Applied Catalysis B: Environmental, 2010. **96**(1): p. 198-207.
32. Louis, B., et al., *Carbon nanofibers grown over graphite supported Ni catalyst: relationship between octopus-like growth mechanism and macro-shaping*. Topics in Catalysis, 2007. **45**(1-4): p. 75-80.
33. Sacco, A., et al., *The initiation and growth of filamentous carbon from α -iron in H₂, CH₄, H₂O, CO₂, and CO gas mixtures*. Journal of Catalysis, 1984. **85**(1): p. 224-236.
34. Boellaard, E., et al., *The formation of filamentous carbon on iron and nickel catalysts*. Journal of Catalysis, 1985. **96**(2): p. 481-490.
35. Kumar, M., et al., *Carbon nanotube synthesis and growth mechanism*, in *Nanotechnology and nanomaterials; Carbon nanotubes-Synthesis, characterisation, application*, S. Yellampalli, Editor. 2011, INTECH Open Access Publisher. p. 148-170.
36. Rostrup-Nielsen, J., et al., *Mechanisms of carbon formation on nickel-containing catalysts*. Journal of Catalysis, 1977. **48**(1–3): p. 155-165.

37. Zhang, Y., et al., *Carbon nanotubes and hydrogen production from the pyrolysis catalysis or catalytic-steam reforming of waste tyres*. Journal of Analytical and Applied Pyrolysis, 2016.
38. Zhang, Y., et al., *High-value resource recovery products from waste tyres*. Proceedings of the Institution of Civil Engineers - Waste and Resource Management, 2016. **169**(3): p. 137-145.

Chapter 7. Conclusions and future work

This research work was aimed at determining the factors that influence the production of hydrogen and carbon nanotubes from the pyrolysis-catalysis of wastes including waste tyres and plastics. A comprehensive series of investigations have been carried out, including the influence of using different types of catalysts such as different transition metals and supports; process conditions such as temperature, water injection rate and sample to catalyst ratio; and different feedstock such as different tyre rubbers and plastics. However, future work is still necessary to understand the research mechanism more in depth and there are still issues in order to develop the processes for potential future commercialization.

7.1 Conclusions

The following conclusions were drawn from this research work.

7.1.1 Pyrolysis-catalysis of waste tyres for hydrogen and carbon nanotubes production

The first step for pyrolysis-catalysis of waste tyre for hydrogen and carbon nanotubes productions was to investigate the four different kinds of catalysts (Co/Al₂O₃, Cu/Al₂O₃, Fe/Al₂O₃ and Ni/Al₂O₃), which the conclusions were drawn as follows:

- The presence of catalysts can boost the waste tyre pyrolysis gasification process to produce more hydrogen production. The Ni/Al₂O₃ catalyst gave the highest total gas yield and the highest H₂ production;
- In the presence of Ni/Al₂O₃ catalyst in the reforming process, the

highest amount of carbon production was found and that the most of the carbon are carbon nanotubes as found by the TPO, SEM and TEM results;

- The Ni/Al₂O₃ catalyst gave the best quality of carbon nanotubes production along with a relatively high yield of syngas in the waste tyre pyrolysis-catalytic reforming process. SEM and TEM results showed that the carbon nanotubes were relatively long, straight and regularly shaped. Raman analysis of the carbons showed them to be high purity, very graphitic carbon nanotubes.
- The second step investigation for pyrolysis-catalysis of waste truck tyre was undertaken to investigate the production of hydrogen and carbon nanotubes in relation to a range of process conditions in the presence of a Ni/Al₂O₃ catalyst, such as water injection rate, catalysis temperature and sample to catalyst ratio. The conclusions were drawn as follows
- The more water injection would be favorable for more hydrogen production, but there was an optimized water injection rate with the highest hydrogen production without saturating the catalyst. Furthermore, the water introduction inhibited filamentous carbon production. As the water injection rate was increased from 0 to 5 ml h⁻¹, the carbon production decreased from 19.0 wt.% to 4.65 wt.% and the filamentous carbon production decreased from 164 to 45 mg g⁻¹. In addition,, the filamentous carbons formed in waste tyre pyrolysis catalytic-reforming process with water introduction were mostly solid carbon fibers and not carbon nanotubes. Water (steam) introduction to the waste tyre pyrolysis-catalysis process resulted in catalytic steam reforming of the pyrolysis gases and the production of hydrogen, reaching a maximum of 34.69 mmol g⁻¹ tyre and a gas composition consisting of 57.06 vol.% H₂, 16.31 vol.% CO, 14.24 vol.% CO₂ and 9.61 vol.% CH₄. In addition, introducing steam to the process reduced the formation of carbon on the catalyst from 8.0 wt.% (no water) to 3.36 wt.%.
- Pyrolysis-catalysis of waste tyres was further investigated to maximise

the production of carbon nanotubes, therefore no steam was added to the process. The highest yield (118.99 mg g⁻¹ tyre) and high graphitic quality of filamentous carbon was produced at 900 °C. The influence of tyre:catalyst ratio on carbon nanotubes production showed that a ratio of 1:1 gave the highest filamentous carbon production reaching a maximum of 201.5 mg g⁻¹ tyre compared to carbon nanotubes produced at 1:0.5 and 1:2 tyre:catalyst ratio.

Overall, for co-producing carbon nanotubes and hydrogen from waste truck tyre by pyrolysis-catalysis, a catalyst temperature of 900 °C and tyre:catalyst ratio of 1:1 without steam addition produced high yields of H₂ and filamentous carbons and thereby carbon nanotubes.

7.1.2 Investigations on different tyre rubbers and tyre pyrolysis oil model compounds for carbon nanotubes and hydrogen productions

Different types of tyre rubbers used in tyre manufacture and tyre pyrolysis model compounds were investigated to further understand the process of hydrogen and carbon nanotube production from waste tyres. Two types of tyres (waste truck tyre and waste car tyre) and three elastomers (natural rubber, butadiene rubber and styrene-butadiene rubber) were investigated. The conclusion were drawn as below:

- From the thermal gravimetric analysis results, the major component of both waste car tire and waste truck tire was natural rubber. The natural rubber content in waste truck tyre was more than the content in waste car tyre, consequently waste truck tyre contained lower contents of butadiene rubber and styrene-butadiene rubber;
- Natural rubber gave the highest hydrogen production and carbon nanotubes compared with the other two elastomers which could be the reason that waste car tyre gave a higher hydrogen production than waste truck tyre;

- Raman analysis of the deposited catalyst carbon showed that waste truck tyre gave the higher quantity of carbon, were more crystalline, and showed less defects compared with waste car tire. Scanning electron microscopy images and temperature programmed oxidization results showed the deposited carbon was filamentous carbon. Transmission electron microscopy images confirmed the filamentous carbons were carbon nanotubes and were multi-walled carbon nanotubes. The higher aromatic contents, in waste tyre pyrolysis oil are because of the thermal degradation of styrene-butadiene rubber. So, the relatively higher content of styrene-butadiene rubber and butadiene rubber in waste car tyre consequently with lower content of natural rubber inhibits the filamentous carbon formation in the pyrolysis-catalysis process. According to all of the results obtained, it was shown that waste car tyre gave relatively lower quality of carbon nanotubes with more structural defects, with less crystallinity of carbon nanotubes comparing with waste truck tyre in terms of crystallization, smooth surface morphologies and yield.

In addition, the production of hydrogen and carbon nanotubes was investigated in relation to five typical tyre pyrolysis oil model compounds (hexadecane, decane, styrene, phenanthrene and naphthalene). The conclusions drawn were as follows:

- The aliphatic model compounds (hexadecane and decane) favour gaseous hydrocarbons formation instead of solid carbon formation in the waste tyre pyrolysis-catalysis process. Hexadecane and decane gave relatively high gaseous productions which were 42.6 wt.% and 37.65 wt.%, respectively. The carbon production was relatively low which were 0.06 g and 0.2 g per gram of tyre equivalent carbon.
- Aromatic compounds (styrene, naphthalene and phenanthrene) dominate the production of filamentous carbon compared to the aliphatic compounds (hexadecane and decane), which gave the relatively high yield of carbon productions, which were 0.4 g, 0.28 g and 0.29 g, respectively. The gaseous production was less than 10 wt. %.

In summary, The chemical structure of decane with shorter linear structure compared with hexadecane favours a higher quantity of filamentous carbon formation that was mostly multi-walled carbon nanotubes. The aromatic model compounds favour solid carbon formation where the majority of carbon formation is filamentous carbon. Comparing the singlering aromatic model compound, the polyaromatic compounds produce more solid carbon nanofibers formation.

7.1.3 Investigation of the hydrogen production along with value-added carbon nanotubes production from waste plastics by pyrolysis-catalysis/catalytic-reforming

High density polyethylene was investigated as an alternative feedstock for the production of hydrogen and carbon nanotubes by pyrolysis-catalysis. The catalyst consisted of Ni loading on a stainless steel mesh catalyst. The different parameters investigated included different catalysis temperatures (700, 800 and 900 °C), and different sample to catalyst ratios (2:1 and 4:1). The conclusions drawn were as follows:

- When the sample to catalyst ratio was 2:1, with the increase of catalysis temperature from 700 to 900 °C, the hydrogen concentration increased only slightly from 50.51 to 51.03 vol. %. A similar result was obtained at the sample to catalyst ratio of 4:1. The hydrogen concentration increased from 34.40 to 35.59 vol. % as catalysis temperature was increased from 800 to 900 °C. However, there was no significant influence of catalysis temperature on carbon yield. In addition, the liquid yield decreased significantly with the increase of catalysis temperature at sample to catalyst ratio of 2:1.
- When the sample to catalyst ratio was increased from 2:1 to 4:1, the gas yield was increased from 51.99 to 59.37 wt. % and 51.13 to 62.62 wt. % at 800 °C, 900 °C respectively. At 800 °C, the liquid yield decreased from 14.00 to 8.5 wt. %, carbon yield decreased from 34.00

to 26.00 wt. % and the hydrogen production decreased from 18.13 to 12.66 mmol g⁻¹.

- According to the scanning electron microscopy results, transmission electron microscopy results and Raman analysis results, the carbon nanotubes produced at 800 °C with a sample to catalyst ratio of 2:1 exhibited the high quality in terms of the purify and uniformity of the produced CNTs.

Further investigation of the production of hydrogen along with carbon nanotubes from waste plastics by pyrolysis-catalysis/catalytic-reforming investigation was to investigate the effect of Fe to Ni ratios (20:00, 15:05, 10:10, 05:15 and 00:20) on hydrogen and carbon nanotubes production from pyrolysis catalytic-reforming of simulated mixed waste plastics. The conclusions drawn were as follows:

- Hydrogen as the targeted product was produced from simulated mixed waste plastics by the pyrolysis catalytic-reforming process. A batch of Fe:Ni ratios (00:20, 05:15, 10:10, 15:05, 20:00) of mesoporous MCM-41 supported catalysts have been investigated for hydrogen production. The iron and nickel bimetallic catalytic effect played a significant role to stimulate hydrogen production from simulated mixed waste plastics. With a Fe:Ni ratio of 10:10 catalyst, the highest hydrogen production and highest hydrogen concentration were obtained which were 46.06 mmol g⁻¹ and 46.73 vol.%, respectively; Associated with the hydrogen, the lowest carbon deposition is 2.43 wt. % and 0.12 g per gram of simulated mixed waste plastics sample, which means less catalyst deactivation occurred.
- There was no observed change in the total pore volume and average radius of catalysts at different Fe:Ni ratios. However, the surface area of (10:10) Fe/Ni/MCM-41 bimetallic catalyst had the largest surface area is 801.90 m² g⁻¹. Along with the stronger metal-support interaction of (10:10) Fe/Ni/MCM-41 catalyst and lowest carbon deposition (2.43 wt.%), the hydrogen production and hydrogen concentration reached the highest at 46.06 mmol g⁻¹ and 46.73 vol. %.

The process involving waste plastics was further investigated using seven real-world waste plastics ((agricultural mixed plastics, plastics from detergent containers, plastics from vehicle fuel tank, plastics from mineral water containers, plastics from motor oil flasks, plastics from household food packaging and plastics from building re-construction) by pyrolysis catalytic-reforming in the presence of the Fe-Ni (10:10)/MCM-41 catalyst. The conclusions drawn were as follows:

- There were large differences in gas yields between the different feedstocks. The hydrogen production produced from building re-construction plastics and mineral water containers were much smaller than the production from other plastic samples, which were between 22.66 and 18.94 mmol per gram of plastics. The calorific values of the produced gases from different plastic samples were in the range of 12.13 - 24.06 MJ m⁻³.
- The carbon nanotubes as a by-product has also been produced from most of the real-world plastic samples, which can be a value added product from the waste plastics pyrolysis catalytic-reforming process.

7.2 Future work

7.2.1 Mechanism study

In-depth study for the understanding of the carbon nanotubes formation mechanism can possibly be investigated to understand more about the process. The prospect investigations are

- More tyre pyrolysis oil model compounds could be investigated. There might be differences in the behaviour of different model compounds, therefore, more complicated structures of model compounds be investigated for carbon nanotubes production by pyrolysis-catalysis.
- The investigation on the carbon nanotubes formation process would be a good point to make efforts on, which could help to compare the particular carbon nanotubes formation mechanism in pyrolysis-catalysis of waste tyres or plastics and the mechanism of carbon nanotubes

formed by the chemical vapour deposition method. Suggested experimental work to be carried out, such as stop the experiments after the waste samples decompose after different periods of time to compare the carbon formed at different reaction points to see the structural difference of the carbons produced.

- In-situ transmission electron microscopy could be a more advanced technique to apply to understand the growth mechanism of carbon nanotubes formed by pyrolysis-catalysis of waste tyres to monitor the carbon formation process.

7.2.2 Carbon nanotubes purifications study

- The nickel loading on stainless steel mesh catalysts has been investigated in section 6.1 and showed the advantages of a novel catalyst support investigation to solve the recovery of carbon nanotubes. Therefore, more types of metals can be loaded on the stainless steel mesh to see if there are significant differences. Also, the stainless steel supported catalysts can be applied in the waste tyre pyrolysis-catalysis process to form carbon nanotubes.
- The conventional purification methods can be involved in the research to firstly remove the amorphous carbon by oxidation of the carbon production at lower temperature, then dissolve the metals into acid to remove the impurities from the catalysts. The further quality analysis for the purified carbon nanotubes are necessary to see how the purification method would affect the quality of carbon nanotubes.

7.2.3 Quality control of carbon production

- More accurate analysis of the quality of carbon formed by waste tyres or plastics by pyrolysis-catalysis/catalytic-reforming are imperative. Such as the in-depth study on Raman shifts.
- The quality control study for carbon nanotubes produced by waste tyres or plastics by pyrolysis-catalysis/catalytic-reforming. Such as the chirality of the carbon nanotubes, the diameter, the length etc.